Role of TRPV4 channels in adverse cardiac remodelling

Laia Yáñez Bisbe

TESI DOCTORAL UPF / 2021

DIRECTORS DE LA TESI:

Dra. Begoña Benito Villabriga

Dra. Anna Garcia-Elias Heras

Departament de Ciències Experimentals i de la Salut

Universitat Pompeu Fabra Barcelona

Al meu pare,

Viure és intentar, proposar i reprendre,

I també atzar, enigma i dubte

Però mai no defallir sota els porxos de la feblesa

Xavier Viñolas

ACKNOWLEDGEMENTS

Aquest viatge de quatre anys arriba a la seva fi. És moment, doncs, de fer balanç i donar les gràcies a totes les persones que m'heu acompanyat al llarg d'aquest camí.

Primer de tot, un reconeixement especial a les meves directores de tesi, a la Bego i a l'Anna. Gràcies per creure i apostar per mi, per la vostra guia i el vostre suport i, sobretot, per haver-me transmès la motivació, l'interès i la passió per la investigació.

A en Rubén Vicente, gràcies per haver acceptat ser el tutor d'aquesta tesi.

A la Marta Tajes i a la Marta Gimeno, per tot el que em van ensenyar en els inicis d'aquesta tesi a l'IMIM.

A tots aquells que han fet possible el treball amb ratolins. A en Ramón i a la Núria Farré, a tot l'equip de l'Eduard Guasch i a la Cristina Plata, per ajudar-me a endinsar-me en el món de la gestió d'una colònia transgènica. També a tot el personal de l'estabulari, en especial a l'Eva i a la Cristina, per cuidar-me tant bé el ratolins.

Al grup de Malalties Cardiovasculars del VHIR, per acollir-me. Marisol, Javier, Antonio, Angeles, Eli i Kelly, gràcies a tots vosaltres per aportar el vostre granet de sorra i d'experiència. Als meus companys de batalla, David, Diana, Marta i Sara, amb els que compartir el dia a dia ha estat una sort i un plaer. I a tots als que han passat pel laboratori, en especial a l'Andrea.

A la família de biotecs: Turias, Turu i Ferran. El que van unir les birres del bar de ciències, les pràctiques i les tardes d'estudi durant la carrera, s'ha convertit en una gran amistat. Gràcies per animar-me a tirar-endavant. Sou essencials.

A l'Ana, per la seva amistat incondicional. Malgrat sonar-te a xino tot el que t'explicava sobre la tesi, m'has sabut escoltar, entendre, i donar-me la força per continuar avançant.

A la meva família política, que tot i que lluny sempre l'he sentit molt a prop. I un gràcies especial a en Joan i a la Maria, pels nostres vermuts i les tardes de Catán, que tant bé anaven per desconnectar.

A tota la meva família, per ser els braços on sempre m'he pogut refugiar. A tots vosaltres, gràcies per ser-hi sempre.

Als meus pares, perquè sempre han sigut el meu port i la meva barca, el meu mar d'il·lusions i de coratge, els meus pilars. Papa, sé que em faries una d'aquelles abraçades que desitjaves que no acabessin mai i em diries: estic orgullós. T'enyoro. Mama, ets el meu oxigen diari, el meu referent. M'agradaria ser algun dia la dona i mare forta i valenta que ets tu per mi. Us estimo!

A en Gabri, per ser el motor de la meva vida, el meu company d'aventures i projectes, el meu suport constant. Amb tu, a la fi del món. T'estimo infinit!

ABSTRACT

The mechanisms that determine the development of cardiac remodelling, either adverse (such as that seen in heart failure) or adaptive (such as that induced by exercise), are not known in detail. Mechanoreceptors, membrane channels capable of transducing mechanical stimuli into intracellular chemical signals, are postulated as key elements in the promotion of both types of remodelling. In this thesis, we provide evidence that there exists a differential expression pattern of mechanoreceptors in adaptive and adverse remodelling, and we highlight the role of the TRPV4 and TRPC6 channels in the promotion of the pathological response. In addition, we study in detail the molecular mechanisms by which TRPV4 promotes fibrosis and demonstrate that the deletion of the channel protects against the development of adverse remodelling. We also examine the particularities of heart failure promotion and recovery, along with changes in TRPV4 expression, associated with ageing.

RESUM

Els mecanismes que determinen el desenvolupament de remodelat cardíac, tant en la seva forma adversa (característica de la insuficiència cardíaca), com adaptativa (induïda per exercici), no es coneixen en detall. Els mecanoreceptors, canals transmembrana amb la capacitat de convertir estímuls mecànics en senyals químiques intracel·lulars, es postulen com elements clau en la promoció d'ambdós tipus de remodelat. En aquesta tesi s'aporten evidències de que existeix un patró d'expressió diferencial de mecanoreceptors en el remodelat adaptatiu i l'advers, i destaquem el paper dels canals TRPV4 i TRPC6 en desenvolupament de la resposta patològica. A més, estudiem en detall els mecanismes moleculars pels quals el TRPV4 promou la fibrosi i demostrem que la deleció del canal protegeix davant el desenvolupament del remodelat advers. Així mateix, també examinem les particularitats en el desenvolupament i la reversió de la insuficiència cardíaca, així com els canvis en l'expressió de TRPV4, associades a l'envelliment.

PREFACE

Cardiac remodelling is defined as a process that results in structural and functional changes in the heart following a sustained cardiac overload. Cardiac remodelling can be found after chronic exercise training or during pregnancy (in these cases, called physiological or adaptive remodelling) or after cardiac injury (in a form known as pathological or adverse remodelling). While adaptive remodelling is characterized by an organized process of beneficial adaptations that help maintain cardiac function over time, adverse remodelling triggers a devastating spiral of maladaptive responses that lead to a progressive dysfunction of the heart and, in the long term, to heart failure (HF). However, to date, it is not well known which are the key factors that, in response to a sustained mechanical stress, determine the development of an adaptive or an adverse cardiac response. In this context, mechanoreceptors, membrane channels that respond to mechanical forces, are presented as potential crucial mediators of cardiac remodelling.

This thesis tries to determine the involvement of cardiac mechanoreceptors, with particular interest on the TRPV4 channel, in the promotion of adaptive and adverse cardiac remodelling. We postulated that TRPV4 channels could play a determinant role in the promotion of pathological remodelling, and as such, investigate the molecular mechanisms that could drive the adverse response once these channels are activated. In addition, this work explores the role of ageing in both the development and the recovery of adverse remodelling, with particular attention to the role of these mechanoreceptors in this context.

Because management of HF remains a major challenge in clinical practice, it has been tremendously satisfactory to dedicate this four-year journey to try to better understand the participation of cardiac mechanoreceptors in cardiac remodelling, and particularly in adverse cardiac remodelling, in an attempt to provide new therapeutic strategies for this common disease.

ABBREVIATIONS

4α-PDD	4α-phorbol 12,13-didecanoate
4α-PDH	4α-phobol 12,13-dihexanoate
5,6-EET	5,6-epoxyeicosatrienoic acid
AA	arachidonic acid
AAR	area at risk
ACE	angiotensin-converting enzyme
ACEI	angiotensin-converting enzyme inhibitors
Akt (PKB)	protein kinase B
ANK	ankyrin
APS	ammonium persulfate
ARBs	angiotensin-receptor blockers
ARD	ankyrin repeat domain
ARNI	angiotensin receptor-neprilyisin inhibitor
AT1R	angiotensin-II type I receptors
AT-II	angiotensin II
AV node	atrioventricular node
AV-plane	atrioventricular plane
BAA	bisandrographolide A
BCL	basal cycle length
BK_{Ca}	large-conductance Ca^{2+}-activated K^+ channel
C/EBPβ	CCAAT/enhancer binding protein-beta
CaM	calmodulin
CaMKII	calcium/calmodulin-dependent protein kinase type II
CICR	calcium-induced calcium release
CM	cardiomyocyte
CRT	cardiac resynchronization therapy
CSA	cross-sectional area
ECM	extracellular matrix
eCSC	endogenous cardiac stem cell
EF	ejection fraction
ER	endoplasmic reticulum
ERP	effective refractory period
ET-1	endothelin-1
FAM	green fluorescent fluorophore 6-cardoxyfluorescein
FB	fibroblast
FC	fold change

FGF	fibroblast growth factor
FS	fractional shortening
H&E	haematoxylin and eosin
HF	heart failure
HFmrEF	heart failure with midrange ejection fraction
HFpEF	heart failure with preserved ejection fraction
HFrEF	heart failure with reduced ejection fraction
HW/TL	heart weight/tibia length ratio
I/R	ischemia/reperfusion
IGF1	insulin-like growth factor 1
IGF1R	insulin-like growth factor 1 receptor
IKK	IκB kinase
IP	intraperitoneal
IP_3	inositol 1,4,5-triphosphate
IP_3R	inositol 1,4,5-triphosphate receptor
IR	insulin receptor
IVS	intraventricular septum
K_{ATP}	ATP-sensitive K^+ channel
KO	knockout
LA	left atria
LAD artery	left anterior descending artery
LV	left ventricle
LVAD	left ventricular assist device
LVDd	left ventricular diameter at the end of the diastole
LVDs	left ventricular diameter at the end of the systole
LVPW	left ventricular posterior wall
MFB	myofibroblast
MI	myocardial infarction
MRA	mineralocorticoid receptor antagonists
MRTFA	myocardin transcription factor A
mTOR	mammalian target of rapamycin
NCX	Na^+/Ca^{2+} exchanger
NFAT	nuclear factor of activated T cells
NRG1	neuregulin-1
OTRPC	osmosensitive transient receptor potential channel
PCR	polymerase chain reaction
PI3K	phosphoinositide 3-kinase

PIP_2	phosphatidylinositol 4,5-bisphosphate
PKA	protein kinase A
PKC	protein kinase C
PLA_2	phospholipase A2
PLC	phospholipase C
PLN	phospholamban
PMA	phorbol 12-myristate 13-acetate
PMCA	plasma membrane Ca^{2+} ATPase
PRD	proline-rich domain
PVC	premature ventricular complexes
RA	right atria
RAAS	renin-angiotensin-aldosterone System
ROC	receptor-operated Ca^{2+} channels
ROS	reactive oxygen species
RT-qPCR	real time quantitative polymerase chain reaction
RV	right ventricle
RVD	regulatory volume decrease
RyR	ryanodine receptor
SA node	sinoatrial node
SDS-PAGE	sodium dodecyl sulphate-polyacrylamide gel electrophoresis
SEM	standard error of the mean
SERCA2a	sarcoplasmic reticulum Ca^{2+}-ATPase
SNS	sympathetic nervous system
SR	sarcoplasmic reticulum
SRF	serum response factor
SVT	sustained ventricular tachycardia
TA	total area
TAC	transverse aortic constriction
TAK1	transforming growth factor beta-activated kinase I
TEMED	tetramethylethylenediamine
TGF-β	transforming growth factor beta
TM	transmembrane domain
TNF-α	tumour necrosis alpha
TREK-1	two pore-domain K^+ channel
TRP	transient receptor potential
TβR1	transforming growth factor beta receptor type I
TβR2	transforming growth factor beta receptor type II

VEGF	vascular endothelial growth factor
VF	ventricular fibrillation
VRL-2	vanilloid receptor-like
VR-OAC	vanilloid receptor-related osmotically activated channel
VTA	ventricular tachyarrhythmias
WT	wildtype
α-MHC	alpha myosin heavy chain
α-SMA	alpha-smooth muscle actin
β-ARs	beta-adrenergic receptors
β-MHC	beta myosin heavy chain

TABLE OF CONTENTS

ACKNOWLEDGEMENTS VI

ABSTRACT VIII

RESUM VIII

PREFACE X

ABBREVIATIONS XII

TABLE OF CONTENTS XVI

1. INTRODUCTION 24

1.1. ANATOMY AND PHYSIOLOGY OF THE HEART 26

1.1.1. ANATOMY OF THE HEART 26

1.1.1.1. Macroscopic anatomy 26

1.1.1.2. Microscopic anatomy 28

1.1.2. CARDIAC PHYSIOLOGY 29

1.1.2.1. Muscular contraction 29

1.1.2.2. Electrical system 30

1.1.2.3. Excitation and contraction coupling 31

1.2. CARDIAC PLASTICITY AND ADAPTIVE REMODELLING 34

1.2.1. REGULATION OF CARDIAC HEMODYNAMICS 34

1.2.2. CARDIAC REMODELLING 36

1.2.3. PHYSIOLOGICAL OR ADAPTIVE CARDIAC REMODELLING. 38

1.2.3.1. Signalling pathways involved in adaptive cardiac remodelling induced by exercise training 39

1.3. PATHOLOGICAL OR ADVERSE CARDIAC REMODELLING AND HEART FAILURE 44

1.3.1. PATHOLOGICAL OR ADVERSE CARDIAC REMODELLING 44

1.3.1.1. Major findings of pathological remodelling 45

1.3.1.1.1. *Pathological hypertrophy* 45

1.3.1.1.2. *Fibrosis.* 46

1.3.1.1.3. *Arrhythmias* 47

1.3.1.2. Signalling pathways involved in adverse cardiac remodelling 48

1.3.1.2.1. *Dysregulation of Ca^{2+} handling* 49

1.3.1.2.2. TGF-β signalling 52
1.3.1.2.3. Inflammation 53
1.3.1.2.4. Oxidative stress 53
1.3.2. HEART FAILURE WITH REDUCED EJECTION FRACTION 54
1.3.2.1. Epidemiology of HF and social burden 54
1.3.2.2. Pathophysiology and current therapy 55
1.3.3. EXPERIMENTAL MODELS OF HF 57
1.3.3.1. Transverse aortic constriction model 58
1.3.3.2. Myocardial ischemia and myocardial ischemia-reperfusion models 58
1.3.3.3. Neurohormonal stimulation models 59
1.4. MECHANORECEPTOR CHANNELS AND CARDIAC REMODELLING 60
1.4.1. TRP CHANNELS 63
1.4.2. CARDIAC TRP CHANNELS AND THEIR ROLE IN CARDIAC REMODELLING 64
1.4.2.1. The TRPA family 64
1.4.2.2. The TRPM family 65
1.4.2.3. The TRPC family 66
1.4.2.4. The TRPV family 68
1.4.3. THE TRPV4 CHANNEL 69
1.4.3.1. Structure and biophysical properties 70
1.4.3.2. Activation and modulation 72
1.4.3.2.1. *Activation by temperature* 72
1.4.3.2.2. *Activation by osmotic and mechanical stimuli* 72
1.4.3.2.3. *Modulation by chemicals* 74
1.4.3.2.4. *Modulation by protein interactions and phosphorylation* 75
1.4.3.3. Physiological function 76
1.4.3.3.1. *Thermoregulation* 76
1.4.3.3.2. *Osmoregulation and mechanotransduction* 77
1.4.3.3.3. *Nociception* 77
1.4.3.4. TRPV4 in the heart and potential role in cardiac remodelling 78
1.4.3.5. The TRPV4-knockout mouse 81
2. HYPOTHESES AND OBJECTIVES 82
3. MATERIALS AND METHODS 86

3.1. ANIMALS....88
3.1.1. THE TRPV4-KO COLONY....88
3.1.1.1. Genotyping strategy....89
3.1.1.1.1. *Genomic DNA extraction*....89
3.1.1.1.2. *Amplification of genomic DNA by polymerase chain reaction*....89
3.1.1.1.3. *Agarose gel electrophoresis*....90
3.2. *IN VIVO* MODELS....91
3.2.1. MOUSE MODEL OF ADVERSE CARDIAC REMODELLING INDUCED BY CHRONIC INFUSION OF ISOPROTERENOL....91
3.2.1.1. Surgical procedures....92
3.2.1.2. Study design and timepoints....92
3.2.2. RAT MODEL OF ADVERSE CARDIAC REMODELLING INDUCED BY TRANSVERSE AORTIC CONSTRICTION....93
3.2.3. MURINE MODELS OF ADAPTIVE CARDIAC REMODELLING INDUCED BY MODERATE EXERCISE....94
3.3. EXPERIMENTAL DESIGN....96
3.3.1. SET-UP OF THE HF MODEL....97
3.3.2. SET-UP OF THE EXERCISE MODEL....97
3.3.3. MECHANORECEPTOR CHANGES IN ADVERSE AND ADAPTIVE CARDIAC REMODELLING....98
3.3.4. CHRONOLOGY OF ADVERSE CARDIAC REMODELLING AND CHANGES IN MECHANORECEPTOR EXPRESSION....100
3.3.5. EFFECTS OF TRPV4 GENETIC DELETION ON CARDIAC ADVERSE REMODELLING....100
3.3.6. EFFECTS OF AGE IN THE PROMOTION AND REVERSAL OF ADVERSE REMODELLING....102
3.4. ECHOCARDIOGRAPHIC STUDIES....103
3.5. HEART WEIGHT....103
3.6. HISTOLOGY....104
3.6.1. HAEMATOXYLIN AND EOSIN STAINING....104
3.6.2. PICROSIRIUS RED STAINING....105
3.7. ASSESSMENT OF ARRHYTHMIAS....105
3.7.1. LANGENDORFF PERFUSION....106

3.7.2. ELECTROGRAM RECORDINGS 106
3.7.3. ELECTROPHYSIOLOGICAL STUDIES 106
3.7.4. INDUCTION OF REGIONAL ISCHEMIA 109
3.8. ISOLATION OF MOUSE VENTRICULAR CARDIOMYOCYTES AND FIBROBLASTS 109
3.9. REAL TIME qPCR 110
3.9.1. SAMPLE PREPARATION FROM LV SAMPLES 110
3.9.2. SAMPLE PREPARATION FROM CARDIOMYOCYTE AND NON-CARDIOMYOCYTE CELLULAR FRACTIONS 110
3.9.3. RNA ISOLATION 110
3.9.4. cDNA SYNTHESIS 111
3.9.5. QUANTITATIVE POLYMERASE CHAIN REACTION 111
3.10. WESTERN BLOTTING 112
3.10.1. SAMPLE PREPARATION AND QUANTIFICATION 112
3.10.2. GEL ELECTROPHORESIS 113
3.10.3. IMMUNOBLOTING 113
3.11. CARDIAC FIBROBLAST CULTURES 114
3.12. FLUORESCENCE CALCIUM IMAGING IN FIBROBLASTS 114
3.13. CALCINEURIN ACTIVITY ASSAY 115
3.13.1. SAMPLE PREPARATION AND PROTEIN QUANTIFICATION 115
3.13.2. CALCINEURIN CELLULAR ACTIVITY ASSAY 116
3.14. NFAT NUCLEAR TRANSLOCATION 118
3.15. STATISTICAL ANALYSIS 119
4. RESULTS 120
4.1. DIFFERENTIAL EXPRESSION OF MECHANORECEPTORS IN ADVERSE AND ADAPTIVE CARDIAC REMODELLING 122
4.1.1. CHRONIC INFUSION OF ISOPROTERENOL INDUCES CARDIAC ADVSERSE REMODELLONG IN MICE 122
4.1.1.1. Chronic isoproterenol infusion promotes ventricular dilatation and hypertrophy and cardiac dysfunction 122
4.1.1.2. Chronic isoproterenol infusion leads to cardiomyocyte enlargement and cardiac hypertrophy 124

4.1.1.3. Chronic isoproterenol infusion promotes cardiac fibrosis 125
4.1.2. EXERCISE TRAINING ON A TREADMILL INDUCED CARDIAC ADAPTIVE REMODELLING IN MICE 127
4.1.2.1. Exercise training induced cardiac hypertrophy with preserved cardiac function.....127
4.1.2.2. Exercise training induced cardiac hypertrophy by increasing cardiomyocyte area 128
4.1.2.3. Moderate exercise does not induce cardiac fibrosis whereas intense exercise induces a slight increase in collagen deposition in our model.....130
4.1.3. TRPV4 AND TRPC6 INCREASE IN MICE RECEIVING ISOPROTERENOL BUT NOT IN MICE SUBJECTED TO MODERATE EXERCISE TRAINING 131
4.1.4. TRPV4 AND TRPC6 ARE OVEREXPRESSED IN RATS SUBJECTED TO ADVERSE REMODELLING BUT NOT IN RATS SUBJECTED TO ADAPTIVE REMODELLING 135
4.1.4.1. Transverse aortic constriction induces cardiac adverse remodelling in rats 136
4.1.4.2. Moderate exercise training on a treadmill induces cardiac adaptive remodelling in rats 137
4.1.4.3. TRPV4 and TRPC6 are differentially expressed in adverse and adaptive remodelling in rats 139
4.2. TIME-COURSE CHANGES IN TRPV4 AND TRPC6 TROUGHOUT THE DEVELOPMENT OF ADVERSE CARDIAC REMODELLING 140
4.2.1. ISOPROTERENOL CAUSES RAPID LEFT VENTRICULAR HYPERTROPHY AND PROGRESSIVE VENTRICULAR DILATION AND SYSTOLIC DYSFUNCTION 140
4.2.2. CARDIOMYOCYTE HYPERTROPHY DEVELOPS SHORTLY AFTER ISOPROTERENOL INFUSION 141
4.2.3. INTERSTITIAL COLLAGEN DEPOSITION INCREASES PROPORTIONALLY TO THE DURATION OF ISOPROTERENOL INFUSION 143
4.2.4. TIME-DEPENDENT RELEATIONSHIP BETWEEN EXPRESSION OF IONS CHANNELS TRPV4 AND TRPC6 AND ONSET OF FIBROSIS 144
4.3. ADVERSE CARDIAC REMODELLING IN THE ABSENCE OF TRPV4 146
4.3.1. DELETION OF TRPV4 PRESERVES CARDIAC STRUCTURE AND FUNCTION AFTER ISOPROTERENOL INFUSION 148
4.3.2. DELETION OF TRPV4 REDUCES ISOPROTERENOL-INDUCED CARDIAC CELL HYPERTROPHY 150

4.3.3. DELETION OF TRPV4 ATTENUATES THE FIBROTIC RESPONSE INDUCED BY ISOPROTERENOL 151

4.3.4. DELETION OF TRPV4 PREVENTS ARRHYTHMIA INDUCIBILITY ASSOCIATED WITH PATHOLOGICAL REMDODELLING 153

4.3.4.1. Ventricular arrhythmias under normoxia 153

4.3.4.2. Ventricular arrhythmias during regional ischemia 153

4.3.5. TRPV4 OVEREXPRESSION IN PATHOLOGICAL REMODELLING INDUCES ENHANCED CA^{2+} INFLUX, IN CARDIAC FIBROBLASTS 155

4.3.6. TRPV4 ACTIVATION IN PATHOLOGICAL REMODELLING MEDIATES FIBROSIS THROUGH THE CALCINEURIN/NFAT PATHWAY 158

4.3.7. POTENTIAL RELATIONSHIP BETWEEN TRPV4 AND TRPC6 CHANNELS IN PATHOLOGICAL REMODELLING 162

4.4. ROLE OF AGEING AND TRPV4 IN REVERSE REMODELLING AND RECOVERY OF VENTRICULAR FUNCTION AFTER ISOPROTERENOL-INDUCED CARDIOMIOPATHY 166

4.4.1. ISOPROTERENOL INFUSION INDUCED HF AT ALL AGES WITH SUBTLE PARTICULARITIES IN AGED FEMALE MICE 166

4.4.2. REVERSE REMODELLING IS DISTINCTLY DIFFERENT IN YOUNG AND AGED FEMALE MICE 170

4.4.3. TRPV4 EXPRESSION IN YOUNG AND AGED MICE WITH ADVERSE REMODELLING AND RECOVERY 173

5. DISCUSSION 176

5.1. EXPERIMENTAL MODELS OF VENTRICULAR REMODELLING 179

5.2. DIFFERENTIAL EXPRESSION OF MECHANORECEPTORS IN ADAPTIVE AND ADVERSE CARDIAC REMODELLING 181

5.3. TIME-COURSE RELATIONSHIP BETWEEN TRPV4 AND TRPC6 AND THE DEVELOPMENT OF ADVERSE CARDIAC REMODELLING 183

5.4. TRPV4 DELETION IMPROVES CARDIAC OUTCOME FOLLOWING ISOPROTERENOL INFUSION 187

5.5. TRPV4 DELETION DIMINISHES ARRYHTHMOGENESIS AFTER CHRONIC ISOPROTERENOL ADMINISTRATION 189

5.6. TRPV4 MEDIATES FIBROSIS THROUGH THE CALCINEURIN/NFAT PATHWAY 190

5.7. TRPV4 AS A REGULATOR OF TRPC6 EXPRESSION 193

5.8. HF INDUCTION AND RECOVERY IN AGED FEMALE MICE 195
5.9. TRPV4 IN THE AGED HEART.....197
5.10. LIMITATIONS AND FUTURE DIRECTIONS.....199
6. CONCLUSIONS.....204
7. REFERENCES.....210

1. INTRODUCTION

1.1. ANATOMY AND PHYSIOLOGY OF THE HEART

The heart is a thick, muscular, contracting organ, whose primary function is to rhythmically pump blood through the circulatory system to maintain the body's homeostasis. Blood provides oxygen and all necessary nutrients for the body and assists in the removal of metabolic wastes.

1.1.1. ANATOMY OF THE HEART

1.1.1.1. Macroscopic anatomy

In humans, the heart is located between the lungs, in the mediastinum, and it is separated from other structures by the pericardium [1]. The heart is a double pump composed of four chambers (two atria and two ventricles) and four valves, which open unidirectionally by differences in pressure to ensure that blood flows in the appropriate direction (Figure 1). The atria and ventricles are divided by the atrioventricular plane (AV-plane), a fibrous structure where atrioventricular valves are inserted. The mitral valve lies between the left atrium (LA) and the left ventricle (LV), whereas the tricuspid valve sits between the right atrium (RA) and the right ventricle (RV) [2]. The semilunar valves (aortic and pulmonary) are located at the outflow tracts of the LV and RV, respectively (Figure 1).

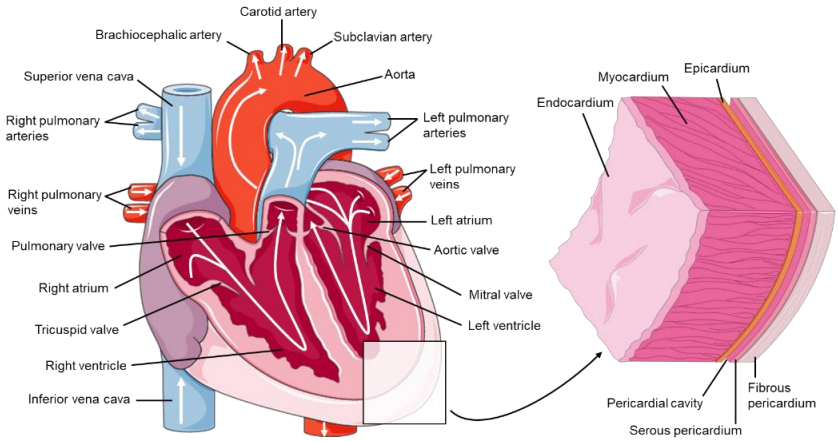

Figure 1. Cardiac anatomy of the heart. Blood flow is indicated with arrows (see explanation in the text). This figure is unique, but some of the elements were downloaded from Smart Servier Medical Art. This applies to all figures in this thesis.

Right cavities receive blood coming from the pulmonary system, which is at low pressure, so their wall is characteristically thin [3]. On the other hand, the LV is a high-pressure cavity, needing to overcome the aortic pressure to eject blood into the systemic circulation, so its walls are the thickest [3]. Cardiac wall in all chambers can be decomposed in three layers, from the inside to the outside: the endocardium, the myocardium, and the epicardium (Figure 1). The endocardium, the thinnest layer, lines the inner heart chambers and heart valves. Composed of endothelial cells, it provides a smooth, elastic, non-adherent surface for blood collection and pumping. The myocardium, the thickest layer, sits in the mid heart wall, and is composed of cardiac muscle fibres, which enable heart contraction. The outer layer, known as the epicardium, is a thin layer composed mainly of elastic fibres and adipose tissue, which protects the inner heart layers. Also found in the epicardium are the coronary blood vessels, which supply the heart wall with blood [4].

1.1.1.2. Microscopic anatomy

The heart is composed of several cell populations that collaborate to maintain its function: cardiac myocytes (CM) and non-myocytes, among which fibroblasts (FB) are the major component. The non-myocyte fraction also includes endothelial cells, pericytes and vascular smooth muscle cells [5]. Other transient cell types, such as macrophages, lymphocytes, mast cells can also be present under certain circumstances, as well as cells derived from the bone marrow (hematopoietic stem cells and mesenchymal stem cells), which are in charge of cell turnover and repair [6].

CM represent the largest volume of the myocardium, but constitute approximately 30% of the cells in the human heart, 50% in the mouse heart and 30% in the rat heart [7]. Containing an exquisitely organized cytoskeleton and contractile elements called sarcomeres, CM generate the rhythmic contractile forces used for heart contraction. Unlike other cardiac cell types, CM become terminally differentiated shortly after birth and lose their ability to proliferate almost completely, although a low level of turnover can occur throughout life [8]. CM can be activated in response to an electrical stimulus through a thoroughly regulated system of transmembrane ion channels that generate the cardiac action potential. Around 1% of CM are constitutively modified, with rudimentary contractile filaments but specific ion chamber dynamics that allow them to spontaneously generate an electrical impulse. These are known as pacemaker cells.

FB make up the largest cell population of the heart, although this appears to vary across different species, especially in mice [9]. Banerjee and collaborators demonstrated that the adult murine heart consists of approximately of 50% myocytes and 50% non-myocytes, being FB the 30% of them [7]. FB are essential for several physiological functions, as they respond to a variety of mechanical, electrical, and chemical stimuli that are key to maintain proper cardiac function

[10]. Additionally, FB contribute to maintain the structural integrity of the heart by regulating the extracellular matrix (ECM).

The ECM is a three-dimensional network where permanent resident cardiac cells lie. It helps to maintain the electrical, chemical, and biochemical responsiveness of the heart, and provides cardiac tissue stability required for normal function. The ECM is a complex meshwork of fibrillar collagens, fibronectin, laminin, fibrillin, elastin, proteoglycans, and glycoproteins in which cardiac cells are embedded [11]. Besides providing structural support, ECM also acts as a signal transducer for cell-cell communication by modulating cell motility, survival, and cell proliferation. The ECM also regulates other molecules in the interstitial space, and importantly, distributes mechanical forces throughout the organ [6].

Overall, the different cell types present in the heart are not isolated from one another but instead interact in a dynamic and coordinated manner and with the components of the ECM. This crosstalk is essential to maintain cellular and tissue homeostasis and to respond to a variety of physiological and pathological stimuli.

1.1.2. CARDIAC PHYSIOLOGY

The primary goal of the heart is to provide an adequate blood supply to all tissues and organs in the body, which is achieved by repetitive mechanical pumping [12]. Both the mechanical and the electrical functions need to work harmonized to ensure an adequate blood supply in all different conditions that an individual may face throughout life.

1.1.2.1. Muscular contraction

Physiological blood flow is achieved by proper functioning of the four heart chambers and the four cardiac valves. Blood low in oxygen flows into the RA from the superior and inferior vena cava. At the RA, blood flow is directed towards the RV through the tricuspid valve [3,13]. Upon RV contraction, tricuspid valve closes, and pulmonary valve opens, allowing blood flow into the pulmonary artery.

Through the pulmonary veins, oxygenated blood returns to the LA, which conducts the blood through the mitral valve into the LV. The LV then initiates contraction, ejecting oxygenated blood towards the systemic circulation via the aorta and its branches [13]. Physiological course of blood flow in the heart is represented in Figure 1.

At the cellular level, contraction takes place in the sarcomeres, the contractile units of CM. Each sarcomere consists of an organized and partially overlapped set of thin (actin and associated proteins) and thick filaments (myosin). The sliding of myosin on the actin filaments shortens the sarcomeres leading to muscle contraction [14].

1.1.2.2. Electrical system

Cell contraction in the heart occurs in response to the electrical activation of CM. Myocardial electrical activity is attributed to the generation of action potentials. An action potential is a sequence of changes in the voltage of the cell membrane that starts with cell depolarization and finishes when transmembrane voltage returns to the resting potential (cell repolarization). Pacemaker and contractile cells have distinct action potentials [15] (Figure 2), which allow the former to generate the electrical impulse and the latter to passively propagate it.

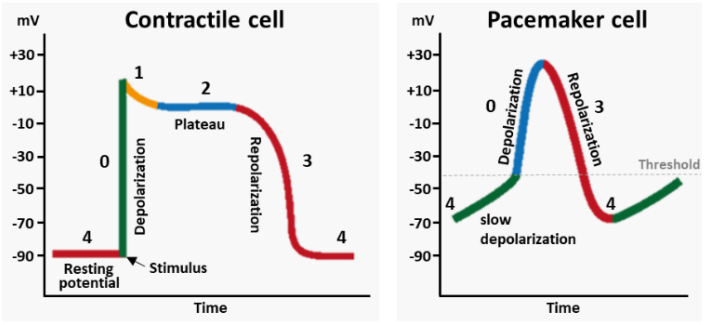

Figure 2. The action potential in contractile and pacemaker CM. Adapted from [15]. Briefly, in contractile cells, depolarization in phase 0 is due to sodium (Na^+) entrance into the cell, whereas repolarization is driven by outward potassium (K^+) currents in phase 3 after a plateau phase (phase 2) where they are balanced against calcium (Ca^{2+}) inward currents. In pacemaker cells, depolarization (phase 0) is mainly carried by Ca^{2+} currents, whereas K+ currents facilitate repolarization (phase 3).

Under normal conditions, the electrical activity is initiated by spontaneous and rhythmic depolarizations of the pacemaker cells conforming the sinoatrial node (SA node), located in the RA [16]. The electrical impulse spreads then throughout the atrial chambers but is also preferentially propagated throughout the conduction system formed by the atrioventricular node (AV node) and the right and left branches of the bundle of His, ending at the Purkinje fibres. The Purkinje fibres contain numerous small branches that ensure that the cardiac impulse is rapidly conducted throughout the ventricular walls to cause ventricular contraction [17] (Figure 3). This sequence of electrical activation ensures a coordinated contraction of all cardiac chambers.

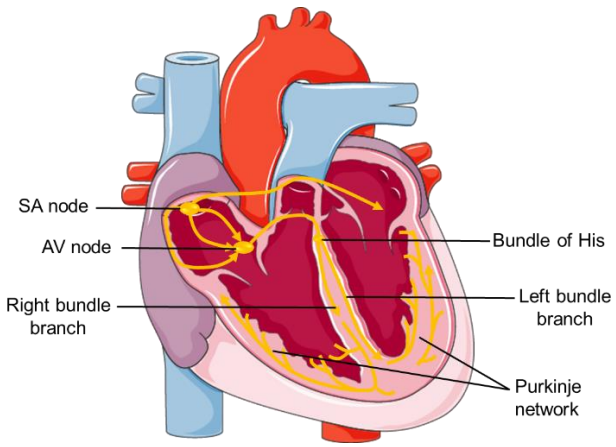

Figure 3. Cardiac conduction system. Electrical impulse begins in the SA node and is conducted to both atria and to the AV node, from where reaches the ventricular myocardium via the His-Purkinje network.

1.1.2.3. Excitation and contraction coupling

Excitation-contraction coupling refers to the process by which an electrical stimulus (excitation) arriving at the CM is transduced into a mechanical signal (cell contraction). Calcium (Ca^{2+}) plays a pivotal role in electro-mechanical coupling, orchestrating heart contraction and relaxation. In phase 2 of the action potential in contractile CM, Ca^{2+} entrance through L-type Ca^{2+} channels, located within the

t-tubules, triggers further Ca^{2+} release from the sarcoplasmic reticulum (SR) by activating the ryanodine receptors (RyR) in a process known as calcium-induced calcium release (CICR) [18,19]. This allows binding of Ca^{2+} to the myofilament protein troponin C, which induces the sliding between myosin and actin, resulting in CM contraction or cardiac systole [20]. After contraction, intracellular Ca^{2+} is transported out of the cytosol either to the extracellular space by the Na^+/Ca^{2+} exchanger (NCX) and the plasma membrane calcium ATPase (PMCA), back into the SR by the sarcoplasmic reticulum Ca^{2+}-ATPase (SERCA2a), or into the mitochondria via the mitochondrial Ca^{2+} uniporter [18,21]. Intracellular Ca^{2+} concentration therefore declines, allowing Ca^{2+} to dissociate from troponin and leading to CM relaxation and cardiac diastole (Figure 4).

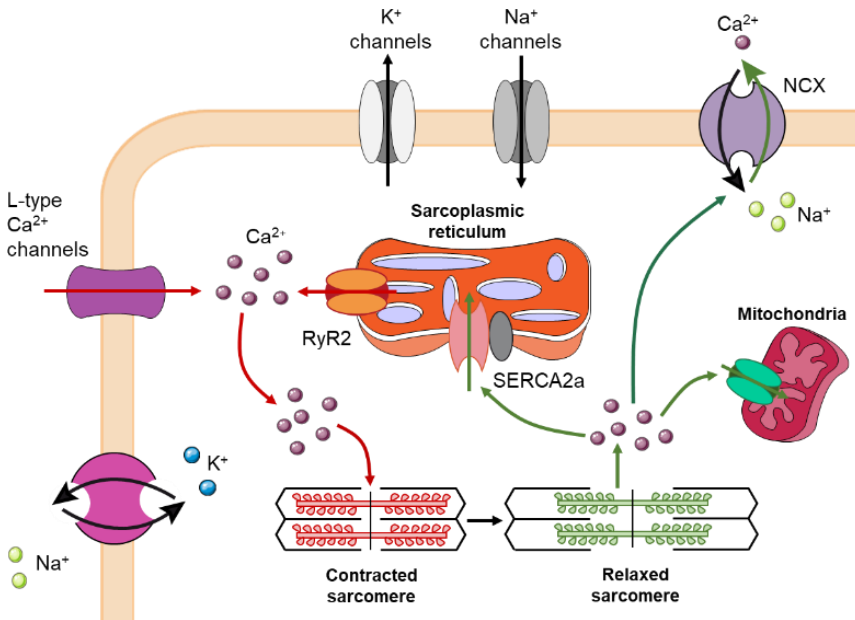

Figure 4. Ca^{2+} signalling in excitation-contraction coupling. Ca^{2+} entrance through the L-type Ca^{2+} channels triggers Ca^{2+} release from the SR through the RyRs. Cytoplasmic Ca^{2+} activates the myofilaments of the sarcomere and leads to contraction. Ca^{2+} is subsequently removed from the cytosol and taken back into the SR by SERCA2a, transported outside the cell by NCX, or taken up by mitochondria.

1.2. CARDIAC PLASTICITY AND ADAPTIVE REMODELLING

To deliver the appropriate blood supply to the tissues over a lifetime, the heart must be extremely adjustable and sustainable. The heart can cope with changing environmental demands and can respond to a variety of stimuli [22]. Control of circulating blood volume is a tightly regulated physiological process, and it is critical for maintaining cardiovascular homeostasis.

1.2.1. REGULATION OF CARDIAC HEMODYNAMICS

Cardiac output is the volume of blood that is pumped out of the heart per unit time and is calculated as the product of the heart rate and the stroke volume (i.e., the volume of blood pumped per beat). Cardiac output is regulated by several neurohumoral mechanisms aimed at improving cardiac efficiency. These include the sympathetic nervous system (SNS) and the renin-angiotensin-aldosterone system (RAAS) [23].

The activation of the SNS leads to an increase both in heart rate and cardiac contractility, increasing cardiac output. Cardiac relaxation is also accelerated to adapt to increased heart rates. The SNS is activated in response to a fall in cardiac output, which is sensed by the baroreceptors, mainly located in the aortic arch

and carotid sinus. The activation of the SNS generates the release of catecholamines (epinephrine and norepinephrine), which bind to the α-adrenergic receptors located in the peripheral vessels, causing vasoconstriction, and to the β-adrenergic receptors (β-Ars) located in the heart, particularly β1-AR. B1-Ars are G-coupled receptors that activate G(s)-protein signalling, converting ATP into the second messenger cAMP through the effector enzyme adenyl cyclase, and inducing secondary activation of protein kinase A (PKA). PKA is a kinase with several targets, including: 1) the L-type Ca^{2+} channels and the RyR2 receptors, in both cases promoting further Ca^{2+} entry into the cytosol to facilitate a stronger cardiac contraction [24,25]; 2) phospholamban (PLN), a modulator of SERCA, which accelerates Ca^{2+} reuptake by the SR, therefore accelerating cardiac relaxation [26]; 3) troponin I and myosin binding protein C, reducing myofilament sensitivity to Ca^{2+} and accelerating relaxation of the myofilaments [27] (Figure 5).

The RAAS system can also be activated by a decrease in cardiac output. The baroreceptors located in the wall of the renal afferent arteriole respond to reduced perfusion pressure by releasing renin [28]. Renin converts angiotensinogen produced at the liver to angiotensin (AT) I, which is subsequently cleaved by the angiotensin-converting enzyme (ACE) generating AT-II [29]. Circulating AT-II is the primary mediator of systemic vasoconstriction in response to volume depletion. In CM, AT-II activates AT-II type I receptors (AT1R), which are G(q)-protein coupled. Activation of AT1 receptors stimulates phospholipase C (PLC) activity via cGMP activation [30]. PLC liberates inositol 1,4,5-trisphosphate (IP_3) from the membrane phosphatidylinositol 4,5-biphosphate (PIP_2). IP_3 diffuses within the cytoplasm and binds the IP_3 receptors (IP_3R) in the SR, which also release of Ca^{2+} from the stores [31], which results in an increase in contractility and force of contraction (Figure 5).

Although the activation of these mechanisms provides an acute hemodynamic compensation to a reduced cardiac output, their sustained activation, together

with the trigger of other signalling pathways discussed below, may induce structural and functional changes in the heart that are globally known as cardiac remodelling.

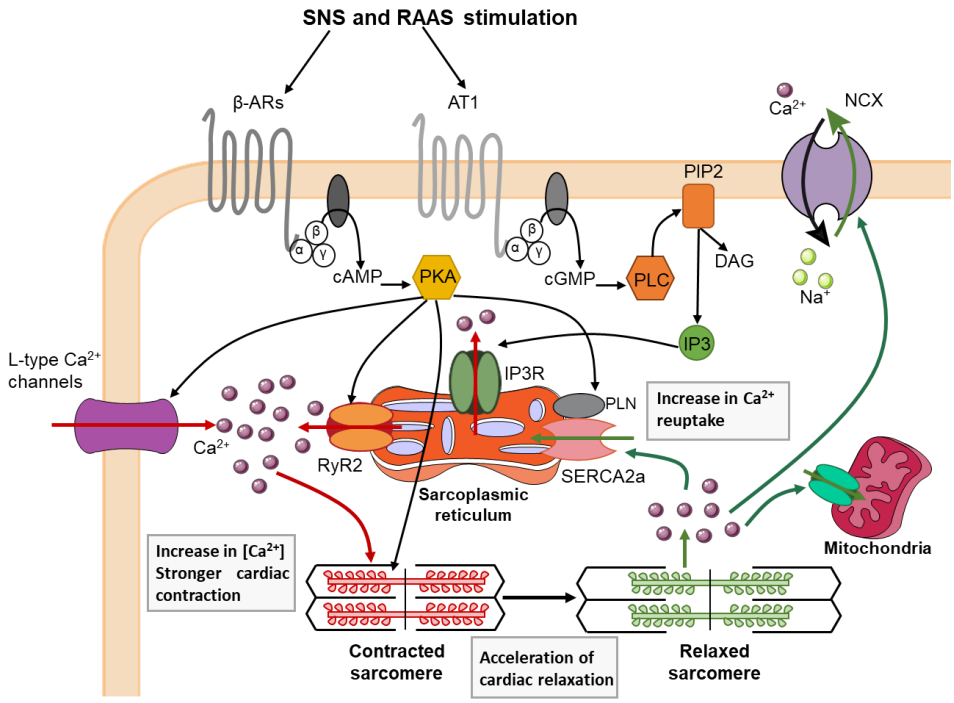

Figure 5. Overview of the molecular mechanisms that are activated in CM upon SNS and RAAS stimulation.

1.2.2. CARDIAC REMODELLING

Cardiac remodelling involves a series of molecular, cellular and interstitial changes that develop in the heart in response to a condition of chronic overload and is primarily driven by the sustained activation of the compensatory mechanisms previously mentioned. At the clinical level, cardiac remodelling translates into changes in chamber size and cardiac function, which try to provide an adequate adaptation to the new hemodynamic load and ensure cardiac efficiency [32]. It develops as an adaptative response, although may turn less favourable over time. Classically, two forms of cardiac remodelling have been

distinguished: physiological or adaptive remodelling, and pathological or adverse remodelling. Adaptive remodelling occurs in healthy individuals following moderate exercise or pregnancy, for example. Characteristically, this remodelling is permanently balanced, not associated with cardiac damage and reversible once the primary stimulus or the overload condition disappears [33]. In contrast, adverse remodelling usually develops in conditions with chronic pressure (hypertension, aortic stenosis) or volume (heart valve disease, dilated cardiomyopathy) overload. In this case, remodelling starts with an adaptive phase that seeks to reduce wall stress and preserve cardiac output, but exhibits over time signs of cellular dysfunction, triggering the transition to heart failure (HF) [34].

Several studies have suggested that it is the intensity and the nature of the stimulus rather than its duration that determines the type of response. Perrino and collaborators demonstrated that exercise training by discontinuous sessions of swimming led to a more benign remodelling compared to chronic aortic constriction, and animals subjected to an interrupted aortic constriction during an equivalent time to the exercise training sessions developed an intermediate remodelling showing adaptive but also maladaptive features [35]. Other authors support that the transition to a maladaptive remodelling is driven by β-adrenergic receptor desensitization [36]. Finally, Ca^{2+} cynetics could also have a role. Unlike abrupt and rapid cytosolic Ca^{2+} accumulation through L-type Ca^{2+} channels and Ca^{2+} release from the SR for effective contraction in the physiological remodeling, it has been suggested that a low and sustained Ca^{2+} entrance through channels other than voltage-dependent Ca^{2+} channels, particularly through receptor-operated Ca^{2+} channels (ROC), could participate in pathological remodelling. ROC channels would be opened by activation of Gq-coupled receptors like AT1R, upon binding of AT-II, endothelin or norepinephrine [37].

Moreover, recent studies indicate that different molecular mechanisms underlie both types of cardiac remodelling, which ultimately exhibit markedly different

prognosis. The following lines review our current knowledge on physiological or adaptive remodelling. Because most of the work of this thesis has been addressed to the study of pathological remodelling and HF, a whole chapter will be later dedicated to review the particularities and the mechanisms involved in this form of non-adaptive, adverse remodelling.

1.2.3. PHYSIOLOGICAL OR ADAPTIVE CARDIAC REMODELLING.

Cardiac remodelling is defined as physiological or adaptive when it displays changes in heart dimensions (usually enlargement) in the presence of a normal or even enhanced heart function.

At the molecular level, a sustained increase in blood demand, such as that occurring during exercise [38] or pregnancy [39], leads to an increase in the muscle mass as a consequence of the growth in both length and width of the individual CM [40]. This process is known as cardiac hypertrophy and is considered the primary contributor to cardiac enlargement, since CM do not proliferate. Nevertheless, recent studies have shown that chronic exercise may lead to CM proliferation and renewal in a small percentage of cells [41], further reinforcing its beneficial effects.

Adaptive cardiac remodelling is characterized by mild heart growth. Typically, athletes show a 10-20% increase in LV wall thickness and a 10-15% increase in both right and LV cavity size [42]. Similarly, pregnancy leads to a 10-20% increase in total heart mass [43]. In both scenarios, cardiac function is preserved. Several studies have shown similar echocardiographic parameters of systolic function in professional athletes and sedentary control individuals [44], with normal or enhanced cardiac filling in diastole and increased stroke volumes in the former [42].

As mentioned, remodelling induced by pregnancy or exercise is fully reversible once the condition is terminated. LV hypertrophy developed during pregnancy normalizes 8 weeks after birth [45], and echocardiographic studies showed that wall thickness and left ventricular mass reverted to normal within a few weeks of

deconditioning in Olympic-trained athletes [46]. One of the important molecular features that could explain the complete reversibility of this type of remodelling is the absence of induction of the molecular foetal gene programme, classically associated with the adverse remodelling. Moreover, the adaptive heart response is not associated with fibrosis, which is one of the main features of the pathologic response (see below). As such, it has been shown that levels of collagen I and α-smooth muscle actin (α-SMA), which confer stiffness to the heart, remain unchanged in LV of rats subjected to endurance training [47].

Given the topic of this thesis, the following chapter summarizes the signalling pathways related to the development of cardiac remodelling exclusively induced by endurance training.

1.2.3.1. Signalling pathways involved in adaptive cardiac remodelling induced by exercise training

The biochemical signals underlying the adaptive cardiac remodelling triggered by exercise are well characterized (Figure 4). The first cardiac response to endurance training is an acute increase in the heart rate and contractility to meet the new metabolic demands of the body, which is primarily mediated by the activation of the SNS. Regular exercise leads to sustained activation of the SNS and a shift in the RAAS system towards the ACE2, with downregulation of the systemic and tissue ACE/AT-II/AT1R axis [48]. Other signalling pathways are activated and play a crucial role in the adaptive response. Among them, insulin and insulin-like growth factor 1 (IGF1), and their downstream phosphoinositide 3-kinase (PI3K)/protein kinase B (PKB or Akt) signalling pathway, have drawn special attention. Insulin is a hormone secreted by pancreatic β-cells, and IGF1, with a structure similar to insulin, is synthetized mostly in the liver. In the heart, IGF1 is predominantly produced and secreted by FB [49]. It has been described that cardiac remodelling in athletes is associated with an exercise-induced increase in IGF1 levels [50]. Insulin and IGF1 bind respectively to the tyrosine kinases insulin receptor (IR) and IGF1

receptor (IGF1R). The activation of these receptors, and their downstream signalling pathways, is sufficient to induce physiological remodelling, as cardiac deletion of the IR adaptor proteins 1 and 2 in mice caused resistance to exercise-induced remodelling [51]. Moreover, mice with genetic deletion of IGF1 were resistant to the adaptive remodelling induced by exercise training [52]. Conversely, hearts of mice overexpressing IGF1R displayed hypertrophy with an increase in CM volume and an increase in systolic function, consistent with an adaptive remodelling, even in the absence of exercise [53]. These hearts also showed increased PI3K and Akt phosphorylation [53]. On the other hand, mice lacking the regulatory subunit of PI3K showed attenuation to exercise-induced remodelling [54].

PI3K enzyme is a heterodimeric protein highly expressed in the heart that is critical for its physiological growth. Transgenic mice expressing a constitutively active dominant negative form of PI3K showed significant hypertrophy in response to pressure overload, but a blunted hypertrophic response to swim training, when compared with non-transgenic mice [55]. Akt is a serine/threonine kinase downstream of PI3K enzyme, which has also been involved in physiological remodelling. In a study using an Akt-knock-out (KO) mouse model, exercise-induced cardiac remodelling was found attenuated, while responses to a pressure overload where preserved when compared to wild-type (WT) mice [56]. These studies suggest that PI3K and Akt mediate specifically cardiac physiological remodelling and do not seem to participate in the pathological response.

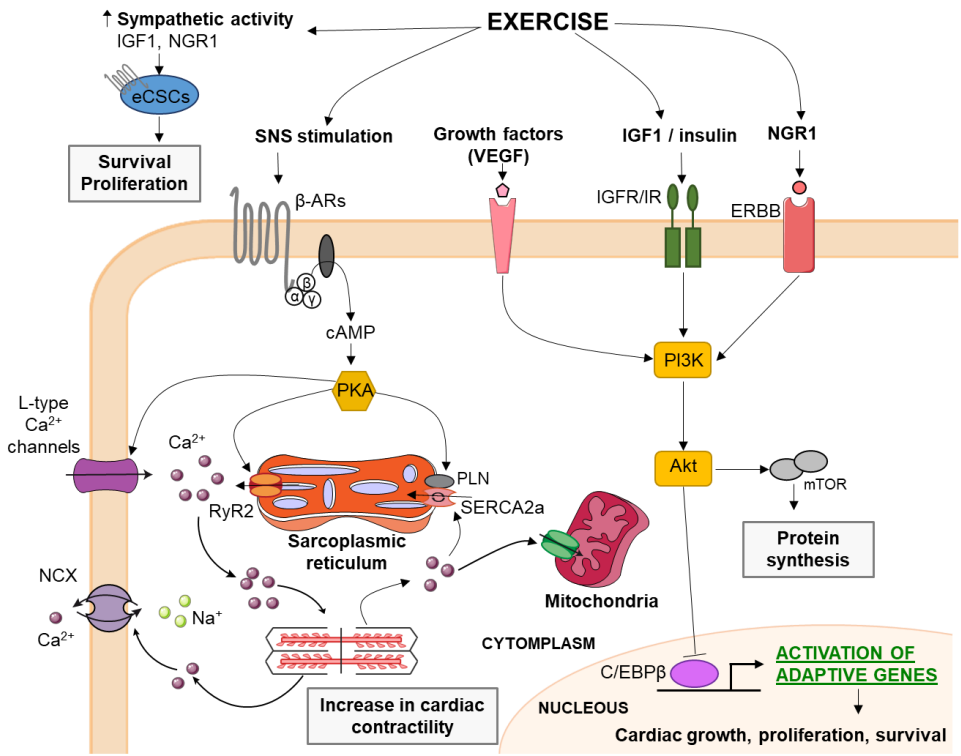

Figure 6. Overview of the signalling pathways involved in the adaptive remodelling induced by exercise.

Among the downstream effectors of PI3K and Akt, the mammalian target of rapamycin (mTOR) and the CCAAT/enhancer binding protein-β (C/EBPβ) are particularly important. Activation of mTOR, a serine/threonine kinase complex, is directly implicated in protein synthesis through promoting ribosomal protein production. On the other hand, C/EBPβ is a transcription factor that controls cellular growth and proliferation by promoting changes in gene expression [57]. Notably, C/EBPβ was found to be specifically downregulated by exercise training [58]. Mechanistically, downregulation of C/EBPβ by Akt allows the expression of beneficial or protective genes that enhance cardiac growth and promotes CM proliferation and survival.

Several studies have shown that other cellular signalling mechanisms can also activate and modulate the PI3K/Akt pathway during the adaptive cardiac remodelling. Epidermal growth factor neuregulin-1 (NRG1), for example, can induce activation of the tyrosine kinase receptors ERBB, which results in the activation of the PI3K/Akt signalling [59,60]. In line with this finding, it has been shown that exercise training increases the expression of cardiac NRG1 and ERBB/PI3K/Akt signalling [61].

Interestingly, some recent observations have shown that the heart seems to have the capacity to produce new CM from endogenous cardiac stem cells (eCSCs) when exposed to exercise [8]. Activated β-ARs, IGF1 and NRG1 have been described as inducers of eCSCs proliferation [62]. On the other hand, an increased proliferation, number and differentiation of eCSCs has been described following physiological overload, either in the form of swimming or treadmill endurance exercise [63].

Finally, angiogenesis, understood as an increase in vessel size and number, is required for maintaining an adequate nutrient and oxygen supply during exercise training. Angiogenesis is triggered by the vascular endothelial growth factor (VEGF), which is secreted in response to exercise, and stimulates endothelial and vascular smooth muscle cell proliferation. VEGF can also activate the PI3K/Akt pathway in CM, in a synergistic hypertrophic response [64].

In summary, current knowledge indicates that the adaptive remodelling is triggered by a small number of intracellular pathways that all converge on the nodal mediators PI3K and Akt, which regulate the transcription of genes leading to a balanced cardiac growth.

1.3. PATHOLOGICAL OR ADVERSE CARDIAC REMODELLING AND HEART FAILURE

1.3.1. PATHOLOGICAL OR ADVERSE CARDIAC REMODELLING

Pathological or adverse cardiac remodelling is described as a maladaptive response to cardiac overload characterized by complex structural and functional changes that lead to LV dilatation, cardiac dysfunction, and consequently, to an adverse clinical outcome [65]. This type of remodelling may occur in response to several acquired conditions, such as hypertension, valvular disease, or myocardial infarction, as well as to certain genetic disorders. Pathological remodelling sets the basis for HF promotion and progression.

Adverse cardiac remodelling is preceded by an initial phase where structural and functional changes are invoked to reduce ventricular wall stress and temporally preserve cardiac pump function. This initial phase is characterized by a concentric hypertrophy of the cardiac chambers exposed to the overload, most commonly the LV, where CM grow in both length and width. At this stage cardiac remodelling is reversible if the primary stimulus or the overload condition disappears. However, if the stress or disease persists, this response

may evolve into a devastating spiral of maladaptive changes [66] that lead to a progressive dysfunction of the heart, and ultimately contribute to the promotion and progression of HF [67]. Characteristic features of the pathological remodelling include pathological hypertrophy, ventricular dilatation, impaired cardiac function, tissue fibrosis and insufficient angiogenesis.

From a cellular point of view, several major mechanisms have been reported to underlie pathological remodelling, affecting both CM and FB.

1.3.1.1. Major findings of pathological remodelling

1.3.1.1.1. Pathological hypertrophy

The transition to pathological remodelling entails changes at the molecular level. CM suffer gene reprogramming with expression of foetal genes and alterations in the expression and function of proteins involved in the excitation-contraction coupling [68]. Both mechanisms contribute to contractile dysfunction in the long term. Foetal genes, including the natriuretic peptides, ANP and BNP, which are normally expressed only during cardiac development, are reinduced during adverse remodelling, Also, relative amounts of the cardiac myosin heavy chain (MHC) isoforms α-MHC and β-MHC change during development, and also during transition to pathological remodelling. Some studies have reported that both isoforms are downregulated in human foetal and failing hearts compared to the adult non-failing hearts. However, the ratio β-MHC/α-MHC increases due to a relative larger repression of α-MHC [69,70]. This shift towards β-MHC, which has a lower ATPase activity, and in consequence, produces a slower contraction, contributes to reduce the myocardial performance [71]. Impaired intracellular Ca^{2+} homeostasis has also been involved in the contractile dysfunction accompanying the pathological remodelling. CM from the failing hearts show alterations in the Ca^{2+} handling proteins, which lead to decreased Ca^{2+} transients, enhanced diastolic Ca^{2+} leak, and diminished SR Ca^{2+} sequestration, impairing contractility and relaxation [72,73].

1.3.1.1.2. Fibrosis.

The transition to maladaptive remodelling includes the proliferation and differentiation of FB into myofibroblast (MFB), which secrete elevated levels of ECM proteins, leading to progressive cardiac fibrosis [74]. MFB are cells with a proliferating, migratory and contractile phenotype that express markers of smooth muscle cells, majorly contractile proteins such as the alpha-smooth muscle actin (α-SMA). Multiple experimental studies have reported that the accumulation of MFB in the interstitial space increases after injury or after a sustained overload, like in myocardial infarction or pressure and volume overload experimental models [75]. The main source of MFB are resident cardiac FB. However, MFB can also differentiate from resident endothelial and epithelial cells via endothelial to mesenchymal transition or epithelial to mesenchymal transition, respectively [76,77].

The transition from FB to MFB is a multifactorial process mediated by several factors, such as cytokines, hormones, ligands (like the transforming growth factor β (TGF-β), AT-II or endothelin1 (ET-1)), and environmental mechanical forces [78]. TGF-β is one of the most powerful direct mediators of FB differentiation and MFB activation [79,80]. Importantly, once activated, MFB can also secrete TGF-β, perpetuating a detrimental positive feedback loop that leads to progressive fibrosis [81]. Along with TGF-β, tensile strength and mechanical stress have also been proven important mediators of FB differentiation into MFB [82]. Furthermore, in the setting of adverse remodelling, other cell types (such as CM, vascular cells, macrophages, and lymphocytes) have been shown to promote MFB differentiation by secreting fibrogenic mediators (like the tumour necrosis alpha, TNF-α), growth factors (TGF-β and fibroblast growth factor, FGF), or other determinant molecules such as AT-II or ET-1 [83].

Irrespective of their origin and their source of activation, activated MFB produce and secrete an aberrant concentration of ECM proteins, especially collagen I and III, as well as growth factors, cytokines, and proteases, which deregulate matrix composition and gradually contribute to cardiac fibrosis. This increases heart stiffness and decreases compliance, impairing myocardial contraction and relaxation [83]. MFB can also modulate CM function and structure, either through paracrine effects (secretion of growth factors and cytokines such as TNF-α, TGF-β, IL-1β or IL-6), or directly through cell-cell interactions via connexins and cadherins [84,85], interfering with the normal CM function and contributing to cardiac dysfunction.

1.3.1.1.3. Arrhythmias

Alongside with increased cardiac stiffness, fibrosis characteristically found in pathological remodelling favours arrhythmia promotion. By disrupting ECM, fibrosis produces a profound impact on electrical activation patterns and timings in the myocardium, creating areas of slow conduction and facilitating reentry. Reentry is a self-perpetuating mechanism by which an electrical wave front propagates repetitively once and again throughout a closed rotational circuit long enough to allow the cardiac tissue to be excitable by the time the wavefront reaches it. Two conditions are essential for reentry to occur: a) unidirectional block of conduction (i.e., successful conduction in only one direction), and b) the circuit cycle has to be longer than any of the refractory periods throughout the circuit, condition that is facilitated by a decreased conduction velocity [86]. Fibrosis favours anatomical block caused by tissue discontinuation and promotes a slower conduction through the viable cells within the fibrotic tissue, representing the optimal substrate for reentry to occur and arrhythmias to develop (Figure 7).

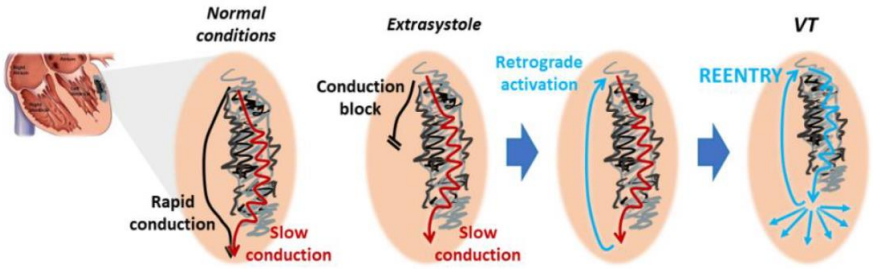

Figure 7. Reentry as one of the most important arrhythmia mechanisms. The electrical impulse faces conduction block in some areas and slow conduction in others, leading to an alternative self-perpetuating circuit.

In the setting of an adverse remodelling, arrhythmias arising from the ventricles, known as ventricular tachyarrhythmias (VTA), have a notorious impact. Among VTA, sustained ventricular tachycardia (SVT) and ventricular fibrillation (VF) pose the greatest threat to patients with HF, because they are directly related to sudden cardiac death, and indirectly related to HF decompensation [87].

1.3.1.2. Signalling pathways involved in adverse cardiac remodelling

The molecular mechanisms responsible for the transition from adaptive to adverse cardiac remodelling are still under intense investigation. Previous literature indicates that neurohormonal activation, as well as exposure to mechanical stress, may play a pivotal role in this maladaptive process. Other mechanisms, such as inflammation and oxidative stress, are also known to participate in the pathological response. Importantly, the signalling pathways that are activated during adverse remodelling are clearly different from those promoting an adaptive response (Figure 8).

1.3.1.2.1. Dysregulation of Ca^{2+} handling

In CM, impaired Ca^{2+} homeostasis is a prominent feature in the transition from compensatory to adverse remodelling. Accumulating evidence indicates that a defective Ca^{2+} signalling is due to an altered function of proteins involved in the excitation-contraction coupling process. Chronic activation of the SNS may contribute to impaired Ca^{2+} homeostasis. Physiologically, stimulation of β-ARs activate PKA, which induces the phosphorylation of L-type Ca^{2+} and RyR receptors, increasing the Ca^{2+} entry into the cytosol, and PLN, enhancing Ca^{2+} uptake into the SR by relieving SERCA2a from inhibition (see Section 1.2.1, Figure 4). However, chronic stimulation of β-ARs leads to a hyperphosphorylation of RyR receptors, which destabilizes their closed state, and results in a pathological diastolic Ca^{2+} leak from the SR that accumulates in the cytosol and impairs contractility and relaxation [88]. Sustained activation of the RAAS also contributes to impaired Ca^{2+} homeostasis, aggravating Ca^{2+} release from the SR by IP_3 receptors, which are activated in response to AT-II/PLC/IP_3 signalling.

Intracellular Ca^{2+} accumulation plays also a critical role in the FB, participating in the differentiation of quiescent FB to active matrix-producing MFB. Unlike CM, whose electrical properties and Ca^{2+} signalling mechanisms are well described, the role of Ca^{2+} signalling in FB is not fully understood. In FB, intracellular Ca^{2+} signals are generated by entry through Ca^{2+}-permeable channels located in the plasma membrane or release from the intracellular Ca^{2+} stores (endoplasmic reticulum, ER) via activation of IP_3R [89]. Among the Ca^{2+} release pathways, no apparent role for RyRs and voltage-gated Ca^{2+} channels has been demonstrated thus far in FB [90]. Similar to other cell types, intracellular Ca^{2+} levels are finely controlled by Ca^{2+} extrusion pumps, including NCX and PMCA in the plasma membrane, and SERCA in the ER.

As in CM, activation of G-protein-coupled receptors, such as β-ARs and AT-II, in FB can contribute to the accumulation of Ca^{2+} in the cytosol, ultimately leading to FB differentiation and cardiac fibrosis [91,92]. Chronic stimulation of PKA, the downstream effector of β-AR signalling, could also participate in the promotion of the pro-fibrotic responses in FB [93]. However, the specific mechanisms by which this would happen are not known. Sustained activation of AT-II receptors in FB seems to produce similar effects to those reported in CM, with production of IP_3 by PLC, causing an aberrant release of Ca^{2+} from the ER via IP_3R and an increase in the cytosolic Ca^{2+} levels. Moreover, AT-II receptor stimulation in FB can also directly activate Ca^{2+}-permeable channels in the plasma membrane, further contributing to Ca^{2+} rising in the cytosol [89].

One of the immediate consequences of increased Ca^{2+} concentration in the cytosol, both in CM and FB, is the activation of the Ca^{2}-dependent protein calmodulin (CaM), which acts as an intermediate messenger regulating intracellular signals. Once bound to Ca^{2+}, CaM activates various target proteins such as the protein kinase C (PKC), the Ca^{2+}/CaM-dependent protein kinase type II (CaMKII), and the serine/threonine protein phosphatase, calcineurin (Figure 8).

Activation of PKC, among others, leads to PLN dephosphorylation, resulting in a reduced reuptake of Ca^{2+} into the SR/ER by SERCA2a, which further contributes to cytosolic Ca^{2+} accumulation. Consistent with this, both SERCA2a and PLN phosphorylation have been shown to be decreased in experimental HF models and in myocardial samples of HF patients [94–96]. Activation of CaMKII, at least in CM, has been shown to promote RyR2 Ca^{2+} leak from the SR [97], contributing to maladaptive remodelling and also arrhythmogenesis [98]. In FB, CaMKII activation might modulate the MFB transition, since CaMKII inhibition has been shown to significantly reduce the expression of collagen I and III [99,100].

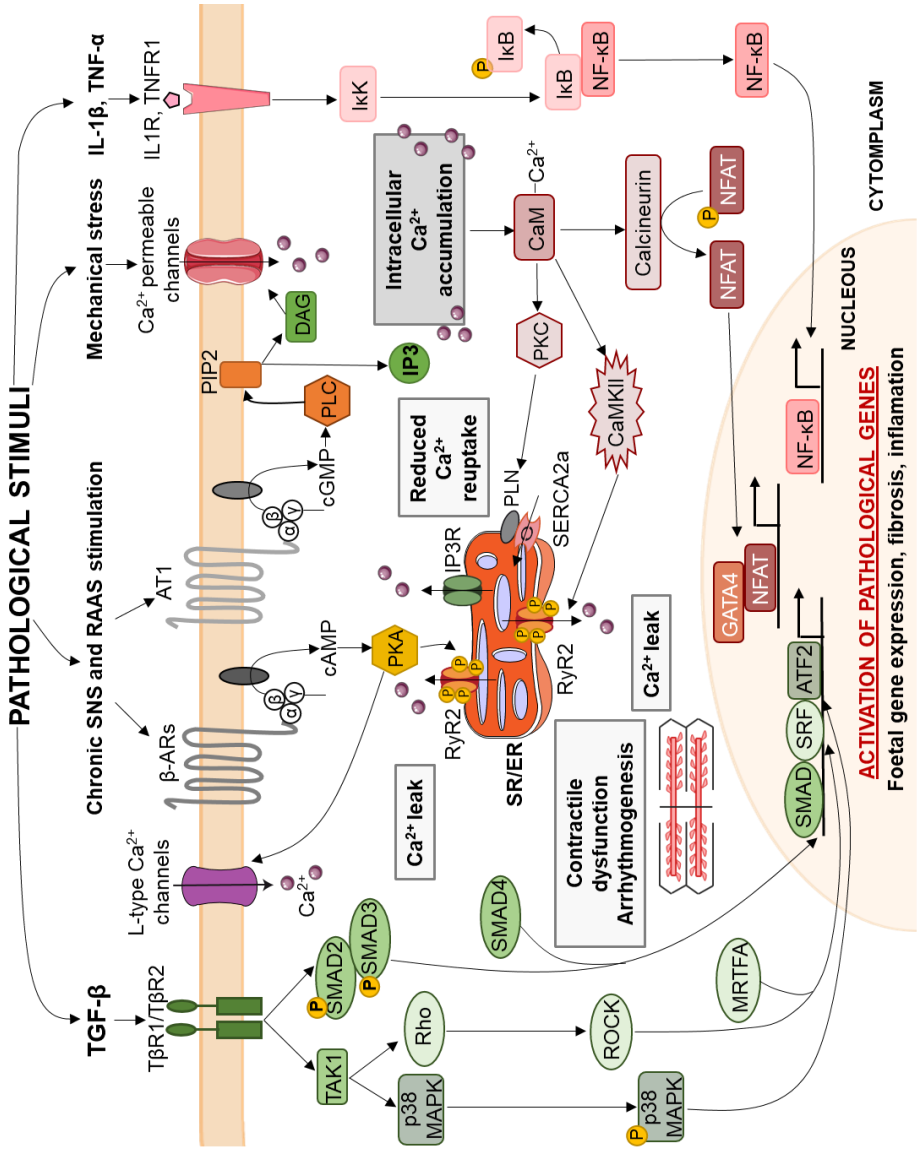

Figure 8. Schematic representation of several signalling pathways involved in the adverse cardiac remodelling in CM and FB.

Ca^{2+}-calmodulin-activated calcineurin binds to its downstream effector, the nuclear factor of activated T cells (NFAT). NFAT transcription factors are normally hyperphosphorylated and sequestered in the cytoplasm, but rapidly translocate into the nucleus after calcineurin-mediated dephosphorylation [101]. NFAT interacts with transcriptional cofactors, such as GATA4, to stimulate hypertrophic and fibrotic gene expression in CM and FB, respectively [101,102]. The Ca^{2+}-calcineurin-NFAT pathway has been found to be both sufficient and necessary for the development of adverse cardiac remodelling [101,103,104]. Transgenic mice that overexpress either active calcineurin or a constitutively nuclear NFAT mutant protein develop cardiac hypertrophy and fibrosis leading to HF [101]. Conversely, mice subjected either to aortic banding o myocardial infarction and treated with an specific calcineurin or NFAT inhibitor presented a significantly attenuated adverse response [103,104].

1.3.1.2.2. TGF-β signalling

Members of the TGF-β family play a major role in a wide range of processes related to cardiac remodelling, especially in FB differentiation and ECM deposition [105]. Secreted by macrophages, infiltrating immune cells, and FB themselves, TGF-β elicits its biological responses through an heteromeric receptor complex comprising two serine-threonine kinase receptors, named TGF-β receptor type 1 and 2 (TβR1 and TβR2). Canonical signalling through TβR1 and TβR2 activates Smad proteins, which are phosphorylated upon receptor activation, and subsequently translocated into the nucleus where they act as transcription factors of fibrosis-related genes [106]. TGF-β receptors can also activate a non-canonical signalling through stimulating the Rho-ROCK and the p38 MAPK signalling pathways. The stimulation of these pathways includes the activation of the TGF-β activated kinase 1 (TAK1), which can contribute to pathological remodelling, and has been reported to induce HF once overexpressed [107]. A study of Small and collaborators also showed that

TGF-β promotes the nuclear translocation of myocardin transcription factor A (MRTFA) through Rho/ROCK signalling. MRTFA is a potent transcriptional activator of the serum response factor (SRF), which induces the expression of a subset of genes consistent with a MFB-like cell type [108]. Similarly, TAK1 can also bind to p38 MAPK leading to its autophosphorylation and translocation into the nucleus, promoting ECM synthesis through the transcription factor ATF2 [109,110].

1.3.1.2.3. Inflammation

Long-term adverse cardiac remodelling is also associated with a chronic infiltration of cytokine-releasing inflammatory cells, which trigger the activation of intracellular pathways that promote a pathological response [111]. Pro-inflammatory cytokine levels, such as TNF-α, IL-1β, IL-4, IL-6, IL-8 or IL-18 have been found increased in patients with HF [111,112]. A key question is whether inflammation plays a role in the establishment of an adverse remodelling, or it appears as a consequence of the remodelling itself and contributes to its progression [113].

Cytokines such as TNFα and IL-1β can activate the canonical NF-κB pathway and contribute to maladaptive remodelling [114]. Accordingly, NF-κB activity is increased in the myocardium of patients with HF [115]. In normal conditions, NF-κB is found inhibited by IκB. IκB phosphorylation by the IκB kinase (IKK) releases NF-κB from IκB, which can translocate into the nucleus regulating the transcription of multiple inflammatory, hypertrophic and fibrotic genes [116117]. Importantly, NFκB can also be activated by the degradation of IκB by calpains, intracellular proteases that are activated by increases in cytosolic Ca^{2+}, thereby linking this pathway with abnormal Ca^{2+} dynamics [118].

1.3.1.2.4. Oxidative stress

Oxidative stress also contributes to the promotion and development of adverse cardiac remodelling. Under physiological conditions, reactive oxygen

species (ROS) act as secondary messengers facilitating signalling pathways that are essential for normal cardiac function. However, upon an imbalance between ROS production and the detoxifying capacity of antioxidant systems, oxidative stress occurs. This has been described in hypertension and HF, among other cardiovascular diseases [119,120]. ROS contribute to the accumulation of oxidized proteins, lipids, and DNA, which can lead to cell death, CM hypertrophy, increased collagen production and deposition by FB, and contractile dysfunction by directly modifying proteins involved in excitation-contraction coupling [121–123].

1.3.2. HEART FAILURE WITH REDUCED EJECTION FRACTION

HF is the common final manifestation of adverse cardiac remodelling, a complex, chronic and progressive clinical syndrome, that represents one of the leading causes of mortality worldwide. The term HF usually refers to the inability of the heart to pump efficiently enough blood to satisfy the metabolic requirements of the body. It is characterized by presenting symptoms such as breathlessness, ankle swelling and fatigue, and is classified in three categories according to the left ventricular ejection fraction (LVEF): HF with preserved ejection fraction (HFpEF, LVEF≥50%), HF with midrange ejection fraction (HFmrEF, 41%≤LVEF≥49%), and HF with reduced ejection fraction (HFrEF, LVEF≤40%) [124,125].

1.3.2.1. Epidemiology of HF and social burden

Chronic HF is a major health problem affecting 1-2% of the adult population and >8-10% of patients aged ≥75 years [126]. It has been estimated that around 26 million people are living with HF worldwide [127]. In the United States, more than 5 million people have HF, with 550 000 new cases and around 1 million hospitalizations per year [128]. In Spain, recent data report a 6% prevalence among patients older than 65 years [129]. HF prevalence increases with age. In a

population-based analysis conducted in Spain with 88 195 HF patients, 68% of them were >75 and 30% were >84 years old [130]. Therefore, it is expected that HF prevelence grows exponentially in the upcoming years, as life-expectancy increases and global population ages.

HF is not only the most frequent cardiovascular disorder, but it is also the one associated with the greatest morbidity and mortality rates. It is the first cause of hospitalization among individuals aged 65 years or older and represents 3% of all hospital admissions [129]. This causes a tremendous burden to the community and health systems, with an estimated cost of $29 billion per year only in the US [128] and gathering up to 7.1% of the total healthcare budget in Spain [131].

The overall prognosis of HF is poor, with mortality rates that, despite advances in management, remain high. A recent meta-analysis including over 1,5 million of all-cause HF patients estimated the 1-, 2-, 5- and 10-year survival rates at 87%, 73%, 57% and 35%, respectively [132]. Most deaths in the HF population are due to cardiovascular causes, mainly HF progression and sudden cardiac death, although up to one third die from non-cardiovascular causes such as malignancies, or underlying comorbidities, which also contribute to a poor quality of life [133]. Among all forms of HF, patients with HFrEF represent a subgroup with particularly high mortality rates and, specifically, high cardiac deaths [134].

1.3.2.2. Pathophysiology and current therapy

The onset of HF relies in a heart exposed to a condition of persistent hemodynamic overload. As reported before, the immediate consequence is usually a fall in blood pressure driven by insufficient cardiac output, which is sensed by carotid, aortic and renal baroceptors to activate the SNS and the RAAS [23]. The consequences of chronic activation of these systems have been extensively discussed in the previous sections of this work and include the

activation of different cascade pathways leading to pathological remodelling, with CM hypertrophy, tissue fibrosis and ultimately cardiac dysfunction.

Multiple therapies are available today for HF treatment, ranging from lifestyle modifications to reduce exposure to risk factors, to pharmacological therapy and the use of implantable devices. All of them contribute in greater or lesser degree to reduce complications and HF progression, but none achieves complete regression of the HF phenotype, and mortality, as mentioned above, remains high.

Current pharmacological strategies for HF treatment reside majorly in the inhibition of the RAAS and SNS systems [135]. Inhibitors of the RAAS such as angiotensin-converting enzyme inhibitors (ACEI) or AT-II receptor blockers (ARBs) have proven effective in reducing hospitalizations and, more importantly, mortality in patients with HFrEF [136,137]. Similarly, numerous studies support the use of betablockers, which reduce all-cause and cardiovascular mortality, sudden cardiac death, and hospitalizations in HFrEF patients [138,139]. In patients under treatment with ACE inhibitors/ARBs and betablockers, further blockade of the RAAS system with mineralocorticoid receptor antagonists (MRA) reduces mortality and HF hospitalizations, especially in patients with a LVEF of 35% or less [140]. The combination of hydralazine and isosorbide dinitrate, resulting in arterial and venous vasodilation, has also proven to reduce major cardiac events in patients with HFrEF. Diuretics, especially loop diuretics, are key drugs in the regulation of fluid retention in patients with HFrEF, with proven clinical benefit [135].

The favourable effects of all these therapies have been recognized for decades, and it was not until recent years that new pharmacological options, attempting other pharmacological targets, appeared. Ivabradine inhibits pacemaker activity by blocking the funny channel (I_f) current. The result is a decrease in sino-atrial heart rate without affecting blood pressure, myocardial

contractility, or intracardiac conduction. Ivabradine has shown to reduce HF hospitalization and HF mortality, and is indicated in patients in sinus rhythm with a heart rate > 70 bpm despite maximally tolerated doses of betablockers. [141]. More recently, the angiotensin receptor–neprilysin inhibitor (ARNI) sacubitril/valsartan showed a reduction in cardiovascular mortality and HF hospitalization when compared with enalapril in patients with chronic HFrEF [142]. More recent data indicate that ARNI could also provide clinical benefits in patients with acute decompensation of HF [143]. Finally, several clinical trials in the most recent years have shown that sodium-glucose cotransporter-2 (SGLT2) inhibitors such as dapaglifozin and empaglifozin [144], and oral soluble guanylate cyclase stimulators like vericiguat [145] provide further benefit, with reduction of hard clinical endpoints, in patients with HFrEF.

Despite the unquestionable benefits of pharmacological therapy and device-based therapy (including cardiac resynchronization therapy or LV assist devices) in HF management, HF remains progressive in a significant proportion of patients, who continue to present high hospitalization and mortality rates. Consequently, it becomes crucial to have a better knowledge of the molecular mechanisms underlying the disease in order to identify new pathways that, in addition to those targeted by current therapies, might be involved in its onset and evolution. In this context, considering that the stimulus that initiates the HF response is a mechanical hemodynamic overload, it seems reasonable to speculate that cardiac mechanoreceptors, membrane channels that respond to mechanical forces, could participate in the initial pathways that drive cardiac remodelling and potentially lead to HF progression.

1.3.3. EXPERIMENTAL MODELS OF HF

Experimental animal models of HF are fundamental to study the complex nature of this disease. Over the last years, several small animal models have been generated to study HF, which have allowed to better understand the

mechanisms underlying the development and progression of HF and have helped identify novel targets for therapeutic intervention and biomarkers of disease progression.

1.3.3.1. Transverse aortic constriction model

The transverse aortic constriction (TAC) is a pressure overload model that mimics the adaptations associated with hypertension and aortic valve stenosis in patients [146]. TAC is achieved by banding the aorta with a suture between the brachiocephalic trunk and the left common carotid artery. Generally, a small piece made from a bended and blunted needle (of 27G in mice and of 20G in rats) is placed in parallel to the transverse aorta and the suture is tied around the vessel and the needle, leaving a 60% of constriction upon removal [147]. TAC quickly increases LV afterload, initially resulting in compensated hypertrophy and progressing over time to HF [148]. One important limitation of TAC is the immediate onset of pressure overload, which is in contrast with the slow progression of clinical hypertension and aortic valve stenosis[149].

1.3.3.2. Myocardial ischemia and myocardial ischemia-reperfusion models

Permanent ligation of the left anterior descending (LAD) artery is used to explore the ventricular remodelling and cardiac function following myocardial infarction (MI) [150]. Occlusion of the coronary circulation in patients can be eventually re-established. However, despite the reestablishment of blood flow is essential to save the ischemic tissue, reperfusion can paradoxically cause further damage to the tissue [151]. The classical models of ischemia-reperfusion (I/R) have attempted to mimic this injury. In those, the LAD is temporally occluded by ligature to produce the ischemic event, and then that ligature is removed to allow reperfusion of the ischemic area [152]. Again, in these models coronary occlusion is sudden, leaving no chance to pre-existent collateral flow through a previously ischemic territory, a scenario that is commonly seen in

patients [153]. Another limitation of these models is that the degree of LV remodelling is very variable among animals, strongly dependent on the size of the infarct [154].

1.3.3.3. Neurohormonal stimulation models

Considering that sustained activation of SNS and RAAS is one of the triggers of the onset of cardiac remodelling, animal models of chronic neurohormonal stimulation are also widely used to induce HF. Administration of AT-II, the effector hormone of the RAAS, and isoproterenol, a non-selective β-adrenergic agonist, are the most frequent chemicals used to reproduce the chronic activation of the SNS and RAAS that occurs in patients with HF [155–157].

Regarding isoproterenol models, two main administration strategies have been described: single daily injections or continuous infusion with osmotic pumps [156,158]. Although both models have been shown to induce HF, the latter seems to generate a more progressive substrate that corresponds better with the slow progression of HF in humans [159].

1.4. MECHANORECEPTOR CHANNELS AND CARDIAC REMODELLING

All organisms, from single-cell bacteria to multicellular animals, must respond to mechanical forces, either environmental or self-generated, for proper growth, development, and health. A variety of proteins and complexes can sense and respond to such forces, in a process known as mechanosensation. Among those proteins, mechanoreceptor channels are considered to be at the origin of the cellular signalling pathways involved in mechanosensation. Embedded in membranes, they convert diverse mechanical stimuli (including membrane tension, membrane thickness, curvature, or matrix-protein interactions) into intracellular electrical and biochemical responses [160]. Mechanoreceptors are ion channels, which, upon mechanical stimulation, open and facilitate an influx or efflux of ions across the cellular membrane, initiating the biochemical response.

Mechanoreceptors are widely expressed in all tissues and cell types, including the heart. The heart is constantly exposed to mechanical signals (stretch, compression, bending, and shear stress), and needs to adapt to such forces to preserve normal cardiac function. Several mechanoreceptor channels have been described in the heart. Those include certain K^+ channels, one member

of the Piezo channels, and several transient receptor potential (TRP) channels (Figure 9) [161].

Figure 9. Mechanoreceptors of the distinct families that have been reported to be expressed in the heart.

Potassium channels allow K^+ flux following the electrochemical gradient. In mammalian cells, activation of K^+ channels located in the cytoplasmic membrane generally hyperpolarizes the membrane, while K^+ channel closure leads to cell depolarization. Specifically in the heart, K^+ channels are key elements in the genesis and duration of the cardiac action potential [162], and can play a secondary role in Ca^{2+} influx into the cytosol: the increase in K^+ currents would shorten action potential duration by reducing phases-2 and -3 of the action potential and therefore Ca^{2+} entrance [163]. In the mammalian heart, several stretch-activated K^+ selective channels have been reported to be functionally expressed, including the two pore-domain K^+ channel (TREK-1), the large conductance Ca^{2+}-activated K^+ channel (BK_{Ca}), and the ATP-sensitive K^+ channel (K_{ATP}).

It seems that TREK-1, BK_{Ca}, and probably K_{ATP} could have cardioprotective effects, probably limiting Ca^{2+} accumulation, although the intrinsic mechanisms have not been fully elucidated. One study showed that TREK-1-KO mice with a permanent coronary artery ligation developed larger-sized infarcts, greater LV diameter, and thinner posterior walls [164], suggesting the role of TREK-1 in protecting against cardiac dysfunction during myocardial infarction. In this regard, some studies have identified that TREK-1 expression

is reduced in patients with HF [165], indicating that the loss of function of this channel could promote the development of such disease. On the other hand, the activation of BK_{Ca}, either pharmacologically or genetically, seems to protect the heart from ischemia-reperfusion injury by modulating the oxidative state of the cell [166–168]. Regarding the K_{ATP} channel, both an increase and a decrease in function results in cardiac impairment. Mice lacking the pore-forming subunit exhibited more susceptibility to pressure-overload following TAC, presenting high fibrosis and myocardial hypertrophy [169]. In addition, K_{ATP}-KO mice had less tolerance to exercise [170]. These results suggest that proper function of this channel is essential for optimal adaptation to both physiological and pathological stresses. On the other hand, the increased activity of K_{ATP} has also been shown to be pro-arrhythmic due to their ability to shorten the AP duration [171].

Piezo channels are the last family of mechanoreceptors to be cloned. The non-selective cation channels Piezo1 and Piezo2 have been described as the only inherently mechanosensitive and the primary sensors of mechanical forces in a wide range of cells and tissues. This finding has revolutionized the field of mechanosensation, to the point of awarding the Nobel Prize of Medicine in 2021 to Ardem Patapoutian, the investigator that described them for the first time [172]. Although both Piezo channels are broadly distributed throughout the body, only Piezo1 has been reported to be functional in the heart. Piezo1 responds to several different types of mechanical stimuli allowing Ca^{2+} inside the cell. It has been shown to be upregulated in experimental animals following myocardial infarction or angiotensin stimulation and in human biopsies from patients with hypertrophic cardiomyopathy [173,174]. Moreover, murine studies have revealed that cardiac overexpression of Piezo1 leads to severe HF and arrhythmias [174]. These findings suggest that Piezo1 could have a role in cardiac remodelling, although further investigation is needed.

Finally, cardiac TRP channels have emerged as novel mediators of diverse physiological and pathological cardiovascular processes. Considering their relevance in the present thesis, their structure and physiology will be explained in detail in the next section.

1.4.1. TRP CHANNELS

TRP channels form a large family of cation channels involved in sensing and transmission of multiple external and internal stimuli. The first TRP channel was discovered in 1969 in the *Drosophila melanogaster* photoreceptors, where a mutation in the *trp* gene led to a transient response to light [175]. Since then, 70 TRP channels with different properties have been described in both invertebrates and vertebrates, among which 28 have been found in mammals so far.

The mammalian TRP channels are classified according to its structural homology into six subfamilies: TRPC (canonical; TRPC1-TRPC7), TRPV (vanilloid; TRPV1-TRPV6), TRPM (melastatin; TRPM1-TRPM8), TRPA (ankyrin; TRPA1), TRPML (mucolipin; TRPML1-TRPML3), and TRPP (polycystin; TRPP1-TRPP3) [176]. TRP channels are believed to share a common topological structure consisting of 6 transmembrane domains (TM1-TM6) with both carboxy and amino-terminal tails facing the intracellular side of the membrane. The pore-forming region is located in a short hydrophobic stretch between TM5 and TM6. Like other pore-forming proteins, TRP assemble as tetramers to form an entire operating pore [177]. Functional TRP channels may form either homotetrameric (consisting of four subunits of the same TRP) or, less frequently, heterotetrameric complexes (formed by the assembly of different TRP subunits), with unique properties [178].

TRP channels are mostly non-selective for cations, often with more permeability for Ca^{2+} than for Na^{+} (P_{Ca}/P_{Na} ratio). Cation permeability varies

from one channel to another. For example, the permeability of TRPV4 to Ca^{2+} ($P_{Ca}/P_{Na} \approx 6$) is greater than that of TRPC6 ($P_{Ca}/P_{Na} \approx 5$) [179], and TRPV5 and TRPV6 exhibit highly Ca^{2+} selectivity ($P_{Ca}/P_{Na} \approx 100$), whereas TRPM4 and TRPM5 are almost impermeable to Ca^{2+} ($P_{Ca}/P_{Na} <1$) [180]. TRP channels are multisensory receptors that respond to a wide variety of physical and chemical stimuli. They can be gated by dynamic changes in temperature, pH, osmolarity, mechanical forces, as well as by a broad range of endogenous or exogenous ligands and natural or even artificial chemicals [181].

1.4.2. CARDIAC TRP CHANNELS AND THEIR ROLE IN CARDIAC REMODELLING

Several TRP channels are expressed in the cardiac tissue, and some can be activated by mechanical forces. This activation allows Ca^{2+} entry into the cell, modulating the cation's homeostasis. Hence, given the importance of Ca^{2+} in the promotion of cardiac remodelling and being the mechanical forces a potential primary stimulus in the onset of such remodelling, TRP channels have been postulated as promising candidates to explain the triggering and development of adaptive and adverse cardiac responses.

Recent advances regarding the role of diverse TRP channels in mediating Ca^{2+} signalling and their potential roles in cardiac remodelling and cardiac diseases are detailed below.

1.4.2.1. The TRPA family

TRPA1, the sole member of the mammalian TRPA family, is a large conductance Ca^{2+} permeable channel. Although present in the cardiac tissue, its role is still unclear. Some data suggest that TRPA1 might be implicated in the process of cardiac hypertrophy and failure. Wang and colleagues found that TRPA1 protein levels were increased in the LV of patients with dilated cardiomyopathy and in a mouse model of pressure overload [182] Moreover,

TRPA1 inhibition ameliorated the development of hypertrophy and fibrosis, and improved cardiac performance in a murine model of pressure-overload [182]. Likewise, another study showed that TRPA1 knockdown increased survival rates, reduced fibrosis, and enhances heart performance after myocardial infarction [183].

1.4.2.2. The TRPM family

The TRPM subfamily includes eight channels (TRPM1-TRPM8) expressed in mammals, although within the heart, only TRPM3, TRPM4, and TRPM7 have been identified as potential mechanotransducers. Previous studies have mainly focused on the cardiac role of TRPM4 and TRPM7, while little is known regarding TRPM3.

TRPM4 channel, which is impermeable to Ca^{2+} but permeable to both Na^{+} and K^{+}, has demonstrated to play a favourable role in cardiac remodelling. Gueffier and colleagues found that *TRPM4* mRNA expression was increased in the LV of mice following 4 weeks of endurance training compared to sedentary mice. Moreover, they showed that endurance training in WT mice was mainly associated with the activation of the PI3K/Akt pathway, which leads to a physiological cardiac hypertrophy. In contrast, they reported that endurance training in $TRPM4^{-/-}$ mice was correlated with the activation of the calcineurin/NFAT pathway, resulting in pathological cardiac remodelling [184]. Interestingly, it has been shown that selective removal of TRPM4 from the heart resulted in increased Ca^{2+} entry via voltage-gated Ca^{2+} channels and prominent hypertrophic growth after chronic treatment with AT-II or β-adrenergic stimulation [185,186]. Together, these studies suggest that TRPM4 might protect the heart to a sustained neurohormonal stimulation by diminishing Ca^{2+} entry and counteracting the pathological remodelling.

Unlike TRPM4, the cardiac role of TRPM7, a channel with high permeability to Ca^{2+}, remains controversial and could be chamber-specific. TRPM7 has been

involved in pathological signalling, but also reported to have cardioprotective effects. A report from Du and colleagues correlated an increased expression of TRPM7 with the development of atrial fibrosis. They reported that TRPM7 expression and activity was upregulated in atrial FB from patients with atrial fibrillation and that knockdown of TRPM7 significantly reduced MFB differentiation in the atria [187]. Nevertheless, another study demonstrated that TRPM7 channels did not play a role in ventricular FB differentiation [188]. These results could indicate that TRPM7 are involved in the FB-MFB transition exclusively in the human atrium. On the other hand, Rios and collaborators reported that mice with global TRPM7 deficiency were more prone to suffer cardiac hypertrophy, fibrosis, and inflammation. This potential protective role of TRPM7 was attributed to its function within infiltrating macrophages cells [189]. Hence, the role of TRPM7 in cardiac adaptive and maladaptive responses is not fully understood and needs further investigation.

1.4.2.3. The TRPC family

The TRPC family comprises 7 members (TRPC1-TRPC7) that are widely expressed in most types of cardiac cells, and, with the exception of TRPC2 and TRPC7, all are thought to participate in the transduction of mechanical stimuli in those cells. Several studies suggest that activation of TRPC channels may be downstream of PLC. When the cell surface density of Gq-coupled receptors (such as AT_1) is increased by their overstimulation, PLC is activated and mediates the production of DAG and IP_3, which are able to induce Ca^{2+} currents through TRPC channels. In this regard, TRPC1, TRPC3, and TRPC6 have been demonstrated to be important mediators of adverse cardiac remodelling and have been shown to be upregulated in patients with HF [190].

TRPC1 plays a relevant role in CM hypertrophy. Independent reports have demonstrated that the increased CM hypertrophy observed in mice and rats subjected to pressure overload is associated with the up-regulation and

activation of TRPC1 [191,192]. Notably, mice with global TRPC1 gene deletion exhibit less hypertrophy and improved cardiac function in response to pressure-overload or neurohormonal stimulation [192]. At the molecular level, it seems that TRPC1 mediates CM hypertrophy by inducing the activation of calcineurin/NFAT and NF-Kb pathways [192,193].

Similarly, TRPC3 overexpression has demonstrated to promote both CM hypertrophy and FB proliferation. In mechanically stressed hearts, Kitajima and collaborators showed that TRPC3 activation triggered an aberrant increase in ROS production leading to a pathological remodelling [194]. In addition, CM of mice overexpressing TRPC3 and subjected to pressure overload or AT-II stimulation showed greater increase of a NFAT-luciferase transgene, indicating that NFAT activation occurs downstream of TRPC3 channel activity [195]. Conversely, the use of dominant-negative TRPC3 mutants or its blockade with a pharmacological agent (Pyrazole 3) attenuated the cardiac hypertrophic and fibrotic responses following either the infusion of a neurohormonal agonist or pressure-overload stimulation [196,197]. However, another study reported that individual activation of TRPC3 is not sufficient to develop HF [198], suggesting that more channels are needed in the deleterious maladaptive cardiac response.

Previous literature has highlighted the relevant role of TRPC6 in initiating the adverse cardiac response that leads to HF. Again, this channel would act on both CM and FB. Kuwahara et al. reported that TRPC6 expression was increased in the hearts of mice subjected to an aortic banding, as well as in failing human heart samples. In addition, they also showed that TRPC6 mediates a pathological cardiac hypertrophy by activating the calcineurin/NFAT pathway in CM. Interestingly, the same study showed that NFAT, in turn, also regulates the expression of TRPC6, suggesting a positive regulatory circuit in the calcineurin/NFAT pathway that could promote the

transition to adverse remodelling [199]. In FB, a recent genome-wide screening identified TRPC6 as a regulator of MFB differentiation. Overexpression of this channel in primary rat cardiac FB promoted spontaneous differentiation to MFB to the same extent as the treatment with the known pro-fibrotic agonists TGF-β or AT-II [103]. Conversely, the loss of TRPC6 in a TRPC6-KO mice attenuated FB differentiation induced by TGF-β and AT-II. The molecular mechanisms by which TRPC6 promotes FB differentiation seem to be, as well, through the calcineurin/NFAT pathway [103]. Consistent with the pro-fibrotic role of TRPC6, silencing the channel with a siRNA approach attenuated the TGF-β-mediated upregulation of α-SMA in the human right ventricle [200]. Moreover, the administration of a pharmacologic antagonist of TRPC6 (BI749327) to mice subjected to a pressure-overload attenuated cardiac fibrosis and dysfunction, with no impact on cardiac hypertrophy [201]. Again, all previous literature on TRPC6 indicates that this channel participates in cardiac pathological remodelling, but its inhibition only has partial protective effects, which suggests that other pathways (and potentially other TRPs) must be also playing a role.

1.4.2.4. The TRPV family

The vanilloid family of TRPs, the TRPV family, is formed by 6 channels (TRPV1-TRPV6), each of them having distinct roles within the body. The first four (TRPV1, TRPV2, TRPV3, and TRPV4) have been found to be functionally expressed in cardiac cells. However, TRPV3 is not modulated by mechanical forces such as stretch [202], but rather responds to temperature changes, so it will not be discussed in this sections despite some reports have suggested a potential contribution of this channel to adverse cardiac remodelling [203].

Within the heart, TRPV1 seems to protect against pathological remodelling and cardiac dysfunction. For instance, studies in mouse models of myocardial infarction suggest that the activity of TRPV1 supresses the adverse cardiac

response in the infarcted region following ischemic injury [204,205]. On the other hand, in a mouse model of coronary occlusion, deletion of TRPV1 increased infarct size, as well as MFB infiltration and collagen production, an effect potentially mediated by the canonical TGF-β-SMAD pathway [205]. The cardioprotective role of TRPV1 was also confirmed in a couple of studies using pressure-overload mouse models [206,207]. Likewise, it has also been demonstrated that the overexpression of TRPV1 attenuates β-adrenergic-induced adverse remodelling by diminishing cardiac fibrosis [208]. However, it is not clear how this channel mediates the protective response at the cellular and molecular level.

Unlike TRPV1, TRPV2 seems to have a deleterious effect in cardiac remodelling. A recent study demonstrated that TRPV2 expression is upregulated in mice following aortic constriction, whereas the absence of functional TRPV2 attenuates the LV remodelling induced by pressure-overload [209]. Moreover, TRPV2 overexpression has also been associated with heart enlargement, increased fibrosis, and myocardial structural defects in patients with dilated cardiomyopathy [210]. Intriguingly, despite the deletion of TRPV2 might have a protective role in pressure-overloaded hearts, its deletion did not produce any beneficial effect against AT-II or β-adrenergic-induced cardiac remodelling [209], suggesting that other this channel could play a role in very specific mechanical conditions and not others.

Because this thesis is focused on studying the role of TRPV4, its structural, functional and cardiac roles will be described extensively in the following chapter.

1.4.3. THE TRPV4 CHANNEL

The TRPV4 channel was first described in the year 2000 [211–213]. Before receiving its current nomenclature, several names according to its functional features

were proposed: OTRPC4 (osmosensitive transient receptor potential channel) [211], VR-OAC (vanilloid receptor-related osmotically activated channel) [212], VRL-2 (vanilloid receptor-like) [214], and TRP12 [213].

1.4.3.1. Structure and biophysical properties

The human *TRPV4* gene is found on chromosome 12 and is composed of 15 exons. The protein contains 871 amino acids and, like the other TRP channels, 6TM domains with linking loops, and both N- and C-terminal tails facing the cytosol. A re-entrant pore loop between TM5 and TM6 forms the central cation permeable pore, while TM3 and TM4 seem to constitute an agonist binding-pocket [215] (Figure 10A). Recently, the crystal structure of the channel has been resolved, which has led to a better understanding of its architecture and unique properties [216] (Figure 10B). Deng and collaborators found that the pore of the TRPV4 channel exhibited a remarkably wide selectivity filter pore (large gate diameter), as compared to other TRP channels, suggesting an explanation for its selective signature, with low preference for cation ions [216] (Figure 10C). Although nonselective, TRPV4 has a higher selectivity for Ca^{2+} than for Mg^{2+} or Na^{+} (Ca^{2+}>Mg^{2+}>Na^{+}), and under normal physiological conditions (if Ca^{2+} is present in the medium), the open channel will generate an influx of Ca^{2+}. In addition to Na^{+}, TRPV4 can also permeate to a lesser extent other monovalent cations, although it discriminates poorly between them (K^{+}>Cs^{+}>Rb^{+}>Na^{+}>Li^{+}) [217]. Concerning the cytoplasmic tails, the N-terminus of the TRPV4 channel contains a characteristic ankyrin repeat domain (ARD), consisting in six ankyrin (ANK) repeats, with important regions for protein-protein interactions with channel regulators [218]. Before the ARD, there is a proline-rich domain (PRD) that has been implicated in the mechanosensitive properties of the channel [219]. On the other hand, the TRPV4 C-terminal tail contains other functional domains, such as the TRP box, implicated in channel

gating, a CaM-binding site and interacting domains with cytoskeletal proteins [220–222].

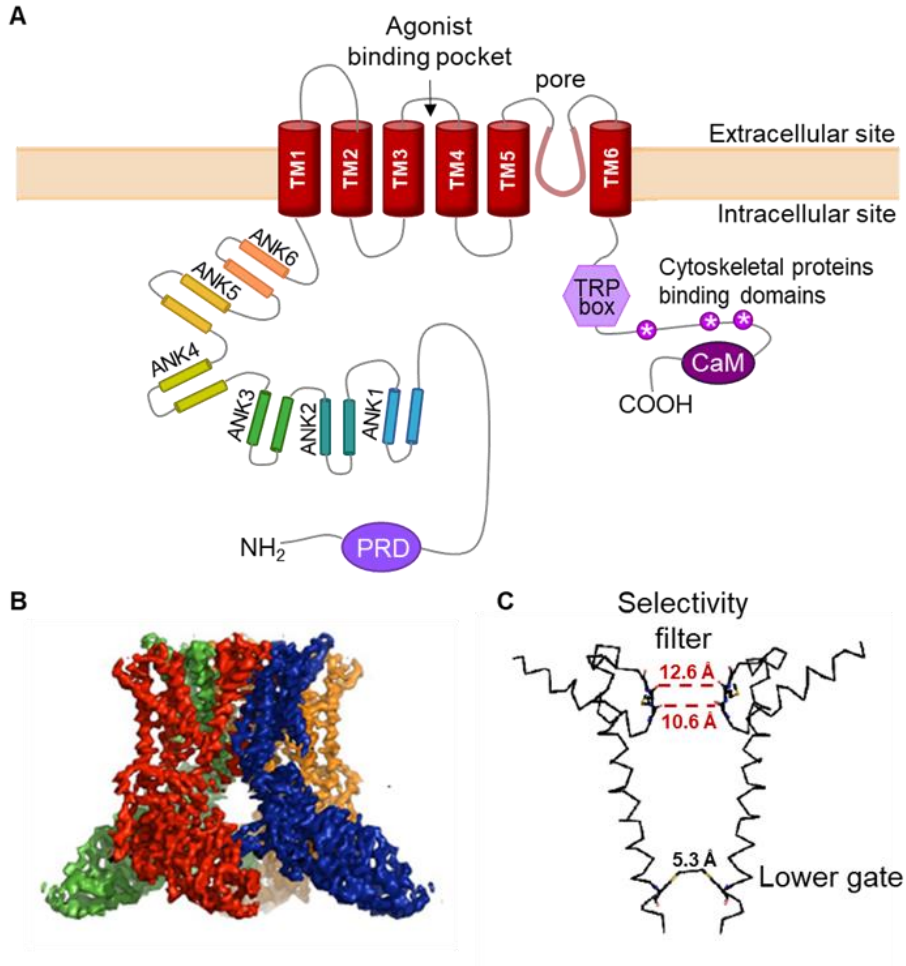

Figure 10. Structure of the TRPV4 channel. A. Topological structure of the TRPV4 channel. B. Crystallography reconstruction of the tetrameric channel. Each subunit is represented in a different colour. C. Details of the ion-conduction pore of TRPV4 channel. The distance (in angstroms, Å) between the residues forming the selectivity filter is represented by a red line. The lower gate of the TRPV4 pore is also showed. This lower gate is a conserved among TRPV channels, and the size of that gate in the TRPV4 channel is sufficient to prevent ion passage when the channel is closed. B and C figures are adapted from [216]. Abbreviations: TM: transmembrane domain, ANK: ankyrin repeats, CaM: calmodulin, PRD: proline rich domain.

To form a functional ion channel, oligomerization of four TRPV4 monomers is required. Although the channel usually assembles in a homotetrameric structure [223], TRPV4 has been reported to occasionally form heterotetramers with other TRP monomers, including TRPC1 [224] and TRPP2 [225], resulting in new channels with different characteristics and functions.

1.4.3.2. Activation and modulation

Like other TRPs, TRPV4 is a multimodal channel regulated by a diverse array of stimuli such as temperature, osmotic and mechanical stimuli, as well as exogenous or synthetic ligands. Different regions within the channel modulate the activation following differential stimuli.

1.4.3.2.1. Activation by temperature

As many members of the TRP channel family, TRPV4 is gated by temperature. Warm temperatures, ranging from 24 to 38°C, activate TRPV4, suggesting that this channel is active at normal body temperature [226]. Deletion of three N-terminal ARD of the TRPV4 abolishes its activation by mild temperatures but does not prevent its activation by osmotic stimuli, indicating that the ANK repeats are necessary for the channel activation by heat, but not by other stimuli [227]. Furthermore, Garcia-Elias et al showed that binding of the plasma membrane protein PIP_2 to the N-terminal tail of TRPV4 is required for its activation by temperature [228]. Physiologically-activating temperatures have shown a synergistic effect with other stimuli, increasing the efficacy of channel activation by other stimuli [229].

1.4.3.2.2. Activation by osmotic and mechanical stimuli

Initially, TRPV4 was described as an osmoreceptor, in charge to detect and respond to changes in the extracellular osmolarity. Specifically, TRPV4 is activated by decreases in extracellular osmolarity (hypotonicity) and inhibited when the osmolarity of the extracellular media increases (hypertonicity) [211].

Although osmotic stress is considered a mechanical stimulus, TRPV4 can also respond to other mechanical forces applied to the cell membrane, such as shear stress or high viscous loading [230,231].

The mechanisms by which TRPV4 channels are activated by mechanical stresses are, to date, not fully understood. In contrast to the Piezo channels, which are directly activated by force, TRPV4 could be activated downstream of the mechanical sensor. Two different mechanisms have been proposed: direct mechanical activation and indirect activation through other molecules or transduction pathways (Figure 11).

The first activation hypothesis, in which TRPV4 may respond directly to the effect of mechanical deformation of the cell membrane, is controversial [232]. It rather seems that the opening of the TRPV4 channel is driven by cell membrane structures attached or in close vicinity to the channel that are the direct sensors of the force [233]. These structures may include accessory proteins, such as integrins, the cytoskeleton, or even the same ECM. Thus, the mechanical forces may be transmitted via these structures, which may directly cause a conformational change that results in TRPV4 activation [234,235].

Alternatively, membrane deformation may cause the release and activation of membrane products which, in turn, effect the gating of TRPV4 channel. It has been reported that TRPV4 osmotic and mechanical sensitivity relies on the activity of phospholipase A_2 (PLA_2). Under mechanical stress, PLA_2 leads to the release of arachidonic acid (AA) metabolites and the consequent production of 5,6-epoxyeicosatrienoic acid (5,6-EET) via the cytochrome P450 [236]. Several reports have shown that 5,6-EET directly activates TRPV4 and that its removal or cytochrome P450-blockade reduces TRPV4 activation [237,238]. 5,6-EET could activate TRPV4 by two mechanisms, either by direct binding to the newly discovered EET-binding pocket localized in the TM2-3 linker of the channel, and/or indirectly by modulating the membrane fluidity around the channel [239].

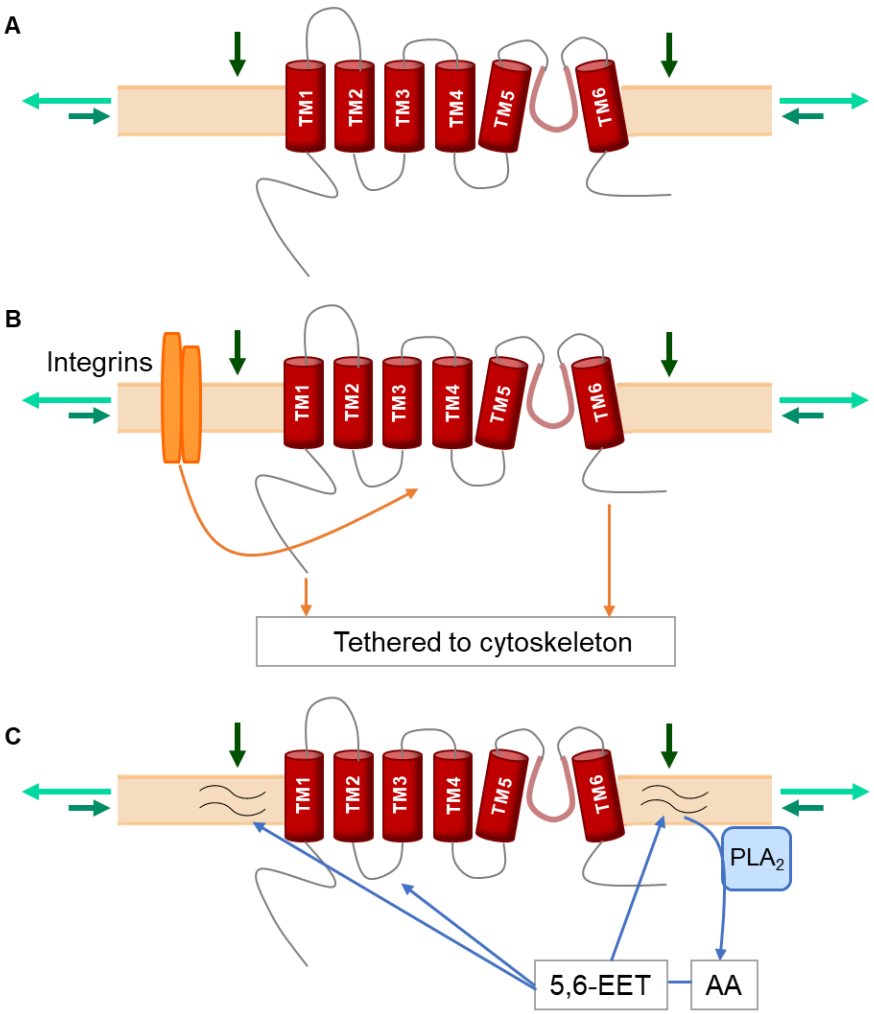

Figure 11. Possible mechanisms of TRPV4 mechanotransduction. A. Deformation of the plasma membrane by mechanical stimuli directly modulates channel opening. B. Channel is gated by tethering to cytoskeletal elements, which are reorganized by mechanical or osmotic stress. Also, mechanical forces may stimulate integrins which, in turn, may cause a structural alteration to the channel leading to its activation. C. Mechanical activation of PLA_2 results in the generation of AA and 5,6-EET, which activate the channel either by binding directly to a pocked formed between TM2 and TM3 or indirectly by altering membrane viscosity.

1.4.3.2.3. Modulation by chemicals

TRPV4 can also be activated or inhibited by several chemicals. These have been of great use to explore the roles of TRPV4. Phorbol esters, including the

4α-phorbol 12,13-didecanoate (4α-PDD), the 4α-phorbol 12, 13-dihexanoate (4α-PDH), and the phorbol 12-myristate 13-actetate (PMA), activate the channel [240,241] by binding directly to a channel pocket formed between TM3 and TM4 segments [242]. Bisandrographolide A (BAA), a compound isolated from an extract of the plant *Andrographis paniculate*, can also activate specifically TRPV4 by directly interacting with the channel [243].

In 2008, Thorneloe and colleagues described the synthetic lipid GSK1016790A to be a potent TRPV4 activator [244]. In fact, this drug is currently employed as the preferred molecular activator of the channel in most experimental studies. Although the specific interaction site is still unknown, a recent study demonstrated that GSK101679A activates TRPV4 to a similar extent that that obtained by hypotonicity, suggesting that this compound activates TRPV4 by mimicking its physiological gating [245].

On the other hand, TRPV4 antagonists were initially non-specific inhibitors with high cross-reactivity with other TRP channels or Ca^{2+} channels (e.g ruthenium red) [246]. However, several selective inhibitors have been finally developed. RN-1734 and HC067047 (very commonly used) were reported to block TRPV4 currents without affecting other channels [247]. Also, a newer antagonist, GSK2193874, which is orally available and highly potent and selective, has been shown to be tolerated in vivo and even to prevent pulmonary edema in a mouse model of HF [248]. Further optimization of the potency and pharmacokinetics of the chemotype led to the development of GSK2798745 [249]. Recently, this compound was tested in clinical trials and demonstrated well tolerability and no significant safety issues in both healthy volunteers and HF patients [250].

1.4.3.2.4. Modulation by protein interactions and phosphorylation

Given that approximately 70% of the TRPV4 sequence is located at the cytosolic site of the plasma membrane, channel modulation by protein

interaction and phosphorylation are proposed to occur in this intracellular region. Posttranscriptional modifications are important to modulate channel trafficking or channel sensitivity to gating stimuli. So far, 38 proteins have been identified to interact with TRPV4, several of them being modulators of channel localization or signalling. For instance, it was found that the membrane localization of TRPV4 is modulated by the cytoskeletal protein PACSIN 3 by directly binding to the PRD region on the N-terminal tail [251]. Sensitization of the channel can also occur through the interaction of the N-terminal domain with the plasma membrane PIP_2, which favours an expanded conformation of the intracellular tails, thereby activating the channel in response to hypotonicity and heat [228]. Similarly, IP_3 receptor binding to the TRPV4 C-terminal CaM-binding side has been reported to sensitize the channel to osmotic stimuli [252]. Finally, TRPV4 activity can also be enhanced via PKA- and PKC-dependent phosphorylation [253,254].

1.4.3.3. Physiological function

In general, TRPV4 plays an essential role in regulating cell function by mediating Ca^{2+} influx, which in turn regulates multiple intracellular proteins required for several physiological processes. Consistent with its involvement in many physiological functions, TRPV4 is ubiquitously expressed, and can be found in the brain, lung, heart, vasculature, bone, bladder, kidney, skin, and liver, among other organs.

1.4.3.3.1. Thermoregulation

The responsiveness of TRPV4 to warm temperatures and its expression in sensory neurons, keratinocytes, and in the hypothalamus, point to a role for TRPV4 in thermoregulation. In fact, a study using TRPV4 transgenic mice showed that $TRPV4^{-/-}$ mice chose warmer floor temperatures on a thermal gradient and responded with prolonged tail withdrawal during acute application of heat to the tail than $TRPV4^{+/+}$ mice [255].

1.4.3.3.2. Osmoregulation and mechanotransduction

Controlling cell volume is a homeostatic imperative process for cells to survive. When exposed to a hypotonic environment, cells rapidly swell, and activate a regulatory response called regulatory volume decrease (RVD) to restore their isotonic volume. This process is normally associated with changes in intracellular Ca^{2+} concentrations which, in turn, activate K^+ and Cl^- channels, permitting an efflux of electrolytes that drag water out. In this sense, TRPV4 is thought to provide the primary Ca^{2+} signal required to activate the RVD response, thereby participating in the cellular homeostasis and in the maintenance of systemic osmoregulation [256,257]. This evidence is further supported by the fact that mice lacking TRPV4 have an abnormal osmotic regulation [258].

TRPV4 can also direct behavioural responses to other mechanical stimuli besides hypotonicity, such as shear stress. For example, in the vascular endothelium the mechanical activation of TRPV4 by changes in shear stress and the subsequent entry of Ca^{2+} into endothelial cells is essential for vasodilatation and for the maintenance of vascular tone [230]. In endothelial cells, an increase in the intracellular Ca^{2+} triggers the synthesis of endothelium-derived vasodilators (such as NO, prostacyclin and EDHF) [259], and in that sense, TRPV4 has been proposed to mediate the flow-induced Ca^{2+} signalling and the subsequent release of vasodilator factors [260].

1.4.3.3.3. Nociception

TRPV4 is expressed in peripheral nociceptive neurons and has been found to play an important role in mediating certain pain sensations. Evidence of TRPV4-mediated nociception was found when TRPV4 gain of function caused an abnormal pain perception in the animal's face and hind paw [261]. On the contrary, TRPV4-KO mice displayed a lower sensitivity to harmful pressure on the tail [262]. In the rat dorsal root ganglia, the activation of TRPV4 results in the

release of nociceptive peptides (CGRP and substance P) and contributes to the transduction of mechanical stimuli to induce hyperalgesia [263]. A further finding demonstrated a potentially key role of TRPV4 in chemotherapy-induced neuropathy. Alessandri-Harper and collaborators showed that administration of antisense oligodeoxynucleotides targeting TRPV4 completely reversed the mechanical hyperalgesia induced by Taxol, the most widely used drug for the treatment of a variety of tumour types [264].

1.4.3.4. TRPV4 in the heart and potential role in cardiac remodelling

TRPV4 have been detected in multiple cardiac cell types, including CM and FB [265], and recent evidence suggest that these channels may be promising candidates as mechanoreceptors involved in the development and progression of cardiac remodelling by acting on both cell types.

Several studies have shown that TRPV4 channel activity significantly increases after I/R injury in both *in vitro* and *in vivo* models. During no-flow ischemia, cellular metabolites equilibrate across the plasma membrane and generate a hyperosmotic environment relative to physiological levels [266]. However, during reperfusion rapid washout of the extracellular fluid creates a hypoosmotic stress on the plasma membrane, which may activate TRPV4 and subsequent Ca^{2+} entry, contributing to the excessive Ca^{2+} overload classically observed during I/R [267]. Consistent with TRPV4 participation in I/R injury, Wu et al. recently reported that TRPV4-mediated Ca^{2+} entry induces ROS production and cell death in cultured H9C2 cells (a cell line derived from rat cardiomyoblasts) and in neonatal rat ventricular myocytes following I/R challenge. Moreover, they found that the TRPV4 agonist GSK1016790A enhanced ROS production whereas inhibition of TRPV4 with HC067047 prevented its production, supporting a key role of TRPV4 in I/R injury [268]. Similarly, it has also been demonstrated that treatment with HC067047

greatly alleviates myocardial I/R injury in mice by also reducing infarct size and improving cardiac function [269].

Importantly, and considering that over 50% of hospital admissions and 80% of deaths due to myocardial infarction occur in elderly individuals, Jones and collaborators demonstrated that TRPV4 expression and function increases in CM with age and that this may contribute to age-related diastolic dysfunction. They showed that the relaxation speed of CM was slower in untreated aged mice compared to those administered with a TRPV4 antagonist [267]. More recently, using a Langendorf perfusion system and intracardiac ECG recordings, Peana and colleagues demonstrated that aged mice hearts had increased incidence of arrhythmia compared with young following I/R. Moreover, by isolating CM from the young and aged mice and by exposing them to hypoosmotic stress, they showed that CM from aged mice had increased Ca^{2+} signals compared to young and aged CM treated with the TRPV4 inhibitor HC067047 [270]. Together, these findings indicate that TRPV4 may be a contributing factor to age-dependent cardiac dysfunction and arrhythmias. There is more evidence suggesting a role of TRPV4 in cardiac remodelling. In CM derived from pluripotent stem cells from patients with dilated cardiomyopathy, TRPV4 channels were found to participate in an aberrant cytosolic Ca^{2+} rise in response to stretch, mediating cytosolic calcium accumulation and leading to the pathological progression of dilated cardiomyopathy [271].

The role of TRPV4 in cardiac remodelling seems to be mostly mediated by their function on cardiac FB. As mentioned previously in this Introduction, the molecular mechanisms underlying the FB transition to MFB are not well known. However, TGF-β and mechanical stress, together with calcium signalling, are recognized as major mediators of FB differentiation. Recently, Adapala and co-workers demonstrated that TRPV4 channels are functionally

expressed in cardiac FB and required for their differentiation to MFB. Notably, they reported that TRPV4 integrates TGF-β signals and mechanical stimuli to promote FB differentiation. In an in vitro model, they found that the inhibition of TRPV4 activity or expression by a TRPV4 antagonist or shRNA knockdown, respectively, significantly attenuated FB differentiation induced by TGF-β, and mechanical stimuli generated by ECM stiffness. Furthermore, they showed that FB treated with TGF-β exhibit enhanced TRPV4 expression and increased Ca^{2+} influx [188]. Finally, a very recent work from the same group, which was published at the late stage of this doctoral thesis, pointed that TRPV4 deletion could protect the heart from the adverse remodelling following myocardial infarction in a mouse model [272]. Using TRPV4 KO mice, the authors observed, after 8 weeks of permanent coronary occlusion, that fibrotic content was decreased in KO mice compared to WT, both in the infarcted area but also in the remote areas. This led to suggest a potential role of TRPV4 in pathological remodelling, which the authors attributed to the activation of the Rho/Rho kinase/MRTF-A pathway [272], previously found to contribute to myogenic differentiation [273].

However, more data are needed to confirm the specific role of TRPV4 in cardiac remodelling, either adaptive or adverse. In this latter example, an animal model mimicking the human chronic phenotype of HF, such as that induced by chronic adrenergic stimulation, would be most desirable. Furthermore, since TRPV4 majorly promotes Ca^{2+} entrance into the cells, which is known to initiate the cardiac response to a mechanical overload, it would be of most interest to study the consequences of TRPV4 activation on calcium-activated cytosolic proteins potentially involved in cardiac remodelling.

1.4.3.5. The TRPV4-knockout mouse

As with many other proteins, TRPV4 deficient mouse models have been widely used to decipher the roles of the TRPV4 channel. To date, two TRPV4 KO mice have been produced by different methods. In mice, the *trpv4* gene is located in chromosome 5 and is comprised of at least 15 exons. Liedtke and colleagues generated the *trpv4*$^{-/-}$ mouse by cre-lox-mediated excision of exon 12, which encodes the pore-loop region and the adjacent TM5 and TM6 domains. The excision of this exon renders a non-functional TRPV4 polypeptide chain that is targeted for degradation [258]. At the same time, another *trpv4*$^{-/-}$ mouse was created by Suzuki et al., in which the exon 4, encoding the ANK repeats domain, was replaced with a neo-cassette, also resulting in a lack of TRPV4 production [262].

Despite the importance of the TRPV4 channel in many body functions, the TRPV4 knockout mice only display minor phenotypes. These include a larger bladder capacity and impaired voiding due to an affected mechanosensitivity in the bladder wall [274], altered osmosensation and subsequent reduction in water intake [258], compromised vasodilatation and pain sensing [262,264,275], and mild hearing [276]. These mice also exhibit thicker bones due to an impaired osteoclast differentiation, which critically depends on TRPV4 signalling [277]. However, they are viable and present normal size, appearance, and growth [262]. This suggest that important physiological responses are redundant and that most probably, the body has compensatory mechanisms to counteract the absence of TRPV4 during development. At the cardiac level, no differential findings have been found in TRPV4 KO mice, which show at baseline similar cardiac dimensions to WT [272]. Therefore, using the TRPV4 KO mouse model seems a very attractive strategy to evaluate the role of this channel in the heart.

2. HYPOTHESES AND OBJECTIVES

Cardiac remodelling develops as a compensatory mechanism to confront a persistent mechanical load over the heart. However, it is not fully understood why in some instances cardiac remodelling remains persistently adaptive while in others it evolves to a maladaptive response, with fibrosis accumulation and cardiac dysfunction. As discussed earlier, one of the hypotheses that have been postulated points to the dynamics of Ca^{2+} entrance into the cardiac cells: a low and sustained Ca^{2+} influx through channels other than voltage-dependent Ca^{2+} channels, most likely activated by G-protein-coupled receptors, would seem to be involved in pathological remodelling [37].

In this context, since the heart is continuously subjected to mechanical stretch, mechanoreceptor channels arise as attractive potential mediators of cardiac remodelling in response to different types of hemodynamic overload. Different mechanoreceptors have been studied in this regard, with different results thus far (see section 1.4.2.). We hypothesized that TRPV4 channels could exert a relevant role in the promotion of pathological remodelling. TRPV4 channels are expressed in both CM and FB and have been previously involved in myocardial scarring following myocardial infarction. Given their high PCa/PNa ratio and high selectivity for Ca^{2+}, we speculated that TRPV4 activation could promote the maladaptive response, and particularly the promotion of fibrosis, through Ca^{2+} entrance and activation of cytosolic Ca^{2+}-dependent proteins, a mechanism that has not been proven thus far.

Therefore, the overall objective of this thesis research is to identify the differential involvement of TRPV4 channels in both forms of cardiac remodelling and determine if deletion of the TRPV4 channel may prevent or alter the progression to the adverse cardiac response.

The specific objectives were:

1) To assess the differential expression of cardiac mechanoreceptors, with particular attention to TRPV4 channels, in physiological or adaptive remodelling using a mouse model of chronic exercise.

2) To assess the differential expression of cardiac mechanoreceptors, with particular attention to TRPV4 channels, in pathological or maladaptive remodelling using a mouse model of chronic β-adrenergic stimulation, which best mimics the sustained neurohormonal activation that occurs in human HF.

The results of these 2 objectives were validated in a rat model where the adaptive and the adverse remodelling were induced by exercise and transverse aortic constriction, respectively.

Additionally, in the setting of pathological remodelling exclusively, using transgenic mice with genetic deletion of TRPV4 ($TRPV4^{-/-}$, KO) and WT ($TRPV4^{+/+}$) animals subjected to chronic β-stimulation for HF induction:

3) To characterize the predominant cell type (CM or FB) over which TRPV4 could exert its main effects in terms of pathological remodelling.

4) To investigate the potential mechanisms by which TRPV4 could promote pathological remodelling and fibrosis, particularly by activation of the Ca-CaM-calcineurin/NFAT pathway.

5) To evaluate the potential role of TRPV4 in promoting arrhythmias related to the HF phenotype.

6) To assess the particularities of HF promotion and recovery in elderly mice, and their association with TRPV4 expression, to evaluate potential age-related differences in the HF phenotype.

3. MATERIALS AND METHODS

3.1. ANIMALS

Experiments were mainly performed in 10-week-old B57BL/6J wildtype (WT) and TRPV4 *knockout* (KO) mice (see below). The ageing study was done with a subset of 10-week-old (young) and 22-months-old (aged) female B57BL/6J mice. Additionally, a small group of 8-week-old (200-250 g) male Wistar rats provided by Dr. Eduard Guasch, from Hospital Clínic-IDIBAPS (Barcelona, Spain), was also used to replicate some of the experiments performed in mice (see Section 3.3.). Animals were kept with undisturbed social interaction (5 animals per cage in the case of mice, 2 in the case of rats) in conventional cages and maintained in a temperature and humidity-controlled environment (22-24 °C, and 60-65%, respectively), on a 12h-light/dark cycle. All animals had *ad libitum* access to tap water and standard diet throughout the whole experimental period.

At their final endpoint, animals were euthanized by intraperitoneal (IP) injection of sodium pentobarbital (100 mg/kg). Hearts were then removed and either cannulated on a Langendorff perfusion system, fixed for histology, or snap-frozen in liquid nitrogen and stored at -80 °C for ulterior analyses.

3.1.1. THE TRPV4-KO COLONY

Transgenic TRPV4 B57BL/6J mice (4 heterozygous females and 2 heterozygous males) were kindly provided by Dr. Wolfgang Liedtke (The Rockefeller University, New York, USA), and the colony was then expanded at the Vall d'Hebron Institute of Research (VHIR) facilities. As previously explained, this model bases gene targeting and generation of the null *trpv4* allele on the *cre-lox*-mediated excision of exon 12 of the *trpv4* gene, which encodes the pore-loop and adjacent transmembrane domain of the TRPV4 ion channel [258].

Animals were housed at the VHIR Animal Facility and crossings were done between heterozygous ($TRPV4^{+/-}$) breeders. Pups were sexed and identified by

ear-notch at 4 weeks old. Mice were used in homozygosis, either WT ($TRPV4^{+/+}$, intact *trpv4* gene and normal expression of the protein) or KO ($TRPV4^{-/-}$, both alleles recombined and no protein expression).

3.1.1.1. Genotyping strategy

3.1.1.1.1. Genomic DNA extraction

Genomic DNA was isolated from a distal tail snip (2mm of tissue) using the Wizard SV Genomic DNA Purification System (Promega). Briefly, the tail biopsy was incubated overnight for digestion at 55 °C with 275 µL of Digestion Solution Master Mix (200 µL Nuclei Lysis Solution supplemented with 50 µL of 0.5M EDTA, 20 µL of 20 mg/ml proteinase K, and 5 µL of 4 mg/ml RNase Solution, pH 8). Afterwards, the sample was centrifuged at 2000 g to pellet undigested hair or cartilage, and supernatant was transferred to 1.5 mL microcentrifuge tube. Then, 250 µL of Wizard SV Lysis Buffer containing ethanol was added to the lysed sample and transferred to the Wizard SV Minicolumn where it was centrifuged at 13000 g for 3 minutes to bind genomic DNA to the silica-membrane. Following nucleic acid binding, the column was washed four times and centrifuged 13000 g for 1 minute to ensure the removal of any residual impurities from the membrane. Finally, DNA was eluted with nuclease-free water by centrifugation at 13000 g for 2 minutes.

Purified genomic DNA was quantified using a Nanodrop 2000 spectrophotometer (Thermofisher,) and samples with a 260/280 ratio of ≥ 1.8 were accepted as pure and used for gene amplification.

3.1.1.1.2. Amplification of genomic DNA by polymerase chain reaction

Polymerase chain reaction (PCR) was performed to amplify the *trpv4* gene fragments using the enzyme Platinum Taq DNA Polymerase (Thermofisher). The reaction was carried out in 0.2 mL tubes containing 17 µL of PCR mixture (PCR Buffer 1X, 0.75 mM $MgCl_2$, 0.1 mM dNTP mix, 1U Platinum Taq DNA Polymerase, and 0.1 µM forward and reverse primers, Table 1) and 8 µL of

purified genomic DNA in an iCycler thermal cycler (Bio-Rad) with the following protocol: 2 minutes at 95 °C, followed by 34 cycles of 30 seconds at 95 °C, 90 seconds at 65 °C, and 3 minutes at 72 °C. A final step of 10 minutes at 72 °C ensured that all gene sequences were at full length. The reaction was then stopped by cooling the samples to 4 °C.

	Primer	Primer sequence (5'-3')	T_m (°C)
Trpv4	Forward	CATGAAATCTGACCTCTTGTCCCC	63
	Reverse	TTGTGTACTGTCTGCACACCAGGC	65

Table 1. Primers for the amplification of *trpv4* gene by PCR. Abbreviation: $T_{m:}$: Primer Melting Temperature.

3.1.1.1.3. Agarose gel electrophoresis

The PCR products were separated by electrophoresis on a 1.2%-agarose gel in 1x Tris-Acetate-EDTA buffer (TAE, 40 mM Tris base, 1 mM EDTA, 20 mM glacial acetic acid, pH 8) that contained SYBR Safe DNA gel stain (Thermofisher). PCR products were diluted 10:1 in TrackIt Cyan/Orange Loading Buffer (Thermofisher), which allowed tracking of DNA migration. The electrophoresis was set at 100 V for 30 minutes in TBE 0.5X. DNA bands were visualized in a Molecular Imager Gel Doc (Bio-Rad) with ultraviolet light and processed with Quantity One Analysis Sofware (Bio-Rad).

Primer sequences were designed to distinguish wildtype, heterozygous, and homozygous KO mice based on the size of the amplicon, showing a single 2.4-kb band in the wildtype mice, a single 1.2-kb band in the homozygous KO mice, and both bands in the heterozygous knockout. Figure 12 shows an example of the different pattern of sequencing depending on the genotype of the animal.

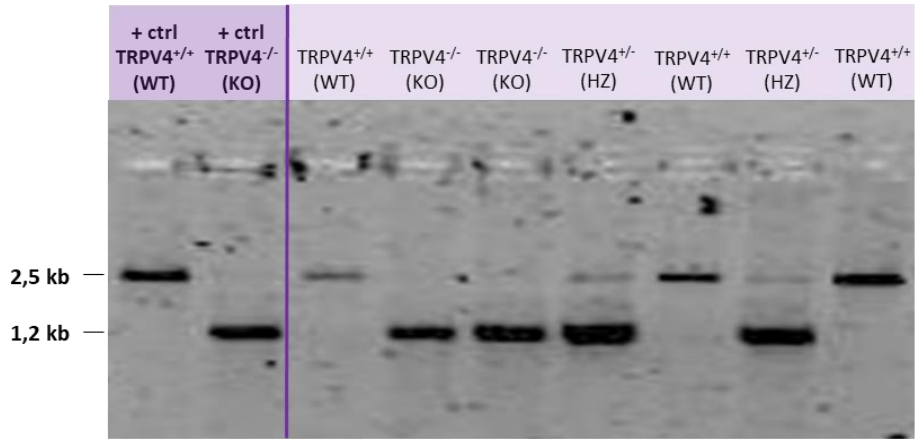

Figure 12. Example of the different pattern of DNA bands obtained depending on the genotype of the animals in an agarose gel electrophoresis. TRPV4$^{+/+}$ (WT) mice show a single 2.5-kb band (intact trpv4 gene sequence). TRPV4$^{-/-}$ (KO) mice show a 1.2-kb band (a part of the trpv4 sequence is excised and, therefore, amplicon size is smaller). TRPV4$^{+/+}$ (HZ) mice show both 2.5 and 1.2-kb bands.

3.2. *IN VIVO* MODELS

All experimental protocols were approved by the Animal Research Ethical Committee of the Institut del Mar d'Investigacions Mèdiques (IMIM), the Experimental Animal Ethical Committee of the VHIR, and the Animal Research Ethical Committee of the Institut d'Investigacions Biomèdiques Agust Pi I Sunyer (IDIBAPS), where all procedures were carried out, Additionally, the whole project received the approval of the Generalitat de Catalunya (CEA-OH/9538_MR1/1).

3.2.1. MOUSE MODEL OF ADVERSE CARDIAC REMODELLING INDUCED BY CHRONIC INFUSION OF ISOPROTERENOL

Pathological remodelling was generated using a validated model of HF induced by 28-day infusion of isoproterenol [36,278]. This model has been shown to mimic the chronic neurohumoral activation of human HF, and probably represents the model of HFrEF with the best resemblance to the clinical setting.

The first experiments were performed using two different isoproterenol concentrations to assess for a potential dose-effect in the cardiac pathological response: a moderate dose of 30 mg/kg/day (from now on, iso-30) and a high dose of 60 mg/kg/day (from now on, iso-60). Control mice received a saline infusion (from now on, sham). Osmotic minipumps (Alzet, 1004) filled with a blunt needle were used to administer either the isoproterenol (dissolved in 0.9% NaCl) or the saline solution. Specifically, the Alzet 1004 model, designed for mice, has a reservoir volume of approximately 100 µL, and allows a continuous and passive infusion of the contained solution at a rate of 0.11 µL/h, expiring after 28 days.

3.2.1.1. Surgical procedures

Mice were anaesthetized in an induction chamber with 4% isoflurane and maintained with 2% isoflurane using a nose mask. Anaesthetic depth was confirmed by loss of the withdrawal reflex in response to a painful stimulus (a pinch) on the hind-paw. When properly anaesthetized, the back neck of the animal was shaved with a depilatory cream (Veet®) and the animal was transferred to a heating pad. Chlorhexidine 2% was applied to the back neck and a ~1 cm incision was made. The skin was brought apart from the underlying connective tissue with blunt-ended scissors, and a pocket was created to allocate the pumps. The skin was then sutured with two interrupted stitches (6-0 Ethicon). At the end of the procedure, analgesia with 0.03 mg/kg of buprenorphine was administered IP, along with 0.5 mg/ml of meloxicam as an anti-inflammatory drug. The animals were then left to recover in a heated box for 15 minutes. Afterwards, mice were transferred to their cages, and monitored regularly to ensure complete recovery.

3.2.1.2. Study design and timepoints

This isoproterenol model was performed with distinct protocols and at different stages of the work to answer several specific aims (see Section 3.3):

- To determine the most adequate dose of isoproterenol promoting the cardiac features of pathological remodelling, 10-week-old WT male mice were infused with either 30 mg/kg/day or 60mg/kg/day of the drug for 28 days. Of note, subsequent experiments were only performed with the dose of 30 mg/kg/day, since this was confirmed to be sufficient to the develop an adverse response. To characterize the chronology of adverse remodelling promotion and the expression of mechanoreceptors over time, a group of 10-week-old WT male mice were infused with isoproterenol for either 3, 7, 14 or 28 days.
- To study the effect of TRPV4 deletion in the protection against adverse cardiac remodelling, 10-week-old $TRPV4^{+/+}$ and $TRPV4^{-/-}$ male and female mice were treated with isoproterenol (iso-30) for 28 days.
- To evaluate the effect of age in the promotion of adverse remodelling, 10-week-old (young) and 22-month-old (aged) female mice were infused with isoproterenol for 28 days.
- To evaluate the effects of ageing on cardiac recovery from isoprotrenol-induced adverse cardiac remodelling, osmotic minipumps delivering ISO over 28 days were implanted, and mice were subsequently kept for 28 additional days without receiving any treatment.

3.2.2. RAT MODEL OF ADVERSE CARDIAC REMODELLING INDUCED BY TRANSVERSE AORTIC CONSTRICTION

An alternative model of pathological remodelling was used in a different animal species in order to confirm the results obtained with isoproterenol infusion in mice. Transverse aortic constriction (TAC) surgery was performed in male Wistar rats with the help of a surgical lens. Rats were anesthetized with 2-3% isoflurane, intubated and ventilated (CWE, Incorporated), and kept

on a heating pad at 37 ºC during the whole experiment (Kent Scientific). Intramuscular buprenorphine (0.03 mg/kg) was used as analgesic. The portion of the aorta between the brachiocephalic trunk and the left carotid artery was isolated through a medial suprasternal partial thoracotomy. A bended and blunted 20G needle was placed next to the aorta, and a piece of 5.0 nylon suture was placed and tied around both the vessel and the needle to restrict blood flow. The needle was subsequently removed in order to yield an aortic constriction of 0.9 mm in diameter. This technique reduces the internal diameter by 60%, generating a constant increase in pressure in the left-hand side of the heart. As sham controls, littermate rats underwent the same surgery, but no needle or constriction were applied. After both TAC and sham surgery, the chest cavity and the skin were carefully sutured. Once recovered from anaesthesia, rats were placed back to their cages and monitored regularly to ensure complete recovery. Rats were sacrificed 8 weeks after surgery, when pathological remodelling should be present according to previous reports [279,280].

3.2.3. MURINE MODELS OF ADAPTIVE CARDIAC REMODELLING INDUCED BY MODERATE EXERCISE

The promotion of an adaptive cardiac remodelling was achieved by subjecting mice to exercise (exercise model). Two training intensities were assessed: moderate intensity (mod-ex) and high intensity (int-ex). Sedentary (sed) mice served as controls. The exercise groups were conditioned to run in a treadmill (LE8710, Panlab). After a 2-week adaptation period in which treadmill speed, slope and training duration were progressively increased, a stable routine was reached and kept for the following 8 weeks. Mod-ex mice ran at a speed of 15 cm/s, with a 6º positive slope during 30 minutes, and int-ex mice ran at a speed of 30cm/s, with a 12º positive slope for 45 minutes. Both groups were trained 5 days a week during 8 weeks (Table 2). The treadmill had different lanes to

allow several animals to run at the same time and a grid in the back that would administer a small electric shock on contact to ensure that the animals ran effectively. The electric shock was of constant intensity (2 mA), sufficient to encourage the animal to run without being harmful, as previously described [281]. All training sessions were supervised by an experienced investigator to ensure proper running and lack of stress. Sedentary mice were housed in the same conditions but did not perform any exercise session.

The adaptation and training sessions were performed in WT male mice aged 10-weeks at the beginning of the exercise protocol at the IDIBAPS in collaboration with the group of Dr. Eduard Guasch.

The results obtained from the mouse model of physiological remodelling were replicated in rats. Male Wistar rats were randomly assigned to one of the following two groups: moderate exercise (ex) or sedentary (sed). Exercise rats underwent daily running training sessions on a treadmill. The treadmill was essentially the same as the one for mice, but lanes were bigger to fit rats. The protocol included a 2-week progressive training program, starting with a 10-minute running session at 10 cm/s, followed by gradual increase over the following days until the steady-state of 35 cm/s and 45 minutes was achieved. Thereafter, animals were trained at this level 5 days/week for 16 weeks. As in the case of mice, rats were supervised during all training sessions to ensure proper running and avoid stress. Sedentary rats were housed and fed in the same conditions but kept with no exercise.

		Monday	Tuesday	Wednesday	Thursday	Friday
MODERATE INTENSITY EXERCISE						
Adaptation to exercise **Week 1**	**Speed**	5 cm/s	10 cm/s	10 cm/s	15 cm/s	15 cm/s
	Slope	-	-	-	-	-
	Duration	10 min	10 min	15 min	15 min	20 min
Adaptation to exercise **Week 2**	**Speed**	15 cm/s	15 cm/s	15 cm/s	15 cm/s	15 cm/s
	Slope		6°	6°	6°	6°
	Duration	20 min	20 min	25 min	25 min	30 min
Exercise routine **Weeks 3-10**	**Speed**	15 cm/s	15 cm/s	15 cm/s	15 cm/s	15 cm/s
	Slope	6°	6°	6°	6°	6°
	Duration	30 min	30 min	30 min	30 min	30 min
INTENSE EXERCISE						
Adaptation to exercise **Week 1**	**Speed**	10 cm/s	10 cm/s	15 cm/s	15 cm/s	15 cm/s
	Slope	-	-	-	6°	6°
	Duration	10 min	15 min	20 min	20 min	25 min
Adaptation to exercise **Week 2**	**Speed**	15 cm/s	20 cm/s	25 cm/s	25 cm/s	30 cm/s
	Slope	6°	6°	6°	12°	12°
	Duration	25 min	25 min	30 min	35 min	45 min
Exercise routine **weeks 3-10**	**Speed**	30 cm/s	30 cm/s	30 cm/s	30 cm/s	30 cm/s
	Slope	12°	12°	12°	12°	12°
	Duration	45 min	45 min	45 min	45 min	45 min

Table 2. Details of the moderate and intense exercise protocols and chronological scheme of the exercise protocol. Male mice of 10 weeks of age were subjected to run on a treadmill either at a moderate or an intense exercise protocol. The first 2 weeks, mice were allowed to adapt to exercise training by gradually increasing the exercise intensity and duration. After adaptation period, mice ran for 8 weeks (week 2-week 10) following a stable exercise routine.

3.3. EXPERIMENTAL DESIGN

This thesis embraces multiple experiments that were designed to address specific questions. The following lines describe and schematize the main sub-projects of the work.

3.3.1. SET-UP OF THE HF MODEL

A first experiment was designed to establish the most appropriate dose of isoproterenol to induce HF, given that different doses have been reported previously with different results [282–284]. Ten-week-old B57BL/6J male mice were infused with two different doses of isoproterenol (30 mg/kg/day or 60mg/kg/day) or with saline (sham). Cardiac phenotype with in vivo echocardiography was assessed at baseline and after treatment. Cardiac hypertrophy and fibrosis were assessed post-mortem with morphology, cardiac weight, histology, and gene expression analyses (Figure 13).

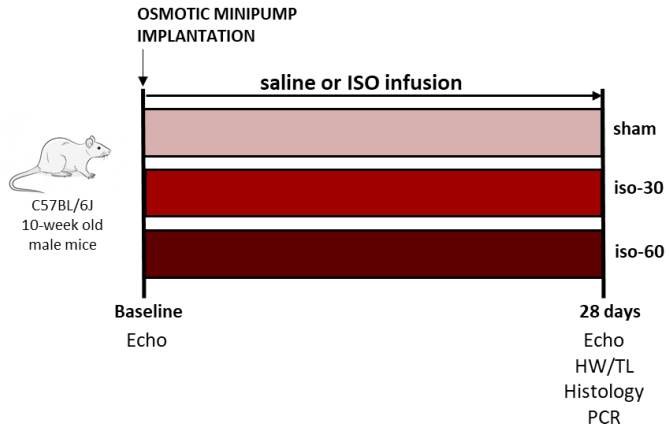

Figure 13. Establishment of the HF mouse model.

As mentioned before, the dose of 30 mg/kg/day was found to be enough to induce pathological remodelling, so this dose was the only used in the following experiments throughout the project.

3.3.2. SET-UP OF THE EXERCISE MODEL

A subsequent experiment was designed to establish the most appropriate exercise training program to induce a physiological cardiac remodelling. B57BL/6J male mice were subjected to two different protocols of exercise training (mod-ex and int-ex, see Section 3.2.3) or remained sedentary

(controls). In vivo echocardiographic studies were performed before exercise and at least 24h after the last training session, to avoid potential artifacts due to acute training (Figure 14). Post-mortem samples were collected after echocardiographic studies. Unlike the int-ex, the mod-ex training was found to induce a complete physiological remodelling, and therefore was the one used for subsequent experiments.

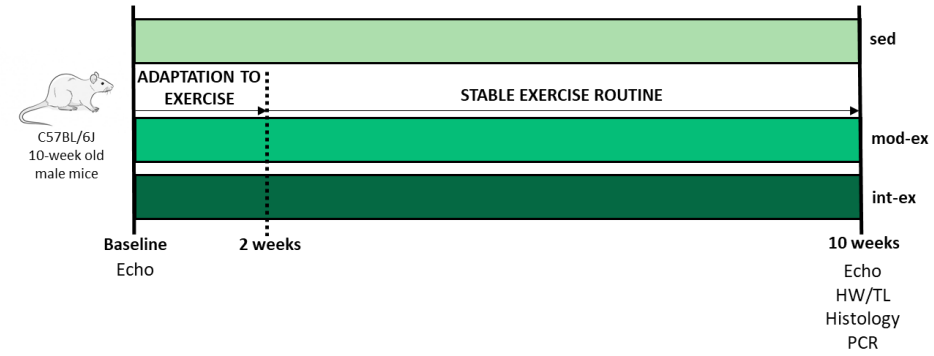

Figure 14. Establishment of the exercise mouse model.

3.3.3. MECHANORECEPTOR CHANGES IN ADVERSE AND ADAPTIVE CARDIAC REMODELLING

This subproject was aimed at exploring the changes in mechanoreceptor expression that took place in the two forms of remodelling (adverse and adaptive). For Subproject 3, only the dose of 30 mg/kg/day of isoproterenol (in the HF model) and the mod-ex training (in the exercise model) were studied. Echocardiograms were performed at baseline and at the end of both protocols. Gene and protein mechanoreceptor expression was explored at the end of each protocol (Figure 15).

This subproject included a confirmatory experiment performed in rats, in which changes in mechanoreceptor expression were assessed after HF induction or exercise training. Ten-week-old Wistar rats were subjected to either TAC surgery or to moderate exercise training (see Sections 3.2.2 and

3.2.3). Echocardiographic studies were performed at baseline and at the end of both protocols. Cardiac remodelling assessment and mechanoreceptor expression analyses were performed at the end of each procedure (Figure 16).

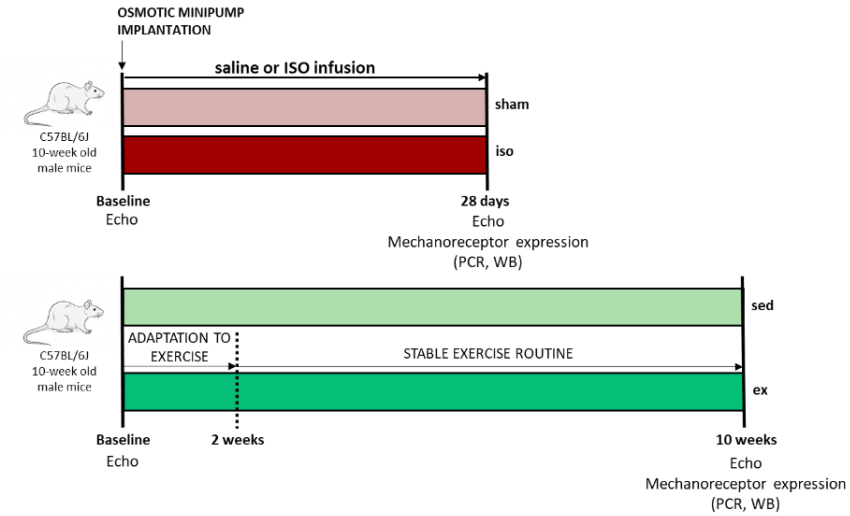

Figure 15. Outline of the procedures and groups of animals used to explore the changes in cardiac mechanoreceptor expression in adverse and adaptive cardiac remodelling.

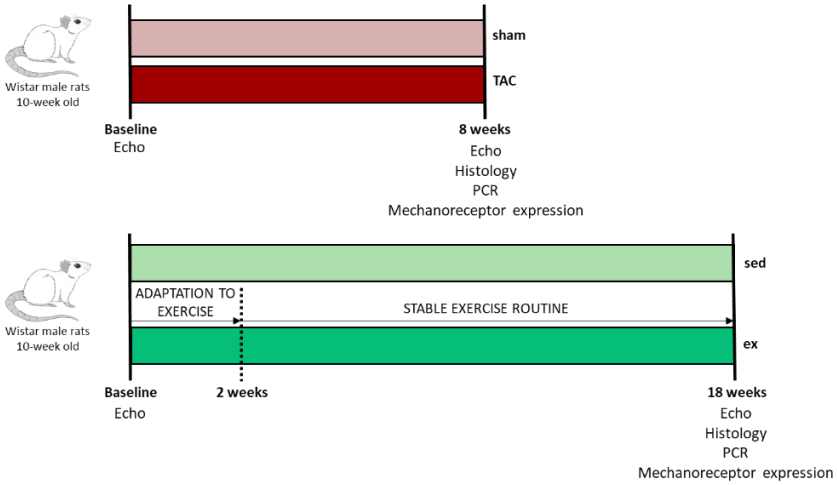

Figure 16. Outline of the validation study of changes in mechanoreceptor expression in adverse and adaptive cardiac remodelling performed in rats.

3.3.4. CHRONOLOGY OF ADVERSE CARDIAC REMODELLING AND CHANGES IN MECHANORECEPTOR EXPRESSION

This experiment was designed to characterize the chronology of adverse remodelling promotion and the expression of mechanoreceptors over time. A group of 10-week-old B57BL/6J male mice were infused with isoproterenol and sacrificed at different timepoints (3, 7, 14 and 28 days). Echocardiographic measurements were taken at baseline, 14 and 28 days, whereas post-mortem studies (cardiac weight, histology and gene and protein expression analyses) were performed after sacrifice (Figure 17).

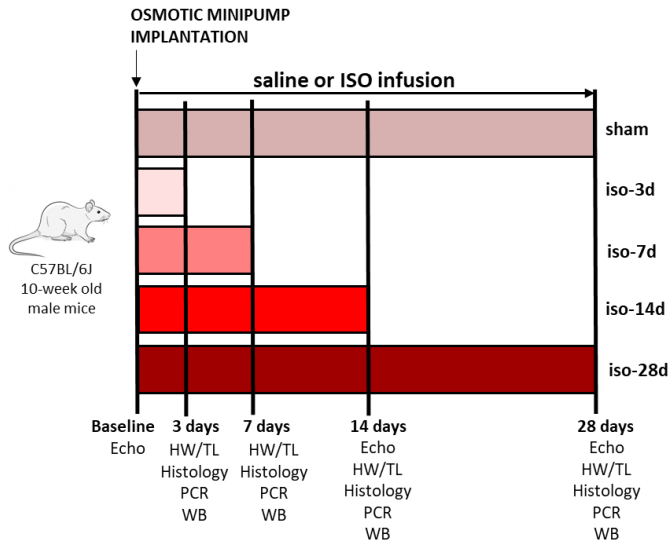

Figure 17. Schematic representation of the groups of animals used to characterize the chronology of adverse cardiac remodelling and mechanoreceptor expression over time.

3.3.5. EFFECTS OF TRPV4 GENETIC DELETION ON CARDIAC ADVERSE REMODELLING

This subproject embraces the majority of experiments performed in the present thesis. To evaluate the effects of TRPV4 deletion in the protection against adverse cardiac remodelling, transgenic TRPV4$^{+/+}$ (WT) and TRPV4^{-}/$^{-}$

(KO) male and female mice were treated with isoproterenol or saline for 28 days. Echocardiographic studies were performed at baseline and after 28 days. Hypertrophy and fibrosis assessment were performed after sacrifice in all study groups by morphology, cardiac weight, histology, and gene expression analyses (Figure 18).

In a subset of animals, arrhythmia inducibility in isolated Langendorff-perfused hearts was assessed in TRPV4$^{+/+}$ and TRPV4$^{-/-}$ mice after HF induction at 28 days (Figure 18). Moreover, in another group of animals, fibroblasts (FB) were isolated and functional and mechanistic were performed at this timepoint (Figure 18). Functional studies aimed to assess Ca^{2+} dynamics in all study groups. Mechanistic studies to study signalling pathways that could be affected by TRPV4 deletion were performed by protein analysis, activity assays and immunofluorescence (IF).

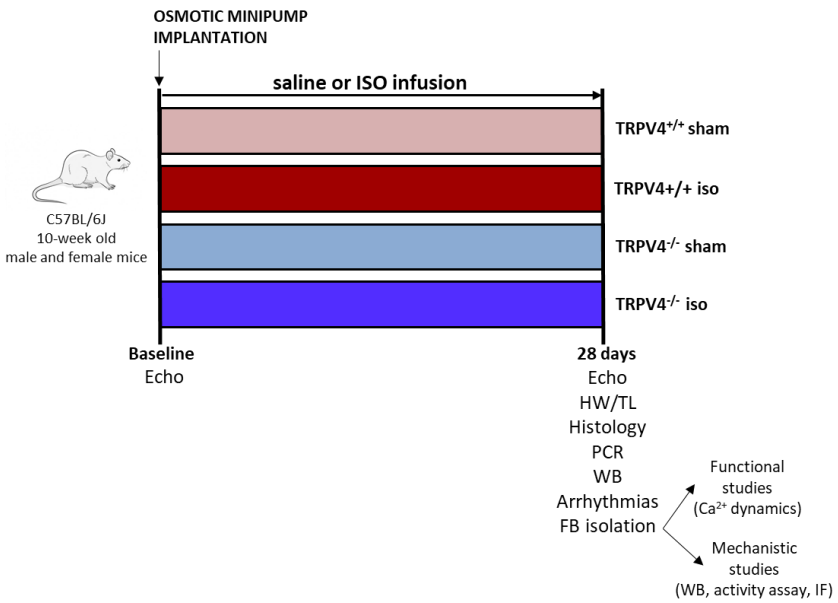

Figure 18. Outline of the experiments performed to evaluate the effects of the deletion of TRPV4 in the protection against adverse cardiac remodelling.

3.3.6. EFFECTS OF AGE IN THE PROMOTION AND REVERSAL OF ADVERSE REMODELLING

This subproject represents a final experiment that aimed to provide preliminary results and set the basis for future experiments about the role of TRPV4 in pathological cardiac remodelling. Ten-week-old (YOUNG) and 22-month-old (AGED) female B57BL/6J mice were infused with isoproterenol or saline for 28 days. A group of animals were sacrificed at 28 days, but another subset was kept for 28 additional days without receiving any treatment to assess for a potential recovery of the cardiac remodelling. Echocardiographic studies were performed at baseline, at 28 days, and additionally at 56 days if indicated (Figure 19). Histology and gene expression studies were performed at the final timepoint for each subgroup of animals.

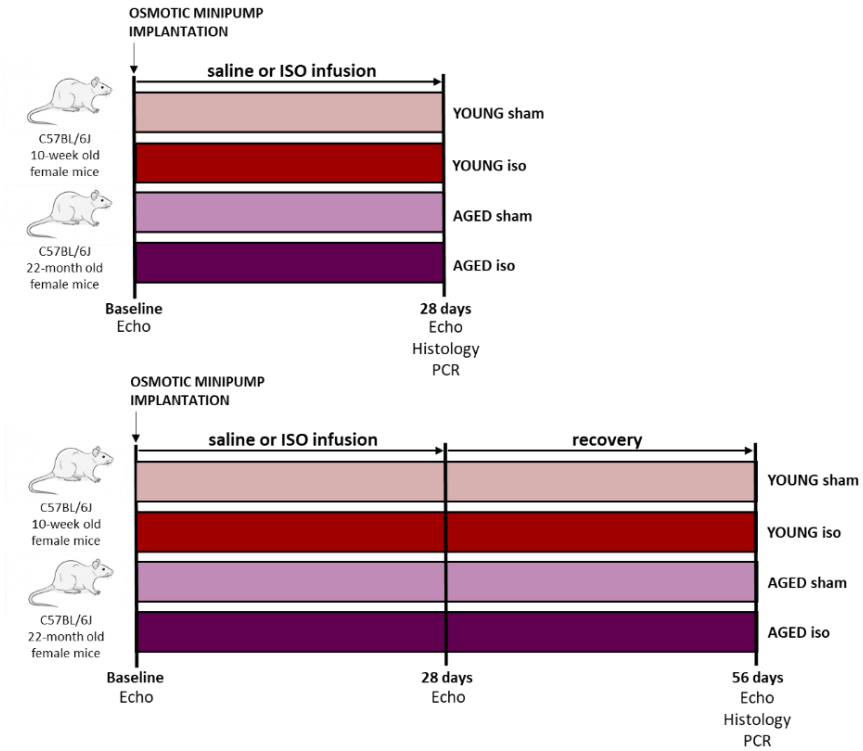

Figure 19. Schematic representation of the groups of animals and experiments performed to assess the effects of ageing in the promotion and recovery of adverse cardiac remodelling and potential role of TRPV4.

3.4. ECHOCARDIOGRAPHIC STUDIES

Repeated transthoracic echocardiographic studies were performed to assess morphological and functional cardiac variations in animal models of ventricular remodelling. Echocardiographic acquisitions were taken at different timepoints depending on the animal model (see Section 3.3). Echocardiograms were carried out under general anaesthesia with 2% isoflurane using a Vivid IQ and L8-18 Linear Array 5-15 MHz echograph (General Electric Health Care, Horten, Norway).

Animals were placed in supine position on a heating pad to maintain body temperature, and its four limbs were fixed. The thorax was shaved with a depilatory cream (Veet®). A thin layer of transmission gel was applied on the left hemithorax to improve ultrasound transduction, and hearts were imaged in parasternal short and long-axis projections. M-mode echocardiograms of the mid-ventricle were recorded at the level of the papillary muscles. M-mode images were used to measure the following parameters of the left ventricle: left ventricular diameter at the end of the systole (LVEDs) and the diastole (LVEDd), intraventricular septum thickness (IVS), and left ventricular posterior wall thickness (LVPW). Systolic function was assessed by LV fractional shortening (FS), calculated by ((LVDd-LVDs)/LVDd)*100 and ejection fraction (EF), calculated by the formula packed in GE Healthcare Ultrasound Vivid 7 system and proposed by the American Society of Echocardiography [285]. The left atrium (LA) diameter was measured in the long axis. The average of 3 consecutive cardiac cycles was used for each measurement. All measures were taken blinded.

3.5. HEART WEIGHT

After euthanasia, the chest was opened, the heart was excised, and the tibia was separated and dissected from the surrounding tissue. The extracted hearts were blotted on dry paper and weighed on a precision balance. Tibial

length was calculated by measuring the exposed tibia with a digital calliper. The heart weight/tibia length (HW/TL) ratio was used as a parameter of hypertrophy.

3.6. HISTOLOGY

The LV of the heart samples were cut in transverse cross-sections and fixed in buffered 4% formaldehyde for at least 24 h to preserve tissues for histological analysis. The day after, tissues were placed in histological cassettes and embedded in paraffin, in order to exchange the tissue water with paraffin. First, tissue sections were dehydrated by soaking them in a series of ethanol solutions (deionized H_2O, 70%, 96%, and 100% ethanol). Next, and because ethanol and paraffin are largely immiscible, tissue sections were cleared using xylene, an intermediate solvent fully miscible with both ethanol and paraffin. Finally, sections were embedded in hot paraffin. After paraffin inclusion, pieces were placed on a steel mold, and paraffin was poured over to form a paraffin block. Afterwards, tissues were cut into 4 µm-thick sections with a manual microtome (Leica). The sections were immediately placed in a hot water bath and floated onto polysine-coated slides.

Slices were then stained with several histological stains. First, heart sections were deparaffinized and rehydrated by immersing sections in xylene, decreasing concentrations of ethanol solutions (ethanol 100%, 96%, and 70%), and tap water. Then, the desired staining was performed, and sections were dehydrated again (ethanol 70%, 96%, 100%, and xylene-eucalipthol) and mounted with DPX mounting media.

3.6.1. HAEMATOXYLIN AND EOSIN STAINING

The haematoxylin and eosin (H&E) stain, a common experimental method, was used to evaluate CM cross-sectional area. Briefly, LV sections were placed in Harris haematoxylin (Sigma), washed with running tap water, quickly submerged in acid alcohol (70% ethanol, 1% hydrochloric acid), and alkaline

water until stains turned blue. Then, the slides were placed in eosin (Sigma) and washed briefly with running tap water.

To evaluate CM hypertrophy, random photomicrographs of each heart section were taken using an Olympus BX60 microscope coupled with a QI-imaging Q-cam at 400x magnification. LV CM cross-sectional area (CSA) was measured by outlining round to cuboidal-shaped nucleated CM. At least 30 random CM from each slice were measured using the ImageJ software (Image J, U.S. National Institutes of Health). All measured were taken and analysed blinded.

3.6.2. PICROSIRIUS RED STAINING

Tissue sections were stained with Picrosirius red for quantification of collagen deposition. In brief, LV sections were placed in picrosirius solution (Saturated aqueous solution of picric acid 0.1% Sirius Red) for 1 hour followed by a wash in acidic water (5% acetic acid). Collagen deposition is stained in red, while intact tissue is stained in yellow.

Ten representative ventricular photomicrographs per animal were acquired at 40X with an Olympus BX60 microscope and a QI-Imagin-Q-cam and quantified as percentage of collagen deposition with an automated colour recognition processing plugin from Image J. Perivascular, pericardial and endocardial collagen were excluded from measurements. All measures were taken and analysed blinded.

3.7. ASSESSMENT OF ARRHYTHMIAS

Spontaneous and inducible ventricular arrhythmias were studied in isolated mice hearts perfused in a Langendorff system. A first evaluation was performed in normoxic conditions, but because arrhythmia triggering in small hearts is characteristically challenging, a second evaluation was performed after inducing regional ischemia.

3.7.1. LANGENDORFF PERFUSION

Immediately after sacrifice, the whole heart was removed and transferred into an ice-cold saline solution as quickly as possible to avoid any detrimental effects of hypoxia. Then, the heart was directly cannulated via the aorta into a standard Langendorff perfusion system. The heart was secured with a 3-0 suture, and the excess of lung tissue was removed. Hearts kept beating with a retrograde perfusion through the aorta at a constant flow with an oxygenated (95% O_2: 5% CO_2) Krebs solution at 37 ºC (118 mM NaCl, 4.7 mM KCl, 1.2 mM $MgSO_4$, 1.8 mM $CaCl_2$, 25 mM $NaHCO_3$, 1.2 mM KH_2PO_4, 11 mM glucose, pH 7.4), adjusted to produce a perfusion pressure of 80-90 mmHg (normoxic environment). LV pressure was monitored using a water-filled latex balloon placed in the LV, inflated to obtain a LV end-diastolic pressure between 6 and 8 mmHg, and connected to a pressure transducer.

3.7.2. ELECTROGRAM RECORDINGS

Arrhythmogenesis under normoxic and ischemic conditions were monitored in isolated mouse hearts by electrogram recordings using stainless steel electrodes (model 6491 unipolar pediatric temporary pacing lead, Medtronic) placed in the LV base and the aortic cannula. Bipolar electrograms between the ventricular electrode and the one placed at the cannula were used to monitor ventricular arrythmias at baseline and during regional ischemia. Signals were amplified, digitized at 2 kHz, and stored for later analysis using PowerLab/8SP data acquisition System and Chart 5.0 (AD Instruments).

3.7.3. ELECTROPHYSIOLOGICAL STUDIES

The electrophysiological study protocols were initiated after 20 mins of stabilization. First, spontaneous arrythmias were examined during 5 minutes before starting the pacing protocol.

Then, arrhythmia inducibility was assessed by ventricular stimulation. Electrical stimulation was achieved using paired stainless-steel electrodes

(model 6491 unipolar pediatric temporary pacing lead, Medtronic) placed in the apex of the LV. Regular pacing was set at 2V using rectangular pulses of 1 ms duration. A modified version of a previously validated stimulation protocol [286] was used to induce ventricular tachyarrhythmias (VTA). First, ventricular effective refractory period was calculated by applying a premature stimulus (S2) at the pacing site after a train of 18 stimuli (S1). The effective refractory period was defined as the longest S1-S2 interval that produced a propagated response. VTA were thereafter induced using a protocol of programmed electrical stimulation, which is represented in figure 20. To begin with, repetitive trains of 18 stimuli (S1) were delivered at a basal cycle length (BCL) of 100 ms, followed by a premature extra stimulus (S2) introduced by 2 ms-decrements, starting at 60 ms or at an interval 5 ms longer than the effective refractory period. Subsequently, a second and third extrastimuli were progressively introduced (S3-S4) following the same principle (Figure 20). Arrhythmia induction was further assessed after burst pacing at rates of 50, 40 and 30 ms during 5 s, each cycle repeated three consecutive times. Induced arrhythmias were recorded if occurred within the first 3 s after the last stimulus. The same stimulation protocol was repeated after regional ischemia.

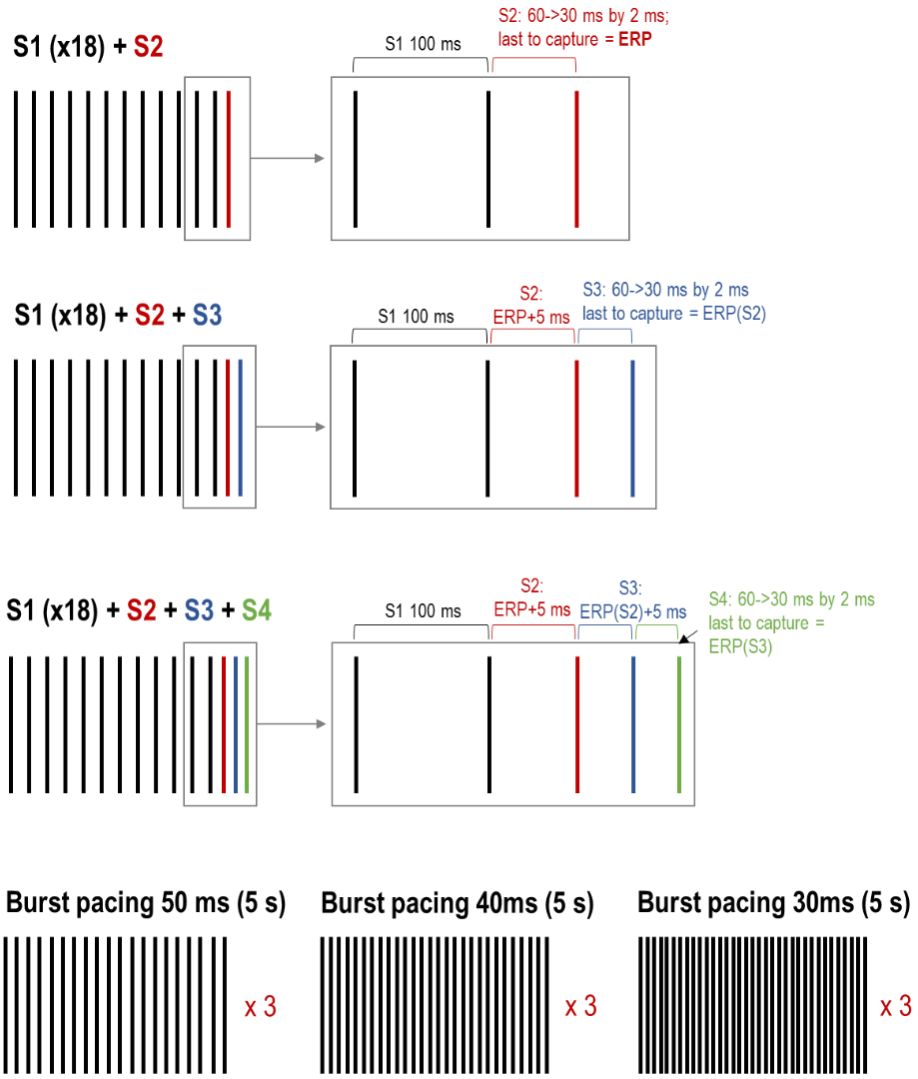

Figure 20. Programmed electrical stimulation protocol used to induce ventricular tachyarrhythmias (VTA) in isolated mouse hearts perfused in a Langendorff system. First, trains of 18 stimuli (S1) at a basal cycle length of 100 ms followed by 1 up to 3 extra stimuli (S2-S4) introduced by 2 ms-decrements, were applied. The protocol finished with 3 cycles of burst pacing at cycles of 50, 40, and 30 ms.

3.7.4. INDUCTION OF REGIONAL ISCHEMIA

In Langendorff-perfused hearts, regional ischemia was induced by ligature of the left descending coronary artery using a 6.0 silk snare placed 2-3 mm distal to its origin. Successful coronary occlusion was verified by assessing changes in the ECG (ST-segment elevation) and an increase in LV perfusion pressures. During ischemia, hearts were immersed in normal saline solution 0.9% NaCl. Spontaneous arrythmias were analysed for a 5-minute period starting 15 min after the ischemia, and inducibility of VTA was tested thereafter.

At the end of the protocol, the size of the ischemic area, or area at risk (AAR), was measured in all hearts. To do so, the hearts were perfused with 0.5 mL of 5% Evans Blue diluted in saline, which stained the entire myocardium, except for the area irrigated by the ligated artery. The non-stained area was considered the AAR. Stained hearts were then cut into 4 transversal slices and photographed under white light. Afterwards, each slice was weighed. Digitized images were measured semi-automatically with the software Image Pro-Plus (Media Cybernetics). The AAR and the total area (TA) of each slice were normalized to the heart's weight. The final AAR and TA were calculated summing up the values of all 4 slices as follows: AAR/TA (%) = ($\sum AAR_{1-4} / \sum TA_{1-4}$) *100.

3.8. ISOLATION OF MOUSE VENTRICULAR CARDIOMYOCYTES AND FIBROBLASTS

Mouse ventricular CM and FB were isolated on a Langendorff setup. Hearts were mounted on the Langendorff system as described in section 3.7.1. First, the heart was retrogradely perfused through the aorta with an oxygenated Krebs solution at 37 °C to wash residual blood. Flow was kept constant, adjusted to produce a perfusion pressure of 80-90 mmHg. Then, the heart was digested with a Krebs solution containing 0.4 mg/mL type 2 collagenase (Worthington, Biochemical Corporation) during 20 minutes. After enzymatic

digestion, the heart was removed from the cannula and the atria were separated. The LV was minced into small pieces and placed in a 15 mL Falcon containing the same enzymatic solution. The digestion was continued by pipetting for 10 more minutes. The resulting cell suspension was then filtered through a 180 µm pore size mesh, to remove any undigested tissue and debris, and centrifuged at 25 g for 3 minutes. The pellets, which contained the CM fraction, were stored at -80 ºC. Supernatants were meshed again through a 40 µm cell stainer (Thermofisher) and the non-myocyte fraction (containing FB) was pelleted by centrifugation at 650 g for 5 minutes.

3.9. REAL TIME qPCR

3.9.1. SAMPLE PREPARATION FROM LV SAMPLES

The LV heart tissue was disrupted by carefully grinding samples to a fine powder using a stainless-steel homogenizer submerged on dry ice. Once ready, lysis buffer RA1, containing denaturing chaotropic ions, 1% β-mercaptoethanol and 1% triton-x-100 (Macherey-Nagel), was added. Additional disruption with proteinase K was performed to remove high levels of proteins and connective tissue. Lysates were then centrifuged at 11.000 g for 1 minute, and the supernatant was kept for further RNA isolation.

3.9.2. SAMPLE PREPARATION FROM CARDIOMYOCYTE AND NON-CARDIOMYOCYTE CELLULAR FRACTIONS

Isolated CM and non-CM (see section 3.8 for isolation process) were lysed by adding directly to the cellular pellet the RA1 lysis buffer supplemented with 1% β-mercaptoethanol. To reduce viscosity, lysates were filtered through an inert column, and filtrates were kept for subsequent RNA isolation.

3.9.3. RNA ISOLATION

Total RNA was isolated using the Nucleospin RNA Extraction Kit (Macherey-Nagel) following the manufacturer's instructions. After the sample lysis, 70%

ethanol was added, and samples were loaded into the columns. Contaminating DNA was removed by an rDNase solution added directly onto the silica membrane. Washing steps with two different buffers were used to remove salts, metabolites, and macromolecular cellular components. Pure RNA was finally eluted under low ionic strength conditions with RNase free H_2O. Total RNA concentration was measured with the NanoDrop 2000 (Thermofisher) and samples with a 260/280 ratio of ≥1.8 were accepted as pure and used for gene expression analysis.

3.9.4. cDNA SYNTHESIS

RNA was reverse transcribed into cDNA using a High-Capacity cDNA Reverse Transcription kit (Applied Biosystems). The reaction was carried out in 0.2 mL tubes containing 10 µL of the desired amount of RNA and 10 µL of retrotranscription mix (2 µL of 10X RT Buffer, 0.8 µl of 25X dNTP Mix (100 nM), 2 µL of 10X Random Primers, 1 µL of MultiScribe Reverse Transcriptase, 4.2 µL nuclease-free water) in an iCycler thermal cycler (Bio-Rad). The thermal cycler was programmed to run a single cycle of 25 °C for 10 minutes, 37 °C for 120 minutes, 85 °C for 5 minutes. Samples were kept at 4 °C until use.

3.9.5. QUANTITATIVE POLYMERASE CHAIN REACTION

cDNA products were used to determine expression levels by real time quantitative PCR (RT-qPCR). Expression levels were measured in triplicate in a 7900HT Fast Real-Time PCR System (Applied Biosystems) using Taqman Universal PCR master mix (Thermofisher) and predesigned gene-specific probes labelled with FAM (green fluorescent fluorophore 6 carboxyfluorescein) (Thermofisher, see Table 3). GAPDH was used as an endogenous control for normalization.

The real-time PCR system enables detection and quantification of nucleic acid sequences, by detecting the changes in fluorescence signalling over the cycles. The amplification program consisted in 40 cycles of 15 seconds at 95 °C

followed by 1 minute at 60 °C. Cycle threshold (Ct) values were obtained for all target genes, and gene expression levels calculated as the difference between the Ct value of each target gene and the one of GAPDH (ΔCT). Experimental groups were compared expressing the relative mRNA levels as fold change (FC) over control group (value=1) following the formula $2^{-\Delta\Delta Ct}$ [287].

Gene	Assay ID	Gene	Assay ID
GAPDH	Mm99999915_g1	TRPM7	Mm00457998_m1
COL1A1	Mm00801666_g1	TRPA1	Mm01227437_m1
COL3A1	Mm00802300_m1	TRPV1	Mm01246302_m1
ACTA1	Mm00808218_g1	TRPV2	Mm00449223_m1
TRPC1	Mm00441975_m1	TRPV4	Mm00499025_m1
TRPC3	Mm00444690_m1	PIEZO1	Mm01241544_g1
TRPC4	Mm00444280_m1	KCNMA1	Mm01268570_m1
TRPC5	Mm00437183_m1	KCNJ8	Mm00434620_m1
TRPC6	Mm01176083_m1	KCNJ11	Mm00440050_s1
TRPM3	Mm01210379_m1	KCNK2	Mm01323942_m1
TRPM4	Mm00613173_m1		

Table 3. Thermofisher code of the predesigned Taqman probes labelled with FAM (green fluorescent fluorophore 6-carboxyfluorescein) and used for the analysis of gene expression by RT-qPCR.

3.10. WESTERN BLOTTING

3.10.1. SAMPLE PREPARATION AND QUANTIFICATION

For Western Blotting experiments, LV tissue were homogenized in RIPA buffer containing: 50 mM Tris Base, 150 mM NaCl, 10 mM EDTA, 0.1% SDS, 0.5% Na-deoxycholate, 1% Triton-X-100, 10 mM NaF, 2 mM Na_3VO_4, and 1% protease inhibitor, pH 7.3. Sample homogenates were centrifuged at 15.000 g for 15

min at 4 ºC, and supernatants were stored at -80 ºC. Protein concentrations were quantified with the Bradford method.

3.10.2. GEL ELECTROPHORESIS

Tissue protein homogenates were resolved on a sodium dodecyl sulphate-polyacrylamide gel electrophoresis (SDS-PAGE) in denaturing conditions. Stacking gel was prepared with 4% acrylamide, 0.125 mM Tris base, 0.1% SDS, 0.05% ammonium persulfate (APS), and 0.1% tetramethylethylenediamine (TEMED) (pH 6.8), to allow proteins to migrate freely and enter the gel all at once. Running gel was prepared with 10% acrylamide, 0.375 mM Tris base, 0.1% SDS, 0.05% APS, and 0.1% TEMED (pH 8.8) to allow proteins to resolve according to their molecular weight. Forty µg of protein homogenates, diluted in Laemli loading buffer 2x, were loaded onto the gels, together with a molecular weight standard ladder (Mini-protean III, Bio-Rad). Gels ran at a constant amperage of 20 mA for 2h in electrophoresis buffer (25 mM Tris base, 192 mM glycine, 0.1% SDS, pH 8.3).

3.10.3. IMMUNOBLOTING

Proteins were then transferred onto nitrocellulose *Hyband ECL* membranes (Amersham Biosciences) at a constant voltage of 100V for 90 min at 4 ºC in transfer buffer (Tris base 25 mM, glycine 20 mM, methanol 20%). Afterwards, membranes were blocked in 5% non-fat milk/Tris Buffered Saline-Tween (TBS-T, 20 mM Tris-base, 150 mM NaCl, 0.1% Tween20, pH 7.4) for 1 h at room temperature and incubated in blocking buffer overnight at 4 ºC with antibodies against TRPV4 (ACC034), Alomone, diluted 1:500 in blocking buffer), TRPC6 (PA5-77308 (1:500) and PA5-29848 (1:1000), Thermofisher) and GAPDH (GT239 (1:10000), Genetex) as the endogenous control. On the following day, membranes were rinsed 3 times with TBS-T and incubated with the secondary peroxidase-conjugated IgG in blocking buffer for 1h at room temperature. After rinsing again, they were developed at room temperature

with ECL Prime Western Blotting Detection Reagent (Amersham Biosciences). Protein bands were captured using an Odyssey FC Imaging System (LI·COR) and band intensities were measured by densitometry scanning using Image Studio Lite software. Target proteins were normalized to GAPDH, that served as a loading control.

3.11. CARDIAC FIBROBLAST CULTURES

Isolated cells from the non-myocyte fraction (see section 3.8 for isolation process) were plated on 6-well plates. Cells were cultured in DMEM (ATCC 30-2002) supplemented with 10% FBS and 2% penicillin/streptomycin and incubated at 37 ºC 5% CO_2 for 2 hours and washed afterwards. At that time, all viable FB are attached on the plate, while other cell types found in the non-myocyte fraction remain floating. Therefore, this washing step is key to purify FB from the other cell types, as well as helping to remove cell debris. After 24 hours, the medium was changed, and FB were allowed to grow until full confluence (approximately at 5 days). Thereafter, FB were trypsinized and seeded for final experiments (see Sections 3.12, 3.13 and 3.14).

3.12. FLUORESCENCE CALCIUM IMAGING IN FIBROBLASTS

Passage-1 FB were seeded at a density of $2x10^5$ cells/well on 96 well-plates and allowed to grow for 24 hours. The calcium sensitive dye Fluo-4 AM (5 µM) was used to measure changes in the concentration of intracellular calcium. Fluorescence was continuously monitored at an excitation wavelength of 488 nm and emission of 528 nm with the microplate reader SpectraMax ID3 (Molecular Devices). To load the cells with the dye, cells were rinsed with an isotonic solution (~300 mOsm) containing: 139 mM NaCl, 3.6 mM KCl, 1 mM $CaCl_2$, 1.2 mM $MgSO_4$, 10 mM HEPES, 5mM glucose, pH 7.4. Then, FB were loaded with Fluo-4 AM for 30 minutes at 37 ºC. Following incubation, cells were washed with isotonic solution for 30 minutes at 37 ºC.

Basal intracellular calcium concentration was first recorded, measuring the fluorescence every 15 seconds during 90 seconds (basal fluorescence, F_0). After that, cells were treated either with one of the following TRPV4 activators: GSK1016790A (GSK, 100 nM) or an hypoosmotic solution (~140 mOsm) containing: 50 mM NaCl, 3.6 mM KCl, 1 mM $CaCl_2$, 1.2 mM $MgSO_4$, 10 mM HEPES, 5 mM glucose, pH 7.4. Measurements were continued every 3 seconds up to 3 minutes. To enhance changes in cytosolic calcium, the calcium reuptake to the endoplasmic reticulum was inhibited by adding 1 µM of thapsigargin, the sarco/endoplasmic calcium ATPase (SERCA) inhibitor. In some experiments FB were preincubated with 10 µM HC067047 (HC), the TRPV4 antagonist, during 3 minutes before adding GSK or the hypoosmotic solution. Both GSK and HC were dissolved in DMSO at a 10 mM stock concentration and were freshly diluted into their working solution just before use. Changes in intracellular calcium were calculated as the ratio of Fluo-4 fluorescence intensity at each time point relative to the basal fluorescence (F/F_0).

3.13. CALCINEURIN ACTIVITY ASSAY

A commercially-available calcineurin activity assay (Enzo, Life Sciences) was used to assess the activity of the phosphatase in cardiac FB. This is a colorimetric assay that measures calcineurin activity based on the changes in absorbance of the malachite green dye once it binds to the free phosphates released by the phosphatase when active.

3.13.1. SAMPLE PREPARATION AND PROTEIN QUANTIFICATION

Calcineurin phosphatase activity was measured in protein extracts collected from isolated non-myocyte fractions. Cells were thawed on ice and lysed with 75 µL of a lysis buffer containing 50 mM Tris, 0.1 mM EDTA, 0.1 mM EGTA, 1 mM DTT, 0.2% NP-40 and supplemented with protease inhibitor. Cell chunks were mechanically dissociated with a 27G needle. Cell lysates were then

centrifuged at maximum speed for 10 minutes at 4 °C, and supernatants were transferred to a fresh tube. Excess phosphate and nucleotides, which could interfere with the assay, were removed from the lysates using a desalting column. Protein concentration was measured with the Bradford Assay and total protein was diluted 1:2 in lysis buffer.

3.13.2. CALCINEURIN CELLULAR ACTIVITY ASSAY

The assay was performed in a 96-well plate. Phosphate standards were prepared by serial dilution of 80 µM of phosphate standard in 1x assay buffer. Calmodulin (CaM), essential for calcineurin activation, was diluted 1:50 in 2x assay buffer.

For each sample, background, total phosphatase activity and EGTA wells were prepared. Background wells contained 20 µL ddH_2O and 25 µL CaM assay buffer. Wells representing total phosphatase activity contained 10 µL ddH_2O and 25 µL CaM assay buffer. EGTA wells contained 10 µL ddH_2O and 25 µL 2x EGTA buffer. The lack of CaM in these wells, combined with the calcium chelator EGTA, resulted in the inhibition of the calcineurin activity. Hence, these wells allow to detect possible activity of other phosphatases in the samples. Positive control wells contained 10 µL ddH_2O and 25 µL CaM assay buffer. Figure 21 shows a schematic representation of the assay.

RII phosphopeptide, which is a calcineurin-specific substrate, was added to all wells except background and phosphate standard wells (Figure 21). To initiate the calcineurin assay, 5 µL of sample lysate was added to background, total, and EGTA wells. Purified recombinant calcineurin was diluted to 8U/µL prior to addition into the positive control wells. The microplate was incubated at room temperature for 30 minutes and after incubation the BIOMOL GREEN reagent was added and incubated for 30 minutes at room temperature. Absorbance at 620 nm was measured using the microplate Reader SpectraMax ID3 (Molecular Devices).

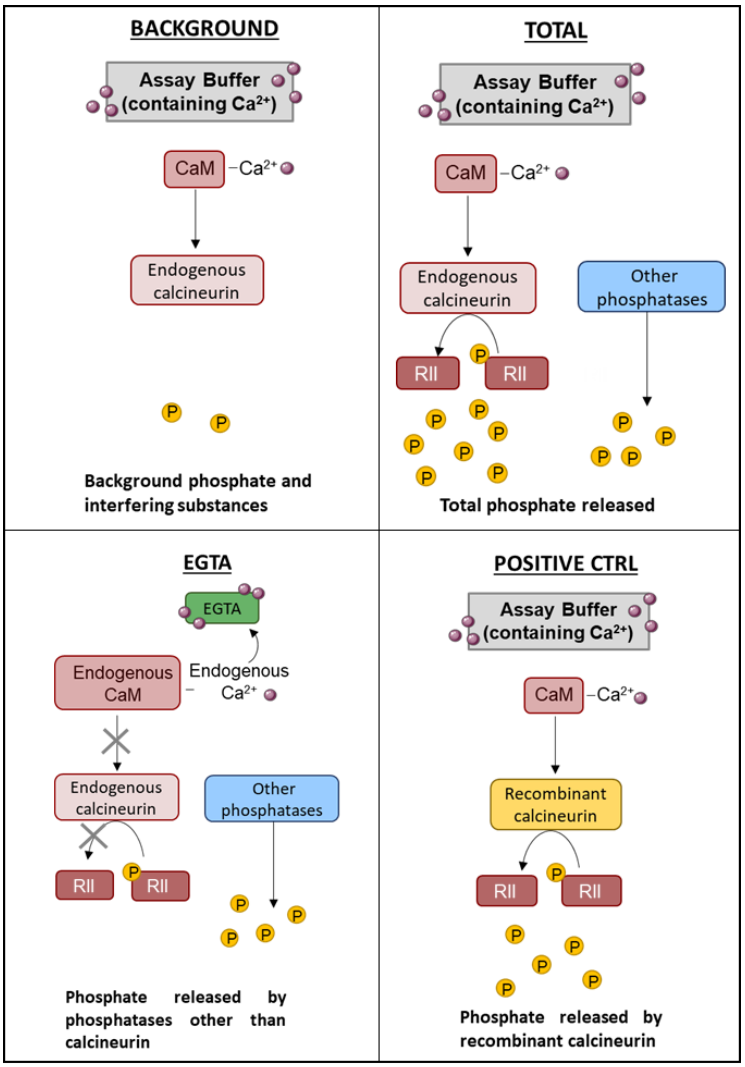

Calcineurin activity = TOTAL - BACKGROUND - EGTA

Figure 21. Schematic representation of the calcineurin activity assay. To assess calcineurin activity, 4 wells were prepared for each sample: background, total, EGTA, and positive control. Background wells, containing the sample and assay buffer with Ca2+ and calmodulin (CaM), were used to determine background phosphate and substances interfering with the assay. Total wells, containing the sample, assay buffer with Ca2+ and CaM, and RII phosphopeptide, were used to determine the total phosphate released. EGTA wells, containing the sample and the Ca2+ chelator EGTA, were used to determine the phosphate released by the activity of phosphatases other than calcineurin. The lack of Ca2+ and the sequestration of Ca2+ by EGTA inhibited the release of phosphate from the RII peptide due to calcineurin activity. Wells containing a recombinant calcineurin, assay buffer with Ca2+ and CaM, and RII phosphopeptide, were used as positive controls. Calcineurin activity was calculated by subtracting the absorbances of background and EGTA wells to that of total wells.

To infer calcineurin activity, absorbance from background and EGTA wells was subtracted. Resulting absorbances were converted to nmol of released phosphate using the standard curve, and this was normalized to total protein. Values were expressed as nmol of released phosphate per microgram of protein.

3.14. NFAT NUCLEAR TRANSLOCATION

As calcineurin activation results in NFAT translocation into the nucleus (See Introduction, Section *1.3.1.2.1*, Figure 8), immunofluorescence was used to determine the cytosolic or nuclear localization of NFAT in cultured FB. Briefly, FB were seeded at a density of $2*10^4$ in 8-chamber culture slides coated with 0.02% gelatin, and 5 µg/ml fibronectin and allowed to grow for 24h. FB were fixed in 4% formol and permeabilized with 0.2% tween-20 for 5 minutes. To block nonspecific binding sites, cells were blocked with 5% rabbit serum in PBS-tween (phosphate buffered saline, 0.1% tween-20) for 1 hour at room temperature. Primary antibodies (NFATc3, mouse ab219063 Abcam) diluted 1:100 in PBS 1% BSA 0.1% tween-20 were incubated overnight at 4 ºC. The day after, cells were washed three times with PBS and incubated with a secondary antibody anti-mouse conjugated to an Alexa Fluor 546 for 1 hour. After washing with PBS (x3), nuclei were stained with 5 ug/ml of Hoechst 3345 for 5 minutes at room temperature and cells were mounted with Immunohistomount media (Sigma Aldrich). Additionally, a negative and a positive control were added. The negative control followed the same protocol but in the absence of a primary antibody. The positive control was performed by inducing an activation of calcineurin by increasing the extracellular calcium concentration. FB were incubated with DMEM media containing 4 mM of calcium (by adding 2.2 mM of $CaCl_2$ to the standard medium) during 2 hours before fixation.

Images were acquired at 400x magnification using an Olympus FV1000 fluorescence microscope and analysed using ImageJ. NFAT translocation was measured as the ratio of mean fluorescence intensity of the nucleus relative to that of the cytosol. At least 30 isolated FB were measured per condition in 3 or 4 independent experiments.

3.15. STATISTICAL ANALYSIS

Analyses were performed using GraphPad Prism 6.0. Data are presented as mean ± the standard error of the mean (SEM). For variables following a Gaussian distribution, statistical analyses were performed using unpaired parametric t-test (for comparisons between 2 groups), or one way (for comparisons between 3 or more groups). If data did not respect normality, non-parametric tests were used. A two-way ANOVA was used to assess differences in the mRNA levels between CM and FB, where factors were cell type, and study group. A Two-way ANOVA was also used in most of the experiments performed in transgenic mice to evaluate the effects of TRPV4 deletion, where factors were genotypes ($TRPV4^{+/+}$ and $TRPV4^{-/-}$) and treatment group (sham and iso). Similarly, in the study addressed to determine the differences in remodelling between young and aged female mice, a two-way ANOVA was used with the factors being age and treatment group. All ANOVA and non-parametric analyses were followed by a Bonferroni post hoc correction when interaction was found. Since arrhythmia inducibility did not follow a Gaussian distribution, differences during normoxia and after ischemia were assessed by a non-parametric equivalent of a two-way ANOVA test (scheiner-Ray-Hare, SRH test). Differences were considered statistically significant when the p-value (p) was less than 0.05.

4. RESULTS

4.1. DIFFERENTIAL EXPRESSION OF MECHANORECEPTORS IN ADVERSE AND ADAPTIVE CARDIAC REMODELLING

We first aimed to determine the potential changes in mechanoreceptor expression accompanying the development of adverse and adaptive cardiac remodelling. Therefore, we established two different mouse models of cardiac remodelling: an adverse model of chronic infusion of isoproterenol (ISO), widely used to mimic HF [288] , and a model of daily training on a treadmill as a paradigm of adaptive remodelling induced by exercise. In addition, we validated our results in a rat model of adverse remodelling induced by TAC and in a rat model of adaptive remodelling induced by exercise.

4.1.1. CHRONIC INFUSION OF ISOPROTERENOL INDUCES CARDIAC ADVSERSE REMODELLONG IN MICE

A group of C57BL/6 male mice were subjected to a sustained perfusion of isoproterenol (for 28 days) by means of an osmotic pump. A first experiment was performed to determine the most appropriate dose of isoproterenol required to promote an adverse remodelling. Mice were infused with either saline (sham), 30 mg/kg/day (iso-30) or 60 mg/kg/day (iso-60) of isoproterenol for 28 days. We evaluated the development of pathological remodelling by assessing cardiac performance, hypertrophy, and interstitial fibrosis (see Sections 4.1.1.1, 4.1.1.2 and 4.1.1.3, Figures 22, 23 and 24).

4.1.1.1. Chronic isoproterenol infusion promotes ventricular dilatation and hypertrophy and cardiac dysfunction

Echocardiographic analyses were performed at baseline (before surgery) and at the end of the isoproterenol infusion (28 days). At baseline, no differences were observed between groups (data not shown). At 28 days, echocardiographic recordings revealed that both isoproterenol groups (iso-30

and iso-60) had increased end-diastolic left ventricular (LVDd) and end-systolic left ventricular (LVDs) volumes (Figure 22 A-B), compared to sham, indicating an LV dilatation. Mice in the iso-30 and iso-60 groups also showed increased intraventricular septum (IVS) thickness and enhanced left ventricular mass (LV mass) (Figure 22 C-D).

These morphological changes were accompanied by a significant decrease in ejection fraction (EF) and fractional shortening (FS) in both groups receiving isoproterenol compared to sham (Figure 22 E-F).

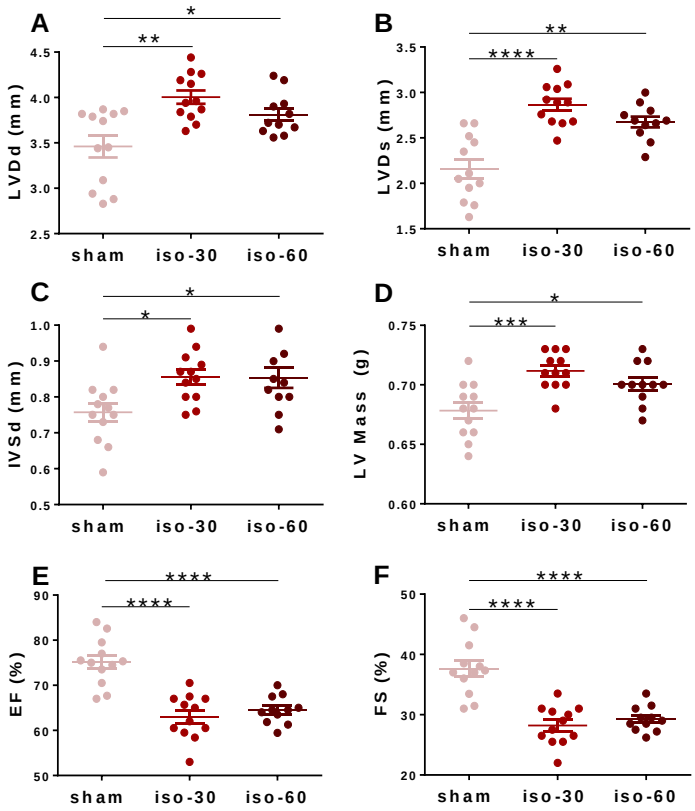

Figure 22. Echocardiographic parameters of male mice after 28 days of exposure to either saline (sham, pastel pink dots), or isoproterenol at a dose of 30 (iso-30, red dots) or 60 mg/kg/day (iso-60, brown-red dots). A) LVDd: End-diastolic left ventricular diameter. B) LVDs: End-systolic left ventricular diameter C) IVSd: intraventricular septum thickness measured in diastole. D) LV Mass: left ventricular mass measured in diastole. E) EF: ejection fraction. F) FS; fractional shortening. N=11-12 per group. * p<0.05; ** p<0.01; *** p<0.001; **** p<0.0001.

These findings indicate that chronic adrenergic stimulation by isoproterenol caused cardiac dilation and hypertrophy, and impaired cardiac function with both doses of isoproterenol.

4.1.1.2. Chronic isoproterenol infusion leads to cardiomyocyte enlargement and cardiac hypertrophy

Cardiac hypertrophy was further confirmed by morphometry, the heart weight/tibia length (HW/TL) ratio, and the CM cross-sectional area (CSA).

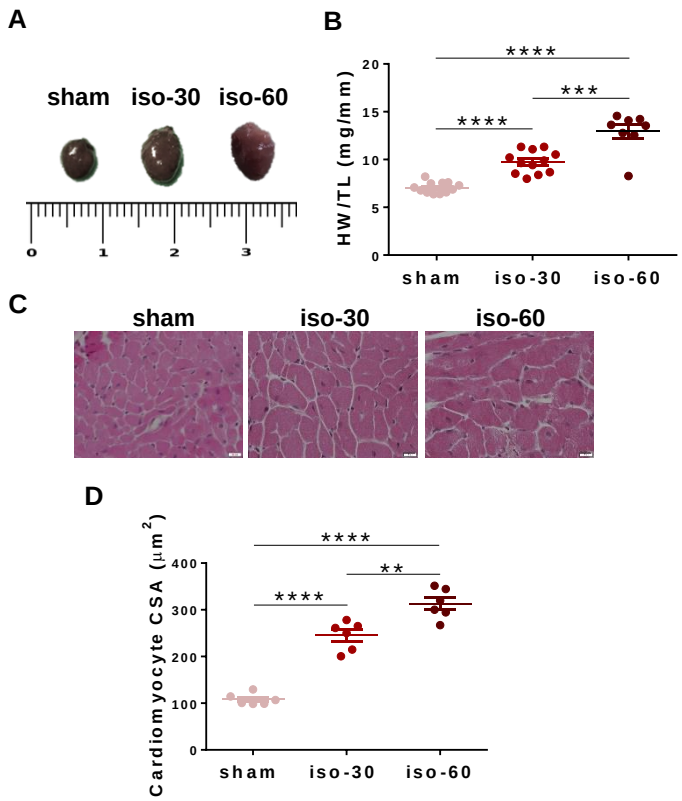

Figure 23. Post-mortem analysis of cardiac fibrosis at 28 days of saline (sham, pastel pink dots), or isoproterenol at a dose of 30 mg/kg/day (iso-30, red dots) or 60 mg/kg/day (iso-60 brown-red dots) infusion in male mice. A) Representative microphotograph (40X) of left ventricular cross-sections areas stained with picrosirius red, and B) Quantification of interstitial collagen deposition, expressed in percentage. Ten representative ventricular microphotographs per animal were measured, N=8 hearts per group. mRNA expression levels, normalized to GAPDH expression and expressed as fold change (FC) of D) Collagen type I (*col1a1*), E) Collagen type III (*col3a1*), and F) a-SMA (*acta1*). N= 8-12 animals per group. * p<0.05; ** p<0.01; **** p<0.0001.

After 28 days of saline or isoproterenol infusion, mice were sacrificed, hearts were extracted, and the length of the tibia was measured. As shown in Figure 23 A, hearts were markedly larger in the isoproterenol groups than in the sham group. Accordingly, the HW/TL ratio was increased in both isoproterenol groups, particularly in the iso-60 group. (Figure 23 B). We next assessed cell hypertrophy by staining heart sections with haematoxylin-eosin (H&E) and measuring the CM CSA. H&E staining revealed that CM CSA was enlarged in the isoproterenol groups compared to the sham group, and, again, the enlargement was significantly greater in the iso-60 then in the iso-30 group (Figure 23 C-D). These data indicate that isoproterenol induced CM hypertrophy that resulted in heart hypertrophy, and that these changes were more pronounced with increasing doses of isoproterenol.

4.1.1.3. Chronic isoproterenol infusion promotes cardiac fibrosis

Cardiac fibrosis was assessed by measuring collagen deposition in picrosirius red-stained LV sections. Fibrosis was further validated by gene expression of the fibrotic makers collagen type I (*col1a1*), collagen type III (*col3a1*), and α-smooth muscle actin, α-SMA (*acta1*) in LV samples. Histological analysis showed that isoproterenol groups had more collagen deposition than the sham group (Figure 24 A-B), which was further supported by increased mRNA levels of *col1a1*, *col3a1* and *acta1* in iso-30 and iso-60 mice compared to sham (Figure 24 C-E). Interestingly, unlike hypertrophy, fibrosis seemed to develop similarly in the two isoproterenol groups, both at the histological and at the gene expression level.

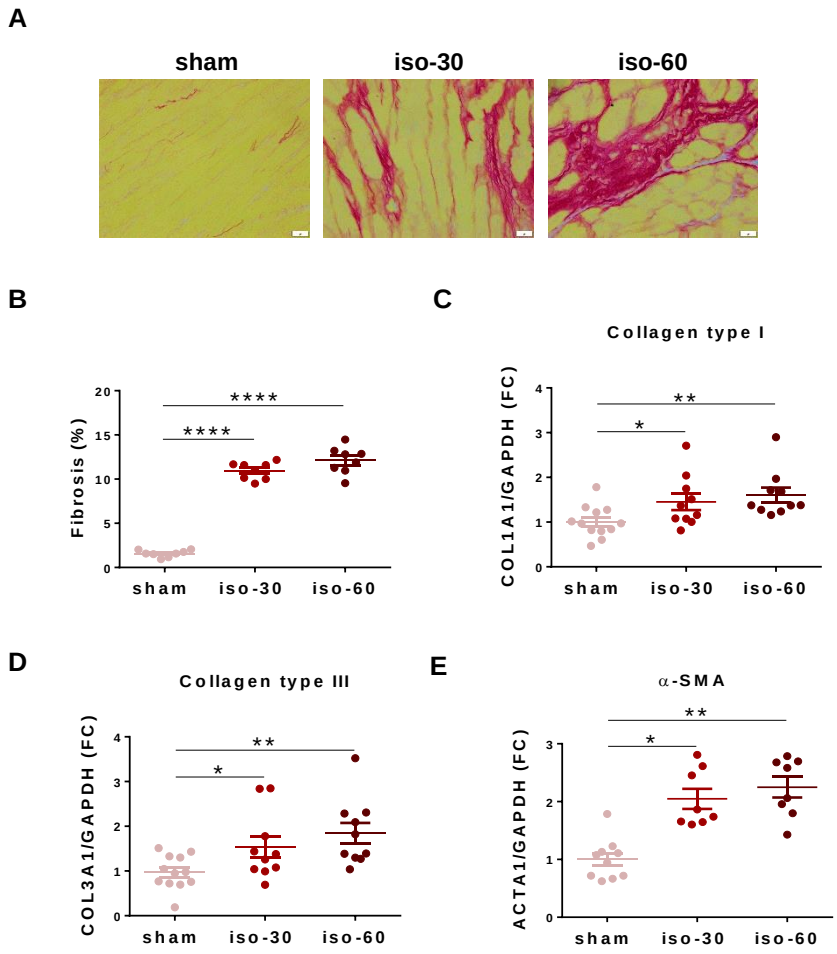

Figure 24. Post-mortem analysis of cardiac fibrosis at 28 days of saline (sham, pastel pink dots), or isoproterenol at a dose of 30 mg/kg/day (iso-30, red dots) or 60 mg/kg/day (iso-60 brown-red dots) infusion in male mice. A) Representative microphotograph (40X) of left ventricular cross-sections areas stained with picrosirius red, and B) Quantification of interstitial collagen deposition, expressed in percentage. Ten representative ventricular microphotographs per animal were measured, N=8 hearts per group. mRNA expression levels, normalized to GAPDH expression and expressed as fold change (FC) of D) Collagen type I (col1a1), E) Collagen type III (*col3a1*), and F) a-SMA (*acta1*). N= 8-12 animals per group. * p<0.05; ** p<0.01; **** p<0.0001.

In summary, chronic infusion of isoproterenol induced dilation and hypertrophy of the LV, and impaired cardiac function. At the cellular level, chronic isoproterenol induced CM hypertrophy and interstitial fibrosis. These

are all characteristic hallmarks of the pathological remodelling and confirm the appropriateness of our HF model. Except for CM and cardiac hypertrophy, which were greater after the iso-60 dose, all the remaining changes, including fibrosis, were similarly seen with the two doses of isoproterenol (iso-30 and iso-60). Therefore, thinking of the welfare of the animals, subsequent experiments were followed using exclusively the smallest dose that induced a HF phenotype, i.e., the iso-30 dose.

4.1.2. EXERCISE TRAINING ON A TREADMILL INDUCED CARDIAC ADAPTIVE REMODELLING IN MICE

A group of male mice were trained to run in a treadmill at a moderate (mod-ex) or an intense (int-ex) exercise routine for 8 weeks. The objective of testing two different programs of training was to determine if there were differential cardiac adaptations depending on the intensity of the exercise sessions. Following exercise training, cardiac function and structure were assessed.

4.1.2.1. Exercise training induced cardiac hypertrophy with preserved cardiac function

Echocardiographic analyses were performed at baseline (at the beginning of the exercise protocol) and after 8 weeks of exercise training. No differences were observed between groups at baseline (data not shown). M-mode images from echocardiographic studies taken 24 hours after the final exercise session revealed that mice in the exercise groups had cardiac dilation and hypertrophy compared to sedentary mice, as reflected by an increase in LVDd, LVDs, IVS thickness and LV mass (Figure 25 A-D)**.** Notably, both EF and FS remained preserved in mod-ex and int-ex animals (Figure 25 E-F)**.** These findings suggest that, in response to both moderate and intense training, our model generates changes consistent with adaptive cardiac remodelling, characterized by eccentric hypertrophy while preserving cardiac function.

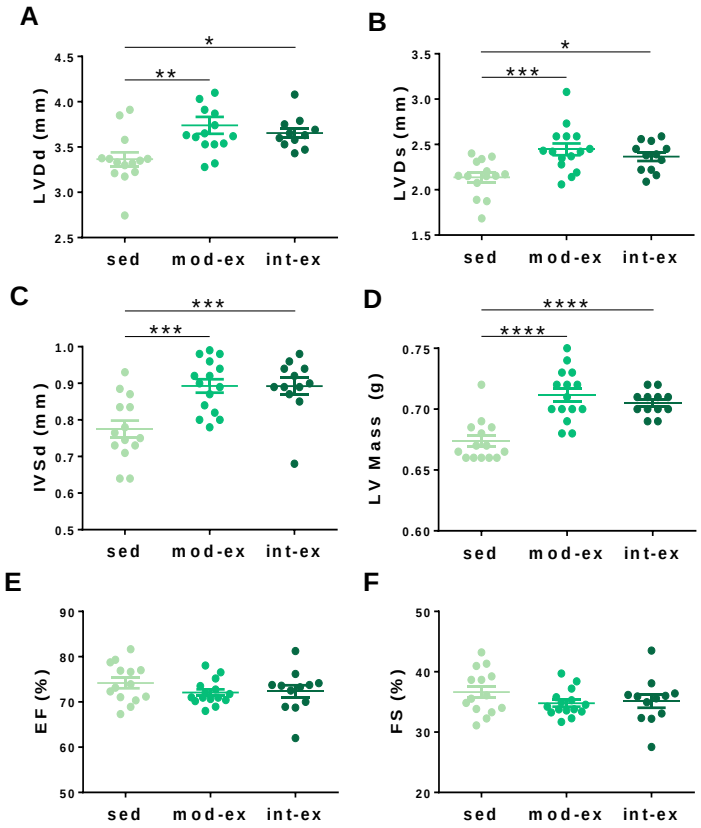

Figure 25. Echocardiographic parameters of male mice following 8 weeks of sedentary (sed, light green dots), moderate intensity exercise (mod-ex, green dots) or intense exercise (int-ex, dark green dots). A) LVDd: End-diastolic left ventricular diameter. B) LVDs: End-systolic left ventricular diameter. C) IVSd: intraventricular septum thickness measured in diastole. D) LV Mass: left ventricular mass measured in diastole E) EF: ejection fraction. F) FS; fractional shortening. N=11-12 per group. * p<0.05; ** p<0.01; *** p<0.001; **** p<0.0001.

4.1.2.2. Exercise training induced cardiac hypertrophy by increasing cardiomyocyte area

Anatomical examination of the hearts of mice following 8 weeks of exercise revealed that animals in the mod-ex and int-ex mice groups had an increased heart size compared to sed mice (Figure 26 A). This observation was validated with the HW/TL ratio, with mod-ex and int-ex animals having an increased ratio, compared to sed animals (Figure 26 B). CM CSA measures of transversal

LV sections stained with H&E also showed enlarged CM in mod-ex and int-ex compared to their sedentary counterparts. Comparing training intensities, we observed that int-ex mice displayed a non-significant trend to develop larger CM area than mod-ex mice (Figure 26 C-D), with no discernible changes in macroscopic hypertrophy.

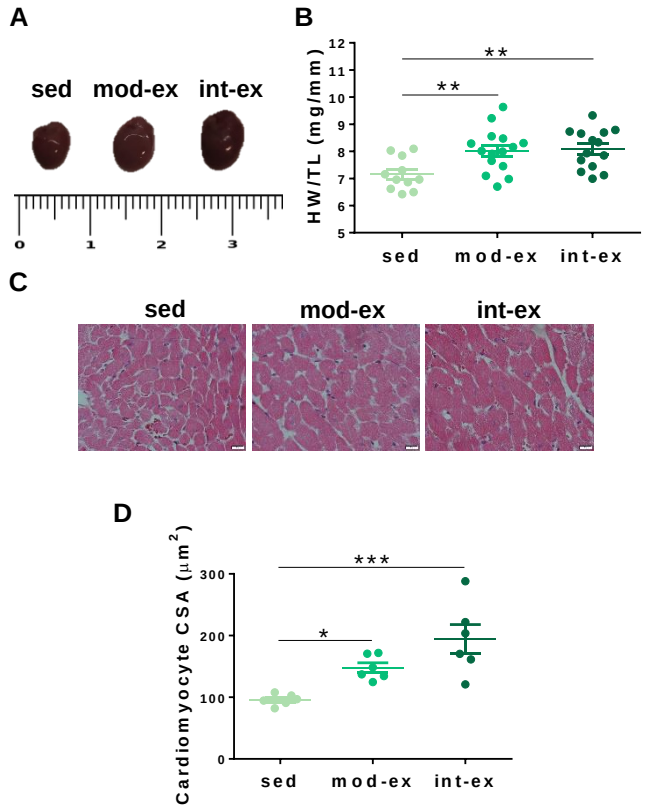

Figure 26. Post-mortem measurement of cardiac hypertrophy of male mice 8 weeks after sedentary (sed, light green dots), moderate intensity exercise (mod-ex, green dots) or intense exercise (int-ex, dark green dots) routine. A) Representative photo of the size of the heart of the different experimental groups, taken just after its extraction. A ruler (in cm) is provided for visual reference of the size. B) Analysis of HW/TL, N=11-15 animals per group. C) Representative microphotograph (40X) of the left ventricular cross-sections stained with H&E, and C) Quantification of the CM CSA. At least 30 cells per heart were randomly measured, N= 6 hearts per group. * p<0.05; ** p<0.01; *** p<0.001; **** p<0.0001.

4.1.2.3. Moderate exercise does not induce cardiac fibrosis whereas intense exercise induces a slight increase in collagen deposition in our model

Histological sections stained with picrosirius red revealed that moderate exercise did not increase collagen deposition, although a slight increase was observed in mice that followed an intense exercise routine (Figure 27 A-B). Note that, although significant, the percentage of fibrosis is still far from the one observed in the isoproterenol model (3.5% in int-ex compared to 13% in iso-30 and iso-60, Figure 24 B). Gene expression confirmed that *col1a1, col3a1* and *acta1*, indicators of FB differentiation, were similar between sed and mod-ex mice, whereas int-ex mice exhibited slightly higher *acta1* expression, with no changes in *col1a1, col3a1* expression (Figure 27 C-E).

In summary, moderate training induced fully adaptive cardiac changes characterized by eccentric hypertrophy with preserved cardiac function, and, at the cellular level, CM hypertrophy without interstitial fibrosis. Intensive training induced similar changes in echocardiographic studies but was accompanied by a mild degree of collagen deposition and increased expression of *acta1*, a fibrotic marker. We therefore conclude that only did the mod-ex group exhibit a full phenotype consistent with physiological remodelling, whereas the int-ex group seemed to show mild maladaptive features most likely due to excessive training potentially leading to animal distress.

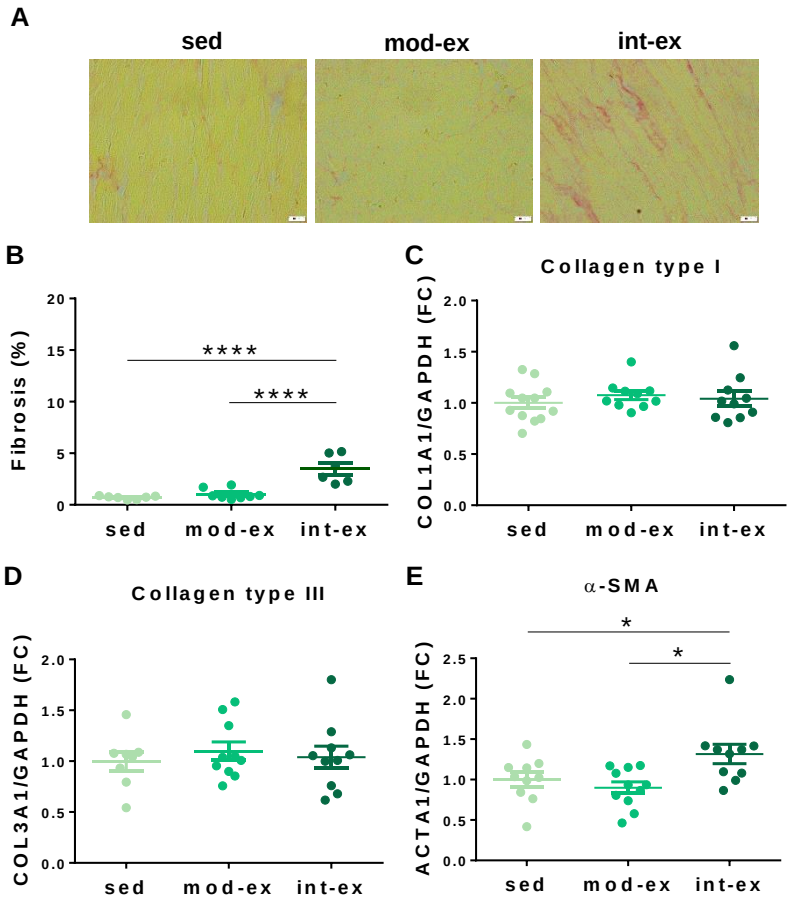

Figure 27. Post-mortem analysis of cardiac fibrosis of male mice 8 weeks after sedentary (sed, light green dots), moderate intensity exercise (mod-ex, green dots) or intense exercise (int-ex, dark green dots). A) Representative microphotograph (40X) of left ventricular cross-sections stained with picrosirius red, and B) Quantification of the interstitial collagen deposition. Ten representative ventricular microphotographs per animal were measured, N=6-8 hearts per group. mRNA expression levels normalized to GAPDH expression and expressed as FC of C) *col1a1*, D) *col3a1*, and E) *acta1*. N= 10-12 animals per group. *p<0.05; ****p<0.0001.

4.1.3. TRPV4 AND TRPC6 INCREASE IN MICE RECEIVING ISOPROTERENOL BUT NOT IN MICE SUBJECTED TO MODERATE EXERCISE TRAINING

Using exclusively the iso-30 dose (from now on referred as iso) and the moderate intensity exercise (from now on referred as ex) as established and

validated models of pathological and physiological remodelling, respectively, we performed a comprehensive qPCR analysis of the expression levels of all channels known to be cardiac mechanoreceptors. Our interest was to determine which mechanoreceptors were differentially expressed in the LV of animals exposed to both models, to identify potential targets that could explain, at least partially, the differential pathways activated in both types of cardiac remodelling.

Results of the gene expression studies are shown in Figures 28 and 29.

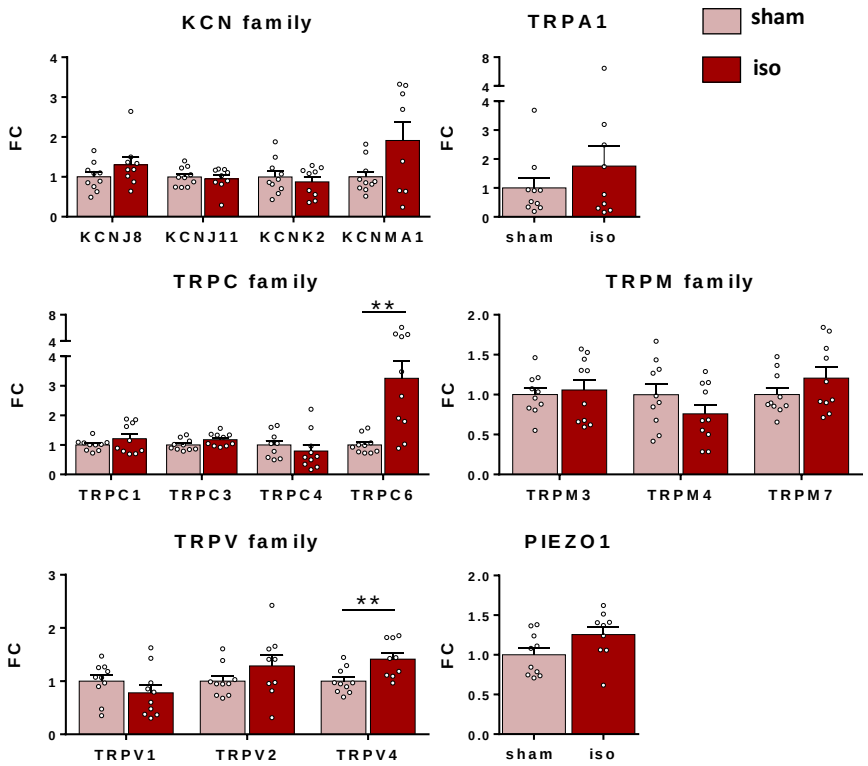

Figure 28. mRNA expression levels of the cardiac mechanoreceptors in the LV in saline (sham, pastel pink dots) and isoproterenol (iso, red dots) infused male mice. From left to right and from top to bottom: potassium mechanosensitive channel family (KCN), transient receptor potential ankyrin family 1 channel (TRPA1), transient receptor potential canonical (TRPC) family, transient receptor potential mucolipin (TRPM) family, transient receptor potential vanilloid (TRPV) family, and Piezo 1 channel. Expression levels were normalized to GAPDH expression and expressed as FC, N=9-10 animals per group. **p<0.01.

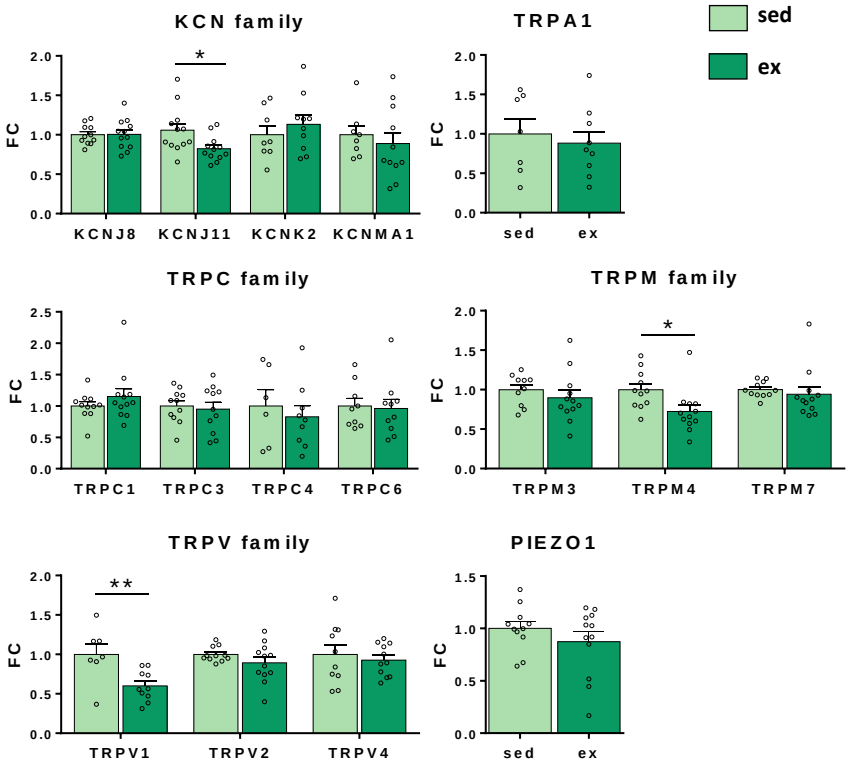

Figure 29. mRNA expression levels of the cardiac mechanoreceptors in the LV in sedentary (sed, light green dots) and exercise (ex, green dots) mice. From left to right and from top to bottom: potassium mechanosensitive channel family (KCN), transient receptor potential ankyrin family 1 channel (TRPA1), transient receptor potential canonical (TRPC) family, transient receptor potential mucolipin (TRPM) family, transient receptor potential vanilloid (TRPV) family, and Piezo 1 channel. Expression levels were normalized to GAPDH expression and expressed as FC, N=6-12 animals per group. *p<0.05, **p<0.01.

Gene expression of TRPV4 and TRPC6 was increased in mice treated with isoproterenol compared to sham (Figure 28). Importantly, neither TRPV4 nor TRPC6 were increased in mice subjected to exercise training compared to sedentary (Figure 29). Additionally, exercise induced the downregulation of KCNJ11, TRPM4 and TRPV1, changes that were not observed in the iso model (Figures 28 and 29). *Trpc5* transcripts were not detected in the heart of any mice, which is consistent with previous studies [289].

To check if changes in mRNA expression levels correlated with changes in protein expression, we performed western blot (WB) analysis of TRPV4 and TRPC6 in both experimental models. Consistent with the mRNA data, TRPV4 and TRPC6 were found to be significantly increased in the LV of mice from the iso group compared to the sham group (Figure 30 A-B), while no difference was seen in the exercise model (Figure 30 C-D). These results further indicate that TRPV4 and TRPC6 are upregulated in response to a pathological stimulus that promotes adverse remodelling, but not in the physiological response that leads to adaptive remodelling.

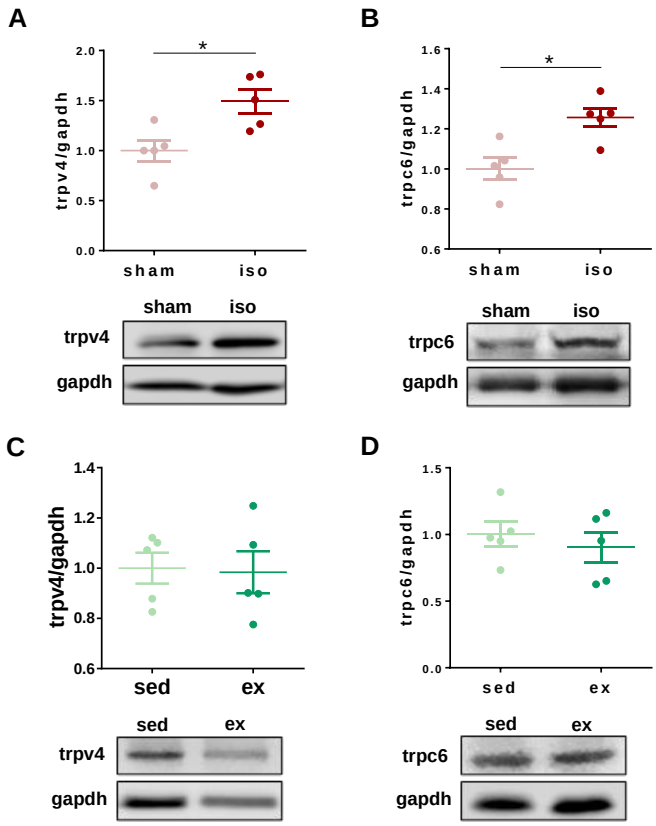

Figure 30. Densiometric analysis and WB representative images of A, B) TRPV4 (A) and TRPC6 (B) protein expression from the ISO model normalized with GAPDH and expressed relative to sham group, N=5 animals per group. C, D) TRPV4 (C) and TRPC6 (D) protein expression from the exercise model normalized with GAPDH and expressed relative to sed group, N=5 animals per group. *p<0.05.

Considering that TRPV4 and TRPC6 are expressed in both CM and FB, where they might exert distinct roles, we also characterized in which cell type these channels were mainly expressed. Our objective was to identify whether the increase in mRNA and protein levels seen in whole tissue was majorly due to changes in a specific cell type. For cell isolation, hearts from sham and iso-treated mice were perfused in a Langendorff system with collagenase type II, and CM and FB from the LV were purified by centrifugation. By qPCR, we found that TRPV4 and TRPC6 were majorly expressed in FB, and both increased in the iso-group compared to sham in this cell type (Figure 31 A-B).

Overall, these results indicate that TRPV4 and TRPC6 gene and protein expression are increased exclusively during adverse remodelling. TRPV4 and TRPC6 overexpression seems to be determinant in cardiac FB.

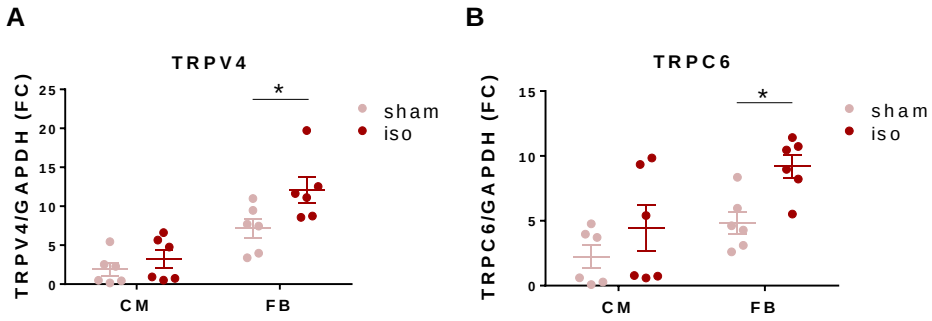

Figure 31. A, B) mRNA expression levels of TRPV4 (A) and TRPC6 (B) in isolated CM and FB analysed in the ISO model. Expression levels were normalized to GAPDH expression and expressed relative to CM from the sham group, N=6 animals.

4.1.4. TRPV4 AND TRPC6 ARE OVEREXPRESSED IN RATS SUBJECTED TO ADVERSE REMODELLING BUT NOT IN RATS SUBJECTED TO ADAPTIVE REMODELLING

The results obtained in mice were further confirmed in two rat models of pathological and physiological remodelling. This experiment was performed in collaboration with Dr. E Guasch from Hospital Clínic-IDIBAPS.

4.1.4.1. Transverse aortic constriction induces cardiac adverse remodelling in rats

A group of male Wistar rats underwent thoracic transverse aortic constriction (TAC), a classical model of adverse remodelling by pressure overload. Eight weeks after surgery, rats were sacrificed, and the hearts extracted. Hypertrophy and fibrosis were assessed.

Analysis of LV cardiac hypertrophy was performed by measuring the area of CM in heart sections stained with H&E. CM size showed a significant increase in TAC rats compared to sham (Figure 32 A-B). Collagen deposition in the LV, assessed in histological preparations stained with picrosirius red, was remarkably higher (~14-fold increase) in TAC rats compared to sham (Figure 32 C-D), and these histological findings correlated with increased expression of fibrotic markers, *col1a1* and *col3a1* (Figure 32 E-F).

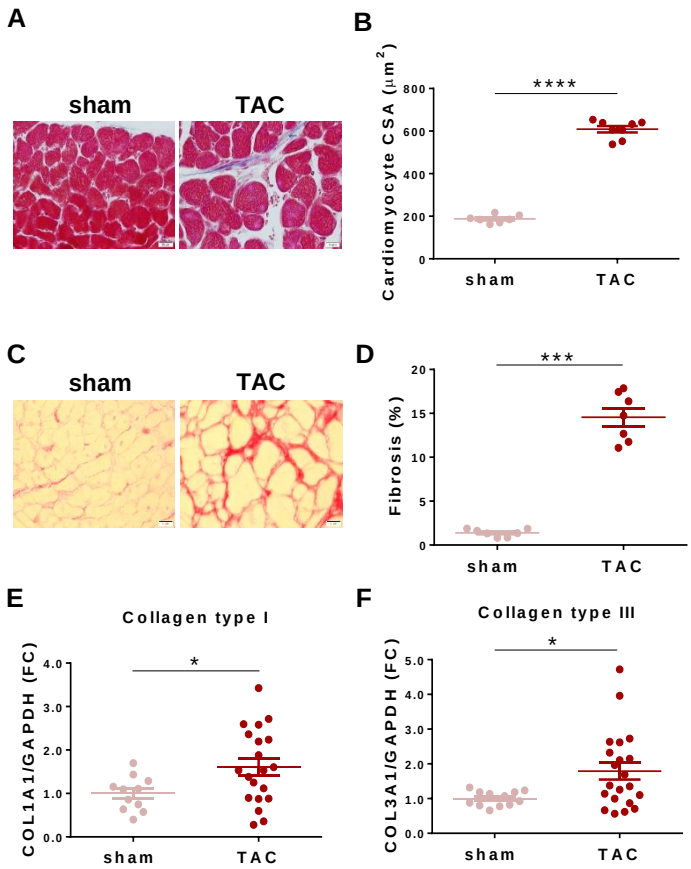

Figure 32. Assessment of adverse cardiac remodelling induced by transverse aortic constriction (TAC) in male rats. A) Representative microphotograph (40X) of the left ventricular cross-sections stained with H&E, and B) Quantification of CM CSA, N= 8 C) Representative microphotograph (40X) of left ventricular cross-sections stained with picrosirius red, and D) Quantification of interstitial collagen deposition, N=7. mRNA expression normalized to GAPDH and expressed as FC of E) *col1a1* and F) *col3a1*. N= 9-10. *p<0.05; ***p<0.001; ****p<0.0001.

4.1.4.2. Moderate exercise training on a treadmill induces cardiac adaptive remodelling in rats

Our results from the adaptive remodelling in mice were also validated in a rat endurance model. Male Wistar rats were conditioned to run on a treadmill at a moderate endurance training protocol (ex, 35 cm/s, 45 min, 5 days/week) for 16 weeks [290]. Following physical training, morphological and molecular cardiac alterations were evaluated.

Rats that followed exercise training showed CM hypertrophy compared to those that followed a sedentary routine (Figure 33 A-B). On the other hand, similar interstitial collagen levels were observed in histological preparations (Figure 33 C-D) and in mRNA expression levels of *col1a1* and *col3a1* (Figure 33 E-F) between ex and sed rats.

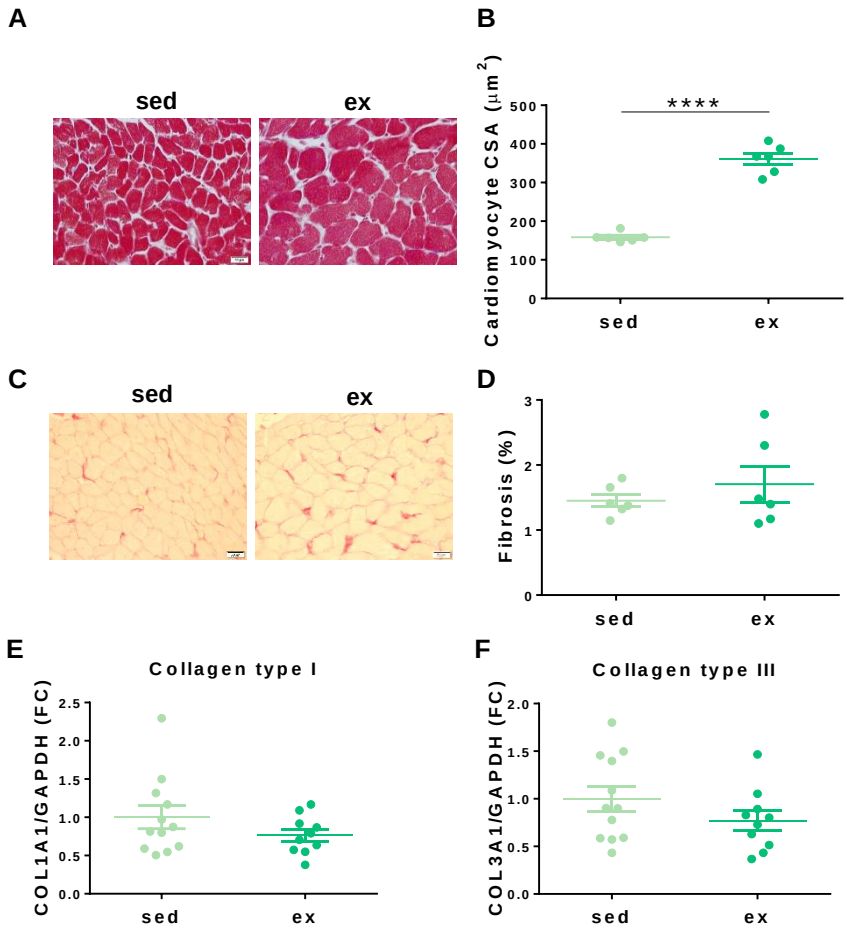

Figure 33. Assessment of adaptive cardiac remodelling in rats conditioned to moderate exercise training A) Representative images (40X) of the left ventricular histological sections stained with H&E, and B) Analysis of CM CSA, N= 6 C) Microphotograph (40X) examples of left ventricular cross-sections stained with picrosirius red, and D) Quantification of fibrosis, N=6. Expression levels assessed by qPCR, normalized to GAPDH expression and expressed as FC of E) *col1a1* and F) *col3a1*. N= 10-12. ***p<0.05.

4.1.4.3. TRPV4 and TRPC6 are differentially expressed in adverse and adaptive remodelling in rats

The expression of TRPV4 and TRPC6 was determined by qPCR in LV samples from both models. Like what had been found in mice, only did TAC induce an increase in gene expression of both TRPV4 and TRPC6 channels, with no differences found in rats exposed to moderate exercise (Figure 34 A-B).

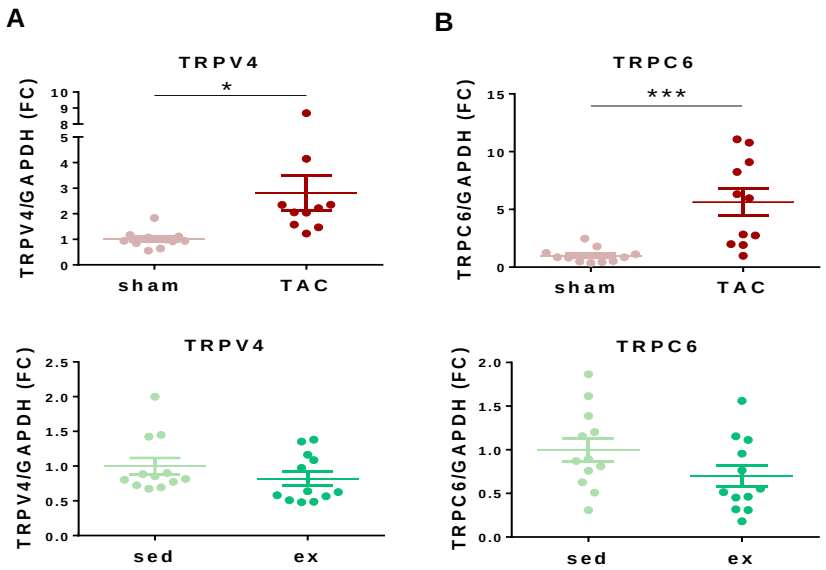

Figure 34. A) mRNA expression levels of TRPV4 (left) and TRPC6 (right) in LV of TAC rats, N=10-11. B) mRNA expression levels of TRPV4 (left) and TRPC6 (right) in LV of exercise rats, N=12. The expression of these genes was normalized to GAPDH expression and is presented as FC. *p<0.05; ***p<0.001.

These results confirm the findings observed in the mouse model and suggest that TRPV4 and TRPC6 seem to be involved exclusively in the development of pathological remodelling.

4.2. TIME-COURSE CHANGES IN TRPV4 AND TRPC6 TROUGHOUT THE DEVELOPMENT OF ADVERSE CARDIAC REMODELLING

Male mice at 10 weeks of age were administered isoproterenol during 3, 7, 14 and 28 days. The goal was to study the temporal evolution towards adverse ventricular remodelling and its correlation with changes in the expression of TRPV4 and TRPC6.

4.2.1. ISOPROTERENOL CAUSES RAPID LEFT VENTRICULAR HYPERTROPHY AND PROGRESSIVE VENTRICULAR DILATION AND SYSTOLIC DYSFUNCTION

For the time-course study, echocardiographic studies were performed at baseline, 14 and 28 days of isoproterenol administration. No differences were observed between groups at baseline (data not shown). Parameters of hypertrophy (IVS thickness and LV mass) appeared significantly increased already at 14 days of isoproterenol infusion, with no further increase beyond that timepoint (Figure 35 A-B). This suggests that hypertrophy is rapidly established after ventricular overload. On the other hand, LV end-diastolic and end-systolic volumes increased at day 14 and further at day 28 (Figure 35 C-D), reflecting the characteristic gradual LV dilation occurring in adverse remodelling. In parallel, mice treated with isoproterenol showed progressive systolic dysfunction, with a significant reduction in EF and FS compared to sham animals at 14 days, and further enhanced at 28 days (Figure 35 E-F).

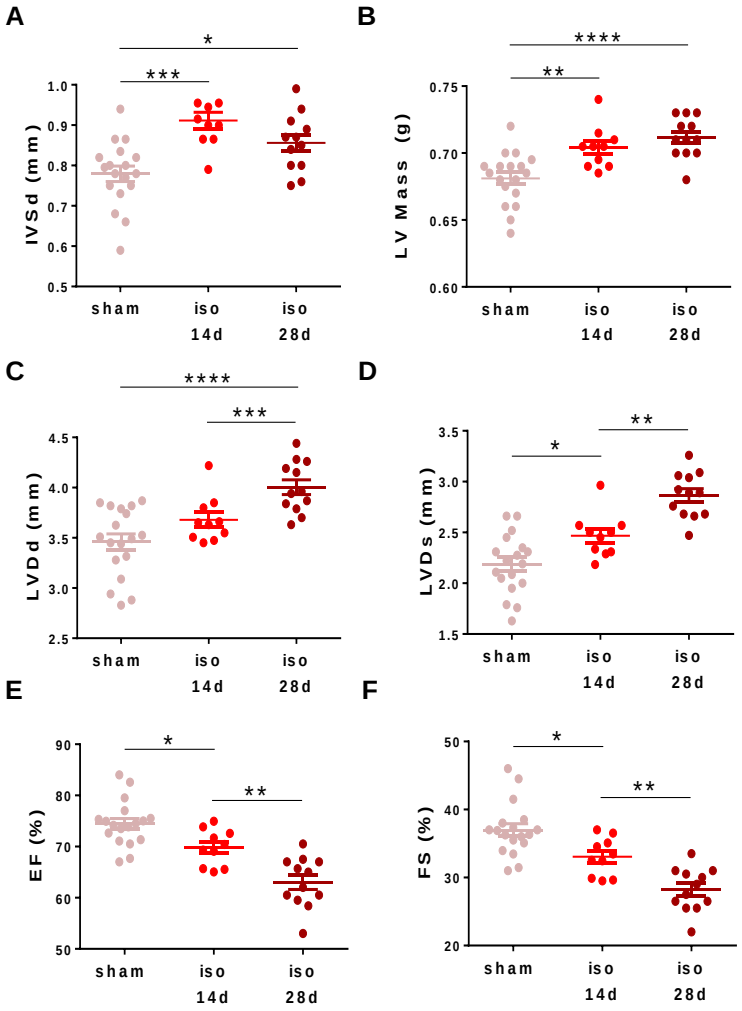

Figure 35. Time-dependent evolution of morphological and functional parameters in mice treated with saline (sham, pastel pink dots) or iso for 14 (iso 14d, orange dots) or 28 (iso 28d, red brown dots) days. A) intraventricular septum diameter measured at the end of the diastole (IVSd), B) left ventricular mass (LV Mass), C) left ventricular diameter at the end of the diastole (LVDd) and D) at the end of the systole (LVDs), E) ejection fraction (EF) and F) fractional shortening (FS) N=10-18 mice per group. *p<0.05; **p<0.01; ***p<0.001; ****p<0.0001.

4.2.2. CARDIOMYOCYTE HYPERTROPHY DEVELOPS SHORTLY AFTER ISOPROTERENOL INFUSION

To further explore the hypertrophic remodelling process over time, mice were sacrificed after 3, 7, 14 or 28 days of isoproterenol infusion, and the hearts

extracted for analysis. The HW/TL ratio revealed that the increase in heart size was already present at day 3 of isoproterenol infusion, and it remained high throughout the whole period, with no further increase with longer isoproterenol treatment (Figure 36 A). CM CSA was also increased already at day 3, but this parameter did increase progressively with longer exposure to isoproterenol (Figure 36 B-C).

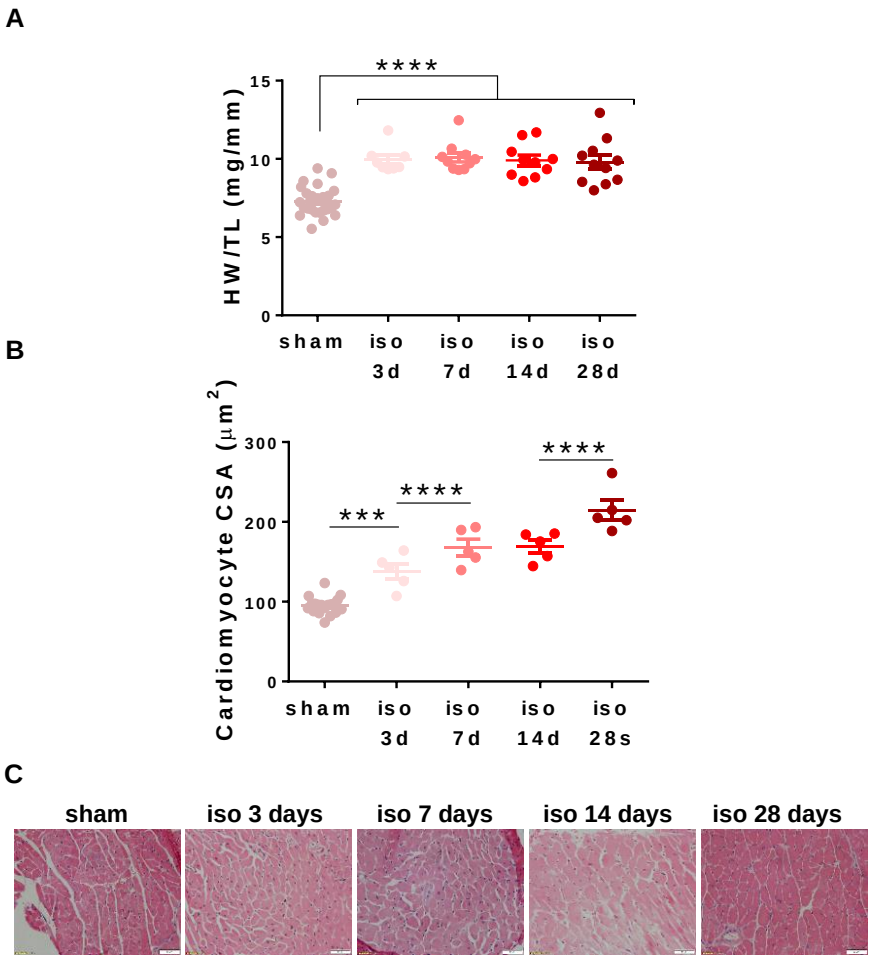

Figure 36. Time-dependent evolution of hypertrophy in animals under saline (sham, pastel pink dots) or ISO during 3 (iso 3d, light pink dots), 7 (iso 7d, salmon dots), 14 (iso 14d, orange dots) or 28 (iso 28d, red brown dots) days. A) HW/TL ratio, N=8 iso animals per group matched with their sham littermates, and B) CM CSA measured in histological sections stained with H&E, N=5 iso animals per group matched with their sham littermates. C) Representative H&E microphotographs (40X). ***p<0.001; ****p<0.0001.

4.2.3. INTERSTITIAL COLLAGEN DEPOSITION INCREASES PROPORTIONALLY TO THE DURATION OF ISOPROTERENOL INFUSION

In picrosirius red-stained LV sections, collagen deposition was already evident from day 3 (although non-significant until day 7), with a fiercely and strong time-dependent progression. The deposition of collagen greatly increased at each time point compared to the previous one (Figure 37 A-B). *Col1a1*, *col3a1* and *acta1* mRNA expression were also upregulated at day 3, with no major changes thereafter. This probably reflects an increased gene expression particularly needed in the first stages of fibrosis formation (Figure 37 C-E).

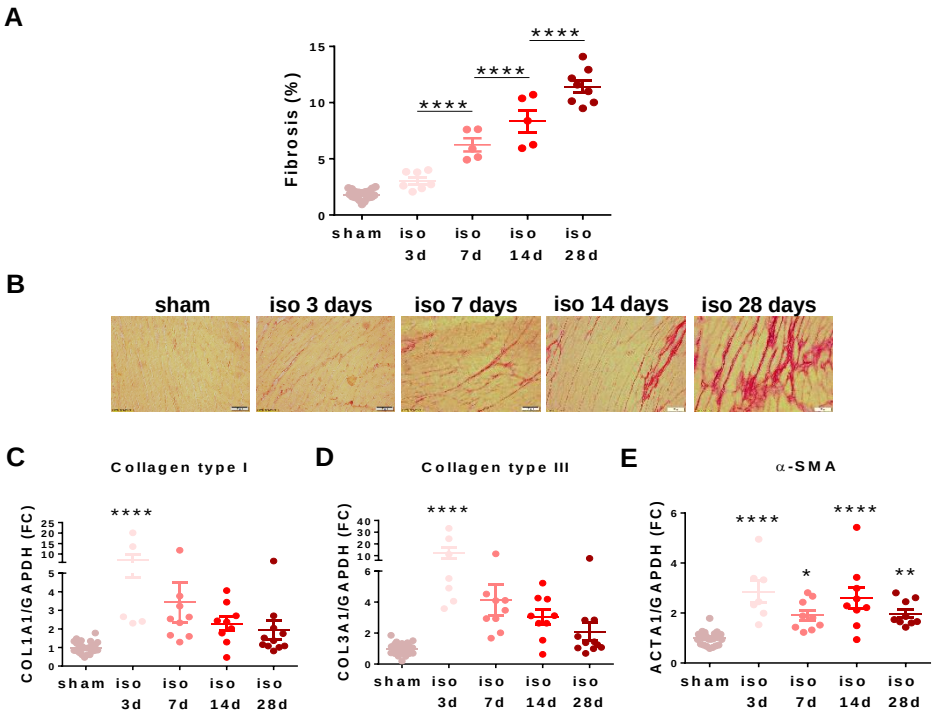

Figure 37. Time-dependent evolution of fibrosis in mice treated with saline (sham, pastel pink dots) or ISO during 3 (iso 3 days, light pink dots), 7 (iso 7 days, salmon dots), 14 (iso 14 days, orange dots) or 28 (iso 28 days, red brown dots) days. A) Quantification of fibrosis in LV heart sections stained with picrosirius red, N=5-8 iso animals per group matched with their sham controls. B) Illustrative images of stained histological samples. C) mRNA expression measured by RT-qPCR, normalized to GAPDH expression and expressed as FC of C) *col1a1* D) *col3a1*, and E) *acta1*, N= 7-11 animals per group matched with their sham controls. **p<0.01; ****p<0.0001.

4.2.4. TIME-DEPENDENT RELEATIONSHIP BETWEEN EXPRESSION OF IONS CHANNELS TRPV4 AND TRPC6 AND ONSET OF FIBROSIS

RNA and protein expression levels of mechanosensitive ion channels TRPV4 and TRPC6 were evaluated at the different timepoints. At the RNA level, isoproterenol promoted a significant and sustained increase in TRPV4 and TRPC6 after 7 days of infusion (Figure X A-B). Western Blot analyses revealed a progressive increase in the protein expression of these channels, although it was not significant until day 28 (Figure X C-D). The lack of significance at earlier time-points could be due to the inherent variability of the WB.

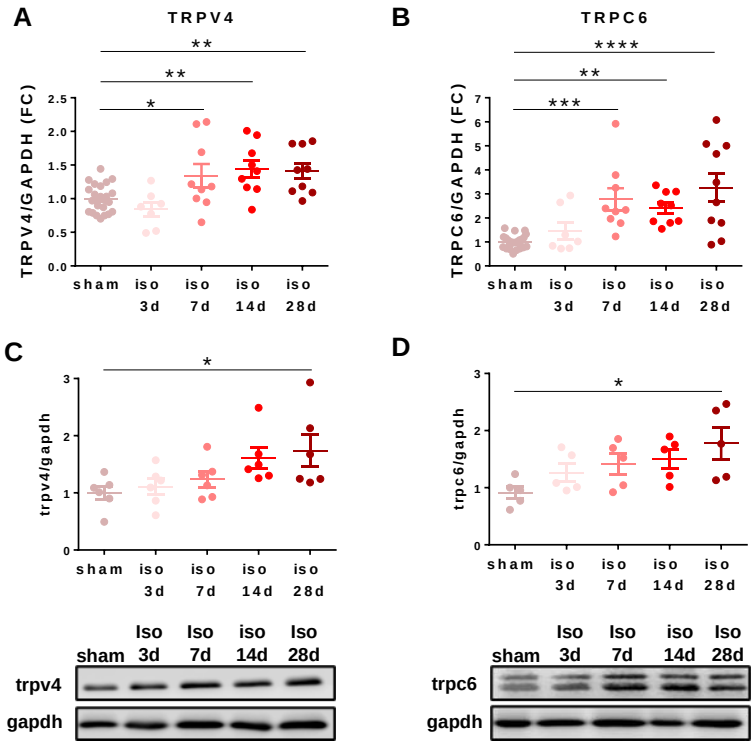

Figure 38. Time-dependent TRPV4 and TRPC6 expression in animals treated with saline (sham, pastel pink dots) or isoproterenol for 3 (iso 3 days, light pink dots), 7 (iso 7 days, salmon dots), 14 (iso 14 days, orange dots) or 28 (iso 28 days, red brown dots) days assessed by qPCR analysis of mRNA expression normalized to GAPDH and expressed as FC of A) TRPV4 and B) TRPC6, N=7-10 mice per group matched with sham controls. Representative WB bands and analysis of protein expression of C) TRPV4 and D) TRPC6 normalized to GAPDH, N=6 mice group.

In summary, these results indicate that cardiac hypertrophy (both at the macroscopic and the cellular level) develops early (after 3 days) following sustained overload with isoproterenol infusion, whereas the fibrotic response, although potentially activated at early stages, translates into later collagen deposition (at 7 days). TRPV4 and TRPC6 overexpression does not precede the pathological response and appears temporally coincidental with fibrosis initiation.

4.3. ADVERSE CARDIAC REMODELLING IN THE ABSENCE OF TRPV4

The results that have been exposed thus far provide evidence showing that TRPV4 and TRPC6 increased expression correlates with adverse cardiac remodelling induced either by sustained infusion of a β-adrenergic agonist or TAC, but not with adaptive remodelling induced by exercise. Our results suggest that mechanosensitive ion channels participate differentially in adaptive and adverse remodelling, and that the overexpression of TRPV4 and TRPC6 could drive, at least partially, the pathological response. Interestingly, some authors have already described the potential role of TRPC6 channel in the promotion of adverse remodelling [103,199]. However, they also demonstrated that its inhibition could not revert such remodelling [199,201], suggesting that more than one mechanosensitive channel may be involved in the promotion and progression of the disease. In this sense, TRPV4 stands as a promising candidate.

To study the role of TRPV4 in adverse cardiac remodelling, we established a TRPV4-KO mouse colony. $TRPV4^{+/+}$ (WT) and $TRPV4^{-/-}$ (KO) male and female mice were used for the experiments. Because the litters of this colony were very small, and to follow the principles of the 3Rs (Replacement, Reduction and Refinement), females were also used. This was possible because no significant differences according to gender were observed neither at baseline nor after HF induction.

We performed a preliminary study to confirm that TRPV4 expression was null in the TRPV4-KO model, and that TRPV4 deletion did not lead to changes in other TRP channels. Figure 39 shows the results of TRP expression in WT versus KO animals.

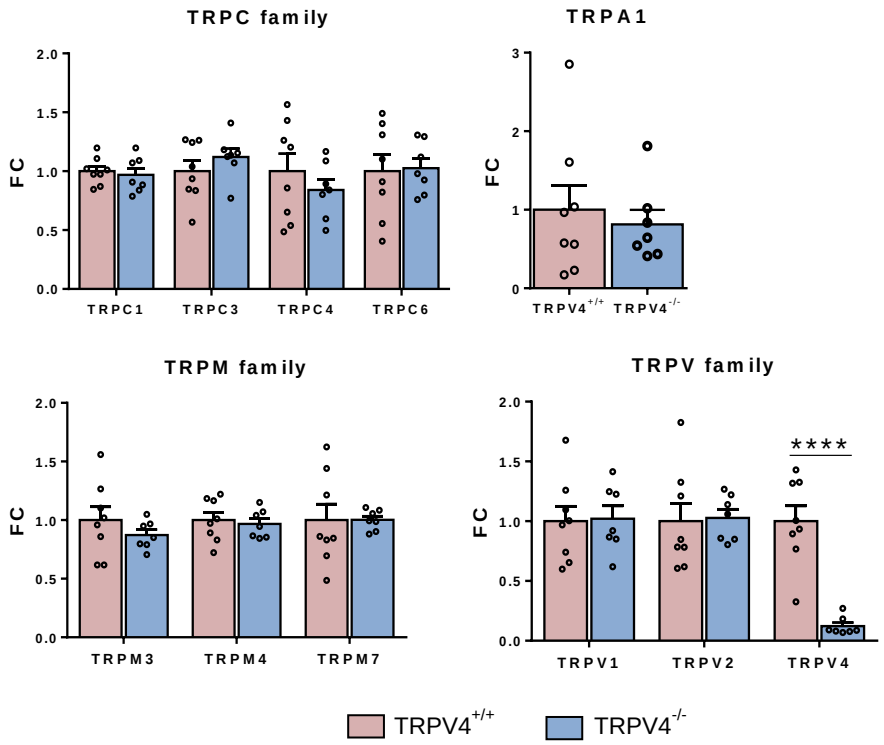

Figure 39. TRP expression in TRPV4$^{+/+}$ and TRPV4$^{-/-}$ animals

As expected, we found a ~ 85% reduction in TRPV4 mRNA expression in TRPV4$^{-/-}$ animals (Figure 39). Since the generation of the null *trpv4* allele was performed by excision of exon 12, which encodes for the pore-loop and adjacent domain [258], a minimal TRPV4 expression was detected by qPCR. However, mRNA TRPV4 transcripts did not translate into the expression of any functional protein. Immunoblotting showed TRPV4 bands were exclusively in TRPV4$^{+/+}$ animals (Figure 40). There was no apparent compensation of other TRPs, as mRNA expression of other mechanoreceptors was similar in WT and KO animals (Figure 39).

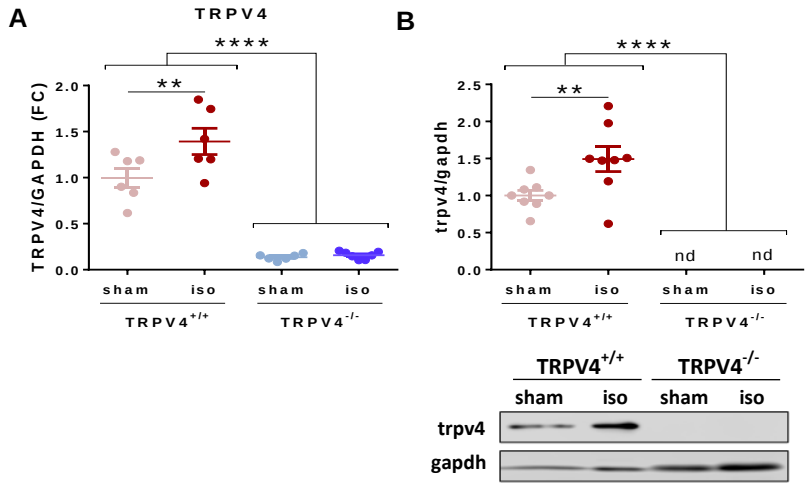

Figure 40. TRPV4 expression in LV samples of TRPV4$^{+/+}$ and TRPV4$^{-/-}$, either treated with saline (sham) or isoproterenol (iso). A) qPCR analysis of mRNA expression normalized to GAPDH and expressed as FC over TRPV4$^{+/+}$ sham, N=6-7 animals per group. B) Representative image of western blot and densiometric analysis of protein expression, N=8 animals per group. **p<0.01; ****p<0.0001.

Next, we exposed our TRPV4$^{+/+}$ and TRPV4$^{-/-}$ male and female mice to chronic infusion of isoproterenol (or saline) for 28 days. As expected, TRPV4 was significantly overexpressed in TRPV4$^{+/+}$ mice treated with isoproterenol compared to sham, whereas TRPV4 expression was insignificant in both TRPV4$^{-/-}$ groups (Figure 40 B). All aspects of cardiac remodelling were evaluated in the 4 study groups (TRPV4$^{+/+}$ and TRPV4$^{-/-}$ mice subjected to isoproterenol or sham infusion).

4.3.1. DELETION OF TRPV4 PRESERVES CARDIAC STRUCTURE AND FUNCTION AFTER ISOPROTERENOL INFUSION

Echocardiographic studies confirmed that, as seen before, TRPV4$^{+/+}$ mice treated with isoproterenol developed increased IVS and LV posterior wall (LVPW) thickness, and LV dilatation, which resulted in significantly greater LV mass (Figure 41 A-C, E-F). In addition, an increase in left atrium diameter (LAD), a secondary parameter associated with ventricular dysfunction, was also observed (Figure 41 D). Accordingly, mice in this group also showed decreased

EF and FS (figure 41 G-H). In contrast, TRPV4$^{-/-}$ mice did not show significant changes in cardiac dimensions after isoproterenol infusion, and cardiac function was preserved in this group of animals, showing comparable parameters to both sham groups (Figure 41).

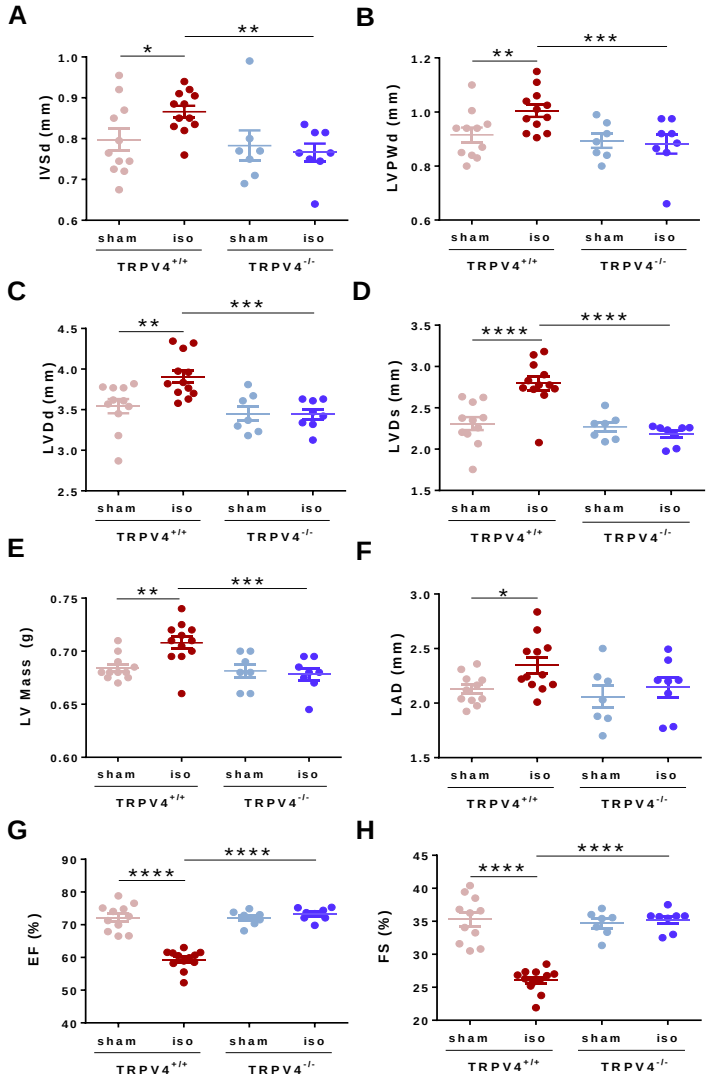

Figure 41. Quantification of echocardiographic parameters of TRPV4$^{+/+}$ and TRPV4$^{-/-}$ mice treated either with saline (sham) or sustained isoproterenol infusion (iso) for 28 days. Cardiac structure was assessed by A) IVS thickness, B) LV posterior wall (LVPW) thickness, C) LV dilatation in diastole (LVDd) and in D) sistole (LVDs), E) LV Mass, F) diameter of the left atrium in diastole (LAD), G) ejection fraction (EF) and H) fractional shortening (FS). N=7-12 animals per group. *p<0.05; **p<0.01; ***p<0.001; ****p<0.0001.

These results suggest that, in the presence of chronic β-adrenergic stimulation, the lack of TRPV4 protects against changes in cardiac dimensions and dysfunction.

4.3.2. DELETION OF TRPV4 REDUCES ISOPROTERENOL-INDUCED CARDIAC CELL HYPERTROPHY

After 28 days of saline or isoproterenol infusion, $TRPV4^{+/+}$ and $TRPV4^{-/-}$ animals were sacrificed, and cardiac structural alterations were assessed by measuring the HW/TL ratio and by quantifying CM CSA in H&E heart sections. Morphological images showed that iso-treated animals from both $TRPV4^{+/+}$ and $TRPV4^{-/-}$ groups exhibited larger heart size than their sham counterparts (Figure 42 A). However, quantification of the HW/TL ratio revealed that $TRPV4^{-/-}$ had less hypertrophy than $TRPV4^{+/+}$ animals (Figure 42 B). Similarly, animals exposed to isoproterenol had increased CM CSA compared to sham littermates but, $TRPV4^{+/+}$ animals exhibited significantly greater CM CSA values compared to $TRPV4^{-/-}$ animals (Figure 42 C-D).

These findings indicate that TRPV4 deletion alleviates the effects of isoproterenol infusion on cardiac hypertrophy by partially buffering the dramatic increase in CM area.

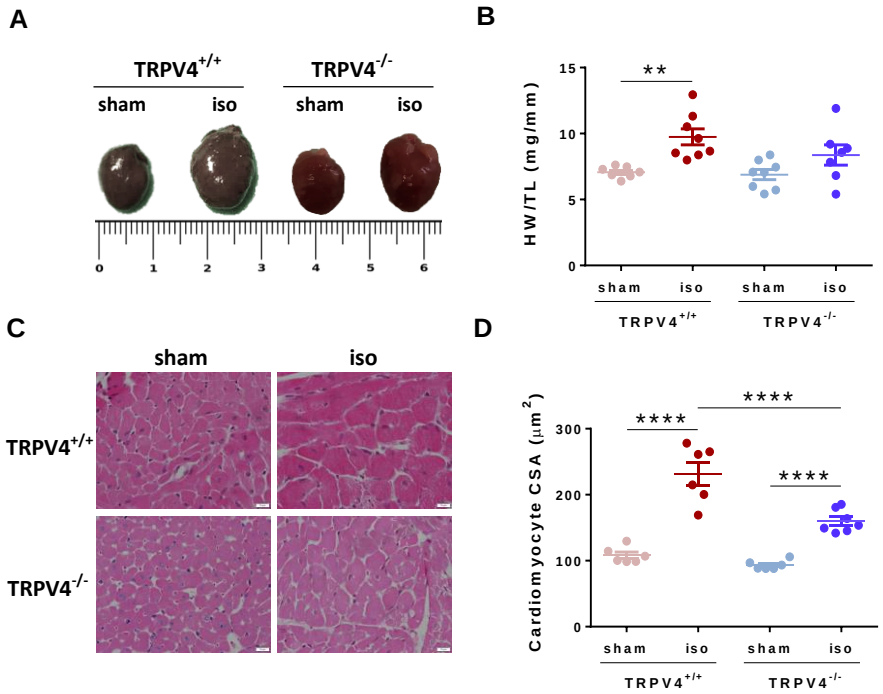

Figure 42. Hypertrophy assessment of TRPV4$^{+/+}$ and TRPV4$^{-/-}$ mice receiving with saline or isoproterenol infusion for 28 days. A) Photographs of the size of the heart of all experimental groups. The scale of the ruler, provided for visual reference, is in cm. B) Measurements of the HW/TL ratio, N=7-8 animals per group. C) Representative images (40X) of stained heart sections with H&E of all experimental groups, and D) quantification of CM CSA in these stained histological sections, N=5-7 animals per group. **p<0.01; ****p<0.0001.

4.3.3. DELETION OF TRPV4 ATTENUATES THE FIBROTIC RESPONSE INDUCED BY ISOPROTERENOL

To determine the effects of TRPV4 deletion on cardiac fibrosis, LV sections stained with picrosirius red were analysed. Histological images showed the expected high collagen content in iso-treated TRPV4$^{+/+}$ mice. In contrast, collagen deposition was significantly and remarkably reduced in TRPV4$^{-/-}$ mice exposed to isoproterenol compared to iso-treated TRPV4$^{+/+}$ mice (Figure 43 A). Notably, iso-treated TRPV4$^{-/-}$ mice exhibited little fibrosis, although still significantly higher than that observed in TRPV4$^{-/-}$ sham (Figure 43 B). Gene expression analyses showed that, while isoproterenol induced an

upregulation of *col1a1*, *col3a1* and *acta1* in the LV tissue of TRPV4$^{+/+}$ mice, these fibrotic genes did not increase in TRPV4$^{-/-}$ animals, which showed similar expression levels compared to their sham littermates (Figure 43 C-E). These data suggest that following isoproterenol treatment, the absence of TRPV4 has profound effects on fibrosis formation, the main hallmark of pathological remodelling, by reducing collagen synthesis and deposition.

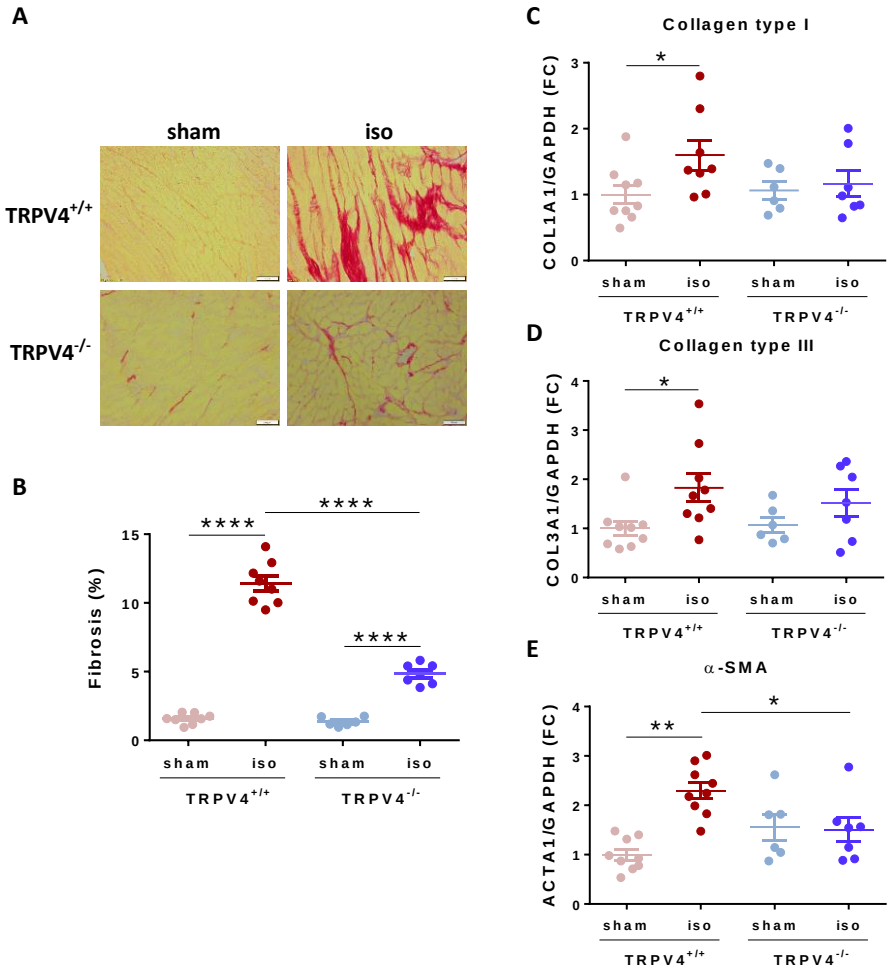

Figure 43. Analysis of LV cardiac fibrosis following 28 days of saline or ISO infusion in TRPV4$^{+/+}$ and TRPV4$^{-/-}$ animals. A) Representative histological sections of all experimental groups stained with picrosirius red (40X) and B) quantification of LV collagen deposition (fibrosis), N=6-8 animals per group. qPCR analysis of LV mRNA expression of fibrotic markers normalized to GAPDH expression and expressed as FC; C) *col1a1*; D) *col3a1* and E) *acta1*. N=6-8 mice per group. *p<0.05; **p<0.01; ****p<0.0001.

4.3.4. DELETION OF TRPV4 PREVENTS ARRHYTHMIA INDUCIBILITY ASSOCIATED WITH PATHOLOGICAL REMDODELLING

Overall, the results of the study with the TRPV4-KO colony indicated that TRPV4 deletion resulted in a remarkable inhibition of the distinctive traits of the pathological remodelling, that is, tissue fibrosis and cardiac dysfunction, with partial attenuation of CM hypertrophy. We then evaluated whether TRPV4 deletion also derived into the prevention of cardiac arrhythmias, another significant hallmark accompanying adverse remodelling and HF.

Whole hearts isolated from $TRPV4^{+/+}$ and $TRPV4^{-/-}$ animals treated with either saline or isoproterenol for 28 days were perfused in a Langendorff system and subjected to a protocol of programmed electrical stimulation. As expected for a small heart, arrhythmia inducibility under normoxia conditions was overall low, and main differences among groups were observed only after regional ischemia.

4.3.4.1. Ventricular arrhythmias under normoxia

No significant ventricular arrhythmias occurred spontaneously in neither group. After programmed electrical stimulation, few premature ventricular complexes (PVC) and non-sustained ventricular tachycardias (NSVT) were observed in all study groups, with no differences among them. Sustained VTA could not be induced in neither group under normoxic conditions.

4.3.4.2. Ventricular arrhythmias during regional ischemia

In order to increase arrhythmia vulnerability, Langendorff-perfused hearts were subjected to regional ischemia by coronary ligation, and inducibility was retested 15 minutes after. Importantly, no differences in the area at risk (AAR) among groups were observed (Figure 44).

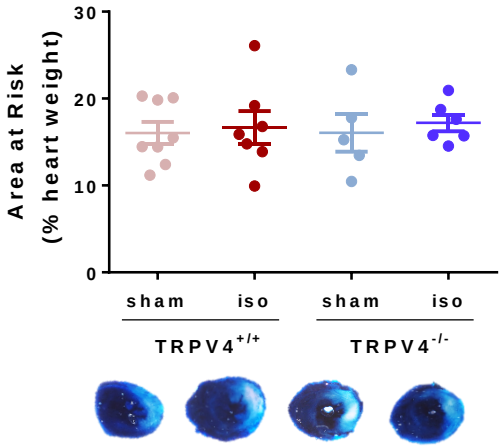

Figure 44. Area at risk (AAR), representing the territory perfused by the ligated coronary artery, expressed as percentage with respect to the heart weight in all four study groups. A representative image is showed for each group, N=5-8.

Overall, programmed ventricular stimulation during ischemia increased the inducibility of ventricular arrhythmias. Total number of VTA was significantly higher in TRPV4$^{+/+}$ animals infused with isoproterenol compared to TRPV4$^{+/+}$ mice treated with saline and their counterpart TRPV4$^{-/-}$ administered with the same isoproterenol protocol (Figure 45 A). Similarly, duration of VTA followed the same trend but did not reach significant differences among groups (Figure 45 B).

In conclusion, despite low arrythmia inducibility in all groups, TRPV4$^{+/+}$ animals subjected to isoproterenol infusion, showed a greater vulnerability to VTA under ischemic conditions compared to their sham littermates and to both TRPV4$^{-/-}$ groups. TRPV4 deletion prevented the increase in arrhythmia inducibility after chronic isoproterenol infusion.

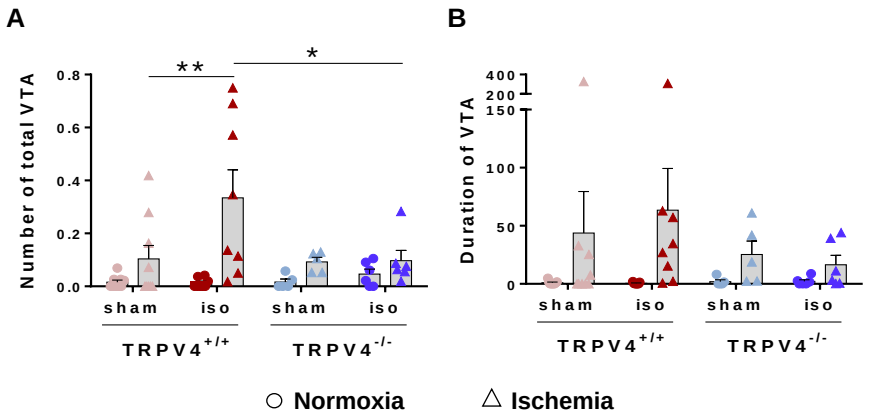

Figure 45. Arrhythmogenesis in isolated hearts from the four study groups in normoxia conditions and after regional ischemia. A) Total number of induced ventricular tachyarrhythmias (VTA) normalized to the number of stimulation events. B) Duration of VTA. N=5-8. *p<0.05, **p<0.01.

4.3.5. TRPV4 OVEREXPRESSION IN PATHOLOGICAL REMODELLING INDUCES ENHANCED CA^{2+} INFLUX, IN CARDIAC FIBROBLASTS

Our findings thus far indicate that TRPV4 could play a key role in the development of adverse remodelling. Therefore, the subsequent experiments were designed to elucidate potential mechanisms by which TRPV4 could activate the pathological response.

TRPV4 channels display a high selectivity for Ca^{2+}, and a sustained increase in cytosolic Ca^{2+} is known to activate intracellular pathways that lead to the expression of fibrotic genes [89]. Since our previous data showed that TRPV4 is mainly expressed in FB, we first aimed to investigate the role of TRPV4 in FB Ca^{2+} dynamics.

Intracellular Ca^{2+} influx was measured in isolated FB from $TRPV4^{+/+}$ and $TRPV4^{-/-}$ mice, either treated with saline or isoproterenol. Cells were cultured until confluence, and cytosolic Ca^{2+} was monitored using the Ca^{2+} sensitive dye Fluo-

4. TRPV4 was selectively activated either with GSK1016790A (GSK), or with a 20% hypotonic solution.

FB from TRPV4$^{+/+}$ iso-treated mice exhibited a robust increase in cytosolic Ca^{2+} after stimulation with GSK, which was greater than in TRPV4$^{+/+}$ sham FB (Figure 46 A). FB from TRPV4$^{-/-}$ animals, exposed to either saline or isoproterenol, did not show any Ca^{2+} influx after GSK treatment, confirming that there is no functional TRPV4 in these cells (Figure 46 A). Further, GSK-induced Ca^{2+} influx was attenuated in the presence of the TRPV4 antagonist, HC067047 (Figure 46 B). Similarly, TRPV4$^{+/+}$ FB exhibited an increase in intracellular Ca^{2+} when stimulated with hypotonic stress, which was also significantly higher in FB from iso-infused animals compared to sham. As well, TRPV4$^{-/-}$ FB failed to induce any Ca^{2+} influx in response to a hypotonic stimulus (Figure 46 C). This hypotonicity-induced Ca^{2+} influx in TRPV4$^{+/+}$ FB was also greatly abolished after adding HC, suggesting that TRPV4 is one of the main players in charge of hypotonic responses in these cells (Figure 46 D).

Taken together, these results indicate that, an increased TRPV4 protein expression translates into a greater influx of Ca^{2+} into cardiac FB when challenged with a TRPV4-mediating stimulus, and this can trigger the downstream pathways leading to adverse remodelling. In contrast, TRPV4 deletion protects against the increased Ca^{2+} influx observed upon chronic beta-adrenergic stimulation.

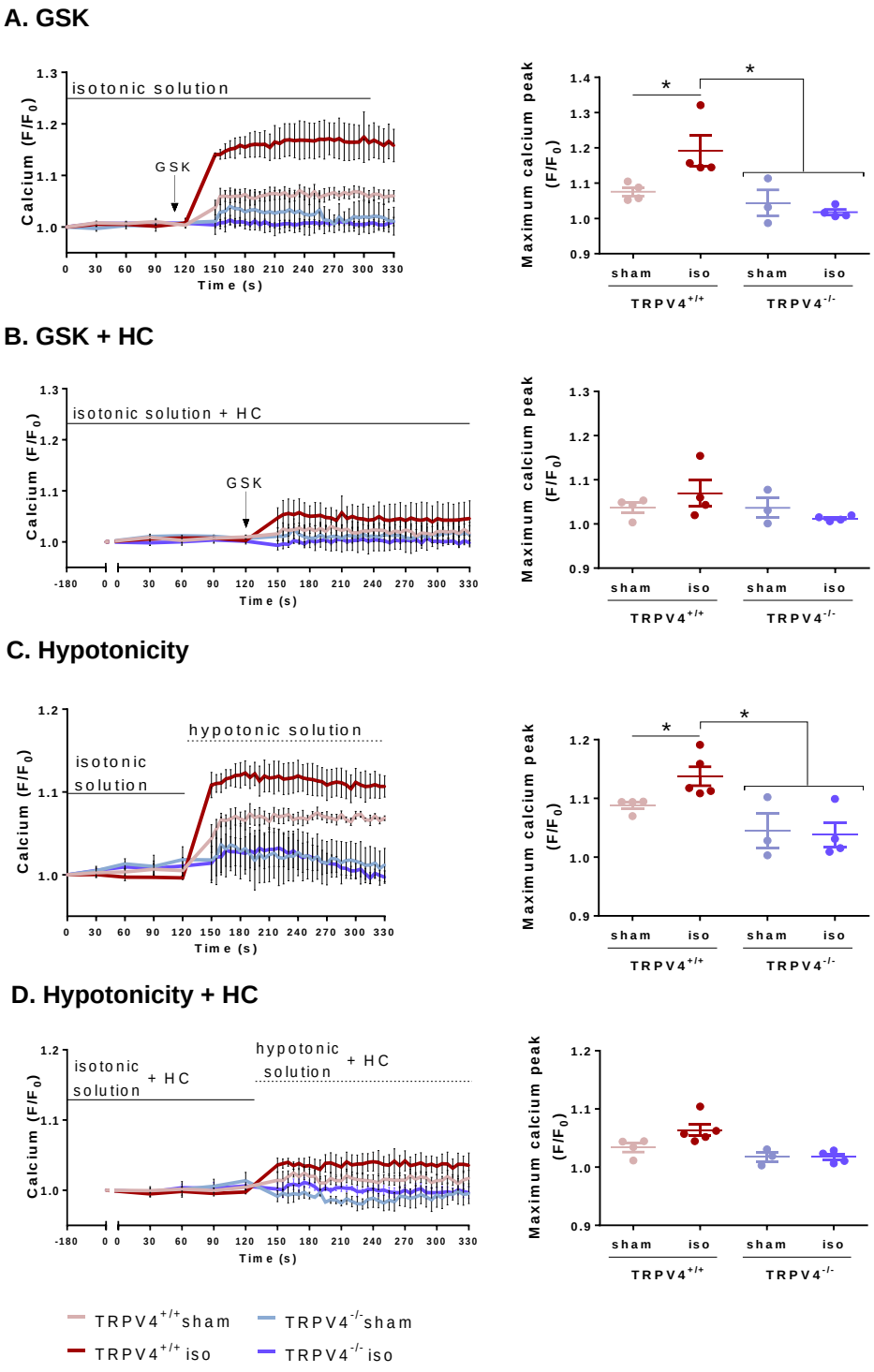

Figure 46. Intracellular Ca^{2+} measures in FB of TRPV4$^{+/+}$ and TRPV4$^{-/-}$ mice infused either with saline or isoproterenol for 28 days and loaded with Fluo-4. Left images of

all panels show average traces depicting Ca^{2+} influx in response to several stimuli, and right images show quantitative analysis of the maximum cytosolic Ca^{2+} influx induced in FB of all experimental groups. A) Calcium influx upon stimulation with TRPV4 activator, GSK 100 nM. Arrow indicates time at which GSK was added. B) Calcium influx upon stimulation with GSK and treated with the TRPV4 antagonist, HC067047 (HC). Cells were pre-treated for 3 minutes with HC before stimulating with GSK. Arrow indicates the time at which GSK was added. C) Calcium influx upon stimulation with 20% hypotonic solution (140 mOsm, dashed line) in FB loaded with Fluo-4. D) Calcium influx upon stimulation with 20% hypotonic solution and treated with HC. Cells were treated with HC for 3 minutes prior to the replacement of the isotonic solution (line) with the hypotonic one (dashed line). F/F_0= ratio of fluorescence intensity relative to time 0. The data is presented as the mean ± SEM of 4-8 replicates per group of 3-4 independent experiments. *$p<0.05$.

4.3.6. TRPV4 ACTIVATION IN PATHOLOGICAL REMODELLING MEDIATES FIBROSIS THROUGH THE CALCINEURIN/NFAT PATHWAY

We have shown that in response to isoproterenol, cytosolic Ca^{2+} in FB increases because of an increased expression of TRPV4. Given that Ca^{2+} entry through TRPV4 may activate downstream signalling pathways that mediate adverse remodelling, we aimed to study the potential activation of such pathways in our model.

In the heart, the Ca^{2+}-calmodulin-dependent serine/threonine phosphatase calcineurin has been shown to be crucial for adverse cardiac hypertrophy and fibrosis [291]. Increased Ca^{2+} concentration binds to calmodulin, which activates calcineurin, and this activation promotes, among other, dephosphorylation of the nuclear factor of activated T-cells (NFAT) [292]. NFAT is located in the cytoplasm but, upon dephosphorylation, it translocates into the nucleus where it complexes with other transcription factors to regulate and drive the expression of hypertrophic and fibrotic genes such as *acta1*, *col1a1* and *col3a1*[103,293]. Consequently, we examined the activation of the calcineurin-NFAT pathway in the FB of our $TRPV4^{+/+}$ and $TRPV4^{-/-}$ mice following 28 days of saline or isoproterenol exposure.

We determined the phosphatase activity and expression of calcineurin in protein extracts from FB of our four experimental groups. We observed that calcineurin phosphatase activity increased in TRPV4$^{+/+}$ FB exposed to isoproterenol, while deletion of TRPV4 prevented this increase (Figure 47 A). This increase was only functional, as protein expression remained the same in all experimental groups (Figure 47 B).

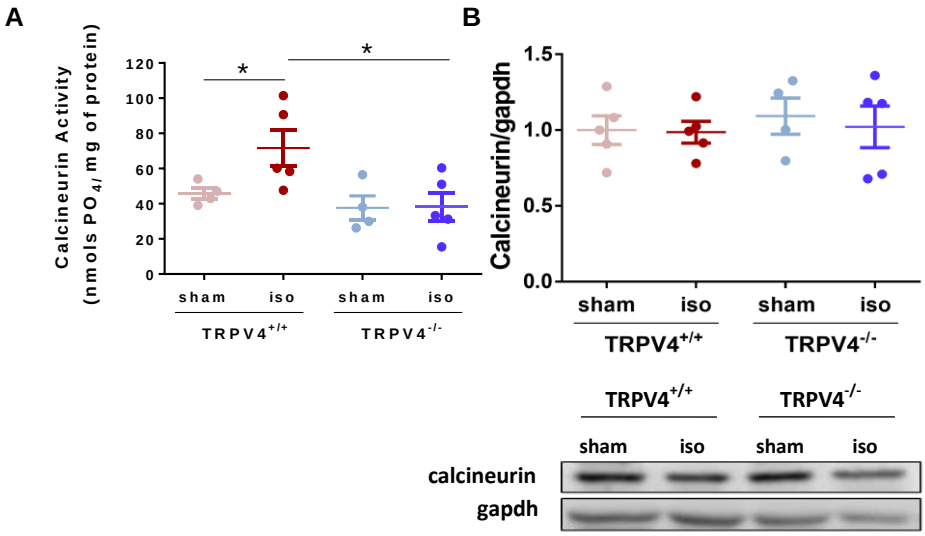

Figure 47. A) Calcineurin activity in FB lysates prepared from TRPV4$^{+/+}$ and TRPV4$^{-/-}$ mice exposed saline or ISO during 28 days, N=4-5 animals per group. B) Upper panel, WB determination of calcineurin expression levels of all experimental groups, N=5 animals per group. Lower panel, a representative image of the blots. N=5 animals per group. *p<0.05.

We then studied whether the increase in calcineurin activity enhanced NFAT translocation, and whether this could be prevented in the TRPV4$^{-/-}$ FB. To do so, we performed NFAT immunostaining to determine its intracellular distribution. As a positive control of nuclear translocation, considering that activation of calcineurin requires a sustained rise in intracellular Ca^{2+}, we treated FB with a high-calcium medium (4 mM) for 3h. Following Ca^{2+} treatment, NFAT localized clearly into the nucleus, as reflected by a

predominantly nuclear staining (positive control, Figure 48). We next quantified the intracellular location of NFAT (whether it was cytosolic or nuclear) in cultured FB from TRPV4$^{+/+}$ and TRPV4$^{-/-}$ mice exposed to saline or isoproterenol. FB from mice exposed to saline had NFAT confined to the cytosol in both TRPV4$^{+/+}$ and TRPV4$^{-/-}$ animals. However, after 28 days of ISO treatment, nearly all NFAT protein in FB from TRPV4$^{+/+}$ translocated to the nucleus, while this translocation was significantly reduced in the TRPV4$^{-/-}$ FB (Figure 48 A-B).

Altogether, these results indicate that in cardiac FB, TRPV4-mediated Ca^{2+} influx stimulates calcineurin activity, which promotes the translocation of NFAT into the nucleus, resulting in enhanced fibrotic gene expression. Importantly, *acta1*, *col1a1* and *col3a1* are target genes of nuclear NFAT, which we previously showed were increased in TRPV4$^{+/+}$ (but not TRPV4$^{-/-}$) animals receiving isoproterenol. Moreover, and considering the results observed in the TRPV4-KO model, one can adventure that the deletion of TRPV4 attenuates adverse remodelling by decreasing the calcineurin-NFAT pathway activation, and therefore preventing the expression of fibrotic genes.

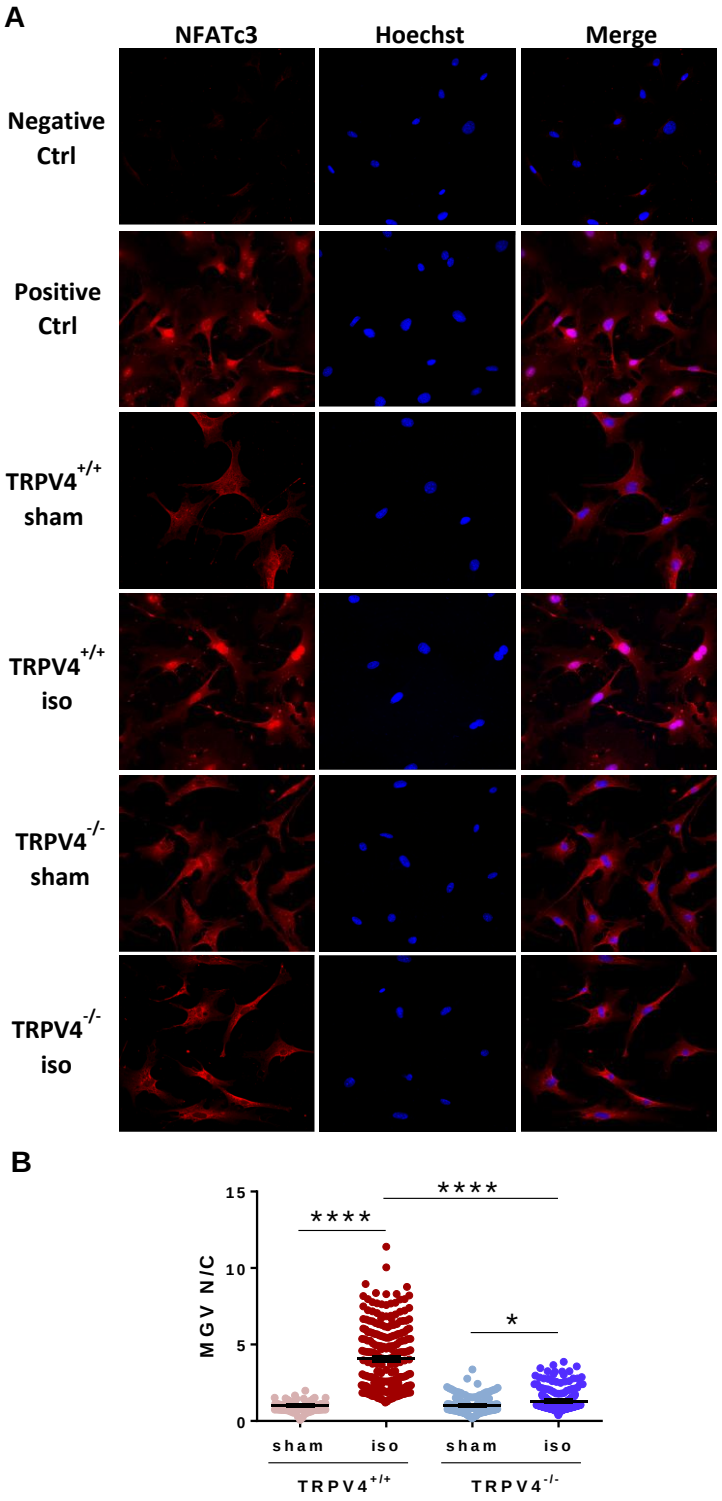
A
NFATc3
Hoechst
Merge
Negative Ctrl
Positive Ctrl
TRPV4+/+ sham
TRPV4+/+ iso
TRPV4-/- sham
TRPV4-/- iso
B
MGV N/C
15
10
5
0
****
****
*
sham
iso
sham
iso
TRPV4+/+
TRPV4-/-

Figure 48. NFAT intracellular distribution in isolated FB from TRPV4$^{+/+}$ and TRPV4$^{-/-}$ mice, either treated with saline (sham) or isoproterenol (iso). A) Representative confocal microscopy images of all experimental groups. Each column represents NFAT staining (left, in red), nuclear staining (centre, in blue) and merge (right). In each row the different experimental conditions and experimental groups are represented. Note: negative control followed the immunostaining protocol but was not incubated with the primary antibody. Positive control was performed by inducing activation of calcineurin and subsequent NFAT translocation by incubating FB with a high-calcium medium (4 mM) for 3 hours. B) NFAT cytoplasmatic and nuclear fluorescence quantification expressed as MGV N/C, the ratio of mean fluorescence intensity (Mean Grey Value) between the nucleus (N) and the cytoplasm (C). N=202-204 FB were measured from 3-4 independent experiments.

4.3.7. POTENTIAL RELATIONSHIP BETWEEN TRPV4 AND TRPC6 CHANNELS IN PATHOLOGICAL REMODELLING

We have demonstrated that, together with TRPV4, TRPC6 is also upregulated after chronic β-adrenergic stimulation. In this regard, some studies have identified TRPC6 as a partial mediator of pathological hypertrophy and as a regulator of FB differentiation, suggesting that this channel has a role in the promotion and development of adverse cardiac response. Thus, we aimed to determine how TRPC6 behaves in the absence of TRPV4, since it is known that mechanoreceptors may change their activity to compensate the loss of other channels with similar functions.

Interestingly, we found that sustained ISO infusion in TRPV4$^{-/-}$ mice failed to induce an upregulation of TRPC6, both at mRNA and protein levels (Figure 49 A-B), suggesting that TRPV4 deletion is somehow altering TRPC6 expression.

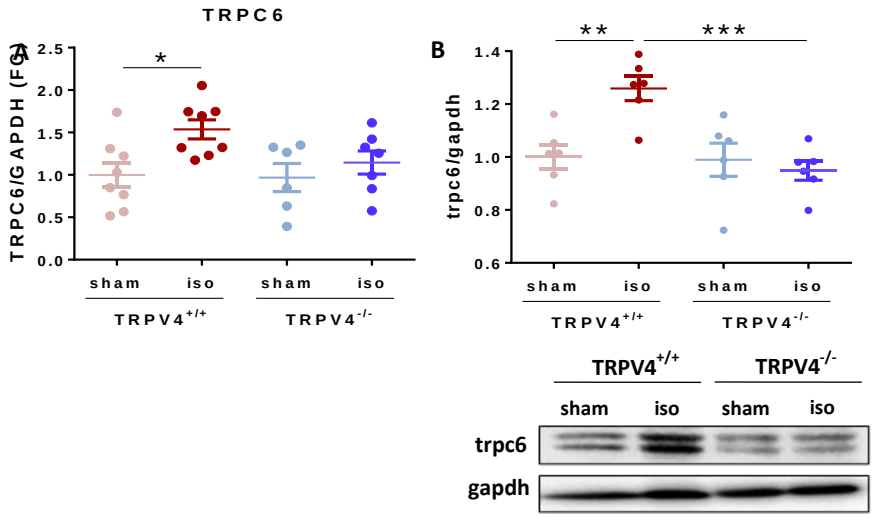

Figure 49. LV TRPC6 expression in TRPV4$^{+/+}$ and TRPV4$^{-/-}$ animals infused with saline (sham) or isoproterenol (iso) for 28 days. A) mRNA expression of TRPC6 normalized to GAPDH and expressed as FC over TRPV4$^{+/+}$ sham, N= 6-8 animals per group. B) Upper panel, WB analysis of TRPC6 protein expression normalized to GAPDH expression. Lower panel, Representative blot, N= 6 animals per group. *p<0.05; **p<0.01; ***p<0.001.

In order to further evaluate the potential regulation of TRPC6 by the TRPV4 channel, we tested if a known TRPC6 promoter was able to induce an upregulation of that channel in TRPV4$^{-/-}$ mice. Previous literature showed that the calcineurin/NFAT pathway regulates TRPC6 expression, both in CM and FB [103,199]. Hence, to bypass the entrance of Ca^{2+} through TRPV4, we induced the activation of calcineurin with a sustained rise in extracellular calcium to trigger NFAT translocation into the nucleus and checked whether TRPC6 expression was increased. Although these experiments were performed at the very end of this thesis and we do not have enough replicates for a statistical analysis, we found that both FB from TRPV4$^{+/+}$ and TRPV4$^{-/-}$ that were incubated with a high amount of Ca^{2+} showed a clear increase in TRPC6 expression compared to those that were grown in regular medium (Figure 50).

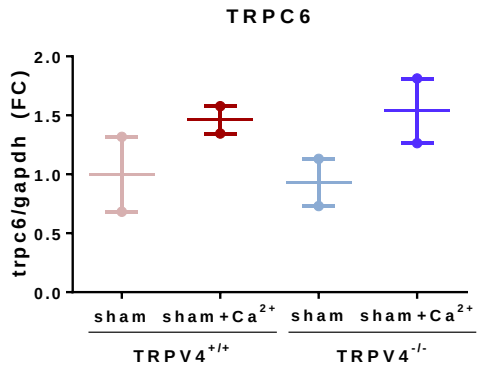

Figure 50. Analysis of the expression of TRPC6 in isolated FB from TRPV4$^{+/+}$ and TRPV4$^{-/-}$ sham animals incubated during 24 hours with regular medium (sham) or medium containing a 4 mM of Ca^{2+} (sham+Ca^{2+}). N=2 animals per group. TRPC6 expression was normalized to GAPDH and expressed as FC over TRPV4$^{+/+}$ sham mice.

Our working model is summarized in Figure 51. Taken together, these results suggest that TRPV4$^{-/-}$ animals can increase expression levels of TRPC6 in response to calcineurin/NFAT activation by supraphysiologic TRPV4 independent increase in intracellular Ca^{2+} (Figure 51 C). Under physiologic conditions, though, it seems that cardiac TRPC6 expression is controlled at least partially by Ca^{2+} entry through TRPV4, and that the deletion of TRPV4 may protect the heart from this response (Figure 51 B). Of note, the fact that the deletion of TRPV4 does not decrease expression of TRPC6, but only hampers its overexpression means that there are other mechanisms by which TRPC6 is controlled, and that this crosstalk between TRPV4 and TRPC6 is probably exclusive of an adverse condition.

This preliminary data warrant future investigation, but altogether suggest that TRPV4 activation could be a primary element in the pathological response, by activating the calcineurin-NFAT pathway, which would induce, not only the expression of fibrotic genes involved in pathological remodelling, but also TRPC6 expression, leading to an enhanced adverse response (Figure 51 A). This hypothesis remains to be confirmed and represents one of the future lines of research following the present project.

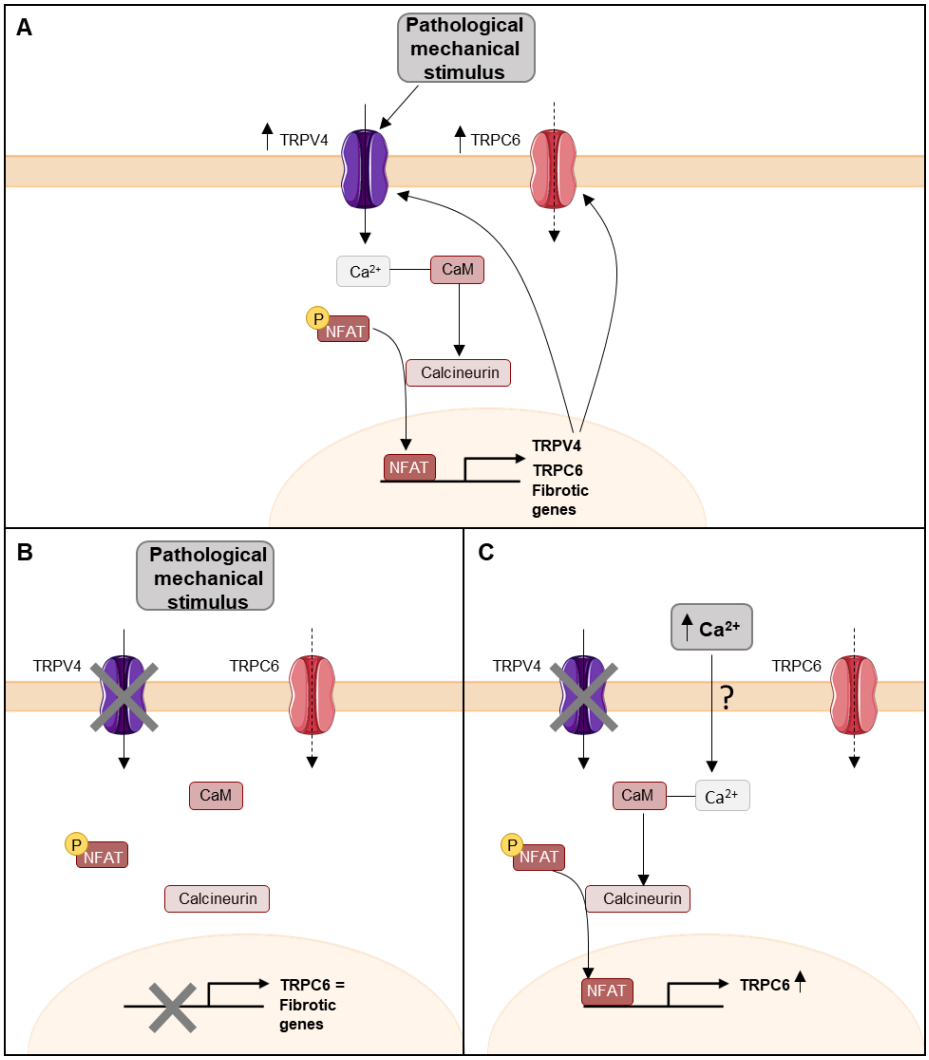

Figure 51. Proposed model outlining the role of the TRPV4 channel in adverse cardiac remodelling and its potential regulation of the TRPC6 channel. A) Pathological mechanical stimulus increases expression of TRPV4, which by increasing Ca^{2+} influx, activates the calcineurin/NFAT pathway and induces the expression not only of fibrotic genes, but also of the TRPC6 channel, enhancing even more the adverse remodelling. B) The deletion of TRPV4 prevents the upregulation of the TRPC6 channel following a pathological stimulus, and also decreases the activation of the calcineurin/NFAT pathway, leading to reduced expression of fibrotic genes. C) In the absence of TRPV4, $TRPV4^{-/-}$ mice can increase the expression levels of TRPC6 in response to calcineurin/NFAT activation triggered by supraphysiologic increase in intracellular Ca^{2+}.

4.4. ROLE OF AGEING AND TRPV4 IN REVERSE REMODELLING AND RECOVERY OF VENTRICULAR FUNCTION AFTER ISOPROTERENOL-INDUCED CARDIOMIOPATHY

We aimed to characterize the HF model induced by isoproterenol infusion, majorly used by us and others [283,284] in young male animals, in elderly female mice. We chose this population of study because both females and aged animals have been largely underestimated in cardiac research, despite cardiac disease affects mainly the elderly and both genders.

Young and aged female C57BL/6J animals were randomized to receive either isoproterenol or saline during 28 days. Additionally, we investigated the potential differences in reverse remodelling and recovery of ventricular function according to age. To that end, another set of young and elderly animals underwent isoproterenol (or saline) infusion during 28 days followed by 28 additional days without receiving any treatment.

The potential involvement of TRPV4 was preliminary assessed in all experimental groups by analysis of TRPV4 expression.

4.4.1. ISOPROTERENOL INFUSION INDUCED HF AT ALL AGES WITH SUBTLE PARTICULARITIES IN AGED FEMALE MICE

To assess the cardiac effects induced by isoproterenol infusion in young and elderly female mice, transthoracic echocardiographic studies were performed at baseline (before osmotic pump implantation) and after 28 days of isoproterenol or saline infusion in all study groups. No differences were observed at baseline among the four study groups (Figure 52, light red and light purple dots). After 28 days, isoproterenol infusion induced an expected increase in both diastolic and systolic LV dimensions in the young population, and a marked reduction in EF and FS, which were not observed in the sham

group (Figure 52, left half of the graphs, red shades). Isoproterenol induced similar morphologic changes in aged mice (Figure 52, right half of the graphs, purple shades), with a non-significant trend to develop less ventricular dilatation compared to the young (9.1% change of LVDd in aged vs. 14.1% change in young animals, p=NS). The decrease of EF and FS was virtually of the same magnitude in young and elderly mice.

Figure 53 shows the histological and gene expression analyses at 28 days. As expected, young mice exposed to isoproterenol (red dots) had CM hypertrophy (Figure 53 A) and greater collagen deposition (Figure 53 B) than controls. So did aged mice of the iso-treated group (purple dots), although both CM CSA (376 μm^2 vs 296 μm^2) and collagen deposition (13.1% vs 11.1%) were significantly higher in aged versus young mice (Figure 53 A-B). It is important to note, however, that aged animals in the sham group had significantly greater basal cardiac fibrosis compared to young controls (6.7% in aged vs 1.1% in young, Figure 53 B). Therefore, the magnitude of increase of tissue fibrosis in mice subjected to isoproterenol versus controls appeared greater in young than in aged mice (by ~10 fold in young compared to ~2 fold in aged mice). As shown in Figure 53 C, mRNA expression of collagen I and III was increased in both iso-treated groups compared to controls, with no relevant differences according to age.

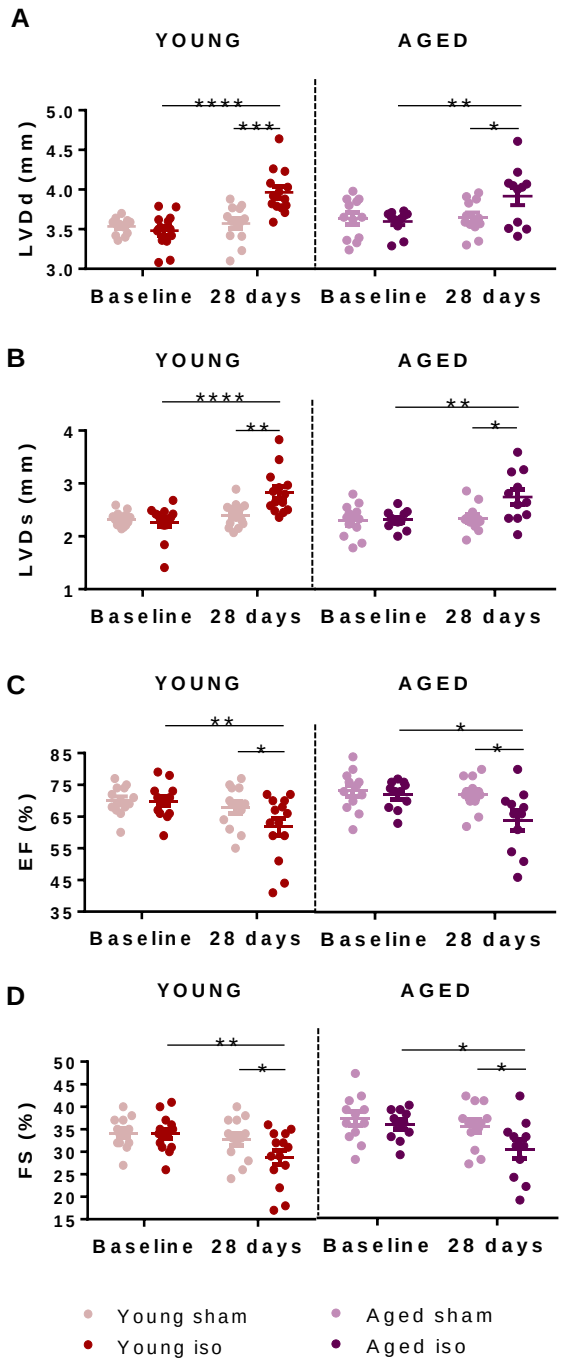

Figure 52. Echocardiographic parameters at baseline and after 28-day exposure to saline or isoproterenol infusion in young and aged mice. A) LVDd: End-diastolic left ventricular diameter. B) LVDs: End-systolic ventricular diameter. C) EF: ejection fraction. D) FS: fractional shortening. *p<0.05; ** p<0.01; ***p<0.001; ****p<0.0001.

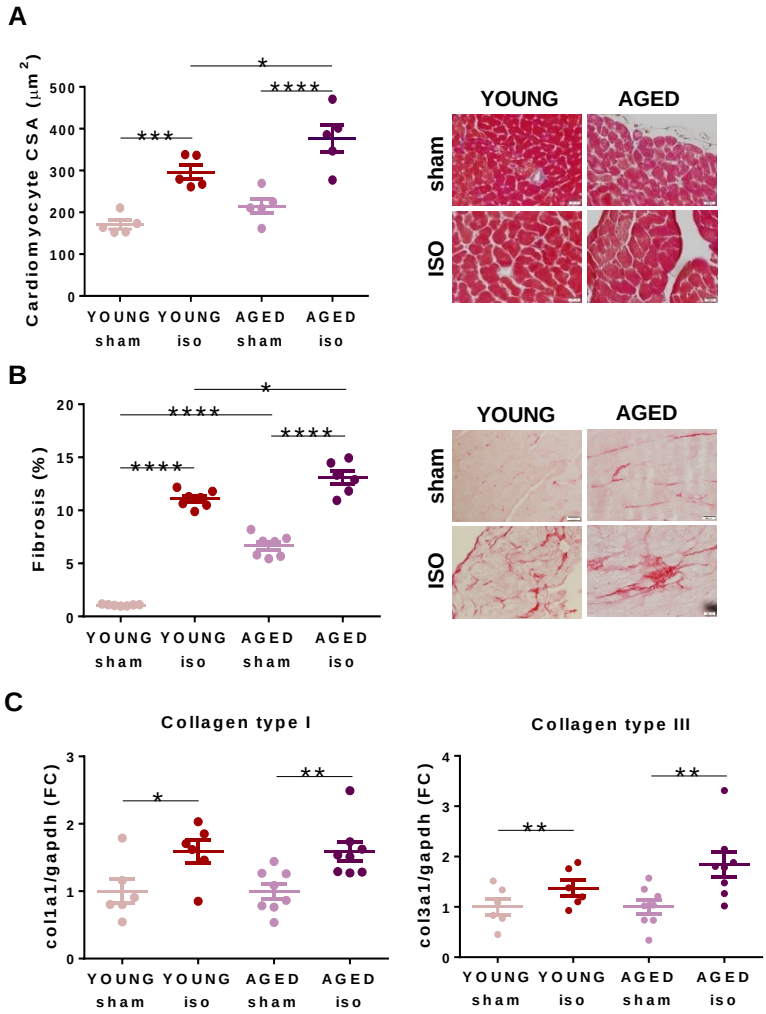

Figure 53. Histological findings and mRNA expression analyses at 28 days after exposure to ISO (iso) or saline (sham) infusion in young and aged mice. A) Left panel, CM CSA in the four study groups, N=5 animals per group. Right panel, representative microphotograph. B) Left panel, quantification of collagen deposition in picrosirius-stained sections in the four study groups, N=5 animals per group. Right panel, representative microphotographs. C) mRNA expression of *col1a1*, *col3a1* in the four study groups, N=6-8 animals per group. *p<0.05; **p<0.01; ***p<0.001; ****p<0.0001.

Together, these results support the suitability of the iso-model as a HF model in aged female mice. Despite exhibiting greater ventricular fibrosis at baseline, aged female animals developed HF features in response to isoproterenol, including LV dilatation and dysfunction and increased histological fibrosis.

Aged mice under isoproterenol also exhibited certain subtle particularities in terms of LV remodelling, including the presence of greater cell hypertrophy and tissue fibrosis compared to young mice.

4.4.2. REVERSE REMODELLING IS DISTINCTLY DIFFERENT IN YOUNG AND AGED FEMALE MICE

The study of reverse remodelling and HF recovery was assessed in a second set of female animals in whom isoproterenol infusion was withdrawn after 28 days of exposure. Figure 54 summarizes the results of the echocardiographic parameters obtained in the four experimental groups at the three study timepoints: baseline, end if iso/saline challenge (28 days, HF induction, HF-28 days), and end of recovery period (56 days, recovery, REC-56 days). Young animals with isoproterenol exposure and subsequent withdrawal exhibited complete reverse remodelling, with LVDd and LVDs values at REC-56d close to those at baseline. Conversely, LVDd and particularly LVDs failed to return to baseline values in aged mice after isoproterenol withdrawal. Furthermore, EF and FS recovered in young animals (values of 66.4%±3.8 and 31.3%±2.7 at REC-56d, respectively) but failed to do so in the elderly (values of 52.7%±7.0 and 23.3%±4.5, at REC-56d, respectively).

Histological analyses of LV tissue sections at 56 days showed that young female animals undergoing isoproterenol infusion and subsequent withdrawal had similar CM CSA and collagen deposition compared to their counterpart sham. Conversely, aged female mice showed CM hypertrophy and significantly greater collagen deposition compared to their corresponding sham, and also compared to young mice undergoing the same protocol (isoproterenol infusion and recovery period) (Figure 55 A-B). Collagen I expression was found increased in aged mice compared to young among those having been treated with isoproterenol (Figure 55 C).

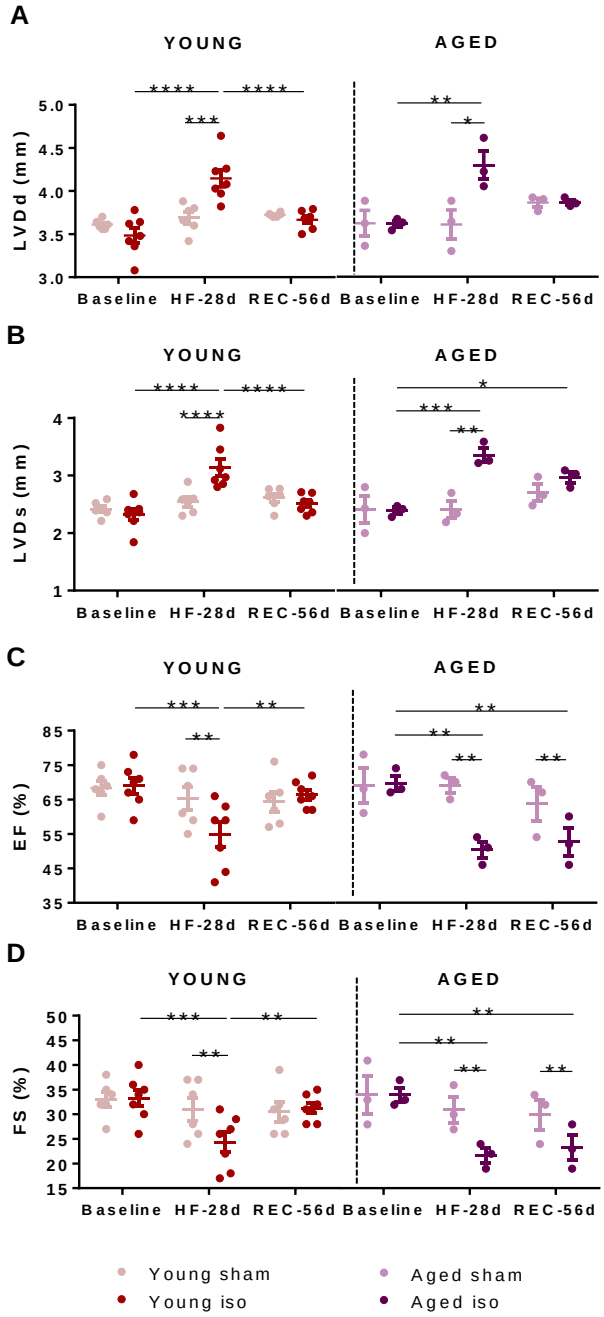

Figure 54. Echocardiographic parameters at baseline, after 28-day exposure to saline or isoproterenol (iso) infusion (HF-28d), and at 56 days after exposure + recovery period (REC-56d) in young and aged mice. A) LVDd: End-diastolic left ventricular diameter. B) LVDs: End-systolic left ventricular diameter. C) EF: ejection fraction. D) FS: fractional shortening. N= animals per group. *p<0.05; ** p<0.01; *** p<0.001; **** p<0.0001.

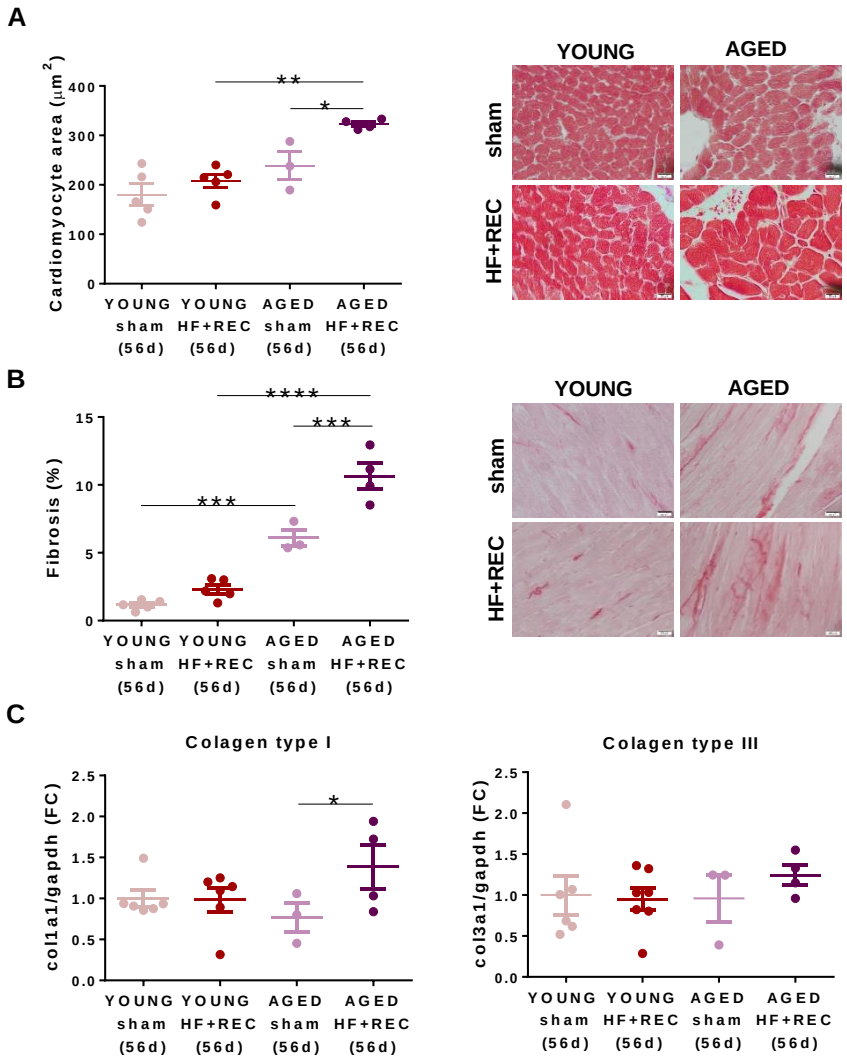

Figure 55. Histological findings and mRNA expression analyses at 56 days, after exposure to isoproterenol (iso) or saline infusion and recovery, in young and aged mice. A) Left panel, CM CSA in the four study groups. Right panel, representative microphotograph. B) Left panel, quantification of collagen deposition in picrosirius-stained sections. Right panel, representative microphotographs of each study group. C) mRNA expression of *col1a1* and *col3a1* in the four study groups. * p<0.05; ** p<0.01; *** p<0.001; ****p<0.0001.

4.4.3. TRPV4 EXPRESSION IN YOUNG AND AGED MICE WITH ADVERSE REMODELLING AND RECOVERY

According to our previous results on TRPV4 (section 4.3), we sought to evaluate whether the differences observed between young and aged mice in response to isoproterenol infusion and withdrawal could be explained, at least in part, by TRPV4 activity. In an attempt to provide a preliminary explanation for such differences, and to open a new door for future investigation, we determined the mRNA expression of TRPV4 in LV homogenates of young and aged female mice of all groups.

According to our previous results, TRPV4 expression increased in both young and aged female mice after 28 days of isoproterenol infusion. Notably, aged sham mice showed an increased upregulation of TRPV4 compared to young controls (~25% increase in aged vs young sham animals), suggesting an age-dependent increase in the channel expression (Figure 56 A). Furthermore, after 28 days of isoproterenol infusion and 28 days of recovery (56 days), expression of TRPV4 was similar to that of sham littermates in young mice. On the contrary, despite withdrawing the isoproterenol stimulus, elderly animals continued to show an increased expression of TRPV4 compared to their matched sham, and also to young animals under the same protocol (Figure 56 B).

Although preliminary and still requiring further investigation, these results suggest that cardiac TRPV4 expression runs in parallel with myocardial fibrosis. Specifically in aged mice, both collagen deposition and TRPV4 expression were increased at baseline compared to young animals. Moreover, elderly animals failed to exhibit reverse remodelling after beta-adrenergic withdrawal, findings that were associated with persistent fibrosis and TRPV4 overexpression.

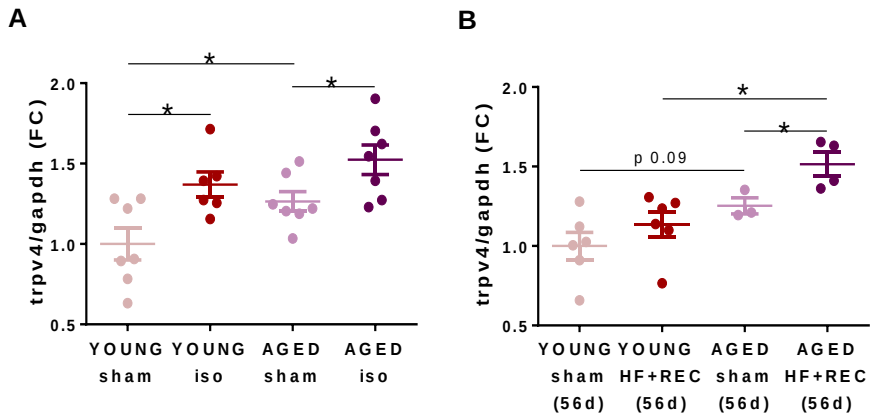

Figure 56. mRNA expression of TRPV4 in LV samples of young and aged mice at A) 28 days, following saline or ISO challenge and B) 56 days, after exposure to saline or ISO infusion and 28 days of recovery. *p<0.05.

5. DISCUSSION

In this work, we demonstrated that cardiac expression of TRPV4 and TRPC6 is increased exclusively in hearts suffering pathological remodelling such as that seen in HF. Both channels did not show appreciable changes after physiological remodelling induced by exercise. In a time-course study, we further demonstrated that cardiac TRPV4 and TRPC6 increase along with the establishment of major features of adverse remodelling, particularly fibrosis. Because, at the time this thesis was designed, TRPC6 had already been studied in the context of adverse remodelling and HF, we moved to explore the role of TRPV4 in the same context, using a model that most resembles the human HF (induced by chronic beta-adrenergic stimulation), and a colony of transgenic mice with genetic deletion of TRPV4.

The results of the study with transgenic mice confirmed that TRPV4 deletion resulted in protection against the HF phenotype induced by chronic infusion of isoproterenol, with a remarkable reduction of fibrosis and attenuation of CM hypertrophy. Moreover, arrhythmia inducibility was also decreased in $TRPV4^{-/-}$ animals receiving isoproterenol compared to $TRPV4^{+/+}$ with the same treatment. These results confirmed that TRPV4 channels are directly involved in the promotion of adverse cardiac remodelling.

We then attempted to identify by means of which molecular pathways TRPV4 could be participating in the pathological response. Because TRPV4 is a membrane channel with high selectivity for Ca^{2+}, we explored the Ca^{2+}-dependent calcineurin/NFAT pathway, extensively involved in pathological remodelling. We demonstrated that, at the cardiac level, TRPV4 channels are mostly expressed in cardiac FB. In FB from $TRPV4^{+/+}$ animals, isoproterenol infusion induced an increase in Ca^{2+} entrance into the cell and calcineurin activation, with subsequent nuclear translocation of NFAT, the transcription factor initiating the expression of fibrotic genes. This response was inhibited in $TRPV4^{-/-}$ animals.

In a final group of experiments, performed to set the bases for future continuation of this thesis' project, we preliminary explored the potential interaction between TRPV4 and TRPC6 in the induction of pathological remodelling, and evaluated the role of aging in HF induction and also HF recovery, and the potential involvement of TRPV4 channels in these processes.

In the following lines, the main findings of the project will be discussed.

5.1. EXPERIMENTAL MODELS OF VENTRICULAR REMODELLING

In order to determine the potential contribution of mechanoreceptors in adaptive and adverse remodelling, we used different animal models that covered several types of chronic stress, all of them associated with the development of distinct types of cardiac remodelling. The study of adverse remodelling was performed using a model of chronic isoproterenol infusion, widely used to mimic the chronic β-adrenergic activation seen in human HF [288], and a model of TAC, a paradigm of HF induced by cardiac pressure overload [147]. Both conditions, irrespective of the primary stimulus, represent good models of chronic HF with reduced ejection fraction, resembling the final stage of cardiac disease. We chose not to use a HF model induced by myocardial infarction because, by definition, this model might generate different injuries across animals and tissue heterogeneity within the heart. On the other hand, to explore the cardiac adaptive remodelling induced by exercise, we used a model of daily training on a treadmill in both mice and rats.

Our results showed that both isoproterenol administration in mice and TAC surgery in rats induced a maladaptive cardiac response, displaying numerous typical characteristics of advanced HF in humans. In particular, 28 of isoproterenol infusion promoted the development of LV dilatation, ventricular

hypertrophy and fibrosis, and impaired cardiac function. We observed that cardiac morphological and functional changes were similar with the two tested doses of isoproterenol (30 and 60 mg/kg/day), although the higher dose resulted in greater hypertrophic response. In this sense, it has been previously reported that the isoproterenol-induced effects over the heart develop proportionally to the dose and duration of the treatment [294]. Moreover, the route and the regime of administration could also determine the adverse cardiac response: whereas daily injections of isoproterenol have been reported to generate severe and rapid ventricular dysfunction [295], continuous release of isoproterenol through osmotic pumps resembles the neurohormonal stimulation seen in human HF, and generates a progressive cardiac remodelling, which corresponds more accurately with the clinical scenario [296]. Similarly, we also showed that rats exhibited a significant increase in hypertrophy and collagen deposition after TAC surgery. However, it is important to note that, although the TAC model has been broadly used to promote an adverse cardiac response, aortic constriction causes an immediate pressure overload that is not usually present in human conditions such as hypertension or aortic stenosis [297]. This is one of the main reasons why we chose to follow our studies using exclusively the isoproterenol model as our gold standard model of human chronic HF.

On the other hand, we showed that mice and rats subjected to exercise training developed a physiological cardiac response, at least at moderate doses. It has been generally accepted that human athletes display heart adaptations that lead to a more compliant and distensible LV that allow increased stroke volume during exercise practise [298]. Several studies have demonstrated that endurance athletes exhibit increased LV wall thickness and greater chamber volume, with unchanged or improved cardiac function [44,299]. Consistent with previously published studies [300,301], we showed that our mice and rat models subjected to exercise developed cardiac morphological

alterations comparable to those described in human athletes. We found that mice following a long-term exercise routine experienced an increase in LV hypertrophy, as well as chamber dilatation, while preserving systolic function.

Of note, we also found that intensive exercise training induced a mild increase in tissue fibrosis (3%) in our model, although far from the one observed in the isoproterenol model (13%). This finding differs from previous publications on the topic, including a rat model of chronic endurance training on a treadmill, which showed mild right, but not left, ventricular fibrosis [281]. We believe these findings are most likely due to some degree of animal distress induced by an excessive training load in this group of animals. We therefore did not use this model in further experiments.

5.2. DIFFERENTIAL EXPRESSION OF MECHANORECEPTORS IN ADAPTIVE AND ADVERSE CARDIAC REMODELLING

Adaptive and adverse cardiac remodelling initially develop in response to a cardiac overload, but they differ greatly in terms of their underlying molecular mechanisms, cardiac phenotype, and prognosis. In recent years, a great scientific activity has focused on defining the mechanisms and the differential factors involved in both forms of cardiac remodelling and the long-term transition from one form to another. To date, it is still unclear what are the determinant factors that, in response to a hemodynamic overload, orchestrate the development towards an adaptive or an adverse response. Since the primary stimulus of overload is mechanic in nature, the study of stretch and mechanosensation of the ventricular wall is especially attractive. In this context, mechanoreceptors, including K^+ selective, Piezo, and TRP channels, are postulated as potential initiators of ventricular remodelling.

Mechanorreceptors function as ion channels, so, upon mechanical stimulation, they open to allow ion movement across the cellular membrane. Among them, those facilitating Ca^{2+} entry into the cell, with the potential to activate Ca^{2+}-dependent intracellular pathways, arise as promising mediators of pathological remodelling, as increases in intracellular Ca^{2+} initiate and sustain the pathological heart response [72,73,302].

In this work, we performed a comprehensive tissue determination of cardiac mechanoreceptors in both types of remodelling. To the best of our knowledge, this is the first time that a complete screening cardiac mechanoreceptor expression in response to different forms of hemodynamic overload is shown. We found that both transcript and protein levels of TRPV4 and TRPC6 were increased in the adverse but not in the adaptive remodelling. Moreover, we demonstrated that these channels followed the same pattern in two additional models (TAC and exercise) generated in rats. Both TRPV4 and TRPC6 channels were mainly expressed in cardiac FB, with minor expression in CM. TRPC6 expression had been previously found increased in experimental models of HF [103,199]. Last year, during the final period of the present thesis, a paper was published reporting a crucial role of TRPV4 in mediating pathological remodelling following myocardial infarction [272]. However, no previous information exists on TRPV4 expression during pathological remodelling induced by chronic isoproterenol infusion, nor in the differential TRPV4 and TRPC6 expression seen between the two forms of cardiac remodelling.

Our results also showed that exercise induced the downregulation of KCNJ11, TRPM4, and TRPV1 channels. Recently, Wang and collaborators demonstrated that exercise training induces the downregulation of some ventricular K^+ channels, which, by prolonging ventricular myocyte action potential duration, increase CM efficiency and contractility [303]. However, contrary to our data,

some reports suggested that TRPM4 and TRPV1 channel activation may improve exercise endurance in mice [184,304]. In this regard, more in-depth studied are needed, as we only checked the expression of mechanoreceptor at the RNA level.

Overall, our results highlight that several mechanoreceptors participate differentially in adaptive and adverse cardiac remodelling, and that the overexpression of TRPV4 and TRPC6 could drive in tandem the pathological response, with no apparent effects on the physiological remodelling.

5.3. TIME-COURSE RELATIONSHIP BETWEEN TRPV4 AND TRPC6 AND THE DEVELOPMENT OF ADVERSE CARDIAC REMODELLING

It is well established that chronic activation of the SNS and the RAAS contributes to HF by activating several Ca^{2+}-dependent pathways that lead to adverse remodelling [305,306]. Such is so, that the current strategies for HF treatment aim to modulate these neurohormonal systems [125]. However, only modest efficacy is seen at the clinical level, revealing a big need to identify alternative therapeutic targets. Emerging evidence suggests that mechanical stimuli and contractile forces applied on cell membranes activate mechanoreceptors, which could trigger signalling pathways critical for the transition and progression of adverse remodelling [307]. We found that TRPV4 and TRPC6 channels are upregulated in adverse cardiac remodelling caused by isoproterenol infusion. To evaluate whether the expression of both channels preceded the onset of the pathological response, we examined the time-dependent progression of cardiac remodelling in relation to TRPV4 and TRPC6 expression.

Sustained β-adrenergic stimulation via isoproterenol infusion caused a noticeable cardiac hypertrophy as soon as 3 days post-pump implantation, which is consistent with previous publications [156,308]. Ventricular wall thickening, consequence of the growth of individual CM, exerts a short-term compensatory response necessary to minimize ventricular wall stress and maintain contractile function [309]. However, under chronical pathological stimulation, this initial adaptive remodelling eventually progresses to ventricular chamber dilatation and molecular changes that alter the functionality of the excitation-contraction coupling system and the sarcomere machinery, promoting a maladaptive heart response that leads to cardiac dysfunction [66]. In line with that, the time-course study in our iso-model showed, besides the expected early LV hypertrophy, a gradual chamber dilatation and a subtle but progressive CM growth throughout the isoproterenol-exposure period. These findings are consistent with previous publications indicating that transition to decompensated hypertrophy is accompanied by a significant CM loss, which is balanced by an enlargement of the surviving CM [310].

Fibrosis, a specific hallmark of pathological remodelling, became significantly evident after 7 days of isoproterenol infusion. In fact, after 3 days, there was already a mild, non-significant increase in collagen deposition, which correlated with the highest levels of *col1a1* and *col3a1* transcripts. This suggests that FB were already activated and began to synthesize collagen after only 3 days of isoproterenol administration. An initial increase in collagen synthesis may be beneficial to support the increase in muscle mass, but in excess it can adversely alter myocardial compliance by increasing myocardial stiffness [311]. Importantly, fibrosis kept increasing remarkably throughout the study period, and proportionally to the duration of isoproterenol administration. This, together with CM hypertrophy, led to a progressive

decline in cardiac performance, reflected by a decreased systolic function, throughout the infusion of isoproterenol.

In our study, the expression of TRPV4 and TRPC6 was closely related to the progression of the adverse cardiac response, and especially to the onset of fibrosis. mRNA expression of both TRPV4 and TRPC6 was significantly increased already after 7 days of isoproterenol treatment, and continued to increase over time, although changes at the protein level became significant at 28 days. The temporal association of TRPV4 and TRPC6 expression with collagen deposition together with the fact that both channels were found mostly in FB, makes it reasonable to think that they may be primarily contributing to the development of myocardial fibrosis.

Two possible scenarios could explain these findings: either the activation of TRPV4 and TRPC6 is secondary to the onset of fibrosis, or their activation precedes the fibrotic response. The first scenario would be supported by the fact that collagen synthesis was already upregulated 3 days after isoproterenol exposure, whereas none of the analysed TRP were differentially expressed at that time. In this case, one could speculate that initial changes in ECM stiffness caused by collagen deposition could alter the mechanical environment and secondarily stimulate the activation and expression of both channels. If that was the case, once activated, TRPV4 and TRPC6 could transduce these mechanical signals and magnify downstream signalling cascades, accelerating the progression of adverse remodelling (Figure 57 A). The second scenario implies that, although without changes in expression, TRPV4 and TRPC6 activity could be increased already at day 3 in response to the persistent hemodynamic overload. This would finally derive in greater expression of both channels at day 7. In this case, Ca^{2+} entry into the cell could precede and drive the fibrotic response, establishing a positive feedback loop that would cause

an increase of their expression and even a greater collagen deposition (Figure 57 B).

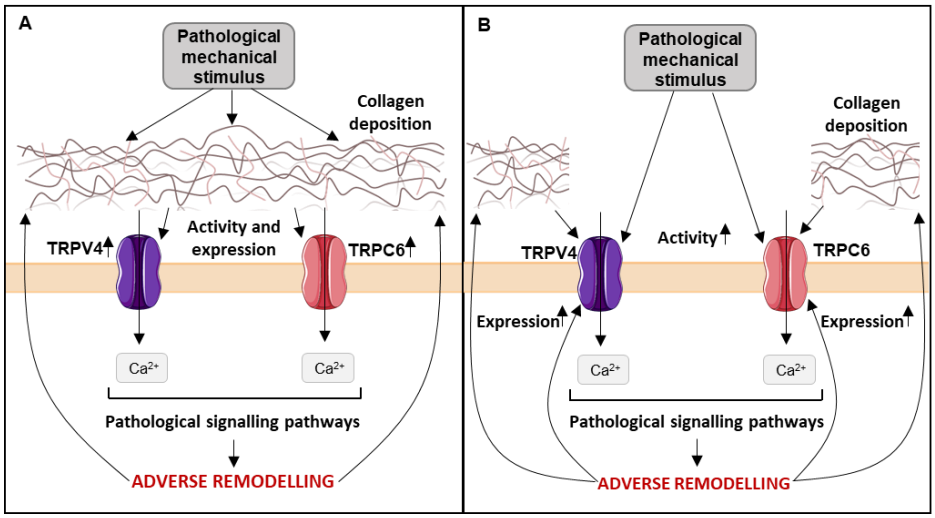

Figure 57. Possible mechanisms of TRPV4 and TRPC6 channel activation. A) Activation of TRPV4 and TRPC6 is secondary to fibrosis onset. Pathological mechanical stimulus induces the synthesis and the accumulation of collagen in the extracellular space, which, by altering the mechanical environment, stimulate the activation and expression of both channels. Once activated, TRPV4 and TRPC6, lead to increased Ca^{2+} influx, magnifying Ca^{2+} -dependent signalling cascades and accelerating the progression of adverse remodelling. B) Activation of TRPV4 and TRPC6 precedes the fibrotic response. Pathological mechanical stimulus increases the activity of TRPV4 and TRPC6, which by promoting Ca^{2+} entry into the cell precede and drive the fibrotic response, creating a positive feedback loop that causes an increase in their expression and greater collagen deposition.

Either way, we suggest that TRPV4 and TRPC6 channels are enhancing the development of fibrosis, leading to the progression of the adverse cardiac remodelling and ultimately to HF. Supporting our results, some authors have already described the potential role of TRPC6 in the promotion of cardiac fibrosis. Using *in vitro* analysis of cultured FB, Davis *et al.* identified that the overexpression of TRPC6 promoted the differentiation of FB to MFB, while the loss of the channel fully inhibited MFB transformation [103]. Further, Lin and collaborators demonstrated that the chemical inhibition of TRPC6 led to a reduction in cardiac fibrosis in mice that had undergone TAC surgery [201].

However, another study pointed out that despite TRPC6 deletion may be beneficial by reducing myocardial fibrosis, its inhibition may exasperate cardiac hypertrophy and CM dysfunction [312]. Therefore, although most literature supports a role for TRPC6 in pathological remodelling, whether TRPC6 is the primary mechanoreceptor that drives the Ca^{2+} influx and the fibrotic response requires further investigation.

5.4. TRPV4 DELETION IMPROVES CARDIAC OUTCOME FOLLOWING ISOPROTERENOL INFUSION

Because the role of TRPC6 in cardiac adverse remodelling has been previously investigated [103,199,201], we evaluated the potential participation of TRPV4 channels. Previous literature has shown that activation of TRPV4 contributes to the intracellular Ca^{2+} accumulation, which could lead to the development of adverse cardiac remodelling. TRPV4 was recently shown to mediate an abnormal cytosolic Ca^{2+} rise in CM from dilatated cardiomyopathy patients, thereby weakening the contractility of the cardiac muscle and worsening the progression of the disease [271]. Consistent with the role of TRPV4 in CM, some authors also reported that TRPV4 inhibition improved cardiac function during ischemia/reperfusion (I/R) injury through the regulation of CM Ca^{2+} transients [268,269]. However, none of those studies investigated the role of the channel in cardiac FB. Only the work by Adapala and colleagues, published when this thesis was entering its final stage, provided evidence that TRPV4 deletion could reduce cardiac fibrosis by inhibiting FB differentiation and improving cardiac function in mice subjected to myocardial infarction, a different cardiac insult that the one used in this work [272]. Although their work partially hampered the originality of our own study, no information on the role of TRPV4 in non-ischemic pathological stimulus is available to date, nor on the

potential Ca^{2+}-dependent signalling pathways activated by TRPV4 that could mediate the pathological process (see below), and this is specifically where the importance of the present thesis comes in place.

Because our results indicated that TRPV4 channels are mostly present in cardiac FB and linked to the development of cardiac fibrosis under sustained isoproterenol exposure, we sought to demonstrate the effect of TRPV4 deletion upon fibrosis and cardiac function under this type of hemodynamic overload. Importantly, we found that $TRPV4^{-/-}$ mice subjected to isoproterenol treatment exhibited significant less collagen deposition and showed preserved systolic function compared to $TRPV4^{+/+}$ mice. These findings have direct clinical implications since they demonstrate that under chronic conditions of β-adrenergic stimulation, the deletion of TRPV4 preserves cardiac performance and markedly attenuates myocardial fibrosis, the main hallmark of the pathological cardiac remodelling, providing the basis for a new therapeutic target in the management of HF

Interestingly, we also found that the absence of TRPV4 significantly reduced CM CSA, preserving the structural integrity of left cardiac chambers. Although we do not know the exact mechanism for this reduced hypertrophy, we speculate that the absence of TRPV4 may modulate CM phenotype in two ways. TRPV4 deletion in CM, may render these less responsive to the mechanical signals that trigger hypertrophy. Alternatively, according to the growing evidence that FB may modulate the structure and function of CM by changing the composition of the ECM or by releasing soluble paracrine mediators [84], the suppression of TRPV4 in FB could crosstalk with CM signalling, leading to an attenuated hypertrophic response. Irrespective of the exact mechanism by which TRPV4 deletion preserves cardiac structure, targeting TRPV4 may also offer a protective effect over pathological cardiac hypertrophy.

5.5. TRPV4 DELETION DIMINISHES ARRYHTHMOGENESIS AFTER CHRONIC ISOPROTERENOL ADMINISTRATION

Ventricular tachyarrhythmias (VTA) are favoured by the molecular changes accompanying the cardiac pathological remodelling.

Cardiac fibrosis, by disrupting the ECM, alters the electrical activation patterns and facilitates re-entry, the most common arrhythmogenic mechanism [313]. However, altered intracellular Ca^{2+} handling in CM [314], inflammatory signalling [315], changes in gap junctional intercellular communication [286], and myocyte-fibroblast crosstalk [316], and other underlying mechanisms have been also been described as responsible for arrhythmogenesis in HF.

In our model of HF, we explored whether TRPV4 channels could also be involved in the generation of VTA.

Our electrophysiological studies demonstrated that, as expected for the mouse heart, inducibility of ventricular arrhythmias at baseline was scarce [270,317]. We therefore conducted the arrythmia inducibility study following regional ischemia, a condition known to facilitate arrhythmogenesis after isoproterenol treatment and previously used to assess arrhythmia vulnerability [318]. Fifteen minutes after induction of regional ischemia (and therefore, past its most acute phase), only $TRPV4^{+/+}$ animals subjected to isoproterenol infusion showed an increase in the number of total VTA and a trend to develop longer episodes. In contrast, $TRPV4^{-/-}$ animals under the same β-adrenergic agonist treatment were not susceptible to increase neither the number nor the duration of total VTA. Considering that fibrosis forms a prominent arrhythmic substrate [319–321], these results could be explained by the fact that $TRPV4^{-/-}$ animals, compared to $TRPV4^{+/+}$, have reduced fibrosis after isoproterenol infusion, so arrhythmia vulnerability in all study groups could be

proportional to the amount of myocardial fibrosis. However, as suggested by several recent publications [270,317], TRPV4 itself could directly participate in arrhythmogenesis by at least three means: 1) increasing Ca^{2+} entry in CM, leading to the activation of the Ca^{2+}-calmodulin-dependent protein, CaMKII, previously involved in arrhythmogenesis [21]; 2) activating NCX secondarily to increased Ca^{2+} entry, favouring Na^{+} entry and potential delayed afterdepolarizations; or 3) increasing CM membrane refractory period [317,322]. In all these cases, TRPV4 arrhythmogenesis would be mediated by direct effects of the channel over CM. In the present work, we did not explore the potential consequences of TRPV4 overexpression and deletion in CM. Whether TRPV4 promotes arrhythmogenesis through fibrosis generation or by combining effects on Ca^{2+} homeostasis in CM remains to be established in future studies.

5.6. TRPV4 MEDIATES FIBROSIS THROUGH THE CALCINEURIN/NFAT PATHWAY

Previous extensive literature has described that Ca^{2+} signalling pathways play a critical role in FB differentiation [187,188,201,323], a key process in cardiac fibrosis and pathological response [324]

We found that FB isolated from iso-treated $TRPV4^{+/+}$ mice had higher Ca^{2+} influx compared to sham mice when stimulated with a TRPV4 agonist (GSK) or when exposed to an hypoosmotic solution. Importantly, GSK and hypotonicity-mediated Ca^{2+} influx was significantly attenuated by pre-treatment with the TRPV4 antagonist HC, indicating that the observed increase in Ca^{2+} was exclusively mediated by the activation of the TRPV4 channel. In addition, our results also confirmed that $TRPV4^{-/-}$ FB failed to induce any Ca^{2+} influx under GSK or hypoosmotic treatment. Together, these results demonstrate that TRPV4 is a functional Ca^{2+} influx-mediator in FB and

that, under conditions of persistent hemodynamic overload, its increased expression contributes to a higher influx of Ca^{2+}.

Several lines of evidence have demonstrated that increased Ca^{2+} entry and sustained elevation in cytosolic Ca^{2+} concentration contributes to FB differentiation and fibrosis by activating abnormal calcium-dependent signalling, especially the calcineurin/NFAT pathway [102,103,183]. A persistent increase in intracellular Ca^{2+} results in Ca^{2+}-dependent binding of CaM to calcineurin, causing a conformational change that exposes its active site [325]. Upon activation, calcineurin leads to NFAT dephosphorylation, usually hyperphosphorylated and sequestered in the cytoplasm, which causes its nuclear translocation to facilitate the regulation of transcription of fibrosis-related genes [326]. In this sense, Molkentin *et al*. showed that transgenic mice expressing a constitutively active form of calcineurin developed cardiac fibrosis and HF [101]. Other authors also reported that fibrosis was reduced after treatment with a calcineurin/NFAT blocker [102,103]. Interestingly, previous literature has highlighted the role of TRPC6 in the activation of this pathway in cardiac ventricular FB and driving the fibrotic response [103]. However, other studies demonstrated that TRPC6 deletion was not associated with complete reversion of fibrosis [199,201], suggesting that other mechanoreceptors could be also involved. On another hand, TRPV4 has been widely linked to the calcineurin/NFAT pathway in other organs and tissues, where it mediates airway smooth muscle cell proliferation [327], osteoclast differentiation [328], or hypoxia-induced pulmonary arterial smooth muscle cell migration [329]. Therefore, we hypothesized that, in cardiac FB, TRPV4 Ca^{2+} signals might be involved in the development of fibrosis by promoting the activation of this signalling pathway.

Our results showed that under isoproterenol treatment, FB of $TRPV4^{+/+}$ mice, with marked myocardial fibrosis and upregulation of TRPV4, had increased

calcineurin activity and nuclear localization of NFATc3. Importantly, diminished fibrosis in TRPV4$^{-/-}$ mice was accompanied with attenuated calcineurin activity and NFATc3 nuclear translocation. The NFAT family consists in five isoforms, NFATc1-c4, NFAT5, each of them performing diverse functions and having unique expression patterns in different tissues [330]. In this work, we chose to determine NFATc3 as this has been majorly involved in the appearance of the fibrotic phenotype of cardiac FB [331]. It is important to note that NFAT signalling regulates the expression, among others, of α-SMA, collagen I, and collagen III, and its pharmacological inhibition leads to an impaired transcription of these genes [102]. This is in line with the results of our study, where the development of pathological remodelling was associated with increased calcineurin/NFAT activity, and also with increased expression of α-SMA, collagen I, and collagen III, a response that was inhibited in TRPV4$^{-/-}$ mice.

In conclusion, these findings define a new regulatory mechanism underlying the differentiation of FB and the production of fibrosis, in which Ca^{2+} influx through TRPV4 channels located in cardiac FB activates the calcineurin/NFAT signalling pathway, promoting the transcription of fibrotic genes (Figure 58). While drugs targeting systematically calcineurin or NFAT can block maladaptive remodelling [102,332], their therapeutic use has been associated with severe side effects, due to the ubiquity of this pathway in the body and its participation in other biological processes[333]. In this regard, targeting specifically TRPV4 could provide a more suitable approach, by inhibiting specifically the pathway activated by mechanical stretch, and leaving the calcineurin/NFAT pathway active for other activating signals.

From our data, we cannot exclude the possibility that other signalling pathways could be activating NFAT, since its nuclear translocation was not completely abolished in TRPV4$^{-/-}$ mice. At the same time, TRPV4 could be also

regulating other fibrotic pathways. In fact, Adapala and collaborators published that following myocardial infarction, TRPV4 regulates fibrosis by activating the TGF-β pathway and the signalling through Rho/ROCK/MRTF-A, which promotes α-SMA expression and its incorporation into stress fibres [272]. Therefore, it plausible that TRPV4 deletion-mediated cardioprotection could be due to the downregulation of more than one signalling pathway.

5.7. TRPV4 AS A REGULATOR OF TRPC6 EXPRESSION

As previously discussed, in our HF model, the expression of TRPC6 was increased in parallel with that of TRPV4 and with the development of fibrosis following isoproterenol exposure. Notably, Davis *et al.* observed that the activation of TRPC6 also induced calcineurin/NFAT signalling to promote FB differentiation [103], which together with our findings suggests that TRPV4 and TRPC6 may cooperate to induce the activation of this pathway and the fibrotic response. Importantly, our results suggested that following a pathologic stimulus, TRPV4 deletion not only prevented adverse remodelling, but also impeded TRPC6 upregulation. One could speculate that TRPV4 and TRPC6 could heterooligomerize in a functional new channel entity, but this has been never reported and although that could still be an option, the most plausible scenario is that TRPC6 expression is partially dependent on TRPV4 activity.

Interestingly, Kuwahara *et al.* demonstrated that the promoter of the *TRPC6* gene contained two NFAT-binding sites, and that during pathological cardiac remodelling the increase in intracellular Ca^{2+} concentration and the activation of the calcineurin/NFAT pathway stimulated transcription of the *TRPC6* gene [199]. Based on these findings, we speculated that the activation of the calcineurin/NFAT signalling pathway by TRPV4 activity could also regulate TRPC6 expression in our experimental model.

Because activation of calcineurin requires a sustained rise in intracellular Ca^{2+}, and we and others have shown that the exposure of FB to increased extracellular Ca^{2+} concentration results in the translocation of NFAT into the nucleus [334], we explored whether primary FB from $TRPV4^{+/+}$ and $TRPV4^{-/-}$ mice were able to increase TRPC6 expression under conditions of Ca^{2+} overload. As expected, and supported by previous works [103,199], we found that FB from both WT and KO mice increased TRPC6 mRNA expression following 24h of Ca^{2+} treatment. Hence, these results demonstrate that mice lacking TRPV4 expression are able to increase TRPC6 expression if there is a sustained rise in intracellular Ca^{2+}, suggesting that TRPV4 deletion prevents TRPC6 upregulation by reducing the entry of Ca^{2+} and the activation of the calcineurin/NFAT pathway.

In conclusion, our findings let us hypothesize that under sustained β-adrenergic stimulation, the activation of the TRPV4 channel is the key promoter of the adverse cardiac response, which by stimulating the activation of the calcineurin/NFAT pathway, not only promotes the development of fibrosis, but might also directly regulate TRPC6 expression to further enhance this remodelling process (Figure 58). This hypothesis sets the basis for future studies specifically addressed to answer this question.

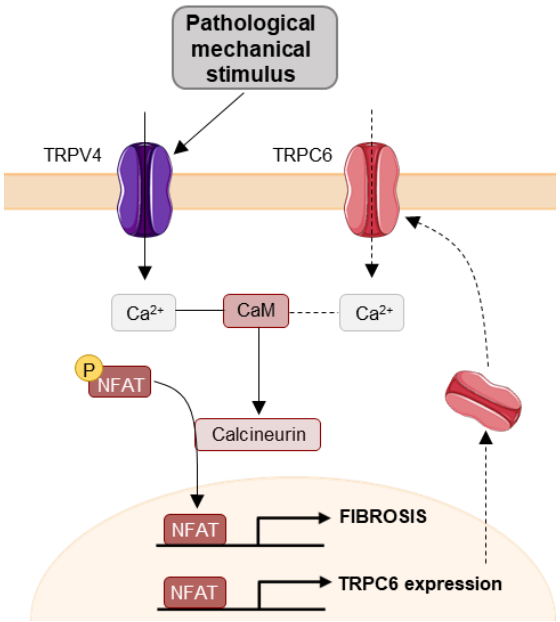

Figure 58. Proposed mechanism by which TRPV4 activation in FB contributes to fibrosis and to TRPC6 gene expression. Isoproterenol induces the entry of Ca2+ through the TRPV4 channel, which by stimulating the calcineurin/NFAT pathway promotes the transcription of collagen1, collagen III and α-SMA, leading to the development of fibrosis and HF. In addition, TRPV4 directly regulates the expression of TRPC6, and the increase in the expression of TRPC6 in FB further activates the calcineurin/NFAT pathway.

5.8. HF INDUCTION AND RECOVERY IN AGED FEMALE MICE

Scarce information exists of HF in women, and the effects of ageing in the female heart. Patients with advanced age and/or female sex have been consistently underrepresented in clinical trials of HF. Similarly, most experimental research in HF has been conducted mainly in young male animals [335]. Importantly, recent real-life data indicate that, among HFrEF patients, 21.9% are aged and 21.6% are women [336], which together represent

significant numbers of affected individuals given the major burden of HF in the whole community.

With this in mind, we aimed to assess the particularities of HF induction using exclusively female mice at different lifespan time-points. At baseline, young and aged female mice had no perceptible differences in echocardiographic parameters, but histological analyses showed a trend to higher CM CSA and significantly higher collagen deposition in aged versus young animals. This is supported by a previous work that showed that CM hypertrophy and fibrosis in mice increased beyond 18 months of age [337]. These findings are also consistent with the morphological changes seen in the ageing human heart, which contribute to cardiac functional deterioration and HF development under chronic hemodynamic overload [338].

In our study, female young mice developed a typical HF phenotype in response to chronic isoproterenol infusion, similar to that reported in males [339,340] More importantly, typical HF traits were also seen in aged female mice in response to isoproterenol. These findings validate the use of the isoproterenol-HF model in aged animals, even though ageing is associated with β-adrenergic receptor dysfunction and desensitization, particularly in women [341,342]. Despite an age-related remodelling of β-adrenergic receptors, chronic isoproterenol stimulation still led to similar structural and functional changes in both young and aged females.

More importantly, our work also confirmed a different behaviour between young and aged mice after removal of β-adrenergic stimulation. Whereas young female animals exhibited full recovery of functional and structural parameters, both at the macroscopic and cellular level, aged mice showed persistent cell hypertrophy, tissue fibrosis and cardiac dysfunction upon β-adrenergic withdrawal. These findings were accompanied by increased

expression of collagen I, the major determinant of myocardial stiffness [343], in elderly animals.

Cardiac reverse remodelling, understood as the restoration of chamber geometry and, at the cellular level, decrease of cell size and tissue fibrosis in previously failing hearts, has not been thoroughly studied. The available data majorly come from clinical studies on response to medical or cardiac resynchronization therapy (CRT) [344,345], left ventricular assist device (LVAD) implant, and ablation of premature ventricular complexes (PVC) in PVC-induced tachycardiomyopathy. Clinical reports have suggested that all these strategies are associated with recovery of LV dysfunction [344–347], and, in some cases, with regression of tissue fibrosis and gene expression [344,345], findings that are consistent with those observed in our young animals.

Importantly, the clinical setting has also highlighted that myocardial reverse remodelling might not always occur to the same extent in all individuals. Several studies suggest that elderly patients might respond comparably to the young after pharmacological therapy or CRT [348–350]. Conversely, data coming from large registries of LVAD support that the incidence of cardiac recovery is 2-fold more likely in individuals aged <50 years [351]. Likewise, ablation of PVCs leads more frequently to reversal of LV dysfunction in younger individuals [352]. These latter findings are in accordance with our results, where elderly animals showed impaired reverse remodelling and recovery of ventricular dysfunction. With the use of an animal model, we could provide new insights into the reverse remodelling in young and aged animals, setting the basis for future research in the field.

5.9. TRPV4 IN THE AGED HEART

Even in apparently healthy individuals, ageing is associated with progressive changes in cardiac anatomy and physiology [353], which increase susceptibility

to cardiovascular diseases [354]. It is well established that Ca^{2+} handling becomes dysfunctional with age, leading to age-dependent cardiac remodelling and Ca^{2+} intolerance under conditions of stress [355]. However, the mechanisms by which intracellular Ca^{2+} is altered with age remain poorly understood.

In this work, we showed that baseline mRNA expression of TRPV4 was increased in female hearts of aged mice compared to the young ones. These findings are consistent with previous studies showing that, in aged CM ,there is an increase in TRPV4 expression and function, that leads to elevated intracellular Ca^{2+} and to a decline in cardiac function [267,356]. Since our results indicate that TRPV4 plays a pivotal role in the promotion of fibrosis, it is plausible that the increase in TRPV4 with ageing may also contribute to the observed age-dependent collagen deposition.

Furthermore, as in young male mice, chronic β-adrenergic stimulation induced an increase in TRPV4 mRNA expression in the young and aged female hearts, although the magnitude of increase of TRPV4 expression seemed higher in the younger population (36% in female young mice vs. 23% in female aged mice). These results suggest that TRPV4-dependent Ca^{2+} influx in response to isoproterenol may also represent a critical regulator of Ca^{2+} signalling in the aged heart, and that TRPV4 inhibition could also provide cardioprotection following cardiac injury in the elderly population.

Notably, our results also revealed age-specific differences in TRPV4 expression after β-adrenergic withdrawal. Whereas TRPV4 expression levels returned to baseline in young females, aged mice exhibited a persistent increase in TRPV4 expression. As shown in other experiments of the project, TRPV4 expression behaved again in close parallelism with fibrosis deposition. Although we did not examine the specific mechanisms by which reverse remodelling appears impaired in elderly animals, sustained activation of TRPV4 could be a potential mechanism that warrants further investigation in future studies.

5.10. LIMITATIONS AND FUTURE DIRECTIONS

In the present thesis we have demonstrated that, under conditions of persistent hemodynamic overload, the mechanoreceptor TRPV4 channel plays a pivotal role in the promotion of pathological remodelling, specifically in fibrosis accompanying HF. In our study, deletion of TRPV4 preserved LV functionality, attenuated cardiac hypertrophy and specially fibrosis, and decreased arrhythmia vulnerability after chronic β-adrenergic stimulation, preventing the development of the main characteristic features of HF.

Nevertheless, our study comes with the inherent limitation of using animal models, which are not always good representatives of the clinical scenario. However, all animal models, and particularly the HF model that was used throughout the study were carefully chosen as the best to mimic the human condition.

Our results open up the possibility of a new potential therapeutic target for the management of HF. Interestingly, although potentially regulated by G-protein coupled receptors such as AT1R [357], TRPV4 channels represent an independent pathway that activates in response to mechanical stress and, therefore, might act independently of the SNS and RAAS activation. TRPV4 inhibition arises therefore as a novel potential approach for the treatment of HF that could offer the possibility of a combined treatment with other drugs already proven effective. In this regard, a few TRPV4 inhibitors have been discovered and developed in the last five years by several research groups and pharmaceutical companies [358]. Scientists from *GlaxoSmithKline* (GSK) identified a potent, selective and orally active TRPV4 channel blocker GSK219374, which showed well tolerability *in vivo* and also demonstrated to prevent pulmonary edema in a rat model of HF [248]. More recently, the optimization of the potency and the pharmacokinetics of the above mentioned chemotype, led to the development of GSK2798745 [249], which has

been recently tested in clinical trials and exhibited no significant safety issues, well-tolerance in healthy volunteers[250], opening the door for future long-term clinical evaluation of the drug in the outcome of HF. However, first it would be desirable to understand the pathophysiological role of the TRPV4 channel in pre-clinical species, and further asses the therapeutic benefits of its inhibition, not only in terms of fibrosis, but also in terms of cardiac hypertrophy and physiological remodelling.

In our study, we did not assess the consequences of TRPV4 deletion on adaptive remodelling. Although TRPV4 did not appear overexpressed in mice and rats subjected to chronic exercise, future work would need to ensure that TRPV4 inhibition does not impair or attenuate the adaptive cardiac response. Further, more experiments are needed to provide more detailed insights into some findings of this work, including a better understanding of the mechanisms by which TRPV4 deletion attenuates hypertrophy and arrhythmias, assessing whether this could be indirectly caused by the reduction of fibrosis or rather by a direct effect on calcium-dependent signalling in CM.

We only explored the effects of TRPV4 deletion in HF promotion and its prevention. It was not investigated whether TRPV4 inhibition might improve cardiac function once HF is already present, a setting that would better mimic the clinical practice. TRPV4 and TRPC6 overexpression did not precede but increased in parallel with the pathological response, and particularly with collagen deposition. However, since fibrosis formation is a continuous and active process in HF, one might speculate that its inhibition at any time might reduce and ameliorate the pathological remodelling. Nevertheless, this hypothesis remains to be confirmed in future studies.

In this study we also demonstrated that persistent β-adrenergic stimulation increases TRPV4 expression and function in cardiac FB, which, by activating

the calcineurin/NFATc3 pathway, leads to fibrosis promotion and potentially regulates TRPC6 expression (previously highlighted as the major contributor of fibrosis [103,201]) to further aggravate the fibrotic remodelling process. However, additional studies are required to validate this mechanism by which TRPV4 would be the key and primary promoter of the adverse response. Importantly, we only explored the calcineurin/NFAT pathway based on previous literature supporting the link between TRPV4 and this pathway. Other authors have recently described activation of other pathways in response to TRPV4 signalling, like the Rho/ROCK/MRTF-A pathway. We cannot exclude that cardioprotection by TRPV4 deletion is due to the downregulation of these pathways simultaneously and potentially others.

Our findings also point out that the TRPV4 channel may contribute to age-dependent cardiac alterations and may also be participating in the adverse response under chronic hemodynamic overload in aged hearts. Likewise, our data also suggest that TRPV4 may compromise the reverse remodelling process upon β-adrenergic withdrawal. These results were obtained from young and aged female mice, because these populations have been classically underrepresented in clinical and experimental studies of HF. However, our results might not be necessarily extendible to males. Therefore, future research should be addressed to respond whether TRPV4 inhibition provides cardioprotection in aged animals (both male and female) and elucidate its potential role in reverse remodelling in both young and aged animals of both sexes.

And to wrap up, a final consideration. As mentioned throughout this thesis, quite a few papers have studied the role of distinct TRPs in cardiac remodelling. And even though some of the published papers seem contradictory, they might be unmasking an important issue. While there are many efforts set in finding pro-fibrotic or pro-hypertrophic targets, these

channels also have very important physiologic roles in both CM and FB and they cannot be categorized as "*The Good, The Bad and the Ugly*", as their function is far more complex. Instead of being sole orchestra directors, it is most probably the conjunction of many factors that will finally evoke in a pathologic remodelling. In this regard, it might be naïve to think that adverse remodelling can be explained by the activity of a few players. In fact, as seen with TRPC6 or other TRPs, the deletion of TRPV4 greatly attenuated but not completely abolished neither the fibrosis nor the hypertrophy, indicating a hypothetic compensatory role via other TRPs or that these processes can be guided by several proteins at the same time. Nevertheless, in depth studies of the individual role of these candidates is needed to dissect their function in each condition and find possible therapeutic strategies that control their function in pathology without altering its physiologic roles.

6. CONCLUSIONS

1. The two HF models that were studied in the present project, induced by chronic isoproterenol infusion and aortic constriction, respectively, emulate the cardiac phenotype of advanced HF in humans.

2. The two models of exercise training that were studied in the present project, at least at moderate doses, have good resemblance with the adaptive cardiac remodelling observed in endurance athletes.

3. Mechanoreceptors seem to participate differentially in adaptive and adverse cardiac remodelling; upregulation of TRPV4 and TRPC6 channels is exclusively associated with the adverse cardiac response.

4. TRPV4 and TRPC6 channels are majorly found in cardiac FB, and their expression does not precede, but is strongly associated, with the progression of the adverse cardiac remodelling, and specifically with the development of fibrosis.

5. Deletion of TRPV4 offers cardioprotection in response to chronic β-adrenergic stimulation. Specifically, absence of TRPV4 remarkably attenuates cardiac hypertrophy and fibrosis, reduces ventricular tachyarrhythmias, and preserves cardiac function following isoproterenol infusion.

6. Under conditions of persistent hemodynamic overload, the increased TRPV4 expression in FB contributes to increasing the intracellular Ca^{2+} concentration and activating the calcium-dependent calcineurin/NFATc3 signalling in mouse cardiac FB, activating the fibrotic process. This response is inhibited in mice with genetic deletion of TRPV4.

7. TRPV4 activity, by activating the calcineurin/NFAT pathway, could promote the upregulation of TRPC6 under sustained β-adrenergic stimulation. Although more experiments are needed, we speculate that TRPV4 channel could be the primary mechanoreceptor driving the fibrotic response, a hypothesis to be addressed in future studies.

8. Chronic isoproterenol infusion induces a similar HF phenotype in young and aged female mice, validating the use of the isoproterenol model in aged animals.

9. Unlike young animals, who exhibit full cardiac recovery upon β-adrenergic withdrawal, aged animals show impaired reverse remodelling with persistent cell hypertrophy, tissue fibrosis and cardiac dysfunction.

10. Increased collagen deposition present in aged mice at baseline is associated with TRPV4 overexpression compared to young animals. Persistent TRPV4 activation in the elderly may compromise heart recovery upon β-adrenergic withdrawal, although further work is needed adequately address this question.

Scientific contribution of this thesis :

- Ageing impairs reverse remodelling and recovery of ventricular function after isoproterenol-induced cardiomyopathy

  Authors: Laia Yañez-Bisbe, Anna Garcia-Elias, Marta Tajes, Isaac Almendros, Antonio Rodríguez-Sinovas, Javier Inserte, Marisol Ruiz-Meana, Ramon Farré, Nuria Farré, Begoña Benito

  Under review

- An article regarding the role of TRPV4 in adverse cardiac remodelling will be written in the next few months.

7. REFERENCES

1. Morton, P. G. Anatomy and physiology of the cardiovascular system. *Crit. Care Nurs. A Holist. Approach.* 193–205 (2013).
2. Humphrey, J. D. & McCulloch, A. D. The Cardiovascular System — Anatomy, Physiology and Cell Biology. *Biomech. Soft Tissue Cardiovasc. Syst.* 1–14 (2003).
3. Mesotten, L. *et al.* Nuclear Cardiology, Part 1: Anatomy and Function of the Normal Heart (1998).
4. Shah, S., Gnanasegaran, G., Sundberg-Cohon, J. & Buscombe, J. R. The heart: Anatomy, physiology and exercise physiology. *Integrating Cardiology for Nuclear Medicine Physicians: A Guide to Nuclear Medicine Physicians* (2009).
5. Camelliti, P., Borg, T. K. & Kohl, P. Structural and functional characterisation of cardiac fibroblasts. *Cardiovascular Research* **65** 40–51 (2005).
6. Baudino, T. A., Carver, W., Giles, W. & Borg, T. K. Cardiac fibroblasts: friend or foe? *Am J Physiol Hear. Circ Physiol* **291**, 1015–1026 (2006).
7. Banerjee, I., Fuseler, J. W., Price, R. L., Borg, T. K. & Baudino, T. A. Determination of cell types and numbers during cardiac development in the neonatal and adult rat and mouse. *Am J Physiol Hear. Circ Physiol* **293**, (2007).
8. Bergmann, O. *et al.* Evidence for cardiomyocyte renewal in humans. *Science* **324**, 98–102 (2009).
9. Souders, C. A., Bowers, S. L. K. & Baudino, T. A. Cardiac fibroblast: The renaissance cell. *Circulation Research* **105** 1164–1176 (2009).
10. Brown, R. D., Ambler, S. K., Mitchell, M. D. & Long, C. S. THE CARDIAC FIBROBLAST: Therapeutic Target in Myocardial Remodeling and Failure. *Annual Reviews* **45**, 657–687 (2004).
11. Rienks, M., Papageorgiou, A.-P., Frangogiannis, N. G. & Heymans, S. Myocardial Extracellular Matrix. *Circ. Res.* **114**, 872–888 (2014).
12. Park, D. S. & Fishman, G. I. The Cardiac Conduction System. *Circulation* **123**, 904–915 (2011).
13. Flanigan, M. & Gaskell, S. M. A review of cardiac anatomy and physiology. *Home healthcare nurse* **22** 45–51 (2004).
14. Cooper, G. M. Actin, Myosin, and Cell Movement. (2000).
15. Kennedy, A. *et al.* The Cardiac Conduction System: Generation and Conduction of the Cardiac Impulse. *Crit. Care Nurs. Clin. North Am.* **28**, 269–279 (2016).
16. Macfarlane, P. W. Comprehensive electrocardiology. (2011).
17. Park, D. S. & Fishman, G. I. Cell Biology of the Specialized Cardiac Conduction System. *Card. Electrophysiol. From Cell to Bedside Sixth Ed.* 287–296 (2014)
18. Bers, D. M. Cardiac excitation–contraction coupling. *Nat.* **415**, 198–205 (2002).
19. Zima, A. V. *et al.* Ca handling during Excitation-Contraction Coupling in Heart Failure. *Pflugers Arch.* **466**, 1129 (2014).
20. Solaro, R. J. Sarcomere Control Mechanisms and the Dynamics of the Cardiac

Cycle. *J. Biomed. Biotechnol.* **2010**, (2010).

21. Bers, D. M. Calcium cycling and signaling in cardiac myocytes. *Annual Review of Physiology* vol. 70 23–49 (2008).
22. Hill, J. A. & Olson, E. N. Cardiac Plasticity. *N. Engl. J. Med.* **358**, 1370–1380 (2008).
23. Hartupee, J. & Mann, D. L. Neurohormonal activation in heart failure with reduced ejection fraction. *Nat. Rev. Cardiol.* **14**, 30–38 (2016).
24. Kamp, T. J. & Hell, J. W. Regulation of Cardiac L-Type Calcium Channels by Protein Kinase A and Protein Kinase C. *Circ. Res.* **87**, 1095–1102 (2000).
25. Morimoto, S. *et al.* Protein kinase A-dependent phosphorylation of ryanodine receptors increases Ca2+ leak in mouse heart. *Biochem. Biophys. Res. Commun.* **390**, 87–92 (2009).
26. Kranias, E. G. & Hajjar, R. J. Modulation of Cardiac Contractility by the Phopholamban/SERCA2a Regulatome. *Circ. Res.* **110**, 1646 (2012).
27. Rosas, P. C. *et al.* Phosphorylation of Cardiac Myosin Binding Protein-C is a Critical Mediator of Diastolic Function. *Circ. Heart Fail.* **8**, 582 (2015).
28. Bock, H. A., Hermle, M., Brunner, F. P. & Thiel, G. Pressure dependent modulation of renin release in isolated perfused glomeruli. *Kidney Int.* **41**, 275–280 (1992).
29. Sayer, G. & Bhat, G. The Renin-Angiotensin-Aldosterone System and Heart Failure. *Cardiol. Clin.* **32**, 21–32 (2014).
30. De Mello, W. C. Renin Angiotensin Aldosterone System And Heart Function. *Endocrinol. Hear. Heal. Dis. Integr. Cell. Mol. Endocrinol. Hear.* 229–248 (2017).
31. Berridge, M. J. Inositol trisphosphate and calcium signalling mechanisms. *Biochim. Biophys. Acta - Mol. Cell Res.* **1793**, 933–940 (2009).
32. Azevedo, P. S., Polegato, B. F., Minicucci, M. F., Paiva, S. A. R. & Zornoff, L. A. M. Cardiac Remodeling: Concepts, Clinical Impact, Pathophysiological Mechanisms and Pharmacologic Treatment. *Arq. Bras. Cardiol.* **106**, 62–69 (2016).
33. Maillet, M., Berlo, J. H. van & Molkentin, J. D. Molecular basis of physiological heart growth: fundamental concepts and new players. *Nat. Rev. Mol. Cell Biol.* **14**, 38 (2013).
34. Schirone, L. *et al.* A Review of the Molecular Mechanisms Underlying the Development and Progression of Cardiac Remodeling. *Oxid. Med. Cell. Longev.* **2017**, 1–16 (2017).
35. Perrino, C. *et al.* Intermittent pressure overload triggers hypertrophy-independent cardiac dysfunction and vascular rarefaction. *J. Clin. Invest.* **116**, 1547–1560 (2006).
36. Schmid, E. *et al.* Cardiac RKIP induces a beneficial β-adrenoceptor-dependent positive inotropy. *Nat. Med.* **21**, 1298–1306 (2015).

37. Watanabe, H., Murakami, M., Ohba, T., Takahashi, Y. & Ito, H. TRP channel and cardiovascular disease. *Pharmacol. Ther.* **118**, 337–351 (2008).
38. Seo, D. Y. *et al.* Cardiac adaptation to exercise training in health and disease. *Pflugers Arch. Eur. J. Physiol.* **472**, 155–168 (2020).
39. Eghbali, M. *et al.* Molecular and functional signature of heart hypertrophy during pregnancy. *Circ. Res.* **96**, 1208–1216 (2005).
40. Bernardo, B. C. & McMullen, J. R. Molecular Aspects of Exercise-induced Cardiac Remodeling. *Cardiol. Clin.* **34**, 515–530 (2016).
41. Waring, C. D. *et al.* The adult heart responds to increased workload with physiologic hypertrophy, cardiac stem cell activation, and new myocyte formation. *Eur. Heart J.* **35**, 2722–2731 (2014).
42. Sharma, S., Merghani, A. & Mont, L. Exercise and the heart: The good, the bad, and the ugly. *Eur. Heart J.* **36**, 1445–1453 (2015).
43. Schannwell, C. M. *et al.* Left ventricular hypertrophy and diastolic dysfunction in healthy pregnant women. *Cardiology* **97**, 73–78 (2002).
44. Pluim, B. M., Zwinderman, A. H., Van Der Laarse, A. & Van Der Wall, E. E. The athlete's heart: A meta-analysis of cardiac structure and function. *Circulation* **101**, 336–344 (2000).
45. Eghbali, M., Wang, Y., Toro, L. & Stefani, E. Heart Hypertrophy During Pregnancy: A Better Functioning Heart? *Trends in Cardiovascular Medicine* **16** 285–291 (2006).
46. Maron, B. J., Pelliccia, A., Spataro, A. & Granata, M. Reduction in left ventricular wall thickness after deconditioning in highly trained Olympic athletes. *Br. Heart J.* **69**, 125–128 (1993).
47. Jin, H. *et al.* Effects of exercise training on cardiac function, gene expression, and apoptosis in rats. *Am J Physiol Heart Circ Physiol* **279**, 46-48 (2000).
48. Goessler, K., Polito, M. & Cornelissen, V. A. Effect of exercise training on the renin-angiotensin-aldosterone system in healthy individuals: a systematic review and meta-analysis. *Hypertens. Res.* **39**, 119–126 (2016).
49. Horio, T. *et al.* Production and autocrine/paracrine effects of endogenous insulin-like growth factor-1 in rat cardiac fibroblasts. *Regul. Pept.* **124**, 65–72 (2005).
50. Neri Serneri, G. G. *et al.* Increased cardiac sympathetic activity and insulin-like growth factor-I formation are associated with physiological hypertrophy in athletes. *Circ. Res.* **89**, 977–982 (2001).
51. Riehle, C. *et al.* Insulin Receptor Substrates Are Essential for the Bioenergetic and Hypertrophic Response of the Heart to Exercise Training. *Mol. Cell. Biol.* **34**, 3450–3460 (2014).
52. Kim, J. *et al.* Insulin-like growth factor I receptor signaling is required for exercise-induced cardiac hypertrophy. *Mol. Endocrinol.* **22**, 2532–2543 (2008).
53. McMullen, J. R. *et al.* The Insulin-like Growth Factor 1 Receptor Induces

Physiological Heart Growth via the Phosphoinositide 3-Kinase(p110α) Pathway. *J. Biol. Chem.* **279**, 4782–4793 (2004).

54. Luo, J. *et al.* Class I A Phosphoinositide 3-Kinase Regulates Heart Size and Physiological Cardiac Hypertrophy. *Mol. Cell. Biol.* **25**, 9491–9502 (2005).
55. McMullen, J. R. *et al.* Phosphoinositide 3-kinase(p110α) plays a critical role for the induction of physiological, but not pathological, cardiac hypertrophy. *Proc. Natl. Acad. Sci. U. S. A.* **100**, 12355–12360 (2003).
56. DeBosch, B. *et al.* Akt1 is required for physiological cardiac growth. *Circulation* **113**, 2097–2104 (2006).
57. Tsukada, J., Yoshida, Y., Kominato, Y. & Auron, P. E. The CCAAT/enhancer (C/EBP) family of basic-leucine zipper (bZIP) transcription factors is a multifaceted highly-regulated system for gene regulation. *Cytokine* **54**, 6–19 (2011).
58. Boström, P. *et al.* C/EBPβ Controls Exercise-Induced Cardiac Growth and Protects against Pathological Cardiac Remodeling. *Cell* **143**, 1072–1083 (2010).
59. D'Uva, G. *et al.* ERBB2 triggers mammalian heart regeneration by promoting cardiomyocyte dedifferentiation and proliferation. *Nat. Cell Biol.* **17**, 627–638 (2015).
60. Fukazawa, R. *et al.* Neuregulin-1 protects ventricular myocytes from anthracycline-induced apoptosis via erbB4-dependent activation of PI3-kinase/Akt. *J. Mol. Cell. Cardiol.* **35**, 1473–1479 (2003).
61. Cai, M. X. *et al.* Exercise training activates neuregulin 1/ErbB signaling and promotes cardiac repair in a rat myocardial infarction model. *Life Sci.* **149**, 1–9 (2016).
62. Brown, M. D. Exercise and coronary vascular remodelling in the healthy heart. *Exp. Physiol.* **88**, 645–658 (2003).
63. Cheryl, W., Daniele, T. & Georgina, E. Cardiac stem cell activation and ensuing myogenesis and angiogenesis contribute in cardiac adaptation to intensity-controlled exercise training. *Japanese J. Phys. Fit. Sport. Med.* **59**, 73 (2010).
64. Wilson, M. G., Ellison, G. M. & Cable, N. T. Basic science behind the cardiovascular benefits of exercise. *Heart* **101** 758–765 (2015).
65. Cohn, J. N., Ferrari, R. & Sharpe, N. Cardiac remodeling-concepts and clinical implications: A consensus paper from an International Forum on Cardiac Remodeling. *J. Am. Coll. Cardiol.* **35**, 569–582 (2000).
66. Tham, Y. K., Bernardo, B. C., Ooi, J. Y. Y., Weeks, K. L. & McMullen, J. R. Pathophysiology of cardiac hypertrophy and heart failure: signaling pathways and novel therapeutic targets. *Arch. Toxicol.* **89**, 1401–1438 (2015).
67. Dorsa Pontes, H. B. & Vieira Pontes, J. C. D. Cardiac remodelling: General aspects and mechanisms. *Curr. Res. Cardiol.* **3**, 79-82(2016).
68. Lehnart, S. E., Maier, L. S. & Hasenfuss, G. Abnormalities of calcium

metabolism and myocardial contractility depression in the failing heart. *Heart Failure Reviews* **14** 213–224 (2009).

69. Lowes, B. D. *et al.* Changes in gene expression in the intact human heart. Downregulation of alpha-myosin heavy chain in hypertrophied, failing ventricular myocardium. *J. Clin. Invest.* **100**, 2315 (1997).
70. Gupta, M. & Gupta, M. P. Cardiac hypertrophy: Old concepts, new perspectives. *Cell. Basis Cardiovasc. Funct. Heal. Dis.* 273–279 (1997)
71. Krenz, M. & Robbins, J. Impact of beta-myosin heavy chain expression on cardiac function during stress. *J. Am. Coll. Cardiol.* **44**, 2390–2397 (2004).
72. Yeh, Y. H. *et al.* Calcium-handling abnormalities underlying atrial arrhythmogenesis and contractile dysfunction in dogs with congestive heart failure. *Circ. Arrhythm. Electrophysiol.* **1**, 93–102 (2008).
73. Gwathmey, J. K. *et al.* Abnormal intracellular calcium handling in myocardium from patients with end-stage heart failure. *Circ. Res.* **61**, 70–76 (1987).
74. Tomasek, J. J., Gabbiani, G., Hinz, B., Chaponnier, C. & Brown, R. A. Myofibroblasts and mechano-regulation of connective tissue remodelling. *Nat. Rev. Mol. Cell Biol* **3**, 349–363 (2002).
75. Kong, P., Christia, P. & Frangogiannis, N. G. The pathogenesis of cardiac fibrosis. *Cellular and Molecular Life Sciences* **71**, 549–574 (2014).
76. Zeisberg, E. M. *et al.* Endothelial-to-mesenchymal transition contributes to cardiac fibrosis. *Nat. Med.* **13**, 952–961 (2007).
77. Moore-Morris, T. *et al.* Resident fibroblast lineages mediate pressure overload-induced cardiac fibrosis. *J. Clin. Invest.* **124**, 2921–2934 (2014).
78. Gibb, A. A., Lazaropoulos, M. P. & Elrod, J. W. Myofibroblasts and Fibrosis. *Circ. Res.* **127**, 427–447 (2020).
79. Khalil, H. *et al.* Fibroblast-specific TGF-β-Smad2/3 signaling underlies cardiac fibrosis. in *Journal of Clinical Investigation* **127**, 3770–3783 (2017).
80. Scharenberg, M. A. *et al.* TGF-β-induced differentiation into myofibroblasts involves specific regulation of two MKL1 isoforms. *J. Cell Sci.* **127**, 1079–1091 (2014).
81. Kuwahara, F. *et al.* Transforming growth factor-β function blocking prevents myocardial fibrosis and diastolic dysfunction in pressure-overloaded rats. *Circulation* **106**, 130–135 (2002).
82. Herum, K. M., Choppe, J., Kumar, A., Engler, A. J. & McCulloch, A. D. Mechanical regulation of cardiac fibroblast profibrotic phenotypes. *Mol. Biol. Cell* **28**, 1871–1882 (2017).
83. Klingberg, F., Hinz, B. & White, E. S. The myofibroblast matrix: Implications for tissue repair andfibrosis. *Journal of Pathology* **229**, 298–309 (2013).
84. Ottaviano, F. G. & Yee, K. O. Communication signals between cardiac fibroblasts and cardiac myocytes. *J. Cardiovasc. Pharmacol.* **57**, 513–521 (2011).

85. Hall, C., Gehmlich, K., Denning, C. & Pavlovic, D. Complex relationship between cardiac fibroblasts and cardiomyocytes in health and disease. *J. Am. Heart Assoc.* **10**, 1–15 (2021).
86. Benito, B. & Josephson, M. E. Taquicardia ventricular en la enfermedad coronaria. *Rev. Esp. Cardiol.* **65**, 939–955 (2012).
87. Singh, B. N. Significance and control of cardiac arrhythmias in patients with congestive cardiac failure. *Heart Fail. Rev.* **7**, 285–300 (2002).
88. Luo, M. & Anderson, M. E. Mechanisms of altered Ca2+ handling in heart failure. *Circ. Res.* **113**, 690–708 (2013).
89. Feng, J. *et al.* Ca2+ Signaling in Cardiac Fibroblasts and Fibrosis-Associated Heart Diseases. *J. Cardiovasc. Dev. Dis.* **6**, 34 (2019).
90. Chen, J. B. *et al.* Multiple Ca2+ signaling pathways regulate intracellular Ca 2+ activity in human cardiac fibroblasts. *J. Cell. Physiol.* **223**, 68–75 (2010).
91. Brilla, C. G., Scheer, C. & Rupp, H. Angiotensin II and intracellular calcium of adult cardiac fibroblasts. *J. Mol. Cell. Cardiol.* **30**, 1237–1246 (1998).
92. Meszaros, J. G. *et al.* Identification of G protein-coupled signaling pathways in cardiac fibroblasts: Cross talk between G(q) and G(s). *Am. J. Physiol. - Cell Physiol.* **278**, 47-54(2000).
93. Lv, T. *et al.* Proliferation in cardiac fibroblasts induced by β1-adrenoceptor autoantibody and the underlying mechanisms. *Sci. Rep.* **6**, 1–15 (2016).
94. Kiss, E., Ball, N. A., Kranias, E. G. & Walsh, R. A. Differential Changes in Cardiac Phospholamban and Sarcoplasmic Reticular Ca2+-ATPase Protein Levels. *Circ. Res.* **77**, 759–764 (1995).
95. Hasenfuss, G. *et al.* Relation between myocardial function and expression of sarcoplasmic reticulum Ca2+-ATPase in failing and nonfailing human myocardium. *Circ. Res.* **75**, 434–442 (1994).
96. Schwinger, R. H. G. *et al.* Reduced Ca2+-Sensitivity of SERCA 2a in Failing Human Myocardium due to Reduced Serin-16 Phospholamban Phoshorylation. *J. Mol. Cell. Cardiol.* **31**, 479–491 (1999).
97. Ling, H. *et al.* Requirement for Ca2+/calmodulin-dependent kinase II in the transition from pressure overload-induced cardiac hypertrophy to heart failure in mice. *J. Clin. Invest.* **119**, 1230–1240 (2009).
98. Swaminathan, P. D., Purohit, A., Hund, T. J. & Anderson, M. E. Calmodulin-dependent protein kinase II: Linking heart failure and arrhythmias. *Circ. Res.* **110**, 1661–1677 (2012).
99. Martin, T. P. *et al.* Adult cardiac fibroblast proliferation is modulated by calcium/calmodulin- dependent protein kinase II in normal and hypertrophied hearts. *Pflugers Arch. Eur. J. Physiol.* **466**, 319–330 (2014).
100. Zhang, W. *et al.* Inhibition of calcium-calmodulin-dependent kinase II suppresses cardiac fibroblast proliferation and extracellular matrix secretion. *J. Cardiovasc. Pharmacol.* **55**, 96–105 (2010).

101. Molkentin, J. D. *et al.* A calcineurin-dependent transcriptional pathway for cardiac hypertrophy. *Cell* **93**, 215–228 (1998).
102. Herum, K. M. *et al.* Syndecan-4 signaling via NFAT regulates extracellular matrix production and cardiac myofibroblast differentiation in response to mechanical stress. *J. Mol. Cell. Cardiol.* **54**, 73–81 (2013).
103. Davis, J., Burr, A. R., Davis, G. F., Birnbaumer, L. & Molkentin, J. D. A TRPC6-Dependent Pathway for Myofibroblast Transdifferentiation and Wound Healing In Vivo. *Dev. Cell* **23**, 705–715 (2012).
104. Jiang, D. S. *et al.* IRF8 suppresses pathological cardiac remodelling by inhibiting calcineurin signalling. *Nat. Commun. 2014 51* **5**, 1–14 (2014).
105. Bujak, M. & Frangogiannis, N. G. The role of TGF-β signaling in myocardial infarction and cardiac remodeling. *Cardiovascular Research* **74**, 184–195 (2007).
106. Creemers, E. E. & Pinto, Y. M. Molecular mechanisms that control interstitial fibrosis in the pressure-overloaded heart. *Cardiovasc. Res.* **89**, 265–272 (2011).
107. Zhang, D. *et al.* TAK1 is activated in the myocardium after pressure overload and is sufficient to provoke heart failure in transgenic mice. *Nat. Med.* **6**, 556–563 (2000).
108. Small, E. M. *et al.* Myocardin-related transcription factor-a controls myofibroblast activation and fibrosis in response to myocardial infarction. *Circ. Res.* **107**, 294–304 (2010).
109. Sano, Y. *et al.* ATF-2 Is a Common Nuclear Target of Smad and TAK1 Pathways in Transforming Growth Factor-β Signaling . *J. Biol. Chem.* **274**, 8949–8957 (1999).
110. Turner & Blythe. Cardiac Fibroblast p38 MAPK: A Critical Regulator of Myocardial Remodeling. *J. Cardiovasc. Dev. Dis.* **6**, 27 (2019).
111. Bartekova, M., Radosinska, J., Jelemensky, M. & Dhalla, N. S. Role of cytokines and inflammation in heart function during health and disease. *Hear. Fail. Rev.* **23**, 733–758 (2018).
112. Torre-Amione, G. *et al.* Tumor necrosis factor-α and tumor necrosis factor receptors in the failing human heart. *Circulation* **93**, 704–711 (1996).
113. Adamo, L., Rocha-Resende, C., Prabhu, S. D. & Mann, D. L. Reappraising the role of inflammation in heart failure. *Nat. Rev. Cardiol.* **17**, 269–285 (2020).
114. Gordon, J. W., Shaw, J. A. & Kirshenbaum, L. A. Multiple Facets of NF-κB in the Heart. *Circ. Res.* **108**, 1122–1132 (2011).
115. Wong, S. C. Y., Fukuchi, M., Melnyk, P., Rodger, I. & Giaid, A. Induction of Cyclooxygenase-2 and Activation of Nuclear Factor-κB in Myocardium of Patients With Congestive Heart Failure. *Circulation* **98**, 100–103 (1998).
116. Hayden, M. S. & Ghosh, S. Shared Principles in NF-κB Signaling. *Cell* **132** 344–362 (2008).

117. Ghosh, S. & Karin, M. Missing pieces in the NF-κB puzzle. *Cell*. **109**, 81-96 (2002).
118. Aluja, D. *et al.* Calpains mediate isoproterenol-induced hypertrophy through modulation of GRK2. *Basic Res. Cardiol.* **114**, 1-16(2019).
119. Keith, M. *et al.* Increased oxidative stress in patients with congestive heart failure. *J. Am. Coll. Cardiol.* **31**, 1352–1356 (1998).
120. Murdoch, C. E., Zhang, M., Cave, A. C. & Shah, A. M. NADPH oxidase-dependent redox signalling in cardiac hypertrophy, remodelling and failure. *Cardiovascular Research* **71** 208–215 (2006).
121. Takimoto, E. & Kass, D. A. Role of oxidative stress in cardiac hypertrophy and remodeling. *Hypertension* **49** 241–248 (2007).
122. Richter, K. & Kietzmann, T. Reactive oxygen species and fibrosis: further evidence of a significant liaison. *Cell and Tissue Research* **365**, 591–605 (2016).
123. Köhler, A. C., Sag, C. M. & Maier, L. S. Reactive oxygen species and excitation–contraction coupling in the context of cardiac pathology. *J. Mol. Cell. Cardiol.* **73**, 92–102 (2014).
124. Ponikowski, P. *et al.* 2016 ESC Guidelines for the diagnosis and treatment of acute and chronic heart failure. *Eur. Heart. J*. **37**, 2127–2200 (2016).
125. Yancy, C. W. *et al.* 2017 ACC/AHA/HFSA Focused Update of the 2013 ACCF/AHA Guideline for the Management of Heart Failure: A Report of the American College of Cardiology/American Heart Association Task Force on Clinical Practice Guidelines and the Heart Failure Society of Amer. *Circulation* **136**, 137–161 (2017).
126. Ziaeian, B. & Fonarow, G. C. Epidemiology and aetiology of heart failure. *Nat. Rev. Cardiol.* **13**, 368–378 (2016).
127. Savarese, G. & Lund, L. H. Global Public Health Burden of Heart Failure. *Card. Fail. Rev.* **03**, 7 (2017).
128. Levy, W. C. *et al.* The Seattle Heart Failure Model. *Circulation* **113**, 1424–1433 (2006).
129. Sayago-Silva, I., García-López, F. & Segovia-Cubero, J. Epidemiology of heart failure in Spain over the last 20 years. *Rev. Esp. Cardiol. (Engl. Ed).* **66**, 649–656 (2013).
130. Farré, N. *et al.* Real world heart failure epidemiology and outcome: A population-based analysis of 88,195 patients. *PLoS One* **12**, e0172745 (2017).
131. Farré, N. *et al.* Medical resource use and expenditure in patients with chronic heart failure: a population-based analysis of 88 195 patients. *Eur. J. Heart Fail.* **18**, 1132–1140 (2016).
132. Jones, N. R., Roalfe, A. K., Adoki, I., Hobbs, F. D. R. & Taylor, C. J. Survival of patients with chronic heart failure in the community: a systematic review and meta-analysis. *Eur. J. Heart Fail.* **21**, 1306 (2019).
133. Mosterd, A. & Hoes, A. W. Clinical epidemiology of heart failure. *Heart* **93**

1137–1146 (2007).

134. Henkel, D. M., Redfield, M. M., Weston, S. A., Gerber, Y. & Roger, V. L. Death in heart failure: a community perspective. *Circ. Heart Fail.* **1**, 91–97 (2008).
135. Murphy, S. P., Ibrahim, N. E. & Januzzi, J. L. Heart Failure With Reduced Ejection Fraction: A Review. *JAMA* **324**, 488–504 (2020).
136. Garg, R. & Yusuf, S. Overview of randomized trials of angiotensin-converting enzyme inhibitors on mortality and morbidity in patients with heart failure. Collaborative Group on ACE Inhibitor Trials. *JAMA* **273**, 1450–1456 (1995).
137. Granger, C. B. *et al.* Effects of candesartan in patients with chronic heart failure and reduced left-ventricular systolic function intolerant to angiotensin-converting-enzyme inhibitors: the CHARM-Alternative trial. *Lancet* **362**, 772–776 (2003).
138. Dargie, H. J. & Lechat, P. The Cardiac Insufficiency Bisoprolol Study II (CIBIS-II): A randomised trial. *Lancet* **353**, 9–13 (1999).
139. Ilton, M. *et al.* The Effect of Carvedilol on Morbidity and Mortality in Patients with Chronic Heart Failure. New Eng J Med **334**, 1349–1355 (2009).
140. Pitt, B. *et al.* The Effect of Spironolactone on Morbidity and Mortality in Patients with Severe Heart Failure. *N. Engl. J. Med.* **341**, 709–717 (1999).
141. Swedberg, K. *et al.* Ivabradine and outcomes in chronic heart failure: A randomised placebo-controlled study. *Lancet* **376**, 875–885 (2010).
142. McMurray, J. J. *et al.* Angiotensin-neprilysin inhibition versus enalapril in heart failure. *N. Engl. J. Med.* **371**, 132–133 (2014).
143. Velazquez, E. J. *et al.* Angiotensin-Neprilysin Inhibition in Acute Decompensated Heart Failure. *N. Engl. J. Med.* **380**, 539–548 (2019).
144. McMurray, J. J. V. *et al.* Dapagliflozin in Patients with Heart Failure and Reduced Ejection Fraction. *N. Engl. J. Med.* **381**, 1995–2008 (2019).
145. Armstrong, P.W. Vericiguat in patients with heart failure and reduced ejection fraction. *N. Eng. J. Med* **382**, 1883-1893 (2020).
146. SR, H. *et al.* Animal models of heart failure: a scientific statement from the American Heart Association. *Circ. Res.* **111**, 78–94 (2012).
147. deAlmeida, A. C., Oort, R. J. van & Wehrens, X. H. T. Transverse Aortic Constriction in Mice. *J. Vis. Exp.* **38** (2010)
148. Bosch, L. *et al.* The transverse aortic constriction heart failure animal model: a systematic review and meta-analysis. *Heart Fail. Rev.* **26**, 1515–1524 (2021).
149. Carlson, W. D. Animal models of heart failure. *Hear. Fail. Second Ed.* 78–94 (2012)
150. Pfeffer, M. A. *et al.* Myocardial infarct size and ventricular function in rats. *Circ. Res.* **44**, 503–512 (1979).
151. Kalogeris, T., Baines, C. P., Krenz, M. & Korthuis, R. J. Cell Biology of Ischemia/Reperfusion Injury. *Int. Rev. Cell Mol. Biol.* **298**, 229 (2012).
152. Michael, L. H. *et al.* Myocardial ischemia and reperfusion: a murine model.

Am. J. Physiol. **269**, 2147-2154 (1995).

153. Gomes, A. C., Falcão-Pires, I., Pires, A. L., Brás-Silva, C. & Leite-Moreira, A. F. Rodent models of heart failure: An updated review. *Heart Fail. Rev.* **18**, 219–249 (2013).
154. Chen, J., Ceholski, D. K., Liang, L., Fish, K. & Hajjar, R. J. Integrative Cardiovascular Physiology and Pathophysiology: Variability in coronary artery anatomy affects consistency of cardiac damage after myocardial infarction in mice. *Am. J. Physiol. - Hear. Circ. Physiol.* **313**, H275 (2017).
155. Ichihara, S. *et al.* Angiotensin II type 2 receptor is essential for left ventricular hypertrophy and cardiac fibrosis in chronic angiotensin II-induced hypertension. *Circulation* **104**, 346–351 (2001).
156. Wang, J. J.-C. C. *et al.* Genetic Dissection of Cardiac Remodeling in an Isoproterenol-Induced Heart Failure Mouse Model. **12**, e1006038 (2016).
157. Grimm, D. *et al.* Development of heart failure following isoproterenol administration in the rat: role of the renin–angiotensin system. *Cardiovasc. Res.* **37**, 91–100 (1998).
158. Ennis, I. L. *et al.* Regression of isoproterenol-induced cardiac hypertrophy by Na+/H+ exchanger inhibition. *Hypertension* **41**, 1324–1329 (2003).
159. Ren, S. *et al.* Implantation of an Isoproterenol Mini-Pump to Induce Heart Failure in Mice. *J. Vis. Exp.* **152** (2019).
160. Jin, P., Jan, L. Y. & Jan, Y. N. Mechanosensitive Ion Channels: Structural Features Relevant to Mechanotransduction Mechanisms. *Annu. Rev. Neurosci.* **43**, 207–229 (2020).
161. Peyronnet, R., Nerbonne, J. M. & Kohl, P. Cardiac Mechano-Gated Ion Channels and Arrhythmias. *Circ. Res.* **118**, 311–329 (2016).
162. Snyders, D. J. Structure and function of cardiac potassium channels. *Cardiovascular Research* **42** 377–390 (1999).
163. Khan, E., Spiers, C. & Khan, M. The heart and potassium: A banana republic. *Acute Card. Care* **15**, 17–24 (2013).
164. Kamatham, S., Waters, C. M., Schwingshackl, A. & Mancarella, S. TREK-1 protects the heart against ischemia-reperfusion-induced injury and from adverse remodeling after myocardial infarction. *Pflugers Arch. Eur. J. Physiol.* **471**, 1263–1272 (2019).
165. Lugenbiel, P. *et al.* TREK-1 (K2P2.1) K+ channels are suppressed in patients with atrial fibrillation and heart failure and provide therapeutic targets for rhythm control. *Basic Res. Cardiol.* **112**, 1-14 (2017).
166. Soltysinska, E. *et al.* KCNMA1 Encoded Cardiac BK Channels Afford Protection against Ischemia-Reperfusion Injury. *PLoS One* **9**, e103402 (2014).
167. Shi, Y. *et al.* Mitochondrial big conductance KCa channel and cardioprotection in infant rabbit heart. *J. Cardiovasc. Pharmacol.* **50**, 497–502 (2007).
168. Xu, W. *et al.* Cytoprotective Role of Ca2+- Activated K+ Channels in the Cardiac

Inner Mitochondrial Membrane. *Science* **298**, 1029–1033 (2002).

169. Yamada, S. *et al.* Protection conferred by myocardial ATP-sensitive K+ channels in pressure overload-induced congestive heart failure revealed in KCNJ11 Kir6.2-null mutant. *J. Physiol.* **577**, 1053–1065 (2006).
170. Zingman, L. V. *et al.* Kir6.2 is required for adaptation to stress. *Proc. Natl. Acad. Sci.* **99**, 13278–13283 (2002).
171. Fedorov, V. V. *et al.* Effects of KATP channel openers diazoxide and pinacidil in coronary-perfused atria and ventricles from failing and non-failing human hearts. *J. Mol. Cell. Cardiol.* **51**, 215 (2011).
172. Coste, B. *et al.* Piezo1 and Piezo2 are essential components of distinct mechanically-activated cation channels. *Science* **330**, 55 (2010).
173. Liang, J. *et al.* Stretch-activated channel Piezo1 is up-regulated in failure heart and cardiomyocyte stimulated by Angii. *Am. J. Transl. Res.* **9**, 2945–2955 (2017).
174. Jiang, F. *et al.* The mechanosensitive Piezo1 channel mediates heart mechano-chemo transduction. *Nat. Commun.* **12**, 1–14 (2021).
175. Cosens, D. J. & Manning, A. Abnormal Electroretinogram from a Drosophila Mutant. *Nat. 1969 2245216* **224**, 285–287 (1969).
176. Samanta, A., Hughes, T. E. T. & Moiseenkova-Bell, V. Y. Transient Receptor Potential (TRP) Channels. *Subcell. Biochem.* **87**, 141 (2018).
177. Gaudet, R. Structural Insights into the Function of TRP Channels. 349–360 (2007).
178. Schaefer, M. Homo- and heteromeric assembly of TRP channel subunits. **451**, 35–42 (2005).
179. Hill-Eubanks, D. C., Gonzales, A. L., Sonkusare, S. K. & Nelson, M. T. Vascular TRP Channels: Performing Under Pressure and Going with the Flow. *Physiology* **29**, 343–360 (2014).
180. Yue, Z. *et al.* Role of TRP channels in the cardiovascular system. *Am J Physiol Hear. Circ Physiol* **308**, 157–182 (2015).
181. Venkatachalam, K. & Montell, C. TRP Channels. *Annu. Rev. Biochem.* **76**, 387 (2007).
182. Wang, Z. *et al.* TRPA1 inhibition ameliorates pressure overload-induced cardiac hypertrophy and fibrosis in mice. *EBioMedicine* **36**, 54 (2018).
183. Li, S. *et al.* TRPA1 promotes cardiac myofibroblast transdifferentiation after myocardial infarction injury via the calcineurin-NFAT-DYRK1A signaling pathway. *Oxid. Med. Cell. Longev.* **2019** (2019).
184. Gueffier, M. *et al.* The TRPM4 channel is functionally important for the beneficial cardiac remodeling induced by endurance training. **38**, 3–16 (2017).
185. Mathar, I. *et al.* Increased β-Adrenergic Inotropy in Ventricular Myocardium From Trpm4−/− Mice. *Circ. Res.* **114**, 283–294 (2014).
186. Kecskés, M. *et al.* The Ca2+-activated cation channel TRPM4 is a negative

regulator of angiotensin II-induced cardiac hypertrophy. *Basic Res. Cardiol.* **110**, 1-14 (2015).

187. Du, J. *et al.* TRPM7-mediated Ca2+ signals confer fibrogenesis in human atrial fibrillation. *Circ. Res.* **106**, 992–1003 (2010).
188. Adapala, R. K. *et al.* TRPV4 channels mediate cardiac fibroblast differentiation by integrating mechanical and soluble signals. *J. Mol. Cell. Cardiol.* **54**, 45–52 (2013).
189. Rios, F. J. *et al.* Chanzyme TRPM7 protects against cardiovascular inflammation and fibrosis. *Cardiovasc. Res.* **116**, 721 (2020).
190. Morine, K. J. *et al.* Endoglin selectively modulates transient receptor potential channel expression in left and right heart failure. *Cardiovasc. Pathol.* **25**, 478–482 (2016).
191. Ohba, T. *et al.* Upregulation of TRPC1 in the development of cardiac hypertrophy. *J. Mol. Cell. Cardiol.* **42**, 498–507 (2007).
192. Seth, M. *et al.* TRPC1 channels are critical for hypertrophic signaling in the heart. *Circ. Res.* **105**, 1023 (2009).
193. Tang, L. *et al.* Inhibition of TRPC1 prevents cardiac hypertrophy via NF-κB signaling pathway in human pluripotent stem cell-derived cardiomyocytes. *J. Mol. Cell. Cardiol.* **126**, 143–154 (2019).
194. Kitajima, N. *et al.* TRPC3 positively regulates reactive oxygen species driving maladaptive cardiac remodeling. *Sci. Rep.* **6**, 37001 (2016).
195. Nakayama, H., Wilkin, B. J., Bodi, I. & Molkentin, J. D. Calcineurin-dependent cardiomyopathy is activated by TRPC in the adult mouse heart. *FASEB J.* **20**, 1660–1670 (2006).
196. Wu, X., Eder, P., Chang, B. & Molkentin, J. D. TRPC channels are necessary mediators of pathologic cardiac hypertrophy. *Proc. Natl. Acad. Sci. U. S. A.* **107**, 7000–7005 (2010).
197. Harada, M. *et al.* Transient receptor potential canonical-3 channel-dependent fibroblast regulation in atrial fibrillation. *Circulation* **126**, 2051–2064 (2012).
198. Seo, K. *et al.* Combined TRPC3 and TRPC6 blockade by selective small-molecule or genetic deletion inhibits pathological cardiac hypertrophy. *Proc. Natl. Acad. Sci. U. S. A.* **111**, 1551–1556 (2014).
199. Kuwahara, K. *et al.* TRPC6 fulfills a calcineurin signaling circuit during pathologic cardiac remodeling. *J. Clin. Invest.* **116**, 3114–3126 (2006).
200. Ikeda, K. *et al.* Roles of transient receptor potential canonical (TRPC) channels and reverse-mode Na+/Ca2+ exchanger on cell proliferation in human cardiac fibroblasts: Effects of transforming growth factor β1. *Cell Calcium* **54**, 213–225 (2013).
201. Lin, B. L. *et al.* In vivo selective inhibition of TRPC6 by antagonist BI 749327 ameliorates fibrosis and dysfunction in cardiac and renal disease. *Proc. Natl. Acad. Sci. U. S. A.* **116**, 10156–10161 (2019).

202. Higashikawa, A. *et al.* Transient Receptor Potential Cation Channel Subfamily Vanilloid Member 3 is not Involved in Plasma Membrane Stretch-induced Intracellular Calcium Signaling in Merkel Cells. *Bull. Tokyo Dent. Coll.* **56**, 259–262 (2015).
203. Zhang, Q. *et al.* Activation of transient receptor potential vanilloid 3 channel (TRPV3) aggravated pathological cardiac hypertrophy via calcineurin/NFATc3 pathway in rats. *J. Cell. Mol. Med.* **22**, 6055–6067 (2018).
204. Huang, W., Rubinstein, J., Prieto, A. R., Thang, L. V. & Wang, D. H. Transient receptor potential vanilloid gene deletion exacerbates inflammation and atypical cardiac remodeling after myocardial infarction. *Hypertension* **53**, 243–250 (2009).
205. Huang, W., Rubinstein, J., Prieto, A. R. & Wang, D. H. Enhanced postmyocardial infarction fibrosis via stimulation of the transforming growth factor-β-Smad2 signaling pathway: Role of transient receptor potential vanilloid type 1 channels. *J. Hypertens.* **28**, 367–376 (2010).
206. Zhong, B., Rubinstein, J., Ma, S. & Wang, D. H. Genetic ablation of TRPV1 exacerbates pressure overload-induced cardiac hypertrophy. *Biomed. Pharmacother.* **99**, 261–270 (2018).
207. Buckley, C. L. & Stokes, A. J. Mice lacking functional TRPV1 are protected from pressure overload cardiac hypertrophy. *Channels (Austin).* **5**, 367–374 (2011).
208. Wang, Q. *et al.* Transgenic overexpression of transient receptor potential vanilloid subtype 1 attenuates isoproterenol-induced myocardial fibrosis in mice. *Int. J. Mol. Med.* **38**, 601–609 (2016).
209. Koch, S. E. *et al.* Transient receptor potential vanilloid 2 function regulates cardiac hypertrophy via stretch-induced activation. *J. Hypertens.* **35**, 602–611 (2017).
210. Iwata, Y. *et al.* Blockade of sarcolemmal TRPV2 accumulation inhibits progression of dilated cardiomyopathy. *Cardiovasc. Res.* **99**, 760–768 (2013).
211. Strotmann, R., Harteneck, C., Nunnenmacher, K., Schultz, G. & Plant, T. D. OTRPC4, a nonselective cation channel that confers sensitivity to extracellular osmolarity. *Nat. Cell Biol.* **2**, 695–702 (2000).
212. Liedtke, W. *et al.* Vanilloid Receptor–Related Osmotically Activated Channel (VR-OAC), a Candidate Vertebrate Osmoreceptor. *Cell* **103**, 525–535 (2000).
213. Wissenbach, U., Bödding, M., Freichel, M. & Flockerzi, V. Trp12, a novel Trp related protein from kidney. *FEBS Lett.* **485**, 127–134 (2000).
214. Delany, N. S. *et al.* Identification and characterization of a novel human vanilloid receptor-like protein, VRL-2. *Physiol. Genomics* **2001**, 165–174 (2001).
215. Nilius, B. & Voets, T. The puzzle of TRPV4 channelopathies. *EMBO Rep.* **14**, 152 (2013).
216. Deng, Z. *et al.* Cryo-EM and X-ray structures of TRPV4 reveal insight into ion

permeation and gating mechanisms. *Nat. Struct. Mol. Biol.* **25**, 252–260 (2018).

217. Voets, T. *et al.* Molecular Determinants of Permeation through the Cation Channel TRPV4. *J. Biol. Chem.* **277**, 33704–33710 (2002).
218. Gaudet, R. A primer on ankyrin repeat function in TRP channels and beyond. *Mol. Biosyst.* **4**, 372 (2008).
219. Goretzki, B. *et al.* Structural basis of TRPV4 N-terminus interaction with Syndapin/PACSIN1-3 and PIP2. *Structure* **26**, 1583 (2018).
220. Valente, P. *et al.* Identification of molecular determinants of channel gating in the transient receptor potential box of vanilloid receptor I. *FASEB J.* **22**, 3298–3309 (2008).
221. Strotmann, R., Schultz, G. & Plant, T. D. Ca2+-dependent potentiation of the nonselective cation channel TRPV4 is mediated by a C-terminal calmodulin binding site. *J. Biol. Chem.* **278**, 26541–26549 (2003).
222. Goswami, C., Kuhn, J., Heppenstall, P. A. & Hucho, T. Importance of non-selective cation channel TRPV4 interaction with cytoskeleton and their reciprocal regulations in cultured cells. *PLoS One* **5**, e11654 (2010).
223. Hellwig, N., Albrecht, N., Harteneck, C., Schultz, G. & Schaefer, M. Homo- and heteromeric assembly of TRPV channel subunits. *J. Cell Sci.* **118**, 917–928 (2005).
224. Ma, X. *et al.* Heteromeric TRPV4-C1 channels contribute to store-operated Ca2+ entry in vascular endothelial cells. *Cell Calcium* **50**, 502–509 (2011).
225. Stewart, A. P., Smith, G. D., Sandford, R. N. & Edwardson, J. M. Atomic force microscopy reveals the alternating subunit arrangement of the TRPP2-TRPV4 heterotetramer. *Biophys. J.* **99**, 790–797 (2010).
226. Güler, A. D. *et al.* Heat-Evoked Activation of the Ion Channel, TRPV4. *J. Neurosci.* **22**, 6408–6414 (2002).
227. Watanabe, H. *et al.* Heat-evoked Activation of TRPV4 Channels in a HEK293 Cell Expression System and in Native Mouse Aorta Endothelial Cells. *J. Biol. Chem.* **277**, 47044–47051 (2002).
228. Garcia-Elias, A. *et al.* Phosphatidylinositol-4,5-biphosphate-dependent rearrangement of TRPV4 cytosolic tails enables channel activation by physiological stimuli. *Proc. Natl. Acad. Sci. U. S. A.* **110**, 9553–9558 (2013).
229. Gao, X., Wu, L. & O'Neil, R. G. Temperature-modulated diversity of TRPV4 channel gating: Activation by physical stresses and phorbol ester derivatives through protein kinase C-dependent and -independent pathways. *J. Biol. Chem.* **278**, 27129–27137 (2003).
230. Köhler, R. *et al.* Evidence for a functional role of endothelial transient receptor potential V4 in shear stress-induced vasodilatation. *Arterioscler. Thromb. Vasc. Biol.* **26**, 1495–1502 (2006).
231. Andrade, Y. N. *et al.* TRPV4 channel is involved in the coupling of fluid viscosity

changes to epithelial ciliary activity. *J. Cell Biol.* **168**, 869 (2005).

232. Christensen, A. P. & Corey, D. P. TRP channels in mechanosensation: direct or indirect activation? *Nat. Rev. Neurosci.* **8**, 510–521 (2007).
233. Kung, C. A possible unifying principle for mechanosensation. *Nat. 2005 4367051* **436**, 647–654 (2005).
234. Pedersen, S. F. & Nilius, B. Transient Receptor Potential Channels in Mechanosensing and Cell Volume Regulation. *Methods Enzymol.* **428**, 183–207 (2007).
235. Matthews, B. D. *et al.* Ultra-rapid activation of TRPV4 ion channels by mechanical forces applied to cell surface β1 integrins. *Integr. Biol.* **2**, 435–442 (2010).
236. Vriens, J. *et al.* Cell swelling, heat, and chemical agonists use distinct pathways for the activation of the cation channel TRPV4. *Proc. Natl. Acad. Sci. U. S. A.* **101**, 396 (2004).
237. Vriens, J. *et al.* Modulation of the Ca2+ permeable cation channel TRPV4 by cytochrome P450 epoxygenases in vascular endothelium. *Circ. Res.* **97**, 908–915 (2005).
238. Watanabe, H. *et al.* Anandamide and arachidonic acid use epoxyeicosatrienoic acids to activate TRPV4 channels. *Nature* **424**, 434–438 (2003).
239. Caires, R. *et al.* Omega-3 Fatty Acids Modulate TRPV4 Function through Plasma Membrane Remodeling. *Cell Rep.* **21**, 246–258 (2017).
240. Watanabe, H. *et al.* Activation of TRPV4 Channels (hVRL-2/mTRP12) by Phorbol Derivatives *. *J. Biol. Chem.* **277**, 13569–13577 (2002).
241. Klausen, T. K. *et al.* Modulation of the transient receptor potential vanilloid channel TRPV4 by 4α-phorbol esters: A structure-activity study. *J. Med. Chem.* **52**, 2933–2939 (2009).
242. Vriens, J., Owsianik, G., Janssens, A., Voets, T. & Nilius, B. Determinants of 4α-Phorbol Sensitivity in Transmembrane Domains 3 and 4 of the Cation Channel TRPV4 *. *J. Biol. Chem.* **282**, 12796–12803 (2007).
243. Smith, P. L., Maloney, K. N., Pothen, R. G., Clardy, J. & Clapham, D. E. Bisandrographolide from Andrographis paniculata Activates TRPV4 Channels. *J. Biol. Chem.* **281**, 29897–29904 (2006).
244. Thorneloe, K. S. *et al.* GSK1016790A, a novel and potent transient receptor potential vanilloid 4 channel agonist induces urin. *J. Pharmacol. Exp. Ther.* **326**, 432–442 (2008).
245. Toft-Bertelsen, T. L., Križaj, D. & MacAulay, N. When size matters: transient receptor potential vanilloid 4 channel as a volume-sensor rather than an osmo-sensor. *J. Physiol.* **595**, 3287–3302 (2017).
246. Duncton, M. A. J. Small Molecule Agonists and Antagonists of TRPV4. TRP Channels as Therapeutic Targets: From Basic Science to Clinical Us*e Academic Press* (2015).

247. Vincent, F. *et al.* Identification and characterization of novel TRPV4 modulators. *Biochem. Biophys. Res. Commun.* **389**, 490–494 (2009).
248. Thorneloe, K. S. *et al.* An orally active TRPV4 channel blocker prevents and resolves pulmonary edema induced by heart failure. *Sci. Transl. Med.* **4**, (2012).
249. Brooks, C. A. *et al.* Discovery of GSK2798745: A clinical candidate for inhibition of transient receptor potential vanilloid 4 (TRPV4). *ACS Med. Chem. Lett.* **10**, 1228–1233 (2019).
250. Goyal, N. *et al.* Clinical Pharmacokinetics, Safety, and Tolerability of a Novel, First-in-Class TRPV4 Ion Channel Inhibitor, GSK2798745, in Healthy and Heart Failure Subjects. *Am. J. Cardiovasc. Drugs* **19**, 335–342 (2019).
251. D'Hoedt, D. *et al.* Stimulus-specific modulation of the cation channel TRPV4 by PACSIN 3. *J. Biol. Chem.* **283**, 6272–6280 (2008).
252. Garcia-Elias, A., Lorenzo, I. M., Vicente, R. & Valverde, M. A. IP3 receptor binds to and sensitizes TRPV4 channel to osmotic stimuli via a calmodulin-binding site. *J. Biol. Chem.* **283**, 31284–31288 (2008).
253. Cao, S. *et al.* Transient receptor potential vanilloid 4 (TRPV4) activation by arachidonic acid requires protein kinase A–mediated phosphorylation. *J. Biol. Chem.* **293**, 5307–5322 (2018).
254. Peng, H. *et al.* Identification of a Protein Kinase C-dependent phosphorylation site involved in sensitization of TRPV4 channel. *Biochem. Biophys. Res. Commun.* **391**, 1721–1725 (2010).
255. Lee, H., Iida, T., Mizuno, A., Suzuki, M. & Caterina, M. J. Altered Thermal Selection Behavior in Mice Lacking Transient Receptor Potential Vanilloid 4. *J. Neurosci.* **25**, 1304–1310 (2005).
256. Becker, D., Blase, C., Bereiter-Hahn, J. & Jendrach, M. TRPV4 exhibits a functional role in cell-volume regulation. *J. Cell Sci.* **118**, 2435–2440 (2005).
257. Pan, Z. *et al.* Dependence of Regulatory Volume Decrease on Transient Receptor Potential Vanilloid 4 (TRPV4) Expression in Human Corneal Epithelial Cells. *Cell Calcium* **44**, 374 (2008).
258. Liedtke, W. & Friedman, J. M. Abnormal osmotic regulation in trpv4-/- mice. **100**, 13698–13703 (2003).
259. Sandow, S. L., Senadheera, S., Grayson, T. H., Welsh, D. G. & Murphy, T. V. Calcium and endothelium-mediated vasodilator signaling. *Adv. Exp. Med. Biol.* **740**, 811–831 (2012).
260. Mendoza, S. A. *et al.* TRPV4-mediated endothelial Ca2+ influx and vasodilation in response to shear stress. *Am. J. Physiol. Heart Circ. Physiol.* **298**, H466-76 (2009).
261. Wei, X., Edelmayer, R. M., Yan, J. & Dussor, G. Activation of TRPV4 on dural afferents produces headache-related behavior in a preclinical rat model. *Cephalalgia* **31**, 1595 (2011).

262. Suzuki, M., Mizuno, A., Kodaira, K. & Imai, M. Impaired pressure sensation in mice lacking TRPV4. *J. Biol. Chem.* **278**, 22664–22668 (2003).
263. Alessandri-Haber, N., Dina, O. A., Joseph, E. K., Reichling, D. & Levine, J. D. A transient receptor potential vanilloid 4-dependent mechanism of hyperalgesia is engaged by concerted action of inflammatory mediators. *J. Neurosci.* **26**, 3864–3874 (2006).
264. Alessandri-Haber, N. *et al.* Transient Receptor Potential Vanilloid 4 Is Essential in Chemotherapy-Induced Neuropathic Pain in the Rat. *J. Neurosci.* **24**, 4444–4452 (2004).
265. Randhawa, P. K. aur & Jaggi, A. S. ingh. TRPV4 channels: physiological and pathological role in cardiovascular system. *Basic Res. Cardiol.* **110**, 1–19 (2015).
266. Jennings, R. B., Reimer, K.A., Steenbergen, C. Myocardial Ischemia Revisited. The Osmolar Load, Membrane Damage, and Reperfusion. *J. Mol. Cell. Cardiol* **8**, 769-780
267. Jones, J. L. *et al.* TRPV4 increases cardiomyocyte calcium cycling and contractility yet contributes to damage in the aged heart following hypoosmotic stress. *Cardiovasc. Res.* **115**, 46–56 (2019).
268. Wu, Q. F. *et al.* Activation of transient receptor potential vanilloid 4 involves in hypoxia/reoxygenation injury in cardiomyocytes. *Cell Death Dis.* **8**, 2828 (2017).
269. Dong, Q. *et al.* Blockage of transient receptor potential vanilloid 4 alleviates myocardial ischemia/reperfusion injury in mice. *Sci. Rep.* **7**, 42678 (2017).
270. Peana, D., Polo-Parada, L. & Domeier, T. L. Arrhythmogenesis in the aged heart following ischaemia–reperfusion: role of transient receptor potential vanilloid 4. *Cardiovasc. Res.* (2021)
271. Lu, J. *et al.* An abnormal TRPV4-related cytosolic Ca2 + rise in response to uniaxial stretch in induced pluripotent stem cells-derived cardiomyocytes from dilated cardiomyopathy patients. *Biochim. Biophys. Acta - Mol. Basis Dis.* **1863**, 2964–2972 (2017).
272. Adapala, R. K., Kanugula, A. K., Paruchuri, S., Chilian, W. M. & Thodeti, C. K. TRPV4 deletion protects heart from myocardial infarction-induced adverse remodeling via modulation of cardiac fibroblast differentiation. *Basic Res. Cardiol.* **115**, 1-14 (2020).
273. Iwasaki, K., Hayashi, K., Fujioka, T. & Sobue, K. Rho/Rho-associated kinase signal regulates myogenic differentiation via myocardin-related transcription factor-A/Smad-dependent transcription of the Id3 gene. *J. Biol. Chem.* **283**, 21230–21241 (2008).
274. Gevaert, T. *et al.* Deletion of the transient receptor potential cation channel TRPV4 impairs murine bladder voiding. *J. Clin. Invest.* **117**, 3453–3462 (2007).
275. Earley, S. *et al.* TRPV4-dependent dilation of peripheral resistance arteries

influences arterial pressure. *Am. J. Physiol. - Hear. Circ. Physiol.* **297**, (2009).

276. Tabuchi, K., Suzuki, M., Mizuno, A. & Hara, A. Hearing impairment in TRPV4 knockout mice. *Neurosci. Lett.* **382**, 304–308 (2005).
277. Masuyama, R. *et al.* Calcium/calmodulin-signaling supports TRPV4 activation in osteoclasts and regulates bone mass. *J. Bone Miner. Res.* **27**, 1708–1721 (2012).
278. Lam, M. P. Y. *et al.* Protein kinetic signatures of the remodeling heart following isoproterenol stimulation. *J. Clin. Invest.* **124**, 1734–1744 (2014).
279. Turcani, M. & Rupp, H. Development of pressure overload induced cardiac hypertrophy is unaffected by long-term treatment with losartan. *Mol. Cell. Biochem. 1998 1881* **188**, 225–233 (1998).
280. Batlle, M. *et al.* Axl expression is increased in early stages of left ventricular remodeling in an animal model with pressure-overload. *PLoS One* **14**, (2019).
281. Benito, B. *et al.* Cardiac Arrhythmogenic Remodeling in a Rat Model of Long-Term Intensive Exercise Training. *Circulation* **123**, 13–22 (2011).
282. Ma, S. *et al.* Cryptotanshinone attenuates isoprenaline-induced cardiac fibrosis in mice associated with upregulation and activation of matrix metalloproteinase-2. *Mol. Med. Rep.* **6**, 145–150 (2012).
283. Galindo, C. L. *et al.* Transcriptional profile of isoproterenol-induced cardiomyopathy and comparison to exercise-induced cardiac hypertrophy and human cardiac failure. *BMC Physiol.* **9**, 23 (2009).
284. Li, X., Zhang, Z. L. & Wang, H. F. Fusaric acid (FA) protects heart failure induced by isoproterenol (ISP) in mice through fibrosis prevention via TGF-β1/SMADs and PI3K/AKT signaling pathways. *Biomed. Pharmacother.* **93**, 130–145 (2017).
285. Lang, R. M. *et al.* Recommendations for cardiac chamber quantification by echocardiography in adults: An update from the American Society of Echocardiography and the European Association of Cardiovascular Imaging. *J. Am. Soc. Echocardiogr.* **28**, 1-39.e14 (2015).
286. Sánchez, J. A. *et al.* Effects of a reduction in the number of gap junction channels or in their conductance on ischemia-reperfusion arrhythmias in isolated mouse hearts. *Am. J. Physiol. Heart Circ. Physiol.* **301**, 2442–2453 (2011).
287. Livak, K. J. & Schmittgen, T. D. Analysis of relative gene expression data using real-time quantitative PCR and the 2(-Delta Delta C(T)) Method. *Methods* **25**, 402–408 (2001).
288. Chang, S. C., Ren, S., Rau, C. D. & Wang, J. J. Isoproterenol-induced heart failure mouse model using osmotic pump implantation. in *Methods in Molecular Biology* **1816** 207–220 (2018).
289. Kunert-Keil, C., Bisping, F., Krüger, J. & Brinkmeier, H. Tissue-specific expression of TRP channel genes in the mouse and its variation in three

different mouse strains. *BMC Genomics* **7**, 1–14 (2006).

290. Sanz-de la Garza, M. *et al.* Severity of structural and functional right ventricular remodeling depends on training load in an experimental model of endurance exercise. *Am. J. Physiol. Heart Circ. Physiol.* **313**, H459–H468 (2017).
291. Berry, J. M. *et al.* Reversibility of adverse, calcineurin-dependent cardiac remodeling. *Circ. Res.* **109**, 407–417 (2011).
292. Crabtree, G. R. Calcium, Calcineurin, and the Control of Transcription. *Journal of Biological Chemistry* **276** 2313–2316 (2001).
293. Wilkins, B. J. & Molkentin, J. D. Calcium-calcineurin signaling in the regulation of cardiac hypertrophy. *Biochem. Biophys. Res. Commun.* **322**, 1178–1191 (2004).
294. Nichtova, Z., Novotova, M., Kralova, E. & Stankovicova, T. Morphological and functional characteristics of models of experimental myocardial injury induced by isoproterenol. *General Physiology and Biophysics* **31** 141–151 (2012).
295. Hohimer, A. R., Davis, L. E. & Hatton, D. C. Repeated daily injections and osmotic pump infusion of isoproterenol cause similar increases in cardiac mass but have different effects on blood pressure. *Can. J. Physiol. Pharmacol*. **83**, 191–197 (2011).
296. Ma, X. *et al.* Distinct actions of intermittent and sustained β-adrenoceptor stimulation on cardiac remodeling. *Sci. China Life Sci.* **54**, 493–501 (2011).
297. Thoonen, R., Vandenwijngaert, S., Beaudoin, J., Buys, E. & Scherrer-Crosbie, M. Translation of Animal Models into Clinical Practice. *Inflamm. Hear. Fail.* 93–102 (2015)
298. Prior, D. L. & La Gerche, A. The athlete's heart. *Heart* **98**, 947–955 (2012).
299. Fagard, R. H. Athlete's Heart: A Meta-Analysis of the Echocardiographic Experience. *Int. J. Sports Med.* **17**, S140–S144 (2007).
300. Kemi, O. J., Loennechen, J. P., Wisløff, U. & Ellingsen, Ø. Intensity-controlled treadmill running in mice: cardiac and skeletal muscle hypertrophy. J. *Appl. Physiol.* **93**, 1301–1309 (2002).
301. Fenning, A. *et al*. Cardiac adaptation to endurance exercise in rats. *Mol. Cell. Biochem.* **251**, 51–59 (2003).
302. Marks, A. R. Cardiac intracellular calcium release channels: Role in heart failure. *Circulation Research* **87** 8–11 (2000).
303. Wang, X. & Fitts, R. H. Cardiomyocyte slowly activating delayed rectifier potassium channel: Regulation by exercise and β-adrenergic signaling. *J. Appl. Physiol.* **128**, 1177–1185 (2020).
304. Luo, Z. *et al.* TRPV1 activation improves exercise endurance and energy metabolism through PGC-1α upregulation in mice. *Cell Res.* **22**, 551–564 (2012).

305. Florea, V. G. & Cohn, J. N. The autonomic nervous system and heart failure. *Circ. Res.* **114**, 1815–1826 (2014).
306. Sigurdsson, A. & Swedberg, K. The role of neurohormonal activation in chronic heart failure and postmyocardial infarction. *Am. Heart J.* **132**, 229–234 (1996).
307. Falcón, D. *et al.* TRP Channels: Current Perspectives in the Adverse Cardiac Remodeling. *Front. Physiol.* **10**, 159 (2019).
308. Zimmer, H. G. Catecholamine-induced cardiac hypertrophy: Significance of proto-oncogene expression. *Journal of Molecular Medicine* **75** 849–859 (1997).
309. Grossman, W., Jones, D. & McLaurin, L. P. Wall stress and patterns of hypertrophy in the human left ventricle. *J. Clin. Invest.* **56**, 56–64 (1975).
310. Gerçek, M. *et al.* Cardiomyocyte Hypertrophy in Arrhythmogenic Cardiomyopathy. *Am. J. Pathol.* **187**, 752–766 (2017).
311. Maulik, S. K. & Mishra, S. Hypertrophy to failure: What goes wrong with the fibers of the heart? *Indian Heart J.* **67**, 66–69 (2015).
312. Oda, S. *et al.* TRPC6 counteracts TRPC3-Nox2 protein complex leading to attenuation of hyperglycemia-induced heart failure in mice. *Sci. Reports* **7**, 1–14 (2017).
313. Disertori, M., Masè, M. & Ravelli, F. Myocardial fibrosis predicts ventricular tachyarrhythmias. *Trends in Cardiovascular Medicine* vol. 27 363–372 (2017).
314. Coronel, R. *et al.* Electrophysiological changes in heart failure and their implications for arrhythmogenesis. *Biochim. Biophys. Acta - Mol. Basis Dis.* **1832**, 2432–2441 (2013).
315. Weber, K. T., Sun, Y., Bhattacharya, S. K., Ahokas, R. A. & Gerling, I. C. Myofibroblast-mediated mechanisms of pathological remodelling of the heart. *Nat. Rev. Cardiol.* **10**, 15–26 (2012).
316. Pellman, J., Zhang, J. & Sheikh, F. Myocyte-fibroblast communication in cardiac fibrosis and arrhythmias: Mechanisms and model systems. *Journal of Molecular and Cellular Cardiology* **94** 22–31 (2016).
317. Chaigne, S. *et al.* Transient receptor potential vanilloid 4 channel participates in mouse ventricular electrical activity. *Am. J. Physiol. Heart Circ. Physiol.* **320**, H1169–H1169 (2021).
318. Du, X. J., Cox, H. S., Dart, A. M. & Esler, M. D. Sympathetic activation triggers ventricular arrhythmias in rat heart with chronic infarction and failure. *Cardiovasc. Res.* **43**, 919–929 (1999).
319. Nguyen, M. N. *et al.* Spontaneous ventricular tachyarrhythmias in β2-adrenoceptor transgenic mice in relation to cardiac interstitial fibrosis. *Am. J. Physiol. - Hear. Circ. Physiol.* **309**, H946–H957 (2015).
320. Lian, H. *et al.* Heart-specific overexpression of (pro)renin receptor induces atrial fibrillation in mice. *Int. J. Cardiol.* **184**, 28–35 (2015).
321. Stöckigt, F. *et al.* Deficiency of cyclase-associated protein 2 promotes

arrhythmias associated with connexin43 maldistribution and fibrosis. *Arch. Med. Sci.* **12**, 188 (2016).

322. AD, W. *et al.* The role of action potential prolongation and altered intracellular calcium handling in the pathogenesis of heart failure. *Cardiovasc. Res.* **37**, 312–323 (1998).
323. Yue, Z. *et al.*Transient receptor potential (TRP) channels and cardiac fibrosis. *Curr. Top. Med. Chem.* **13**, 270–282 (2013).
324. Fan, D., Takawale, A., Lee, J. & Kassiri, Z. Cardiac fibroblasts, fibrosis and extracellular matrix remodeling in heart disease. *Fibrogenes. Tissue Repair* **5**, 1–13 (2012).
325. Rumi-Masante, J. *et al.* Structural basis for activation of calcineurin by calmodulin. *J. Mol. Biol.* **415**, 307 (2012).
326. Lighthouse, J. K. & Small, E. M. Transcriptional control of cardiac fibroblast plasticity. *J. Mol. Cell. Cardiol.* **91**, 52 (2016).
327. Zhao, L., Sullivan, M. N., Chase, M., Gonzales, A. L. & Earley, S. Calcineurin/Nuclear Factor of Activated T Cells–Coupled Vanilliod Transient Receptor Potential Channel 4 Ca2+ Sparklets Stimulate Airway Smooth Muscle Cell Proliferation. Am. J. Respir. Cell Mol. Biol. **50**, 1064-1075 (2014)
328. Cao, B., Dai, X. & Wang, W. Knockdown of TRPV4 suppresses osteoclast differentiation and osteoporosis by inhibiting autophagy through Ca 2+ – calcineurin–NFATc1 pathway. *J. Cell. Physiol.* **234**, 6831–6841 (2019).
329. Parpaite, T. *et al.* Effect of hypoxia on TRPV1 and TRPV4 channels in rat pulmonary arterial smooth muscle cells. *Pflugers Arch. Eur. J. Physiol.* **468**, 111–130 (2016).
330. Kitamura, N. & Kaminuma, O. Isoform-Selective NFAT Inhibitor: Potential Usefulness and Development. *Int. J. Mol. Sci.* **22**, 1–14 (2021).
331. Saliba, Y. *et al.* Transient Receptor Potential Canonical 3 and Nuclear Factor of Activated T Cells C3 Signaling Pathway Critically Regulates Myocardial Fibrosis. *Antioxidants Redox Signal.* **30**, 1851–1879 (2019).
332. Tokudome, T. *et al.* Calcineurin–Nuclear Factor of Activated T Cells Pathway–Dependent Cardiac Remodeling in Mice Deficient in Guanylyl Cyclase A, a Receptor for Atrial and Brain Natriuretic Peptides. *Circulation* **111**, 3095–3104 (2005).
333. Martinez-Martinez, S. & Redondo, J. Inhibitors of the Calcineurin / NFAT Pathway. *Curr. Med. Chem.* **11**, 997–1007 (2005).
334. Al-Daraji, W. I., Grant, K. R., Ryan, K., Saxton, A. & Reynolds, N. J. Localization of calcineurin/NFAT in human skin and psoriasis and inhibition of calcineurin/NFAT activation in human keratinocytes by cyclosporin A. *J. Invest. Dermatol.* **118**, 779–788 (2002).
335. Rich, M. W. *et al.* Knowledge Gaps in Cardiovascular Care of the Older Adult Population. *Circulation* **133**, 2103–2122 (2016).

336. Chioncel, O. *et al.* Epidemiology and one-year outcomes in patients with chronic heart failure and preserved, mid-range and reduced ejection fraction: an analysis of the ESC Heart Failure Long-Term Registry. *Eur. J. Heart Fail.* **19**, 1574–1585 (2017).
337. Grilo, G. A. *et al.* Age- and sex-dependent differences in extracellular matrix metabolism associate with cardiac functional and structural changes. *J. Mol. Cell. Cardiol.* **139**, 62–74 (2020).
338. Strait, J. B. & Lakatta, E. G. Aging-associated cardiovascular changes and their relationship to heart failure. *Heart Fail. Clin.* **8**, 143 (2012).
339. Yang, Y. H. *et al.* Specific α7 nicotinic acetylcholine receptor agonist ameliorates isoproterenol-induced cardiac remodelling in mice through TGF-β1/Smad3 pathway. *Clin. Exp. Pharmacol. Physiol.* **44**, 1192–1200 (2017).
340. Zhang, J. *et al.* Qiliqiangxin attenuates isoproterenol-induced cardiac remodeling in mice. *Am. J. Transl. Res.* **9**, 5585 (2017).
341. de Lucia, C., Eguchi, A. & Koch, W. J. New insights in cardiac β-Adrenergic signaling during heart failure and aging. *Frontiers in Pharmacology* **9** (2018).
342. Lindenfeld, J. *et al.* Sex-related differences in age-associated downregulation of human ventricular myocardial β1-adrenergic receptors. *J. Hear. Lung Transplant.* **35**, 352–361 (2016).
343. Norton, G. R. *et al.* Myocardial stiffness is attributed to alterations in cross-linked collagen rather than total collagen or phenotypes in spontaneously hypertensive rats. *Circulation* **96**, 1991–1998 (1997).
344. Kim, G. H., Uriel, N. & Burkhoff, D. Reverse remodelling and myocardial recovery in heart failure. *Nature Reviews Cardiology* vol. 15 83–96 (2018).
345. N, K. & DA, K. Reverse remodeling in heart failure--mechanisms and therapeutic opportunities. *Nat. Rev. Cardiol.* **9**, 147–157 (2011).
346. Yokokawa, M. *et al.* Recovery from left ventricular dysfunction after ablation of frequent premature ventricular complexes. *Hear. Rhythm* **10**, 172–175 (2013).
347. Berruezo, A. *et al.* Mortality and morbidity reduction after frequent premature ventricular complexes ablation in patients with left ventricular systolic dysfunction. *Europace* **21**, 1079–1087 (2019).
348. G, C. *et al.* Pharmacological left ventricular reverse remodeling in elderly patients receiving optimal therapy for chronic heart failure. *Eur. J. Heart Fail.* **7**, 1040–1048 (2005).
349. Palazzuoli, A. *et al.* Effects of carvedilol on left ventricular remodeling and systolic function in elderly patients with heart failure. *Eur. J. Heart Fail.* **4**, 765–770 (2002).
350. H, Y. *et al.* Impact of age on mid-term clinical outcomes and left ventricular reverse remodeling after cardiac resynchronization therapy. *J. Cardiol.* **77**, 254–262 (2021).

351. Wever-Pinzon, O. *et al.* Cardiac Recovery During Long-Term Left Ventricular Assist Device Support. *J. Am. Coll. Cardiol.* **68**, 1540–1553 (2016).
352. Lee, A., Denman, R. & Haqqani, H. M. Ventricular Ectopy in the Context of Left Ventricular Systolic Dysfunction: Risk Factors and Outcomes Following Catheter Ablation. *Hear. Lung Circ.* **28**, 379–388 (2019).
353. Lakatta, E. G. & Levy, D. Arterial and Cardiac Aging: Major Shareholders in Cardiovascular Disease Enterprises. *Circulation* **107**, 346–354 (2003).
354. M, S. & G, L. Cardiac aging and heart disease in humans. *Biophys. Rev.* **9**, 131–137 (2017).
355. Janczewski, A. M. & Lakatta, E. G. Modulation of sarcoplasmic reticulum Ca2+ cycling in systolic and diastolic heart failure associated with aging. *Heart Fail. Rev.* **15**, 431 (2010).
356. Veteto, A. B., Peana, D., Lambert, M. D., McDonald, K. S. & Domeier, T. L. Transient receptor potential vanilloid-4 contributes to stretch-induced hypercontractility and time-dependent dysfunction in the aged heart. *Cardiovasc. Res.* **116**, 1887–1896 (2020).
357. Saifeddine, M. *et al.* GPCR-mediated EGF receptor transactivation regulates TRPV4 action in the vasculature. *Br. J. Pharmacol.* **172**, 2493–2506 (2015).
358. Lawhorn, B. G., Brnardic, E. J. & Behm, D. J. Recent advances in TRPV4 agonists and antagonists. *Bioorg. Med. Chem. Lett.* **30**, 127022 (2020).